The Study of Charge Carrier Transport in the Semiconductor Lattice

James R Leitch

Submitted for the Degree of
Doctor of Philosophy
from the
University of Surrey

Microwave and Systems Research Group
School of Electronics and Physical Sciences
University of Surrey
Guildford, Surrey GU2 7XH, UK

August 2002

To my father James Reid Leitch of the James Watt College.

ACKNOWLEDGMENTS

I would like to thank my supervisor Prof. Mike Underhill for his support and encouragement throughout the duration of this research. Thanks also to my employer Altera Corporation for their support, and also my previous employer Communications and Control Electronics in the University of Surrey Research Park for their support at the start of the work. Special thanks to my wife Janice for her continued support of my work, without which this research would not have been possible. This work has been funded by support from the two companies mentioned above, and from personal funds.

ABSTRACT

Leitch, James R. Ph.D., Surrey University, August, 2002. . .

This thesis explores the physical origins of noise in semiconductors. A novel method of analysing the electron and hole carrier flow in the junction is developed, and the results are analysed with the objective of comparing the model against physical measurements made on actual semiconductor junctions. The current state of the art for commercial device fabrication is currently about $100nm$ device length, and new approaches to modelling device behaviour and noise mechanisms are required as the technology shrinks. In addition higher order transport models are needed due to smaller transistor sizes, and the need to account for current crowding effects in high current density situations. The various known forms of noise are reviewed, and prioritised in terms of their contribution to a pre-selected demonstration vehicle, in this case a BJT, and their contribution to the BJT's overall noise figure. The alternative methods of analysing noise are considered, and compared against the objective of reducing noise in this selected semiconductor structure. Many simulation techniques are available offering 1, 2 and pseudo three dimensional (2 1/2-D) approaches. The continuing trend to reduce the dimensions of the active devices requires more accurate models, and so more detailed physical correlation, especially at higher current densities. The models should be able to run as quickly and efficiently as possible with this increased complexity. The minority carrier based operation of the Bipolar Junction Transistor or BJT is selected, and this is used as an example in the model , with the intention of validating the model against a mature and very predictable technology. The model is also validated using well known and established simulation methods and then the model is applied to evaluate new structures, in order to propose

a low noise BJT or LNBJT. The dominant noise in BJT devices is shown to be due to shot noise at mid to high frequencies. The noise mechanism known as shot noise, has been assumed in the past to be a fundamental noise form that limits the noise performance of bipolar structures. This work develops and demonstrates a method for modelling the carrier transport in theory of devices down to geometries of $15nm$ between the emitter and collector, using a true 3D simulation model called JAMES (Junction Atomistic Modelling of Extrinsic Semiconductors), based on a multi-carrier model, and able to model a large number of carriers in realistic simulation times. The thesis then goes on to develop the model for studying the nature of the individual carrier flow, and proposes a physically consistent explanation of electrical shot noise, and the carrier transport intrinsic in the BJT current flow. The work demonstrates the use of the model to redesign the bipolar junction transistor, and by modifying its doping structure and biasing, the spectral density of the *shot noise* S_v can be reduced by $-26.4dB$ at frequencies approaching DC, and greater than $-10.75dB$ reduction at $1Ghz$. The mechanism used to reduce the shot noise is to re-thermalise the minority carriers which have been grouped into "noise quanta" , by introducing a semiconductor region to return the individual carriers to a classically chaotic state before they reach the collector. This new proposed structure is a dual base LNBJT capable of not only reducing the shot noise and total device noise, but also increasing the AC voltage gain, and increasing the transition frequency when it is used as a switch. A proposed new constant will be introduced, referred to as K_{SA} , defined as the ratio of reduction in the spectral density as a result of adding a new structure. The work offers as one result, a design methodology to minimise the impact of noise in integrated and discrete BJT's. The noise attenuation mechanism proposed can also reduce other noise forms however, but to a smaller extent. The mechanism proposed here is effective in attenuating shot noise because the noise quanta given by $\Delta Q = n.q$ is relatively small, where q is the carrier charge, and n is the number of charge carriers in the quanta. Low frequency noise forms can have a larger noise quanta, and so the attenuation of these forms is therefore smaller.

PREFACE

The layout of this thesis is briefly summarised below:

1. Introduction

2. A review of noise mechanisms

3. Atomistic simulation

4. The research question

5. A review of the current approaches to noise modelling

6. Review of the methodology and mechanisms used in the model

7. A brief introduction to the new structure to be modelled

8. The JAMES model using a true 3D approach to noise modelling

9. Carrier transport mechanisms in the semiconductor junction.

10. The JAMES algorithm applied to a BJT semiconductor as validation of the model.

11. Results from the JAMES model

12. Conventional analysis of the new BJT structure

13. Analysis of the results from the JAMES model in relation to the new structure

14. Novel aspects of the work

15. Conclusions

Glossary

3D Three dimensions

Alternating current

AC Alternating current

BJT Bipolar junction transistor

CCA Charge control Algorithm

CAD Computer Aided Design tools [EDA]

CPLD Composite programmable logic device

dB Deci-bel

DC Direct current

EDA Electronic Design Automation

FCC Face centred cubic

FET Field Effect Transistor

G-R Generation - recombination

Hexadecimal notation with states 0 to 15(F)

JAMES Junction atomistic modelling of extrinsic semiconductors

K_{SA} New proposed constant - Shot Noise attenuation factor

LNA Low noise amplifier

LU Lattice unit

LUT Look up table

MOSFET Metal Oxide Semiconductor Field effect transistor

MP Measurement plane

NDTU Non Dimensional time unit

OP Observation plane

RF Radio frequency

rms Root mean squared value

ROM Read only memory

SD Spectral density

SEM Spatial Evolution Matrix

SNA Spectral noise attenuation

SNR Signal to noise ratio

TABLE OF CONTENTS

LIST OF FIGURES

1. INTRODUCTION

The study of *noise phenomena* [2] has *long* been a topic of concern in electronic engineering. The limits of amplifying signals has been determined by the level of noise present along with the signal. The study of these mechanisms represents research into the deviation of the actual behaviour of the carriers, from the simplified numerical *idealised* models used to predict noise magnitudes. As the speed of electronic systems and devices increase, the need to use active devices at higher frequencies, lower noise and also more precise timing constraints increase. The presence of noise in active devices is a direct consequence of the physics of conduction, and so requires a better understanding of the design of the active devices to minimise noise and improve the predictability of system timing. The main objective of this research is to provide a vehicle to obtain insight into these effects, and to form the basis for a new generation of EDA (Electronic Design Automation) tools. The existence of shot noise has long been accepted as an intrinsic mechanism that cannot be reduced in magnitude and as a fundamental limit in the design of low noise minority carrier semiconductor amplifiers and systems.

Noise is not an error, but a facet of the electrical behaviour of the actual underlying physics of the semiconductor lattice [7, 66]. This thesis describes the current status of research aimed at studying the *discrete nature of current flow* in sub-micron semiconductor junctions, and relating this to one of the fundamental noise forms [67]. The importance of noise is increasing in RF design in the area of Low Noise Amplifier (LNA) design.

The basis for electrical and electronic sciences has been based on the study of *large carrier populations* in conducting materials, or on macro properties of devices. The use of semiconductor devices at the extremes of operation i.e. very low currents or very high frequencies, or at very low noise levels, begins to show apparently anomalous behaviour.The existing models begin to break down in terms of their ability to predict the behaviour of the device. This research looks at achieving a better understanding of noise mechanisms, and the ability to more accurately model the underlying mechanisms. This modelling of the electrical behaviour allows certain simplifications in the way the conduction behaviour is described e.g. Resistance describes the average value of the charge carrier flow resulting from the application of an electric field.

The study of individual charge carrier behaviour can be made, but of course at the expense of complexity, and the resultant increased time to make the analysis. The application of such a technique, to the study of noise behaviour, is one such situation that seemed appropriate , and would benefit from this approach. The study of electrical noise phenomena in semiconductor devices has been ongoing for many years, with many important papers published [1, 80, 81, 82, 42]. The treatment has been largely empirical, with formula for the various forms of noise being developed, with the exception of thermal and shot noise. More recently more papers have appeared with the objective of describing noise phenomena by using finite element analysis techniques [40].

This work approaches the subject of noise analysis from an attempt to understand and describe the functional level of the individual carriers, rather than using a behavioural approach such as thermodynamics. The

approach developed here was selected for several reasons. The continuing reduction in transistor size, and the requirement for higher performance, including reduced phase noise, means active device lengths are approaching $100\,nm$. The active device is rapidly approaching the size that allows the possibility of 'Atomistic Simulation' to be used in order to analyse the behaviour.

The increase in computing power also means that this technique is now becoming practicable. The evolution of EDA see Appendix: {J.1} over the next ten years will mean that transistor geometry will shrink to tens of nano-meters. The transistor shrinking to atomic dimensions will mean that electrical behaviour can no longer be described adequately with macro descriptions. using traditional approaches.

The accurate modelling of active devices is fundamental to the semiconductor industry, as the EDA tools are used to predict the behaviour of the system, before committing a design to actual silicon. This requirement and the dual requirement of accurately predicting noise parameters would seem to require a common solution. The analysis of the behaviour suggests that the mechanisms can only be controlled, by a more complete understanding of the behaviour of the current flow, through the junction. One problem has been the accuracy with which noise levels can be specified, and tend to vary widely, indicating the basic mechanisms are not well understood and hence controlled.

The random nature of electrical noise has attracted more attention to the discrete nature of current flow, and so this approach was felt to link the physics of the underlying mechanisms involved to the observed phenomena. The noise in an active amplifying device creates a constraint on its usable limits, and so any change in the design that reduces the noise also

increases the usable electrical range for a given device. This thesis shows that a better understanding of the underlying mechanisms, i.e. the charge transport phenomena in the device, can explain the observations more accurately. A simple Bipolar Junction Transistor is used as a demonstration vehicle to show how the application of a new 3-D simulation model, using individual charge modelling, called the JAMES model, see Chapter 3, can be used to reduce the noise in the structure. Noise will occur in an ideal transistor i.e. a device based on the known physical operation of a BJT, even if it is manufactured perfectly, and so the use of an idealised model does not detract from the use of software to analyse the underlying behaviour.

The reduction of noise in an amplifying device is possible by simply reducing the bandwidth of the system, an example of this is thermal noise [15]. The reduction of noise in a broad-band amplifier requires the underlying device noise contribution to be reduced, but requires the bandwidth to be large. These are contradictory requirements and must be addressed by reducing noise without reducing the bandwidth of the amplifier. The measure of electrical noise is the rms noise voltage or spectral density S_v, where the spectral density is defined as the integration of the noise voltage power over the entire frequency spectrum. The spectral noise density S_v of a simple PN junction can be shown to be $2.14 \times 10^{-19}\, V^2/Hz$, at a current of $1mA$ and at an absolute temperature of $300^o K$. These standard conditions will be referred to as Ref_{IT} Appendix: {D.4} from this point forward. This work shows the modification of a simple NPN BJT to reduce this spectral noise density to $5.29 \times 10^{-22}\ V^2/Hz$ in Ref_{IT} Appendix: {D.4}. The reduction of noise in BJT current sources is another important area in IC design, where it is important to reduce noise at DC bias levels, while using high frequency AC collector signals. This approach would pro-

vide a natural end-point to this research, and would result in the design of a Low Noise BJT device, that is able to be evaluated for future signal processing applications. The JAMES model could be used to analyse and enhance other types of semiconductor structures, and certainly other substrate materials apart from silicon. The model would require calibration for other materials in terms of hole and electron mobilities.

1.1 Background Information

1.1.1 A Brief Review of Noise and Noise modelling

The conventional treatment of noise theory [32, 36, 13] from a gross behavioural, or macro-level, will be shown below. These equations do not use individual carrier models to describe them, but use techniques based on the assumption of large numbers of carrier populations. Thermal noise and shot noise are both precisely understood mechanisms, but Flicker noise [52] and Burst noise [15, 53] are defined by more experimentally empirical approaches.

Noise is a measurement of the purity of an electrical signal. When the noise level is low the signal is more pure. When a high level of noise is present then the signal is inaccurate or distorted, or contains a random component which obscures the signal of interest. Noise is the measure of difference between an anticipated ideal signal and the actual signal obtained , due to the imperfections of the system. The basic underlying imperfection, is the physics of the mechanism of current flow in a conductor (or semiconductor) , due to the fact that current flow is a discontinuous flow of individual charge carriers in the conductor. This granularity of carriers limits the continuity of the signal in the conductor. Conventional noise theory [83] shows there are four main types of observed noise in a semiconductor junction.

HOW IS NOISE MEASURED ?

Noise is normally expressed as the amplitude of the noise, as a peak to peak or rms voltage or current in units of $V/\sqrt{Hz}$ or $A/\sqrt{Hz}$. Alternatively noise can be measured as the Spectral Density of the observed signal in units of v^2/Hz or i^2/Hz .

1.1.2 Noise modelling

There are several forms of electrical noise present in BJT [85], and the degree of understanding of these mechanisms vary. The two forms of noise that are well understood and accurately defined are thermal noise [54], and shot noise [51, 55]. The other noise forms that are more empirically defined include 1/f noise, burst noise [3], and (GR) noise [56]. This is evident by the use of empirically derived constants used in the equations describing the state of the art definition of these noise types [15]. Noise has until recently [15, 36] been observed as a macro process, and equations have been used [15] to relate certain parameters of the system to the magnitude of the noise. The parameters might be *temperature* or *current* [54, 51]. Within the last few years the underlying nature of noise has been used to relate the nature of the carriers to the magnitude [57] and type of noise [12]. Thermal noise and shot noise are probably the best understood, as they can be derived [58, 35] from the basic application of thermodynamics and statistics to the mechanisms. The current approach [15] to quantifying noise is to use certain equations describing the different noise forms. This allows the magnitude of each noise component to be determined, and gives an amplitude which can be used to quantify the performance of the system [59]. The equations Eqs. 1.1 and 1.4 do not give any temporal dimension to the noise, and do not relate the noise to the underlying physical processes. They are therefore not immediately helpful as tools for designing new semiconductor devices , and for providing a method for comparing one device design against an other. The modelling of these noise factors is by means of equations which have given a best fit results for a particular physical design or fabrication process. The processes of shot noise and thermal noise are statistically based derivations, and because the underlying mechanisms of charge transport in a semiconductor are best described statistically they are based on fundamentals. More recently [60] the modelling of charge transport has started using modelling techniques that attempt to describe the underlying mechanisms. This work attempts to create a modelling mechanism that aids visualisation , and therefore make the the interpretation of results more

directly related to the physical reality. This iterative approach allows an idea to be quickly evaluated for an improvement. The ease of use of the model allows practical measurements to be carried out on the representation of the device being analysed. The different forms of noise will now be briefly described.

1.1.3 Thermal Noise [1, 10, 18, 33, 35]

This is perhaps the best known form of noise, and is due to the random movement of charge carries in the semiconductor. The voltage created by this random movement of charge, through any intrinsic resistance in the device, gives rise to thermal noise. Thermal noise is a direct consequence of the temperature of a device above absolute zero, and can only be reduced through lower temperatures, or lower resistance.Thermal noise is caused by the random motion of the individual charge carriers within the semiconductor lattice. The energy of the carriers in the lattice is due to the thermal energy stored in the semiconductor and increases with temperature. The energy at absolute zero causes the random movement to cease, and so the noise is zero when measured between two reference planes at this temperature. At temperatures above absolute zero see Appendix: {B.1} the thermal energy stored in the structure of the lattice, and electrons, cause the electrons energy to increase, and so the random fluctuations to increase. The noise voltage can be shown, to be proportional to the absolute temperature. This is the best understood of all the noise forms and can be predicted from the thermodynamics of the solid at a given temperature. Spectral density is a common method for quantifying noise, and is expressed in a form that equates to the noise power in a component or system. The spectral density of thermal noise is given by

$$S_i = \frac{4kT}{R} A^2/Hz \tag{1.1}$$

where k is Boltzmanns constant, T the temperature in K and R the resistance, and

$$S_v = 4kTR\,V/Hz \tag{1.2}$$

[6], where S_i and S_v are the spectral densities of the current and voltage of the junction, respectively. The thermal noise is represented in the Atomistic model in a

natural way as a result of the use of a random movement of the carriers. The thermal noise voltage is given by

$$\nu_n^2 = 4kTR\Delta f \tag{1.3}$$

where Δf is the bandwidth of the measurement system in Hertz, giving

$$\nu_n rms = 4n \ \ V/\sqrt{Hz}$$

at the reference bias {B.1}, and $R = 1k\Omega$, The thermal spectral density of the current is given by

$$S_i = v_n^2/R^2 = 1.6 \times 10^{-23} \ A^2/Hz$$

this is the same amplitude as the shot noise of a P-N junction at a current of $50uA$ at room temperature.

1.1.4 Shot Noise [1, 10]

Shot noise, the physical explanation of which is given in more detail in Appendix: {E.1}, is a major form of noise present in modern minority carrier semiconductor devices. Shot noise and Thermal noise are identical mechanisms, the only difference is thermal noise results from random movement of charge carriers, while shot noise is bounded by the presence of a unidirectional electric field. This field exists in the depletion region of the junction and is proportional to $(\psi_0 - V)$, where V is the voltage across the junction and ψ_0 is the contact potential. Shot noise is well understood, and due to the discrete charge carriers crossing a potential barrier. The noise is created by the individual charge carriers arriving at the measurement plane, at varying times, and causing a unit impulse between the measurement planes. Shot noise is due to the flow of discrete charge carriers over a POTENTIAL-BARRIER JUNCTION [37]. Shot noise is defined by the physics of the charged carriers as they cross a voltage gradient such as the potential-barrier between a N and a P type semiconductor in a semiconductor junction. When carriers in a conductor diffuse in a completely uncorrelated way, the

noise magnitude reaches the well know Poisson limit [48] for a given average DC current I_d is given by

$$2qI_d \tag{1.4}$$

where q is the electronic charge. In all other cases, except for some special cases such as transport in resonant-tunnelling diodes, shot noise is proportional to the average current times a real number. This number is called the Fano factor [13]. Appendix{A.3} . The Shot noise is the fluctuation in I and is defined as

$$\overline{i^2} = \overline{(I - I_d)^2} = \int_0^{1/T} (I - I_d)^2 dt \tag{1.5}$$

giving the mean squared current $\overline{i^2}$in terms of the mean diode current I_d , and Δf the bandwidth of the measuring system in Hz.

$$\overline{i^2} = 2\,q\,I_d\,\Delta f\ (A^2) \tag{1.6}$$

where q {B.1} is the electronic charge. Solving for i_{rms}

$$i_{rms} = \sqrt{2I_d\,qB} \tag{1.7}$$

The spectral density is given by

$$S_i = 2qI_d\ A^2/Hz \tag{1.8}$$

where I_d is the average current through the junction, q is the electronic charge, and B is the bandwidth of the measuring system in Hz. The amplitude of shot noise varies randomly with time, and can only be specified, by a probability density function. This can be shown to have amplitude distribution which is Gaussian in nature. If σ is the standard deviation, then $\sigma^2 = \overline{(I - I_d)^2}$where I is the instantaneous noise and I_d is the average value of the current, and $\sigma = \sqrt{2qI_d\Delta f}$. Calculating the shot noise in the emitter-base junction of a BJT, at a current of $50\,\mu A$, at a bandwidth of $1MHz$ giving a spectral density

$$S_i = 2\,q\,I_d = 1.6 \times 10^{-23}\ A^2/Hz$$

$$\overline{i^2} = 2 \cdot 1.6 \times 10^{-19} \times 50 \times 10^{-6} \times 1 \times 10^{6} = 1.6 \times 10^{-17}\ A^2$$

so $i_{rms} = 4.0 \times 10^{-9}$ or $4.0\ nA$. Providing an example of the shot noise in a BJT as an example, with $I_e = 50uA$, and a bandwidth $B = 1MHz$.

$$I_{rms} = \sqrt{2 \cdot 1.6 \times 10^{-19} \times 50 \times 10^{-6} \times 1 \times 10^{6}} = 4.0\ nA$$

If the collector load $R_L = 50k\ \Omega$,

$$v_{rms} = 4.0 \times 10^{-9} \times 50 \times 10^{3} = 200uV$$

This is the magnitude of the shot noise measured at the collector of a typical BJT at this current and load before the introduction of any noise reduction mechanisms.

1.1.5 Burst Noise or Popcorn noise [15]

This is a Low frequency noise, and is a form of noise that appears to cause a modulation of the current flow through the semiconductor under various conditions. This causes as the name suggests fluctuations in the current at low frequencies. This is also a low frequency noise, and appears to be due to heavy-metal ion contamination. Gold doped devices show very high levels of burst noise. Burst noise shows bursts of noise on a number (two or more) of discrete levels. The spectral density is given by [15, 53] assuming the bandwidth equals $1Hz$.

$$\overline{i^2} = \frac{K_2 I^c}{1 + (\frac{f}{f_c})^2}.\Delta f \tag{1.9}$$

where K_2 is a constant for the particular junction, c is a constant between 0.5 and 2, I the average current, f the operating frequency, and f_c is the corner frequency for a given noise process. Burst [16] noise is still the subject of considerable research, but is thought to be due to the presence of contamination within the relatively pure crystalline lattice of the silicon.

1.1.6 (GR) or (Generation-Recombination) Noise [10, 16]

This form of noise is caused by the basic mechanisms involved in current flow in a semiconductor, and is attributable, to the behaviour of the electrons in the lattice of the semiconductor. The continuous trapping and de-trapping of the carriers, cause a fluctuation in the number of carriers in the conduction and valence bands. The noise is thought to be due to traps in the silicon [56]. In the observed noise spectra, the corner frequency of this noise is dispersed, implying a range of lifetimes. If the current that flows through a semiconductor structure is due to (GR), then the equation Eq. 1.10 for this type of noise applies. When the structure is a potential barrier junction device, the applied voltage increases the injection rate over the barrier, and the noise will show a close approximation to shot noise. This type of noise [16] is Lorentzian in nature, and is given by Eq. 1.10, where f is the operating frequency and τ_n is the lifetime in the conduction band

$$S_n(f) = \frac{<(\Delta_n)^2> 4\tau_n}{(1+(2f\tau_n)^2} \tag{1.10}$$

where $<(\Delta_n)^2> \propto I^2$. For a typical process, and doping, a typical electron lifetime τ_n is $1nS - 100uS$ [61].

1.1.7 Flicker noise [15, 21, 5, 79]

This form of noise, is thought to be caused by traps associated with contamination in the silicon, or lattice defects, forming traps in the BJT emitter-base depletion region. Flicker noise has a $1/f$ dependence, and hence the name Flicker noise.

$$i^2 = k_1 . \frac{I^a}{f^b} \Delta f \tag{1.11}$$

with $b = 1$, and $a = 0.5$ to 2.0, I is the average current flowing, Δf the bandwidth, and k_1 is a constant for a particular BJT structure. Taking a typical collector current level of 200×10^{-6}, or $200\mu A$ for a typical "mesa" bipolar transistor.

$$\overline{i^2} = k_1 \frac{(.05 \times 10^{-3})^2}{f} \Delta f \tag{1.12}$$

with $b = 1$, $a = 1$, $I = 50uA$, and $\Delta f = 10^3$ the current spectral density

$$S_i = 200 \times 10^{-6}.\frac{50 \times 10^{-6}}{10^3} \times 0.1 \times 10^3 = 10^{-16}\ A^2/Hz$$

The presence of these imperfections, or contaminant atoms in the lattice, give rise to recombination centres that cause the average transit time of the individual charge carriers to be changed, resulting in bursts of charge crossing the measurement plane. This is typically found in semiconductor junctions containing impurities [16]

2. WHAT IS ATOMISTIC SIMULATION ?

Atomistic simulation is based on the atomic structure and dynamics of the physical mechanisms in the semiconductor lattice. The simulation models the behaviour of the individual charge carriers , say electrons, and uses their behaviour to explain the macro electrical properties of the semiconductor. No reference to the modelling of a large numbers of individual carriers, in a true 3-D simulation environment, in an attempt to describe noise mechanisms in semiconductors, has been uncovered to date.

However many attempts to model carrier transport have been published, using different methods and analysis techniques, and they are reviewed in this section for completeness. The traditional paradigm has been to use the study of the macro properties of a given noise mechanism by measuring the noise levels with electronic instrumentation. This of course measures averages of reasonably large carrier populations or "macro" measurements. This is performed in the SPICE simulators commonly used in engineering, by assuming the noise is an AC sine-wave, calculating the magnitude of the noise type for a given device in the system, and then referring the noise to the output port through the AC transfer function of the system. The new trend in analysis has been to represent the charge carriers at an individual level, using numerical analysis. The available technologies for analysing noise are summarised as follows:

1. Modelling by noise equations

2. Simulation by means of AC analysis e.g. Spice software

3. The use of numerical simulation to solve the equations describing carrier transport.

2.1 The Research Question

The basic research attempts to answer the question: Can the inherent carrier noise in an active semiconductor device be substantially reduced to produce very low noise BJT transistor amplifiers, with a Noise Figure much lower than that currently achievable today ? This section will show that many attempts have been made to answer this question, but have been unable to provide a physically accurate representation of the semiconductor lattice, and also use mechanisms to describe the different carrier flows in a similar manner to the underlying physics of the carrier transport process. This is proven by the absence of semiconductor devices designed using CAD tools, with an approach based on the analysis of the charge transport processes and the direct consequences of these discrete carriers on the resultant noise.

2.1.1 Quantifying low noise performance

The fundamental limit for a simple, minority carrier device, based on the P-N junction, due to shot noise, has been shown in Appendix: {D.5}, to be $463pV\ rms$ at the standard test conditions, see Ref_{IT} Appendix: {D.4}. This assumes an ideal diode with no series resistive component. In practice the junction will have series resistance , and will have an additional thermal noise component of $v_{\mathrm{n}rms} = \sqrt{4kTR_s}$, where R_s is the series resistance. The limit of $463pV$ at the test conditions Ref_{IT} in Appendix: {D.4} is therefore an apparent fundamental constraint for an ideal diode based only on the shot noise component. The state of the art design in the fabrication of semiconductor amplifiers attempts to use the purest crystal, and the best silicon fabrication techniques, to produce a low noise amplifier structure. The minimisation of the device current will reduce the shot noise component, and the lowest resistance achievable in a given design will minimise the thermal noise contribution. There are other additional noise sources, which tend to be related to the quality of the manufacturing process as described previously. The "state of the art" [62] design for a simple silicon BJT can achieve at 300^0K, a total noise level of $S_v = 0.02\,fV^2/Hz$, or using alternative measurements, a noise factor $F = 1.2$ or a noise temperature $T = 60^oK$.

2.1.2 Importance of finding lower noise structures

The whole field of Electronics is affected by the common issue of underlying noise performance. The ability to detect and process smaller signals gives rise to new insights into physical mechanisms. This minimum detectable signal (MDS) { G.8 on page 200} level is affected by the amount of noise in the measuring device, or transducer. The field of telecommunications and transmitting signals over long distances is likewise affected by the levels of noise in the various components. The field of *radio reception* is an extreme example of the need to *detect* smaller and smaller signals, and this is directly affected by the noise floor in the *receiver input stage.* The development of space exploration means detecting signals from distant sources or man made vehicles transmitting information back, and this also depends directly on the noise floor achievable. Although noise levels can be reduced by techniques such as cooling to reduce thermal noise, the need for technologies available at low cost enables new applications to open up at a greater rate.

2.2 The State of the art in Noise modelling

The previous approaches to noise modelling are now reviewed. The approach to noise analysis in the past has been through characterisation and modelling of the individual noise mechanisms. The analysis of active systems can then use an equation describing the particular noise, its position in the electrical network, and then use the transfer function between that component and the output to calculate the total contribution to noise. Numerous papers have been published in recent years proposing methods for analysing the behaviour by numerical means, of individual charge carriers [30, 63, 60, 24], in an attempt to provide a model for conduction behaviour more accurately. However due to the practicalities of computation time, and complexity, different methods have been mainly limited in the number of dimensions (2-D) they can handle [64] . A large amount of work has been carried out [65, 57, 69,] in modelling devices and also simulation of current flow, but no work was found exploring the phenomena of noise in minority carrier devices by modelling individual carrier flow in a 3-D lattice. There have been some attempts to model noise through numerical

analysis [86, 40] to provide a more accurate insight into noise mechanisms. The following sections of this chapter look at the modelling that has been developed up to this point.

2.2.1 Ghione and Filicore

Ghione & Filicori [12], outlines a model to predict noise in majority-carrier semiconductor devices. This paper presents an approach to the simulation based on parametric sensitivity and noise in majority-carrier semiconductor devices. The model is build by using a Greens function akin to Shockley's impedance field method. The solution of this function is solved within a discretized physical model of the semiconductor, using inter-reciprocity concepts and based on an adjoint device. The evaluation of the discretized scalar-impedance field within the framework of a frequency-domain small signal numerical device simulator is a straightforward but computationally intensive task.

2.2.2 Gruzinskis

Gruzinskis [47], proposes a closed hydrodynamic approach coupled with the field-impedance method, to evaluate the spectra of sub-millimetre $n^{+}n^{++}$ diode generators. The approach taken by Gruzinski et. al. in "Hydrodynamic approach to noise spectra in uni-polar structures" uses a variation of the classical hydrodynamic model which has been used extensively to study "hot electron" phenomena in sub-micron devices. The classical hydrodynamic model is composed of nonlinear conservation laws for particle number, momentum, and energy, coupled with Poisson's equation for the electric potential.

2.2.3 Asenov

Asenov[14] studies the InP diode to model the behaviour of this device when the applied fields near the onset of self-oscillation, and the presence of a sharp peak in the current spectral density at the generation frequency. This novel technique coupled with Shockley's field-impedance method enables the small signal and noise characteristics of uni-polar devices to be calculated. The approach uses a one-dimensional model under current driven operation. This model is then validated by comparing it

with results obtained by using a Monte Carlo simulation method.

2.2.4 Wein

The Monte Carlo method is recognised as having significant benefits for time averaging of a many-particle history. This paper by Wein [24] uses a simulation technique to extract the device current from the solution of the non-linear Poisson's equations at low drain voltage. The drain voltage at low levels does not have significant coupling to current, and so this technique is used to resolve the effect of random dopants on the gate threshold voltage. A uniform $1nm$ grid is devised to assist in the solution of those equations. The average number of dopants in the transistors channel is calculated by integrating the continuous doping distribution within it.

2.2.5 Sarantini

Sarantini [23] proposes an efficient two-dimensional Poisson solver, to be used in the analysis of realistic semiconductor devices. The multi-grid method described provided a method for simulation semiconductor inhomogeneous devices with irregular boundary conditions. The model was applied to two different electronic devices, a GaAs High electron mobility transistor, and a metal oxide semiconductor. The approach used a solution of Boltzmann's transport equation and Poisson's equation to represent the carrier flow. The mechanisms required to explain noise in the semiconductor seemed basic, and present in all forms of semiconductor device, and so the model should be based on as simple a structure as possible.

2.2.6 Stanford University PISCES 2-D simulator.

The Pisces 2-D semiconductor structure has been around for many years, and is able to handle P-N devices, BJT's and MOSFET's. The simulator is based on a Drift-Diffusion (DD) 2-D approach , and solves the linear differential equations based on a mesh approach using type III-IV MODELS. The simulator represents the 2-D semiconductor by attempting to solve the Poisson and Continuity equations for the semiconductor profile provided to it. The surface of the mesh is placed around the main features of the device such as junctions and contact areas. The mesh is then sub-divided into triangles. This grid structure can be repositioned during the program

run, to dynamically adjust the internal nodes of the mesh, and aid convergence.

2.2.7 Review of the previous approaches to noise modelling

The method outlined by Ghione [12] uses an approach which is equivalent to Shockley's Field Impedance method. The Field Impedance method [40] uses the approach of two independent factors: local fluctuations and their propagation to terminal electrodes. To avoid spatial correlation, local fluctuations are modelled using current noise sources that bridge each "lumped" segment in the region of interest. The lumped segment being an integration of the individual elements or paths connected in parallel between two measurement points. The propagation using the impedance field gives a current noise power at the drain electrode of the device. The method seems more suitable to studying specific spatially constrained noise sources , and is not appropriate for studying both major carrier transport noise and specific noise source locations in the lattice. The Gruzinski approach was aimed at modelling a specific phenomenon, in a particular semiconductor structure, and not a general approach and methodology suitable for a large range of semiconductor structures. The approach taken by Asenov uses the field impedance method also as covered previously. This approach was based on a one dimensional model, and was not considered accurate enough for the more general application to producing 3-D contours of carrier plasma in a BJT. The method used by A. Asenov [14] was related to MOSFETs, and also rejected on the basis that the vehicle was not as predictable as a bipolar semiconductor. This simple and efficient 3-D Atomistic simulation of random dopant induced threshold voltage, gives a vehicle for simulating sub 100nm MOSFETs, and was rejected again as being unsuitable for bipolar modelling. The approach taken by Wein in using Monte Carlo simulation as an approach, is in some ways similar to the Stanford Pisces-II approach in using a regular mesh of $1nm$ to subdivide the area of interest. A $1nm$ grid was felt to be an unacceptable constraint for future device geometries and sizes. Monte Carlo methods originated at Los Alamos National Laboratory in the early years of the nineteen forties [24], and is a very powerful analytical tool. The Monte Carlo approach to device simulation has been employed in many areas of

physics [71, 72] and is a very valuable tool for analysing semiconductor devices. This type of simulator solves the Monte Carlo algorithm for integration numerically. by solving Shroedingers wave equation, and operates on probability densities [73]. The algorithm tends to converge rapidly in any dimension, regardless of the smoothness of the operand [74]. The algorithm is also simple, and performs only two major operations , sampling and point evaluation [74]. This approach however does not work well on many-dimensional domains, especially when the integrand is not smooth [75]. The Monte Carlo approach can be used for noise analysis, however the simulation is excruciatingly slow for white noise analysis [76], which is the type of noise form being analysed in the study of shot noise phenomena. The Monte Carlo approach is usually limited to two carriers [64], which is inadequate for studying current crowding effects. The run times also make it prohibitive to use on a small PC. The approach taken by Sarantini [23] and associates was rejected, on the basis of being only two dimensional, and unable to allow 3-D internal structures for the purposes of noise reduction to be evaluated, and again not having been applied to Silicon bipolar structures. The Pisces-II simulator from Stanford offers a choice of only one or two carrier solutions, and this was felt to be inadequate. The Pisces program does not provide any noise analysis, only an AC analysis capability, and as such was not suitable for addressing the research problem. Although the simulator gives fairly reasonable execution times, it does not provide some of the features required for designing a new structure , and deciding on 3-D profiles to minimise noise. The need to observe current crowding effects in 3-D was felt to be a mandatory requirement, given the very small structures to be studied for future generations of VLSI sub-100nm geometries. The need to have multi carrier simulations with many carriers representing typical current densities, meant a logical representation of the problem would be more likely to process the state and evolution of the model in a short time. The other approaches reviewed did not permit an instant by instant evolution of the carrier density to be observed in true 3-D.

2.3 General problem Solution and Methodology

The proposed BJT demonstration vehicle will now be used to build a methodology, and show the value of this approach. One remaining significant contributor to the BJT's overall device noise level is shot noise. The design of a modern BJT optimised for high frequency performance, and low-noise, requires an understanding of the 3-D effects such as current crowding [77], base spreading resistance [77], and charge profiles in the very thin device regions i.e. the base region . The lack of a 3-D approach reduces the value and usefulness of the results, and hence the practical optimisation of device profiles becomes very difficult. This is demonstrated by the absence of any BJT devices available with shot noise suppression. Traditionally the approach in predicting noise has been to use one of the empirically derived equations for that particular type of noise, and control those parameters within the design by empirical methods. There is no evidence found in the literature of a systematic and scientific approach to this end. The object of this research is to develop a model able to represent the mechanisms of noise at a fundamental level, and to use the model produced as a tool, to design lower noise structures. Here it is argued that the approach of using a much more accurate 3-D simulation approach to model the carrier behaviour in a typical semiconductor device, would allow progress to be made in designing devices with the lowest level of noise achievable. The spectral noise density S_v of a simple PN junction was shown to be $2.14 \times 10^{-19}\ V^2/Hz$ see Appendix: {D.4}, at standard test conditions, defined in Ref_{IT} Appendix: {D.4}. This is the currently accepted fundamental limit achievable for this current flowing across a potential-barrier, without attenuation, which has been the case historically with a single base. A way has been found, using the 3-D JAMES simulation model to analyse and reduce the propagation of this fundamental shot noise level from the PN junction, by intercepting the minority current flow with a new, specific high recombination region, designed to alter the behaviour of the minority carrier flow, and so reduce the spectral density of the carriers before they are swept into the collector depletion region. The methodology chosen was to pursue the evaluation of different

conceptual structures with this end in mind. This required a modelling environment to achieve this objective , using a process of iterative optimisation. The use of a *physically mapped* simulation was felt to provide an intuitive environment and the degree of visualisation and speed, required for interpreting the results of the various mechanisms, while allowing properties such as the doping profile, layer widths etc. to be easily entered into the model. The approach was to look at the contribution of all the noise types in a typical BJT device, calculate their magnitudes, and to prioritise the dominant mechanisms. The noise forms could then be prioritised according to their magnitude, and by tackling the most significant, this would give the best reduction in overall noise for a limited resource. The use of a 3-D, physically mapped model, was required in order to obtain an accurate representation of the crystal. This normally requires a large amount of computer random access memory in order to represent the lattice and the carriers, to obtain fast execution times, and to make the tool useful. The model had to be able to scale as different device sizes were used. From todays transistor lengths of $100nm$ down to the point, in theory anyway, where lattice mono-layers could be used. The methodology selected for this research was to build a software model using mechanisms derived from the current understanding of the physical phenomena. The approach of solving transport equations was abandoned in favour of using a model partly inspired by the quantum conductance approach of modelling charge transport through quantum conductance channels, and the use of transmission coefficients, as described by Landauer and others [46, 44, 45]. The use of the transmission and scattering matrices [46] seemed a promising basis, because matrix manipulations can be handled very rapidly and effectively by some high-level software languages. The approach taken however was to allow the matrix to evolve completely randomly rather than manipulate the matrices as a result of any deterministic sequential process. The basis for the model would use a simple, ideal crystal of silicon, and then once the model was behaving as expected, compare the results with results from practical observations in the laboratory. A correlation would be made to the predictions made from a practical behavioural observation of

the structure. A comparable semiconductor structure could be represented using two different impurity profiles for P and N materials. This would form a diode and an actual device could be found at each stage to provide a comparison.The first comparison would be made to a diode, which is the first step in complexity, and then the next step would be to use a transistor. A new structure would then be created based upon the understanding of the mechanisms involved to propose a new low-noise active device. Further noise mechanisms could then be explored by testing various scenarios on the model of the bipolar device, which was known to be accurate in predicting the simpler mechanisms involved. This would also form a more generic model which, could be developed and enhanced at some point in the future. The model would need to represent the diffusion mechanisms [17] of the carriers, and represent the two doped regions of P and N type silicon. The model would also need to comprehend the presence of an $E - Field$, and represent the effect of this field on the charge carriers, with some degree of accuracy. The diffusion mechanisms without the constraints of an $E - Field$, are essentially random in nature, and the models time evolution relies on the interaction between this field and the carrier behaviour. A software architecture was also required that would naturally evolve with the time available to enhance the different features. A basic operating framework was required, which could then be added to in a natural way, as further sophistication was added. The initial validation of the model would be focused on understanding individual carrier transport events and their contribution to shot noise. This approach would provide a natural end-point to the research, and would result in the design of a Low Noise BJT device, that is able to be evaluated for future signal processing applications. The JAMES model could be used to enhance and analyse other types of semiconductor and certainly other substrate materials apart from silicon. The model would require calibration for other materials in terms of hole and electron mobilities.

2.3.1 Choice of the vehicle to be modelled by the simulator

One of the most mature technologies and best understood semiconductor devices is the *Bipolar transistor* (BJT). The current state of the art devices can minimise the

problems that dominated the original technology, such as flicker noise. The current devices are dominated by two fundamental types of noise, thermal noise and shot noise. In order to make a dramatic reduction in a bipolar transistor noise, it would be necessary to make a reduction in one of those fundamental factors. The noise of a typical BJT is analysed in Appendix:{D.1} in order to prioritise the magnitude of the different noise types. This analysis shows that for a typical BJT , the noise mechanisms can be prioritised according to their *contribution to total noise.* This has been shown to be

$$\frac{\overline{v_{in}^2}}{\Delta f} = 4kT(R_S + r_b + \frac{1}{2gm}) + 2K_{SA}\, R_S^2 q[I_B + \frac{I_C}{\mid \beta(jf) \mid^2}] \qquad (2.1)$$

where k is Boltzmann's constant, T the temperature, Δf the bandwidth, R_s is the signal source resistance, r_b the intrinsic base resistance, gm the BJT transconductance, K_{SA} the proposed new shot attentuation factor, I_B the BJT base current, I_C the collector current, f the operating frequency, and β the device gain. The first term represents the total thermal noise and the second term is the shot noise contribution to the total device noise. The analysis of the shot noise mechanism is therefore the primary focus of this study, and identifying a mechanism for reducing this is a focus of the remainder of this work. Shot noise is a mechanism particular to the transit of carriers across a potential-barrier. By analysing the behaviour of the model and the physical structure , it is found that the shot noise in a bipolar transistor is not generated in the collector junction, it is only generated by carriers crossing the emitter-base potential-barrier. Some text [15] show shot noise generators in the base and collector networks of the noise equivalent circuit. This may be a convenient way of analysing the shot noise source, but is not felt to accurately represent the physical processes of the carriers in the structure. There is no physical mechanism to create shot noise as carriers are swept across the reverse biassed collector-base junction. The JAMES model suggests the cause of shot noise is due to the simultaneous crossing of the potential barrier by a number of carriers, at the same instant in time. This is shown in the JAMES model output graph of Figure: 5.6, with the carriers crossing the emitter-base potential barrier. The relatively small recombination current in the

base of the BJT is due to its gain β, which will reflect the shot noise fluctuations in the emitter current. This fluctuation is not generated in the base, it is merely a reflection of the shot noise already generated in the emitter, and attenuated by the gain of the BJT. This is represented in the text [15] as a shot noise generator in the base of the BJT see Figure: 7.3. The JAMES model shows the injection of carriers over the emitter-base barrier creates the largest degree of disorder or spectral density in the device, and this disorder spreads throughout the base region towards the collector. The collector junction of a BJT is normally reverse biased, and does not constitute a potential-barrier. The base emitter junction is forward biased , and this causes the shot current, and since approximately 99% of the emitter current flows to the collector, this is the source of the shot noise. The initial estimates show that reducing the effect of this fundamental mechanism will deliver a significant improvement, and so this thesis is limited to studying this one mechanism, as the analysis of the G-R and Flicker noise would be beyond the scope of this initial part of the research. The solutions identified will however reduce other noise mechanisms by a much smaller degree. Initial estimates from the JAMES simulator, indicate that $_{K_{SA}}$ can have a value of 2.47×10^{-3}, giving a reduction in noise of $-26dB$. The development of a new constant K_{SA} is introduced to express the attenuation of the shot noise , where the SA sub-script stands for SHOT ATTENUATION see Appendix: { C.1}.

2.4 Relationship between Thermal Noise and Shot Noise

A relationship between Thermal Noise and Shot Noise is developed in Appendix: {E.1}. Thermal noise and Shot noise are treated in many text as being different mechanisms, and in fact they have a common origin. For the Base Emitter diode of a BJT it is shown in the Appendix: {E.1} that the shot noise is related to the thermal noise by the physical properties of the two regions. It is believed that this may be new, but further investigation of this is necessary.

3. THE JAMES MODEL FOR ATOMISTIC SIMULATION OF CARRIERS

The initial use of the JAMES simulator was to study the transport of the carriers within the silicon lattice, with a view to finding a way of reducing the noise levels. The basis of the approach was, that if the mechanisms can be understood, and clearly visualised, then the objective for reducing noise becomes clear. The model was used to measure the spectral density of the noise, at given current levels, and to experiment with ways of reducing this by physically realisable means. A new proposed attenuation factor K_{SA} , first used in Eq. 2.1 for quantifying the reduction in shot noise is described. This reduction factor was measured by using the K_{SA} factor in the equation shown in Appendix: {C.1}. By reducing K_{SA} the input referred noise will be reduced, and this will improve the minimum usable input signal to the BJT amplifier. The input noise spectral density of a typical BJT , S_i is shown in Appendix: {D.1}. The low frequency end of the spectrum is dominated by the $1/f$ (or low frequency noise). This type of noise is characterised by the increase in noise as the frequency is reduced over the range $DC - 10^4 Hz$. The mid-band region , the flat part of the frequency range, see Figure: D.1 is typically used in circuit applications. The high frequency end of Figure: D.1 shows a rapid increase of input referred noise due to the BJT's gain reducing as the frequency increases. The high-frequency part of Figure: D.1 is an area typically used by ultra-high frequency amplifiers, where the limit of the device performance is employed, and the SNR (signal to noise ratio) deteriorates here. Any reduction in the shot noise contribution, and hence input referred noise, will provide a significant impact on the performance of the device in this upper frequency region. The initial objective for the model, is therefore to

focus on the shot noise mechanisms, with a view to reducing the contribution to the overall device noise. Once this objective has been achieved, and a correlation with the "macro" simulations achieved, then the model can be used to help predict geometrical and doping profile dependencies impacting the shot noise contributions.

3.1 Towards a new paradigm

The use of traditional equations to describe the noise mechanisms are useful for a rapid assessment of the noise amplitude, but not detailed enough for use in exploring, evaluating and optimising the physical properties of a new device design. The equations e.g. 1.1, 1.8 also do not provide any insights into the temporal reality of the noise mechanisms. The study of individual charge transport was felt to be more effective when it was applied to a semiconductor model, which has been around for a significant time i.e. the BJT. This has led to a better understanding of the physical mechanisms involved, and a more exact understanding of its basic operation [56]. The very powerful set of rules describing current flow in meshes and networks are known as Kirchoff's Laws, and they form a powerful analytical tool for use in circuits with *large currents* and or *large periods of time.* The time period used in the JAMES simulator is extremely small, and at this limit of simulating individual carriers, the laws do not accurately describe the current flows into and out of the transistor being modelled. This is due to the time taken for diffusion and drift in the physical regions of the device. The model commonly shows different carrier counts entering the device, from those leaving it, over short time intervals. This difference tends to reduce when very long simulation times of carrier populations are used. This however requires very long simulation times to observe. The analogy here is the difference between classical Newtonian mechanics and quantum mechanics.

The structure of the BJT was felt to give an initial vehicle that could be analysed at an extrinsic semiconductor level, and then built up into a fully representational model of a BJT by adding dopant impurities to form the active device. This was a more rigorous and gradual approach to ensure success. The model and approach here can be used to represent any idealised semiconductor structure with modifica-

tions. The need to have a geometrically representative model, seemed to be essential in simplifying the problem as much as possible, in order to increase the ability to visualise the physical mechanisms and spatial relationships involved. The method of modelling the individual carriers also needed to be based on a technique that could be manipulated very rapidly by a computer. This approach would have the best chance of reducing the simulation times of larger structures to practical levels. The benefit of the computer model is that many different scenarios can be evaluated in a short time, allowing an iterative approach to problem solving. A 3-D model mapped to a three dimensional output record, would also make data gathering, and measurements more easily obtained from each simulation run.

3.2 Data to be represented

The main storage requirement of the model is to define the silicon lattice and store the spatial position of each charge carrier at any point in time. The method which required the least storage was to represent the bond-states within an array in the model. This approach meant that the silicon lattice would be represented as a fixed array of bond positions in the lattice in which an electron for example would be temporarily held. This simplification has many advantages, the most important being that the lattice is reduced to a binary representation where a bond state is empty or full at any given time. This is also true in the real crystal, where an atom in the lattice would have a bond empty or full. The normal situation in the lattice is that the electrons would only have fixed positions at a temperature of absolute zero, and at any temperature above this, the electrons would move randomly around the lattice bond locations, by moving to adjacent vacant positions. Although the model does not have a quantitative mechanism at this time for representing temperature, the diffusion mechanisms represented do cause random movement of the electrons within the lattice. The different types of semiconductor i.e. P and N type are held in two identical arrays, and manipulated by the program. The basic data above could then be manipulated by algorithms within the software to represent physical properties.

3.3 3-D Atomistic modelling

The use of a model describing the atomistic behaviour of the semiconductor should approximate to the macro behaviour, given a large enough population of carriers. The larger the population used in this model the longer the simulation time, and due to the practical limits of computation time, the results will need to be interpreted in terms of this reduced population. A compromise needed to be made between the population size and the practicalities of the analysis time. The atomistic modelling of the current flow is a complex undertaking, involving the simulation of relatively large numbers of individual carriers evolving in a constrained but deterministic manner. There is no theoretical limit to the number of carriers used, only the practical limit of computation time. A typical current density of $1mA/\mu m^2$ would involve 14 carriers in a lattice structure of area $75A^o \times 75A^o$ or $5.63 \times 10^3 sq\, A^o$.

3.3.1 The design of a model to satisfy the following conditions:

1. Be as simple as possible

2. Diffusion based carrier transport

3. Support 3-D electric fields and hence drift

4. Represent 3-D geometrical shapes

5. Have reasonable execution times for normal current densities

6. Be able to simulate 3-D geometrical shapes up to $200nm$ in a 48-hour period

7. Be capable of being enhanced in a modular form

8. Easily accessible computing resources

9. Represent model P and N type regions

10. Portable model; for ease of transfer between different computing platforms

11. Observe Space charge neutrality.

12. Observe Kirchoff's laws (for simulations with large carrier populations)

The model should also allow simulation over extended time periods much greater than the basic unit of analysis (the NDTU).

3.4 The specific Model Features required are:

1. The design of the model needed to satisfy the following specific conditions:

2. Represent temporal evolution

3. Allow hole p and e carrier types simultaneously

4. Represent impurity doping levels profiles

5. Represent N and P type regions

6. Allow certain types of defect to be placed in the lattice

7. Represent hole and current flow

8. Permit measurement planes to be created

9. Represent infinite recombination surfaces

10. Integrate behaviour of a large population

11. Report various properties and results after a run

12. Represent E-field in 3-D.

13. Use random carrier movement

14. Ability to create centres of noise creation at any 3-D bond coordinates

3.5 Features not included in this version of the model

1. Photon or Phonon interactions
2. Thermal behaviour of the lattice
3. Infinite resolution of applied E-field
4. Inter region intrinsic fields
5. Carrier transport scattering
6. Band structure of the atoms

3.6 Assumptions made in the model

1. The crystal lattice is ideal (no lattice defects)
2. Shot noise mechanism only is implemented
3. The recombination surfaces are ideal
4. The bond-bond transition energy is constant for all lattice sites.
5. A set of bond transition 'rules' as covered in detail in later sections 4.2 and 4.2.1.

3.7 The basis for a model

The restrictions placed on the model are not felt to be significant given the model is primarily being used to analyse the shot noise mechanism. Recombination surfaces at contact regions in a BJT are close to ideal, and so do not introduce significant inaccuracies. The fixed bond-bond transition energy will constrain the number of discrete energy states in the lattice, and this was considered as a necessary trade off between the execution time of the model against the additional resolution obtained by adding a variable bond-bond transition energy. A simple functional model was chosen as a starting point, allowing the functionality to be initially separated from the actual physically quantitative representation of the individual charge carriers.

The functional model selected was a binary array holding the bond states of the crystal and the physical mapping which allowed the array to correspond to the three dimensions of the lattice. This allowed the basic functional behaviour to be enhanced as inaccuracies arose, and so to make the model more precise. A visual representation of an atom isolated but still part of the lattice, with its outer electron shells, and its valence bonds using the Schroedinger model is shown in Figure:3.1. This shows a Silicon atom with 4 bonds. The bonds repel one another due to the similar charges , and form an equidistant spatial arrangement to minimise the forces. In this case the angle is 109.5^o between the bonds.

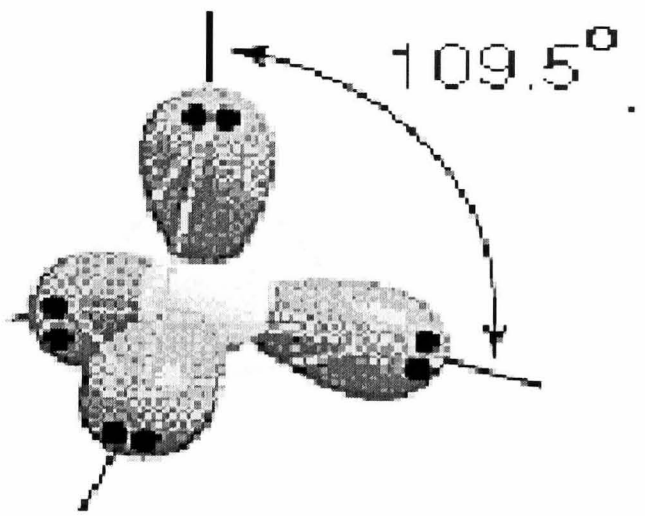

Fig. 3.1. Isolated silicon atom as part of the lattice with electron bonds

3.8 The functional description

The model will use an idealised representation of a pure silicon crystal, and this would support the ongoing objective of semiconductor manufacturing research into finding purer materials. The functional model could be enhanced at a later stage to include a more accurate representation of the physical behaviour, as more accuracy was required. One example of this would be to deliberately create defects in the otherwise ideal lattice, with particular characteristics, to study the effects they would have on the current flow, and hence the noise contribution. The model would recalculate the position of each carrier at each time step, and so the simulation would evolve for

the assigned run time. This is a reasonable simplification as silicon is available in a highly pure state.

3.9 Matrix model Structure

The basis of the model was chosen to be a matrix representation of the silicon lattice. The matrix could be physically mapped, in terms of the 3-D coordinates. to the atomic sites of the atoms in the crystal lattice. The atomic sites were then each assigned covalent bond positions representing the bonds formed between the atoms in the crystal. This simplification meant it was not necessary to describe the temporal state of each of the charge carriers, but only their positional states in the lattice. Certain tradeoffs were inevitable to use this model, for example behaviour of the lattice with temperature, however once the model was working, more accuracy could be added back in, computing time permitting. A set of rules derived from a physical understanding of the silicon, were then constructed to determine the conditions for movement of the individual carriers and the various 'bond states' between the atoms. This meant the concept of an electric field could be built into the model, which is essential for studying the behaviour of the charge transport.

The lattice unit cell LU is shown in Figure: 3.2, and contains 4 unique atoms in the cell body and the 4 valence bonds associated with each of those atoms. The silicon atom forms covalent bonds with 4 adjacent neighbouring silicon atoms. The remaining atoms in the cell are shared with other neighbouring atoms in adjacent cells. This array must be transformed into a form that can be represented in a linear array or matrix in the computer memory. The complete crystal can be visualised by imagining identical units stacked against each other in the three dimensions. The movement of carriers are assumed to require a net of zero energy in moving from one bond state to the next, i.e. the average energy is independent of the thermal vibrations.

3.9.1 Transformation of Crystal to Matrix representation

A matrix is a very convenient way to represent a large number of regular structures. and to be able to handle them easily in software. The dimensions of the array can

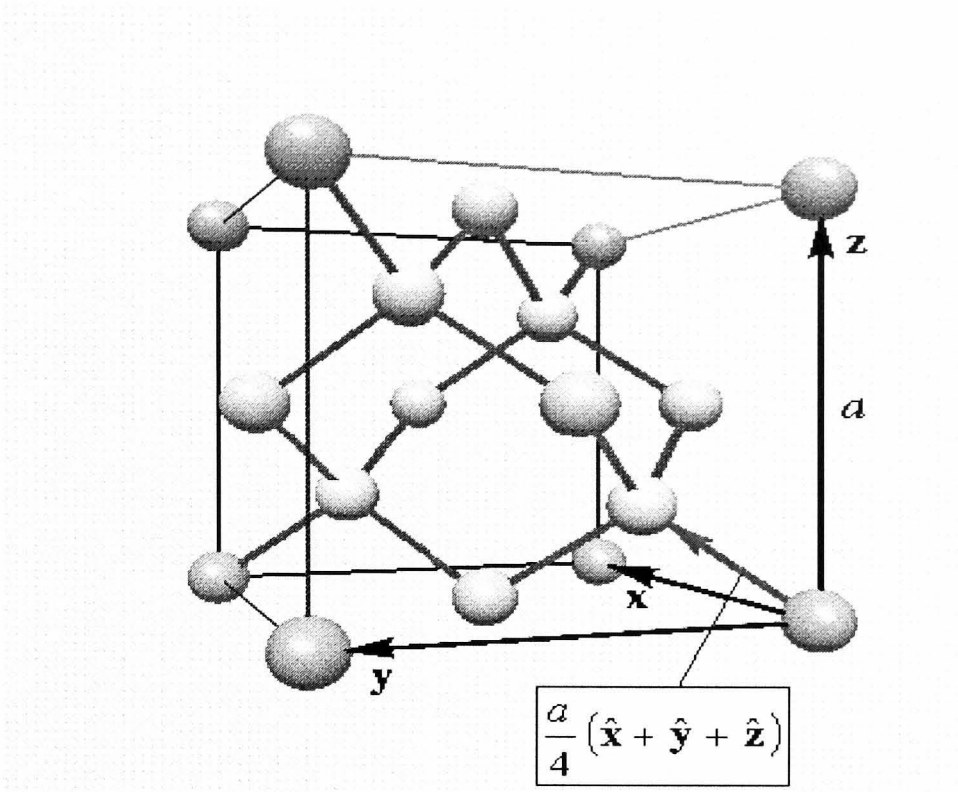

Fig. 3.2. The diamond lattice unit cell of silicon

map to the dimensions in space in this example, enhancing the visualisation of the processes.

3.10 Problems to be overcome

1. Representation of the crystal lattice
2. Representing the temporal evolution of the system
3. Data storage and manipulation
4. Representing the Diffusion mechanism
5. Representation of Drift in an Electric field
6. External electrical connections
7. Recombination
8. Space charge neutrality

9. Doped regions to represent extrinsic properties

The initial problem was finding a way of representing large amounts of data corresponding to the number of atoms in the lattice, and the state of each inter atomic bond related to that atom. This had to be represented in both the N and P type regions. The second problem was representing a large physical model efficiently, for easy manipulation by the algorithms, and with the lowest simulation time. The third problem was how to create a time evolution of the matrix from its initial state, in a random manner, as would happen in the real situation. The next problem was how to create an algorithm that could represent the diffusion mechanism that occurs in many metallurgical and chemical analogies. This would include the diffusion of holes and electrons. Another problem was how to represent the effects of an electric field on the two carrier types, to represent the drift experienced when a voltage is applied to the lattice. The presence of an electrical connection to a particular region of the semiconductor structure is made through a low resistance ohmic contact. This allows access to the device for external biasing components, and circuit elements used in the design of a particular electrical function. Recombination is the continuous process of hole-electron interactions within the lattice. This is the mechanism that controls the complementary populations of both carrier types in given regions of the silicon. The base silicon is intrinsic in its natural state, and requires regions to be defined as extrinsic in nature. This means separate regions must maintain their doping profile regardless of the carrier flux within the model. The above problems had to be solved while maintaining an intuitive approach to the representation and use of the model, as well as a modular approach for future enhancements.

3.11 Representation of the semiconductor structure

GENERAL BACKGROUND

The model designed for this purpose was named **JAMES** which is an acronym for "**J**unction '**A**tomistic' **M**odelling of **E**xtrinsic **S**emiconductors". The available programming languages and operating system environments were studied, and a selection

made against the criteria above. The Unix operating environment was chosen, and the Unix clone named Linux, was chosen because of its efficient kernel and fast execution times. The C^{++} programming language was chosen to allow portability, and fast program execution of the program kernel. A simple functional model was chosen as a starting point, allowing the functionality to be initially separated from the actual physically descriptive representation of the individual charge carriers. The model would use an idealised representation of a pure silicon crystal, and this would support the ongoing objective of semiconductor manufacturing research into finding purer materials. The functional model could be enhanced at a later stage to include a more accurate representation of the physical behaviour, as more accuracy was required.The model would recalculate the position of each carrier at each time step, and so the simulation would evolve for the assigned run time.

3.11.1 Semiconductor Junctions

A semiconductor junction consists of regions of differently doped regions, in order to modify the intrinsic regional properties such as intrinsic $E - Field$, and conductivity. The model represented the two different types of region by using two different matrices, one for acceptor doped regions or P type, and one for donor doped regions or N type. The data in each matrix was the complement of the other to represent the concept of hole and electron flow. They both evolve concurrently in the simulation but also interact with one another. The use of a matrix allowed the doping profile, i.e. the 3-D position of each different impurity to be selected during the initialisation of the matrix. Any number of different profiles shapes and concentrations can be defined at the start of the simulation.

3.11.2 Temporal Evolution

The concept of temporal evolution of the matrix is introduced by assigning a time step for updating the evolution of the carriers in the matrix. This is not a real time representation, as it is a functional model. The concept of real time is introduced by analysing the actual time of events on an atomic level, and calibrating the model time step against real time events.

3.11.3 3-D space

The matrix mapping in terms of actual 3-D physical space is achieved through the unit of inter-atom spacing in the crystal lattice. The object under analysis can then be defined in terms of physical size with this unit as the maximum resolution.

3.11.4 Measurement Planes

The model is designed to allow the insertion of any 2-D reference plane into the matrix orthogonal to the carrier transport direction. This is assumed to be in the z direction. This facilitates the creation of carrier measurements, such as the population crossing the plane, and concentration at any point in time. The matrix can be scanned at any time during a run, to calculate parameters such as space charge, current density, or capacitance anywhere in the crystal lattice. The 3-D profile of charge carriers can be determined at any instant in time, to observe current crowding effects, by logging to a log file. There are limits however to the accuracy of this approach. The model uses a simple algorithm that uses a simple rule to define an observation instance. The detection of a carrier that is currently in the measurement plane (MP_z), where z is the coordinate on the z axis, and is about to move to $z+1$ is defined as the only condition counting as a measurement event. The condition $z- > z-1$ is ignored. A more sophisticated measurement plane algorithm could be created if required. The main objective is to measure the current (carriers) leaving the plane , and to record the time and coordinate position. The time of the carrier (electron or hole) leaving the MP_1 or MP_2 plane is used to calculate the spectral density at that point.

3.11.5 Boundary conditions

The matrix is programmed with a set of boundary conditions that constrain the evolution of the state of the system at the edges of the x, y and z edge planes. This corresponds with the actual edge discontinuities of the crystal, at the edge of the crystal. The boundary is treated somewhat ideally for the purposes of this model in that the carriers can occupy any location up to the last location near the edge.

3.11.6 Infinite recombination centres

An infinite recombination surface is as the name implies, a semiconductor contact, usually a contact point, where the recombination or generation of carriers is effectively infinite at this point, without creating a significant potential drop. The infinite recombination centres exist at external contacts between the crystal and external circuits. These are an ideal approximation to the contacts present between the aluminium contacts and the semiconductor surface. The contact potential is therefore assumed to be zero.

3.11.7 Representing the semiconductor Lattice Structure

The silicon crystal is a type IV material, and the form of the lattice structure must take account of the four directional bonds [18] as silicon $S_{28.1}^{14}$ has a valence number of four. These bonds are equally distributed in three-dimensional space, due to the repulsion force between the electrons within the bonds. The arrangement is each atom forms a covalent bond with four adjacent atoms in the lattice. The tetrahedral arrangement means each silicon atom, is surrounded by four others with a coordination number of four. Three primitive basis vectors $\overrightarrow{a}$, $\overrightarrow{b}$ and $\overrightarrow{c}$ describe a crystalline solid such that the crystal structure remains invariant under translation through any vector that is a sum of integral multiples of these basis vectors. In other words, the direct lattice sites can be defined by the set [18].

$$\overrightarrow{R} = m\overrightarrow{a} + n\overrightarrow{b} + p\overrightarrow{c}$$

where m, n, p are all integers. For a given set of the direct basis vectors, a set of reciprocal lattice [27] basis vectors $\overrightarrow{a}^*$, $\overrightarrow{b}^*$, $\overrightarrow{c}^*$can be defined such that

$$a^* = 2\pi \frac{\overrightarrow{b} \times \overrightarrow{c}}{\overrightarrow{a} . \overrightarrow{b} \times \overrightarrow{c}}, \overrightarrow{b}^* = 2\pi \frac{\overrightarrow{c} \times \overrightarrow{a}}{\overrightarrow{a} . \overrightarrow{b} \times \overrightarrow{c}}, \overrightarrow{c}^* = 2\pi \frac{\overrightarrow{a} \times \overrightarrow{b}}{\overrightarrow{a} . \overrightarrow{b} \times \overrightarrow{c}}$$

so that+

$$\overrightarrow{a} . \overrightarrow{a}^* = 2\pi; \overrightarrow{a} . \overrightarrow{b}^* = 0$$

and so on; and in general the reciprocal lattice vector is given by

$$\vec{G} = H\vec{a}^* + k\vec{b}^* + l\vec{c}^*$$

where H, k, l are all integers. It therefore follows that the product

$$\vec{G}.\vec{R} = 2\pi \times integer$$

and therefore each vector of the reciprocal lattice is normal to a set of planes in the direct lattice. The volume v^*c, of each cell of a unit cell, is then the reciprocal lattice, and is inversely proportional to the volume

$$V_c = \vec{a}.\vec{b} \times \vec{c}$$

A convenient method of defining the various planes in the crystal is to use Miller indices. They are determined by first finding the intercepts of the reciprocals of these numbers and reducing them to the smallest three integers having the same ratio. Silicon is a diamond lattice, and is a lattice structure, belonging to the tetrahedral phases; that is each atom is surrounded by four equidistant nearest neighbours, which lie at the corners of a tetrahedron [18]. The band structure of a crystalline solid is defined by the energy-momentum $(E - k)$ relationship, and is usually obtained by solving the Schroedinger equation of an approximate one-electron problem. Bloch's theorem , states that if a potential energy $V(r)$ is periodic with periodicity of the lattice, then the solutions $\Phi k(r)$, of Schrodinger's equation, see reference [18] are given by

$$\left[-\frac{\hbar^2}{2m\Delta^2} + V(r)\right] \cdot \Phi k(r) = E_k \Phi k(r)$$

and are of the form

$$\Phi k(r) = e^{jk\vec{k}.\vec{r}} U_{n(k,r)}$$

this gives (Bloch's function)[28]. The electron band diagram for a silicon atom as part of the lattice is shown if Figure: 3.3. The energy bands in the lattice structure are more complex than those of a conceptualised single atom considered as separated from the lattice. When the atoms are packed into the lattice in the condensed state.

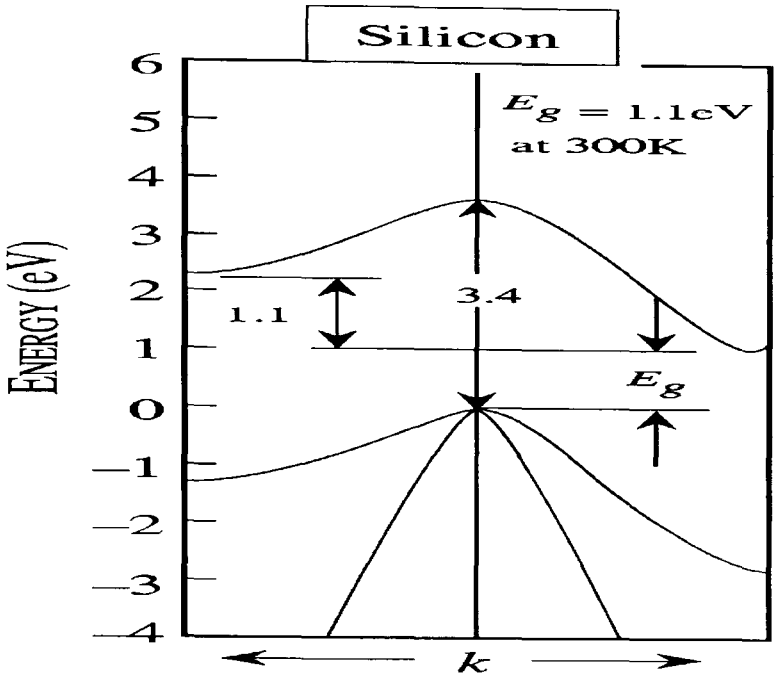

Fig. 3.3. Band structure of a silicon atom

such as in a silicon wafer, the bands broaden. The Pauli exclusion principle explains why each electron must have unique properties, and can not occupy identical bands with another silicon atom. The analysis of periodic potentials is required to find the energy levels and uses periodic wave functions, called Bloch's functions, see 3.11.7. The filling order of the silicon atoms bonds would be

$$1s^2 2s^2 2p^6 3s^2 3p^2 \tag{3.1}$$

by Hunds rule.

A simplification is possible however, since we are only interested in the electrons responsible for electrical conduction, and the carrier transport model can be limited to the top and bottom bands of Figure: 3.3. The highest almost filled band and the lowest almost empty band are the two responsible for conduction, and so the energy diagram can be reduced to the one shown in Figure:3.4 and shows the arrangement of the constant energy bands in the lattice. The bulk lattice constant a shown in Figure: 3.2 is 5.43095 A^o for Silicon [18]. The crystal lattice in the model is assumed to be of $< 101 >$ direction for ease of representing the number of bonds associated with each atom. The x-axis of the model is assumed perpendicular to the $< 101 >$

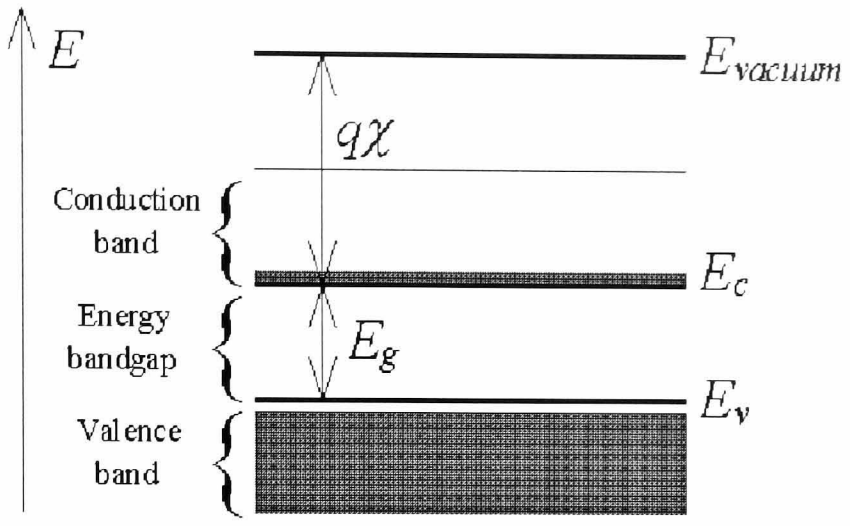

Fig. 3.4. Simplified band diagram

plane. The lattice parameter (the distance along the edge of the cube), is represented by above, for a silicon crystal. The band gap for silicon, the energy gap E_g between the valence and the conduction bands, as shown in Figure: 3.3, is $1.12eV$ [18], and in Appendix: {O.2}. The concept of an energy step within each valence band is not built into the model, the functional model could be refined to include this at some point. The model assumes that the energy-state of each covalent band is the same, and that the electrons are just below the conduction band. The individual electron states are not included at present, as this would increase the size of the matrix and the memory required, to store the state of the systems spatial and temporal evolution. The simulation time would also increase with more states requiring processing. The crystal is also assumed free from defects such as vacancies, stacking faults, dislocations etc.

3.11.8 Lattice representation in the model

The crystal orientation has been assumed to lie in the $< 101 >$ direction, and the injection of carriers from the external contacts into the lattice are assumed to be orthogonal to the $< 101 >$ plane. This orientation was assumed in order to provide the contact surfaces with a known number of contact points for each lattice unit,

as this true 3-D model accurately represents current crowding by representing the carrier flow through each atom site. The direction can be visualised from Figure: 3.2. The current flow would be vertical to the right hand face of the LU with its edges defined by the x and z vectors. The diagram in Figure: 3.2 shows the crystal of silicon represented by the two different integer matrices used to hold the crystal state. The current through the crystal is composed of two carrier types, hole and electrons. In an actual semiconductor the hole is just the absence of an electron, however holes and electrons behave differently under the influence of an electric field, and must be represented separately. The two mathematical matrices, defined as bit arrays are used to represent the bond states in a regular silicon crystal. The four covalent bonds present in each silicon atom have stable states for the electrons, and those are represented in the array. Each array element represents a LU position x, y, z in the crystal structure. The LU contains four unique atoms, with each atom having four bond states associated with it in the matrix. The holes are in reality spatially mobile bond vacancies, with the ability to move in the lattice. A hole can also absorb an electron as it diffuses through the lattice. One matrix represents the atoms and each bond for the electrons, and the other represents the same atoms, except has the bonds representing holes or mobile bond states. The P type semiconductor can then be defined in terms of the intrinsic material with impurity locations defined in the matrix representing holes. The N type material can similarly be defined in the second matrix for the different impurity locations, representing electrons. The outer edge of the crystal is a physical discontinuity, and is represented as a barrier of 1-atom thickness in the matrix. This is the region consisting of broken or 'dangling' bonds at the surface. The outer surfaces of a semiconductor device in practice would be passivated with a silica glass S_iO^2 layer to terminate the bonds and reduce surface effects.

3.11.9 Carrier Diffusion

The model represents the 'hole' population and the electron population in two identical matrices. For a given E-field the electrons e, drift in one direction, and

the holes p, drift in the opposite direction due to their opposite charge. The two populations of carrier are regarded as entirely separate for simplicity. The holes are in reality valence bonds without an electron, and are more directly linked. The holes however are subject to $E-Fields$ and will migrate independently through the lattice. The choice of separating the two populations should not detract significantly from the net behaviour at reasonable carrier population numbers. The program checks the state of the matrices at each dimensionless unit of time called a "NDTU" , and if there is a superposition of a hole and an electron at exactly the same 3-D coordinate position, the hole and the electron recombine. The overall population of holes and electrons can not reduce due to space charge neutrality. A 'hole' is just a mobile vacancy and so if it combines with an electron, the hole-density reduces, and another hole must be created from an external contact, or recombination surface. If an electron leaves through an external contact, another must replace it in the bulk, in order to satisfy the space charge neutrality.

3.11.10 Carrier recombination

The two populations are therefore represented in the two separate Matrices, however they do interact, and this feature has been incorporated in the model. The interaction is controlled at both the regional level i.e. in the emitter , base regions and the collector by charge control algorithms, however an overall mechanism is required. A recombination algorithm is therefore also required operating at a Matrix to Matrix level regardless of the particular region . The recombination algorithm compares the hole and electron population and if a hole and electron appear at identical locations, then the hole is removed, and an additional hole is injected to maintain the carrier population.

3.12 Overview of Semiconductor structures

By combining P and N type materials in the same crystal, new electrical properties can be created such as current amplification. This is a physical process defined by the physics of the carriers at the atomic level as they traverse the silicon structure. The actual temporal, and spatial behaviour of the carriers, cause the phenomena known

better as noise. The individual charge carriers of charge q, as they fluctuate across the measurement planes, normally the device contacts, create these electrical fluctuations. These fluctuations are known as noise. In electronic design the models used by designers regard this amplifying structure as the relationship between a variable representing input current, and another variable representing output current. This form of macro-behavioural model does not comprehend the behaviour of the actual internal physical process operating in the silicon.

3.12.1 Doping the intrinsic silicon

The basic semiconductor starts with an intrinsic piece of silicon, with a very low impurity level. This silicon is a very pure material, and in-practice an impurity-level as low as 1 part 10^{23} in can be obtained. The intrinsic silicon is an insulator, and does not conduct well in its natural pure state. This is due to the low density of donors or acceptors in intrinsic silicon. The theoretical resistivity ρ of the ideal intrinsic silicon used in wafer fabrication is $2.6 \times 10^5\,\Omega - cm$ at $300^o K$. The electrical properties of the semiconductor are altered by adding controlled impurities levels into the material. $N - type$ material is created by introducing Phosphorus into the semiconductor e.g. 1 part in 10^{22} , creating excess electron carriers, and Boron is used to create excess-holes.

3.12.2 Electron Energy states

The energy of the electron is given by the expression $E_k = \frac{\hbar k^2}{2m}$, where $\hbar$ is Planck's constant, k the wave number, see the x-axis on Figure: 3.3, and m the electron mass. Where $\hbar$ is Planck's constant, k is the wave number, and m the electron mass. The energy distribution of the electrons can be derived from Boltzmann's distribution law, where the probability of an electron having, energy E, is given by

$$p(E) \propto exp\frac{-E}{kT} \tag{3.2}$$

where k is Boltzmann's constant,and T is the absolute temperature. The Fermi-Dirac distribution [18] expresses the energy at which a quantum state has a 50% chance of

being occupied, at a given temperature, given by

$$f(E,T) = \frac{1}{exp\{(E - E_F)/(kT)\} + 1} \tag{3.3}$$

where E_F is the Fermi energy level, see Appendix: {I.1}. In order to maintain reasonable computing times at large crystal lattice dimensions, the electron energy levels are simplified to a single energy level. This can be refined at a later stage to include additional accuracy at the expense of processing time and memory storage. The matrix is assumed to be in the state, where the electrons are at the energy level of $E - kT$, and each electron requires a fixed $1.12eV$ to move it into the conduction band. This is a simplification of the situation in a real crystal where the energy will have a statistical distribution. The assumption of a fixed energy level reduces the processing time for each bond, in order to keep the computation time down. The model is simplified by expressing a single energy level for all the bonds, in this simplified functional model. The two planes P1 and P2 are arbitrarily positioned planes used to measure the carrier densities and the times the individual carriers cross them. The diffusion of the carriers is subject to many factors, in the dynamics of the crystal lattice, with a dependency of many physical factors. Some of these factors are the crystal temperature, the purity of the crystal, impurity defects, electric field, boundary conditions etc. The conductivity, σ is given by

$$\sigma = ne\mu_n + pe\mu_p \tag{3.4}$$

Where n is the number of electrons available for conduction per unit volume, e the electronic charge, and p the number of holes available for conduction per unit volume, $\mu_n$the mobility of electrons in silicon, and $\mu_p$the mobility of holes in silicon.

3.12.3 Intrinsic Silicon

The assumption of an ideal crystal of silicon is the starting point, and it can be shown that the following law holds. The product of the carrier densities is equal to the square of the intrinsic carrier density in pure silicon, i.e.

$$p_0 n_0 = n_i^2 \tag{3.5}$$

where p_0 and n_0 are the equilibrium densities of the p and n carriers respectively, and n_i is the intrinsic carrier density at a given temperature.

3.12.4 Thermal activity

The carriers within a semiconductor crystal are assumed to move as if they were free particles , which are not affected by the presence of the atoms in the material, except for the fact that it effectively changes the mass of the particle. For an electron this changes from m to m^*. The carriers can be either electrons or holes, which carry one negative (positive) unit of charge. These carriers move even when there is no electric field applied, because of the thermal energy associated with all the particles in the lattice. The thermal energy of non-relativistic electrons equals

$$kT/2 \tag{3.6}$$

for each possible degree of freedom. At room temperature the thermal velocity of the electrons in bulk semiconductors is about $10^7 cm/s$.

3.12.5 Introduction to Drift

As an electric field ($E-Field$) is applied to a semiconductor , the electrostatic force causes the carriers to first accelerate, and then to reach a constant average velocity, v , as the carriers are scattered due to impurities and the lattice vibration. The ratio of the velocity to the applied field is called the mobility. The velocity saturates at high fields reaching the saturation velocity. Additional scattering tends to occur when carriers flow at the boundary of a semiconductor, resulting in a lower mobility due to surface or interface scattering mechanisms. The carriers move through the crystal until a collision occurs. The collisions, also called scattering events, are due to defects, impurities or the emission/absorption of phonons. The dominant types of collision mechanisms are charged impurity scattering and phonon emission/absorption. These collisions cause an abrupt change in the carrier velocity and energy at the time of the collision. The resulting carrier motion is semi-random due to the frequent changes in direction and velocity. Carrier transport in a semiconductor in the presence of an applied field can also be visualised as being semi-random except that in addition

the individual carriers also accelerate between collisions. Even although the random velocity greatly exceeds the average velocity to the applied field, it can be ignored since the random motion does not result in net flow.

3.12.6 Drift current

The motion of a carrier drifting in a semiconductor due to an applied field is illustrated in Figure: 3.5 . The field causes the carrier to move with an average velocity v . Assuming all the carriers in the semiconductor move with the same velocity, the current can be expressed as the total charge in the semiconductor divided by the time needed to travel from one electrode to the other, or:

$$I = \frac{Q}{t_r} = \frac{Q}{L/v} \tag{3.7}$$

where t_r is the transit time of a carrier, travelling with velocity v, over a distance L . The current density can then be rewritten as a function of either the charge density, ρ , or the density of carriers n in the semiconductor.

$$\overrightarrow{J} = \frac{Q}{AL}\overrightarrow{v} = \rho\overrightarrow{v} = qn\overrightarrow{v} \tag{3.8}$$

By analogy electrons in a non-degenerate and non-relativistic electron gas have a thermal energy as given by $kT/2$ per particle degree of freedom. The thermal velocity is around $10^7 cm/s$, which is much higher than the typical drift velocity in semiconductors of $10^5 m.s^{-1}$. The effect of this is the distribution of velocity around a given plane through the semiconductor would be a Poisson distribution with an average drift of zero, see Figure: 3.5. The steady state situation is now considered, where the carrier has accelerated to its constant average velocity. Under these conditions the velocity is proportional to the applied E-field ξ. The mobility is defined as the velocity to field ratio

$$\mu = \frac{|\overrightarrow{v}|}{|\overrightarrow{\xi}|} = \frac{q\tau}{m} \tag{3.9}$$

The mobility of a carrier in a semiconductor is therefore expected to be large if its

mass is small and the time between scattering events is large The drift current can then be rewritten as a function of mobility, yielding

$$\overrightarrow{J} = qn\mu_n \overrightarrow{\xi} \tag{3.10}$$

This derivation assumes the mass of the electron is m. However in order to incorporate the effect of the periodical potential of the atoms in the semiconductor we must use the effective mass m^* , rather than the free particle mass.

$$\mu = \frac{q\tau}{m^*} \tag{3.11}$$

The linear relationship between the average carrier velocity and the applied field breaks down when very high field are applied, however this will not be considered for this model. The current is equal to the charge transported per unit time through the semiconductor. The drift current is given by

$$I_n = Aen_{vd} \tag{3.12}$$

Where n is the density of electrons, each of charge e, drifting at velocity v_d .

Mobility is defined as

$$u_n = \frac{v_d}{E} \tag{3.13}$$

where E is the Electric field (E-field). This gives a current density

$$J_n = en\mu_n E \tag{3.14}$$

3.12.7 Diffusion mechanisms

Diffusion current is proportional to the carrier density gradient, and flows from high -density regions to low density regions. The density gradient is equal to $\frac{dn}{dx}$ so this gives

$$J_{diff} = eD_n \frac{dn}{dx} \tag{3.15}$$

Where D_n is the diffusion constant for silicon. For drift and diffusion currents of both holes and electrons

$$J_n = en\mu_n E + eD_n \frac{dn}{dx} \tag{3.16}$$

and

$$J_p = ep\mu_p E - eD_p \frac{dp}{dx} \tag{3.17}$$

where

$$J_n = \frac{I_n}{A} \tag{3.18}$$

and

$$J_p = \frac{I_p}{A} \tag{3.19}$$

Since

$$\frac{J_n}{E} = \sigma_n \tag{3.20}$$

the conductivity σ_n is then

$$\sigma_n = ne\mu_n \tag{3.21}$$

There is also a relationship between the diffusion coefficient constant D and the carriers mobility given by Einstein's relation

$$\frac{D_p}{\mu_p} = \frac{D_n}{\mu_n} = \frac{kT}{e} \tag{3.22}$$

where k is Boltzmann's constant [18]. The effects of generation and recombination can be shown in the case of a stable distribution of minority carrier population, for example flowing into the base of a BJT from the emitter, and can be shown by

$$| \frac{-1dJ_n}{edx} = \frac{n_e}{\tau_n} \tag{3.23}$$

where n_e is the excess electron carrier population in the base region ,and τ_n is the electron lifetime in this region. This will be explored in more detail later. The equation in 3.23 is called the continuity equation.

3.12.8 Effect of charged carriers and impurity Ions

The force F on an electron of charge $-e$ in a field of strength E is given by

$$F = -eE \tag{3.24}$$

Guass's law states that the total flux of electric field (product of field and surface area) crossing the surface of a volume is proportional to the total charge inside the

volume. For a charge density within the silicon of ρ, the total charge within the volume is

$$\rho A \delta x \tag{3.25}$$

Guass's law can be expressed as

$$\delta E x A = \frac{\rho A \delta x}{\varepsilon} \tag{3.26}$$

where ε is the relative permittivity of the silicon. If δx tends to zero, then the equation above becomes

$$\frac{dE}{dx} = \frac{\rho}{\varepsilon} \tag{3.27}$$

This is the one-dimensional form of Poisson's equation. The total permittivity is given by $\varepsilon = \varepsilon_o.\varepsilon_r$. where ε_o {B.1} equals the permittivity of free space, and ε_r {B.1} equals the permittivity of Silicon. In the semiconductor the charge density ρ is made up from charges on the electrons and holes ,n and p respectively, and on the fixed donor and acceptor impurity ions defined as N_d and N_a respectively. Therefore,

$$\rho = e(p - n + N_d - N_a). \tag{3.28}$$

Poisson's equation then becomes

$$| \frac{dE}{dx} = \frac{e}{\varepsilon}(p - n + N_d - N_a) \tag{3.29}$$

for p-type material N_d is zero, and n is very small, and in n-type material N_a is equal to zero, and p is very small. The current flowing in the semiconductor crystal is given by

$$I = D_p N_p.q + D_e.N_e.q$$

where D_p is the diffusion constant of holes in the silicon and D_n is the diffusion constant of the electrons, N_p and N_e is the population of each, and q is the electronic charge. Drift occurs when an $E - Field$ is applied between two faces, with the holes diffusing in one direction, and the electrons in the other. The electrons cross the arbitrarily defined measurement planes, at different instants in time, determined by

the dynamics of the lattice. For a given single-dimensional E-field applied along the axis, between the ends of the crystal, the resultant current is given by Eq. 3.14. In the absence of a field the population of carriers can be visualised as randomly moving around the crystal, but confined to the body of the structure. This is the situation defining thermal noise. The random movement of the carriers due to thermal energy in the crystal at temperature T, crossing the measurement planes concurrent with the end planes of the crystal. The energy spectrum of the thermal noise reflects the large number of energy states associated with the inter-atomic bonds in the crystal.

3.12.9 Drift of Carriers in an E-Field

The distribution shown in Figure: 3.5 shows the electron velocity distribution, assuming the free electron gas model, due to the Fermi-Dirac energy distribution. The velocity v of the free electrons is given by $\frac{1}{2}mv^2 = E$ where E is the energy and m the mass of the electron. The velocity of the highest energy electron is given by $v_F = \left(\frac{2E_F}{m}\right)^{1/2}$ and is called the Fermi velocity.

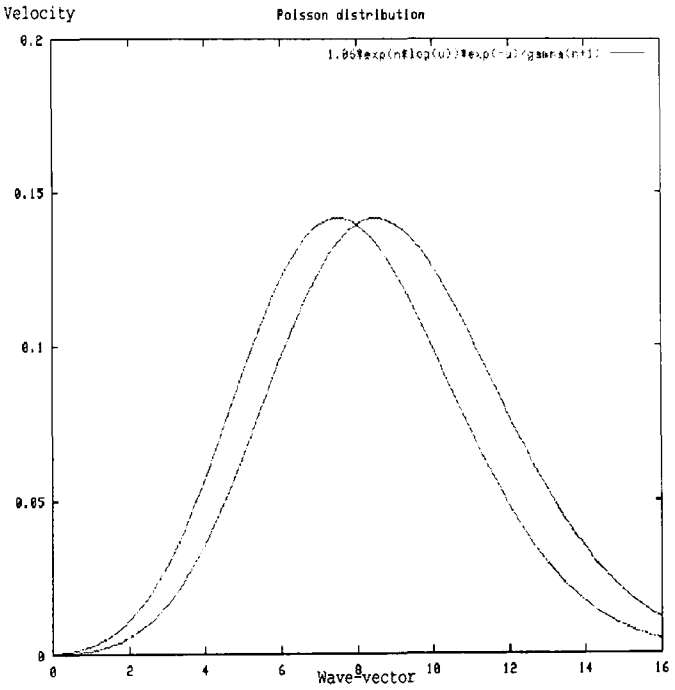

Fig. 3.5. Electron velocity vs wave-vector

The higher the electron energy level in the bands, the higher the electron velocity. For every electron with a velocity of $+\nu$ there is one with a velocity of $-\nu$. The

average velocity is therefore equal to zero, assuming the absence of scattering. the electrons randomly moving with a symmetrical distribution around zero. Deliberately simplifying the actual process, when an electric field is applied the whole distribution shifts slightly by drift velocity ν_d, assuming there are vacancies available. Every electron therefore shifts into the state just vacated by its neighbour on the velocity diagram. The graph in Figure: 3.5 shows velocity vs the wave-vector. Therefore, the distribution can shift in this way. The distribution is made up of a thermal distribution component and a drift component. Since the drift velocity is much smaller than the Fermi velocity, this motion is a small perturbation upon the normal motion of the electrons.

3.12.10 Metal contact to Semiconductor

A metal contact to the semiconductor is essential to connect the device to an external circuit. This junction requires a metal to semiconductor contact that is able to convert the electrons in the wire and the contact into the appropriate charge carriers in the silicon. This is achieved by defining an infinite recombination centre at the contact point. This means that when currents are flowing through these metallic contacts, the densities of electrons and holes, n and p respectively, are equal to their equilibrium densities.

3.13 Representation of above features in the model

The representation of the electronic motion within the lattice requires a random carrier velocity. The distribution will be symmetrical in zero field conditions. The model uses a random number generator to determine the direction and adjacent bond the electron will move to, at each Non Dimensional Time Unit 'NDTU' or time step. This happens for each bond of each atom and at each NDTU. The mechanism of drift is more precisely modelled within the lattice , as this is the primary mechanism giving rise to current flow in the semiconductor under an $E - Field.$ This mechanism is very important in describing the charge transport, while the mechanism of diffusion is also required to describe the dynamics of the carriers within the lattice, and to describe the behaviour of minority carriers. The mechanism of diffusion however, is

more naturally represented by this type of model. The program checks the occupancy of each adjacent bond state, and will move the carrier only if it is vacant. The model checks adjacent occupancy states before moving the carrier, and so if a region of high carrier concentration is present, the only available empty states are in the lower concentration or density positions. This naturally provides an intrinsic concept of diffusion to the model, and so the carriers move away or diffuse from regions of high density, towards regions of low density. The diffusion constants of the different carriers can then be represented by the probability of a transition occurring to another state. These parameters are well defined parameters for given impurity carriers and semiconductor types i.e. P or N.

3.14 A new structure to reduce shot noise.

The analysis of the different noise forms in Appendix: {N.1} showed that the shot noise was the next major contributor to thermal noise in a BJT device. The shot noise has been shown to be the natural consequence of electrons crossing a potential-barrier. The conventional low noise BJT design optimises the base for achieving a high current gain or β, and as low an intrinsic base resistance as possible. The approach selected here was to preserve these parameters as much as possible, but to reduce the spectral density of the noise as it emerges from the base region into the reverse collector base field.

The underlying cause of shot noise in a BJT has been shown to be the simultaneous arrival of minority carriers in the base region injected from the emitter region, and the random arrival time of these charge quanta in the base region, as shown in Chapters 5 and 6. The mechanism of shot noise is not present in majority carrier devices such as the Field Effect Transistor, as these devices rely on controlling the conduction of a single majority carrier channel type for its operation. The use of a mechanism devised to re-thermalise these injected and synchronised quanta of minority carriers in the base region of the BJT would reduce the shot noise. The minority carriers could then be localised at or near the edge of the base-collector depletion region, and would then be released into the collector base reverse field. This would create a more random

timing of transit across this junction, and the spectral density of the transport could be reduced to a level approximating the mechanism in a majority carrier device. This can be demonstrated in the simple example. If a current of $100uA$ flows in a normal metallic conductor, the number of electrons crossing the measurement plane would be

$$n = \frac{100 \times 10^{-6}}{1.6 \times 10^{-19}} = 6.25 \times 10^{14}$$

since this number of electrons flow in 1 second, the time for a single electron to cross the measurement plane would be given by

$$\frac{1}{6.25 \times 10^{14}} = 1.6 \times 10^{-15} seconds \tag{3.30}$$

or 1.6 fS at a current of 100 uA. This would be a consistent result, with, in theory a spectral density of $S_i = 0$, i.e. all the carriers are equally spaced in time, and giving a base frequency spectrum of 62.5 $PetaHz$. This time period gives an order of magnitude for the underlying transport process of carriers moving from lattice to lattice location. A mechanism is therefore required to randomise the transfer of electrons with a low variance in the carrier period from the base into the collector-base reverse field. The transit of the electrons across this constant $E - Field$ should not increase the spectral density of the arrival time, and the carriers will then arrive as majority carriers in the collector region. An important feature of a capacitor is its ability to reduce the spectral density of a fluctuating voltage. The current through a capacitor is given by

$$i = C\frac{dV}{dt} \tag{3.31}$$

where

$$\frac{dV}{dt} = \frac{i}{C}$$

the larger the value of C the smaller the value of $\frac{dV}{dt}$ and the smaller the spectral density S_v for a given current i. Creating a mechanism where the recombination rate of the minority carriers in the base could be increased locally, and the above properties of the capacitor applied, would be the basis for a solution. This would

reduce the spectral density without affecting the normal signal base recombination rate , and would allow the spectral density of the current to be reduced , after the potential barrier junction.

A new BJT structure is now created see Figure: 4.1, where a second base region adjacent to the first signal base is created. This new base region is called the BASE2 region. The second base is in essence a region of high recombination, independent of the signal base as much as possible, forcing recombination of the minority carriers. This causes an additional *external* DC BASE2 current to flow, and also provides a low impedance external path to a capacitance $C_{ext.}$ When the local charge in the BASE2 region *exceeds* the equilibrium charge, a balancing charge flows to or from the external capacitance $C_{ext.}$ The addition of a p^{++} region, in the case of the NPN structure, modifies the minority carrier behaviour in the base region. This region might typically have a donor concentration of $N_A = 10^{23}.\, m^{-3}$, a factor of around ten times the BASE1 p-region doping level. This structure will increase the COLLECTOR-BASE2 capacitance due to the thinner depletion region, where BASE2 is immediately adjacent to the base-collector junction . The original depletion zone boundary and the new position are shown in Figure: 3.6.

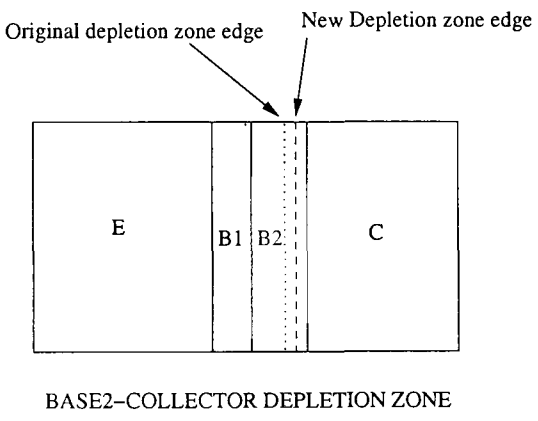

Fig. 3.6. BASE2-collector depletion zone

The recombination rate in this BASE2 region is required to be higher than the SIGNAL-BASE region, in order to achieve the objectives of reducing noise, the opposite objectives for the signal base (BASE1). This can be accomplished in many different

ways, but the most straightforward is to increase the BASE2 majority doping level N_A relative to BASE1. This will increase the minority carrier recombination rate, in this case electrons. This is the opposite design objective for the signal base, where the object is to minimise the minority carrier recombination rate . The increased recombination rate in BASE2 causes the BASE2 external DC current to be increased in order to maintain the charge equilibrium. The minority carrier density will decay from any level above the equilibrium level once the source of minority carriers is interrupted. The average diffusion length is given by L_n in Figure: 3.7.

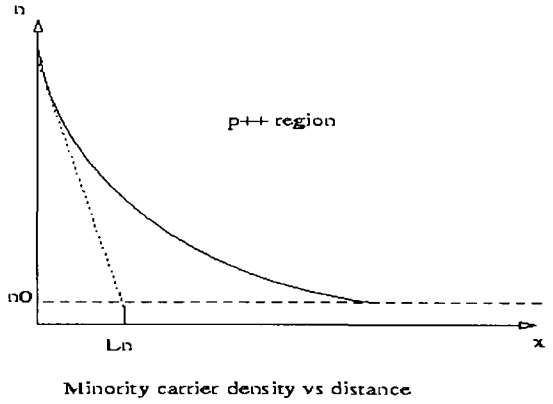

Fig. 3.7. Minority carrier density vs BASE2 length

This highly doped region introduces a low resistance region, where the minority carrier density equilibrium is partly controlled by the new BASE2 contact. The minority carrier population and carrier lifetime controls the recombination rate in this region, and this in turn is determined by the BASE2 current. Since the BASE2 is connected to an external capacitance, the minority carrier flow at the collector side of the BASE-COLLECTOR depletion zone boundary is regulated. The proportion of the minority carrier charge in the BASE1 region is greater than the B_2 charge for similar lengths of the two regions, and lower majority doping level N_{ab1}. The increased doping level N_{ab2} reduces the change in minority charge at this edge, due to noise, reducing the spectral density of the noise. There is still a signal base unaffected by BASE2 and so B_1, still provides the signal gain, providing normal emitter efficiency at lower frequencies. This new BASE2 region requires a low resistance from the external

B_2 contact to the main concentration of minority carriers passing through BASE2. This means the capacitance will remove minority carriers if the equilibrium density is increased, and supply minority carriers if the equilibrium density is reduced. The B_2 contact on the p^{++} region allows connection to a small external capacitance to improve the high frequency response of the device. This second AC {B.1} base provides direct connection to the majority charge in the region of the BASE2 side of the collector-base depletion region. This also allows de-coupling of the collector bulk capacitance from the base B_1 . Any change in this minority charge is met by a similar hole flow from the infinite recombination contact on B_2 . The intrinsic capacitance between the new highly doped region and the collector will be increased slightly. This is due to the shorter length of the depletion zone, in the p^{++}region, caused by the higher doping level. The length of the overall base region may also be increased due to the insertion of the p^{++} region. This will reduce the device β , and hfe, the gain, when compared with similar feature geometries on a standard BJT, if the BASE2 cannot be established inside the BASE1 region. The slightly longer diffusion path caused by the BASE2 p^{++}region over the conventional p region, will increase the transit time τ_1 slightly, and also act to oppose the gain-bandwidth slightly. The JAMES model permits an $E - Field$ vector $\overrightarrow{E_{x,0,z}}$ or $\overrightarrow{E_{0,y,z}}$ with a y or x component to be individually controlled within the BASE2 region. This allows the effects of the field difference caused by the BASE2 recombination surface, in turn controlled by C_{ext} to be active in the model. The reduction in the shot noise and the validation of K_{SA}, can be seen from the reduction in the actual spectral density calculated during the program run and shown in the JAMES model output shown in Algorithm: 45. This is the ratio of the values marked by "<=**T**" and "<=**A**", and gives $K_{SA} = 3.47 \times 10^{-3}$. The second validation of the reduced spectral density obtained from the introduction of the BASE2 region is observed from the graphs of noise attenuation in Chapter 7 obtained by conventional SPICE analysis in a later section e.g. Figure: 7.7.

4. THE JAMES MODEL AND SIMULATION KERNEL

The JAMES kernel is a *functional* model of the silicon crystal lattice. The approach used was to separate the "*Functio*nal" and the "*Behavioural* aspects" into two categories. The functional aspect defines how a mechanism or process takes place, such as a carrier moves from one coordinate to another, and a Behavioural aspect which is defined say, as the carrier takes t seconds to move. The model does not use real-time as its basis, although this can be implied by comparing the functional results with the measured results obtained from experimental observations. The model uses a functional basis for time, which is defined as being the time to complete a complete scan of the lattice and make any changes relating to the functional aspects. The computer model once initialised and started will evolve in a random way, to emulate as closely as possible the behaviour of the real crystal. The state of the crystal can be determined at any point during the execution, but due to the large amount of data generated, only certain important measurements are logged to either external files or to the console. The measurements can be made without disturbing the state of the carriers, however the actual position of the carrier can only be determined at one instant. The carrier may fluctuate around the measurement plane , and so the exact position has some uncertainty attached to it. The model is the basis for further enhancements towards a more behavioural approach, in that the algorithms that control the manipulation of the main matrix can be intercepted to perform more detailed calculations, involving external parameters. The approach has been structured to allow this *gradual refinement* to be adopted as the computing power becomes available. The program was written in $C - code$ to provide good portability between computing platforms, and to give a good balance between high level coding and fast execution time.

4.1 Debug methodology

An important part of writing a complex model is the ability to test the model and the code for its functional accuracy. Certain de-bug modes had to be incorporated into the model to allow the code execution to be retraced and compared with expectations as the model was progressively expanded. The use of a random evolution of the simulation meant it was necessary to be able to repeat the code execution path to examine it for inherent bugs and correct them. This problem was solved by using a pseudo random number generator. The pseudo random generator does approximate to a random number, but does so with the same time sequence when the same program is run again. This meant the model steps could be re-traced to detect the code errors. Once the program code has been validated the random number generator can be changed to a true random number algorithm, without a repeating sequence, to maximise the entropy of the generator. A special mode had also to be incorporated that allowed much more detailed de-bug information to be printed to the console, and to allow internal states to be traced.

4.2 The main lattice array

The main lattice was represented as a 3-D array corresponding to the $3D$ crystal lattice. The array had to represent the x and y coordinate of each cell LU, and also represent the *bond state* corresponding to each atom. Since bonds are shared between adjacent atoms, a method of defining the spatial location of each bond to its atom is fixed for all the atoms. The correspondence between the matrix and the physical lattice is now measured in *'lattice units'* (LU) {B.1}. The LU is the *smallest unique structure* within the semiconductor lattice, and is able to be stacked in any plane end to end to represent the complete lattice structure. The LU is represented in the case of Silicon (Si) as a cube, as shown in Figure: 3.2. To be precise as a face-centred cube or diamond structure. The LU of Silicon is sometimes referred to as two inter-penetrating FCC structures. The LU has four unique atoms, with four bonds for each atom giving a total of 16 unique bonds per LU . The other atoms at each corner of the cube and at the centre of each face have shared bonds with adjacent $LU's$.

The addressing of the matrix, to address a particular atomic bond, is simply the index of each of the three dimensions of the array, which addresses a particular LU. A further sub address is required to uniquely identify a particular bond. The matrix for each atom needs to store information on each bond state allocated to it, and because this is a functional model only at the lattice level , the bond state is represented by the binary states 0 and 1. The Binary 1 state represents an occupied bond for the particular electron or hole matrix. The use of a bit array is the most efficient way of storing this information, and so 16 bits are required to hold the state of each LU in the lattice. This is a compromise between model accuracy and the complexity of the program. The atom state is regarded primarily as the state of each covalent bond. These bonds are shared between atoms and so a simple algorithm assigns which particular bond is being addressed by each of the eight bits. The combination of the lattice x, y, z position and the 16 "bond state" bits, creates a unique address for each bond state. The presence of a bit in the matrix corresponds to an occupied state. The 16 states used here could be increased to add additional accuracy such as *atomic shell energy information* etc. as briefly discussed in section 3.12.2. The basic array is an integer array, and this is then directly addressed through the array dimension integers, and the bit position in the word at that address. Two identical arrays are defined, one for the electrons,the E matrix, and one for holes, the P matrix. These matrices are both manipulated concurrently. The $E - Field$ causes a drift in one direction for electrons, and the holes to drift in the other direction.

4.2.1 The movement of carriers within the matrix

The rules for carrier movement from one bond state to another are controlled by another algorithm referred to as the Spatial Evolution Algorithm or SEA. This algorithm determines which type of movement can be made by the carrier, as it moves from one LU to another. The electron is always constrained to move from one state to a physically adjacent state, as opposed to jumping to a non-interacting bond in another adjacent position. The atom can be considered as a conduit through which an electron can move to reach another bond position.

A particular electron in reality is shared between different bonds, and since each bond terminates in an atom, the electron can then move to another covalent bond through the atom central shell. The consideration here is that the most probable moves are defined by the closest energy level, and this requires the least energy to accomplish. The SEM vectors were calculated by a secondary $3D$ spatial analysis program, developed for JAMES, which translates coordinates and bonds linking each LU to an adjacent one. The SEM vector is assigned to an index representing the particular bond being addressed, and returns all the available bonds which are accessible for a carrier transition. The rules for the carrier movements are therefore built in to this register array for access by the algorithm controlling the spatial evolution. The SEA is computed from the LU structure, in this case for Silicon shown in Figure: 3.2, and is held in a Read Only Memory or ROM or Look Up table LUT. The ROM is now used to provide constraints on how a carrier may move internal to the LU or from one LU to another adjacent LU. This LUT and combined algorithm is referred to as the Spatial Evolution Matrix or SEM . The SEM can be executed at any point in the spatial and temporal evolution of the lattice state, when a decision is needed on how a carrier should move. This algorithm provides no constraints other than the path an individual carrier can take to satisfy the physical and energy constraints of the lattice. The arrays are initialised at the start of the program execution, and then programmed as part of the program initialisation to the values stored in the $SEM - LUT$. The carrier can move if permitted by the SEM , and also the next bond state is unoccupied. The algorithm controlling this movement or diffusion within the lattice is controlled by the Spatial movement algorithm or SMA. The direction of carrier drift is controlled by the $E - Field$ LUT contains the probabilities derived from the Poisson distribution, in relation to the direction of the carrier movement as the $E - Field$ magnitude increases. The SMA algorithm examines the direction of the $E - Field$ vector and then makes a selection of the next LU and adjacent bond position for possible occupation. The SMA algorithm will examine the selected bond state that has been randomly selected and if it is vacant will permit

the move, and if the selected bond state is occupied, then the move will be prevented for this particular time step. A limit is placed on the number of attempts to find the next randomly selected vacant bond, and if the move has not been made, the carrier will remain in its present location. This is of course reviewed at the next sweep of the matrix.

4.2.2 Diffusion of carriers

The mechanism of testing the next selected bond state before moving the carrier was selected to implement the process of carrier diffusion in the lattice. The processes here have been reviewed in section: 3.12.7. The diffusion process in essence means the carriers will diffuse away from areas of high density to regions of lower carrier density. When the SMA tests the availability of a bond in the reverse direction from the $E - Field$, the probability of finding a vacant state diminishes rapidly with increasing carrier density, and so the probability shifts to the regions of lower carrier density. This will usually be in the direction of the $E - Field$, but of course means lateral diffusion occurs where the current flow spreads out across the crystal to some extent. The outer edges then re-direct the diffusion again in the direction of the $E - Field$. The diffusion constants are set to the same value in the program, although the hole diffusion constant is lower for holes.

4.2.3 The Lattice edge boundary

The edge boundaries are defined by writing the unique hexadecimal code FFF_{16} see Appendix:{B.1} into each lattice boundary location. This in effect represents the bond states of the atoms in this location are all occupied, and not available in the address space of the lattice. This means carriers may *not* diffuse into these boundary regions of the lattice, and a the carriers are constrained within the lattice boundaries. This method matches the reality of conduction at the crystal edge, except a little more idealised. The boundaries are represented by the section of the lattice shown in Figure: 5.4.

4.2.4 External connections to the crystal

The physical properties of semiconductor structures are accessed through metallic contacts to the semiconductor at appropriate points on the device. These physical contacts are in fact infinite recombination centres where carriers flowing in the device can be generated or absorbed, and give rise to the electron current flow in the external wires and circuit. The assumption is that these recombination centres are ideal, in that each carrier has a one to one correspondence between generation of holes and electron absorption. This is also close to being true in the actual semiconductor. An idealised representation of the physical semiconductor structure, defined in this program, is shown in Figure: 4.1.

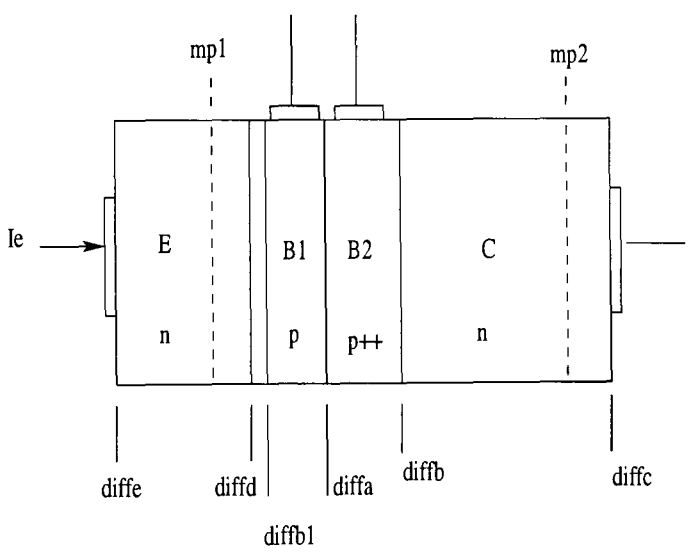

SIMULATION MODEL

Fig. 4.1. NPN semiconductor structure

4.2.5 The **Emitter and Collector contacts**

The two contacts are placed at either end of the silicon crystal, and so are defined as *infinite recombination surfaces* . These surfaces are defined in a similar way to the boundary layer of the crystal, except they have a special algorithm that maintains an empty or full surface state for the particular carriers, depending on which type of contact is present.

4.2.6 The base contacts

The base contacts are defined on the walls of the crystal with their axis orthogonal to the main axis of the carrier flow through the device. These regions are defined as 'windows' in the boundary regions at the edge of the crystal. They are controlled, as in the case of the emitter and collector contacts, as an infinite recombination centre. The type of algorithm will depend on the type of doping region they reside in. The measurement planes in Figure: 4.1 are able to be positioned anywhere across the lattice, and allow carrier densities to be observed in the base regions. The measurement planes are covered in more detail in section: 4.4.1.

4.2.7 Representing electrons and holes in the array

A hole is the majority carrier in a P region of the semiconductor, and an electron is the majority carrier in a N region. The presence of an electron or hole in the matrix is represented by a logic one in the appropriate bond position. A matrix with all carriers programmed to logic '1' would effectively represent an ideal silicon lattice, with no carriers available. This is in effect an ideal intrinsic crystal.

4.2.8 Doped regions

The model described, effectively models the intrinsic semiconductor, however to model extrinsic semiconductors further refinement of this model is required. The difference between the intrinsic and extrinsic conduction is the presence of carriers in the material to allow conduction to take place. The intrinsic silicon lattice can be described by using the basic matrix structure outlined in the previous section. The problem of defining regions of the lattice with different doping levels, was resolved by creating partitions to define each separate doped region. The partitions for example P-type, have a different $N.p$ product, and this ratio must be maintained on average, measured over any time period. The method used to model this, was to monitor all the individual carriers entering and leaving the region, and to ensure the product $N.p \rightarrow 0$, on average, is constant for any given time period. This is the charge control algorithm for each region. Without this algorithm the concentration of dopant in the region would diffuse out of the region to adjacent regions where the carrier density

is lower. In an actual crystal, the carriers from the more highly doped region would diffuse towards adjacent regions, however as they diffuse to regions of lower density an electric field is set up in the boundary between the different regions, which acts to present further diffusion. This creates a natural equilibrium that contains this 'out' diffusion. Because this model has not been enhanced to represent this mechanism, at this stage, by means of an intrinsic local $E-Field$, the charge containment algorithm or CCA provides this function e.g. Algorithm: 37.

4.2.9 Initial Doping

The initial doping is defined after the base matrix structure has been configured, and uses predefined algorithms to program the dopant carriers at the required location in the initial crystal state. This allows any impurity density to be programmed to represent the desired crystal to be studied. Carrier populations are printed to the console at the start of each program run. The typical doping levels in a N or P type semiconductor is of the order of $N = 10^{22}$ which means 1 dopant atom per 10^{22} atoms of silicon. The feature sizes are $100nm$ per side in a current state of the art device, this gives approximately 200 cell $LU's$ per side, or a LU array of 8×10^6, or approximately $\simeq 5.12 \times 10^{10}$ bond states available. The programming of the two different types of region have complementary states. The presence of a high acceptor concentration in a P region, would have a low concentration of n_p carriers in the region and vice versa.

4.3 The P-N junction

The contact of an N and a P type region creates a diode structure , which has certain properties that need to be represented in the model. Again, the properties will broadly describe the functional behaviour of the carriers as they cross the boundary, but the model at this stage does not model the voltage drop associated with the diode.When the two regions are defined with an abrupt junction a migration of holes from the P type and electrons from the N type material migrate across the interface and set up an 'internal field'. The electrons are able to cross from the N type material to the P type material with the correct direction and amplitude of the $E - Field$ applied.

4.3.1 Depletion region.

This region is defined by user input, as a narrow (typically a few cell $LU's$) depletion region, where the region is depleted of carriers. Any carriers moving across this region are assumed to move from the entry to the exit edge immediately the entry conditions are met. The depletion region exists because the collector base junction is reverse biased, and the high $E - Field$ across this narrow region means carriers arriving at this edge are swept rapidly across the region into the bulk collector.

4.3.2 Potential-barrier

The contact potential between the emitter and base creates a region known as a potential-barrier, and is the region responsible for shot noise in a diode or BJT. The carriers are able to cross the potential-barrier, from the N to the P region, given a high enough $E - Field$ and appear as minority carriers in the P region. The carriers are not in general able to cross the barrier in reverse, however in the case of this NPN device, holes however can cross the barrier in the reverse direction, as happens in the real semiconductor.

4.4 Temporal evolution of the matrix state

The dimension of time is created by defining a dimensionless unit, which represents the time a particular process takes to complete in the program. This is a functional model, and so this artificially defined unit of time used , or "NDTU" , has to be calibrated against real time by relating real world behaviour to the models behaviour. There is in effect no real time constraints on how the model is defined. The basic time unit is defined to be the time taken to scan the entire arrays, both the electron and the hole arrays, and to execute any algorithms during this entire process. This in effect means scanning every atomic lattice position, and each bond state, in both arrays. This process or "NDTU" is repeated as many times as required during the simulation to represent the total time the analysis is required. The calibration of the "NDTU" can be made by measuring the number of carriers flowing through the device for a given field, and relating this to the current flowing.

4.4.1 Measurement planes

The measurement planes (MPs) are a vital part of observing the state of the matrix during the analysis, and also quantifying the results. The measurement planes are defined as a 2-D plane orthogonal to the z axis of the crystal between the emitter and collector junctions. They can reside on any $[0, y, z]$ plane within the boundary edges of the main matrix. The MPs can observe any carrier transition across the plane. The MPs can be superimposed as a check on the integrity of an observation i.e. they should provide exactly the same results. If the planes are moved apart by 1 LU then the differential results may be observed. The MPs observe the carrier traffic across the plane by counting the carriers departing from the plane in a positive or negative direction along the z axis. The positive direction is defined as the direction in line with the $E - Field$ vector $\overrightarrow{E_{x,y,z}}$. The current at each time step is calculated, and since the instantaneous state is stored in an array for final calculations at the end of the program, the spectral density SD_i at each plane can be calculated. This provides the current and spectral density to be stored,and to be printed in the run summary, or allows the individual temporal state to be stored a a series of planes in an output file. The temporal evolution of the matrix can then be analysed for any point in the lattice at the end of the simulation run. There are also two fixed planes which monitor the recombination states at either end of the crystal, in this case the emitter and collector contacts.

4.4.2 Analytical calculations

The advantage of using MPs, allows the instantaneous calculation of more meaningful physical, statistical or electrical parameters such as the carrier flux distribution, the instantaneous current, the variance, or the spectral density.

4.5 Carrier behaviour

The carrier behaviour in the model has been constrained to use three of the main mechanisms present in the silicon, Drift, Diffusion and recombination. There are many other second order mechanisms which could be described, but many of them

would require the introduction of temperature, and this was not necessary for the basic objective of studying the electrical noise phenomena.

4.5.1 Random carrier motion

The movement of carriers in the lattice with no $E - Field$ present is essentially random. The behaviour is due to the thermal energy stored in the lattice, and due to the relatively low activation energy necessary to move a carrier from one bond state to another in an adjacent atom, means the carriers will move randomly, constrained only by the boundaries of the crystal. The mechanisms used in the model must be similar to the reality of the crystal, and to resolve this problem the program uses a random number generator to determine which direction the carrier should move. Although this is similar to introducing the concept of temperature into the model, their is no attempt made to make this a behavioural aspect. The random motion in terms of velocity will increase with temperature in a real crystal, and this would require the addition of further information to be stored in the matrix to represent the different energy levels associated with this quantitative aspect if added. Certain simplifications and constraints were employed

1. The rule that a carrier can only move from one bond to an adjacent bond location.

2. The carrier can only move to a new location if it is empty.

3. The relative activation energy required to move a carrier from its bond location to its adjacent location is $1.1eV$.

4. The number of attempts to find an adjacent available state has been constrained to 32 times.

5. The carrier state remains unchanged if no adjacent state is available or the computer can not find a location in 32 attempts (This constrains the computation time in crowded carrier situations).

If individual carriers could be detected as a unit impulse in time, say crossing a reference plane, see Figure: 5.6 due to the flow of the current, a Poisson distribution would result , as shown in Figure: 3.5. The key mechanism which represents the carrier behaviour, is common to the processes of drift and diffusion , that is the testing of a potential new location, before the move is permitted.

4.5.2 Diffusion

The diffusion of carriers in the crystal is very similar to diffusion in chemical systems and gases. The behaviour is in general for a population to diffuse from regions of high density, to regions of lower density. This sets up a diffusion gradient which permits a form of transport through the silicon lattice. This mechanism can be transient or steady state depending on the nature of the biasing, in the case of semiconductors. The problem of representing the diffusion mechanism in the model was addressed by ensuring the testing of each adjacent bond state, before moving the carrier. This means that given the situation shown in Figure: 4.2, where the area to the left hand side of the carrier in a particular LU is highly populated, shown as the darker area A, and the right hand side, region B, is relatively un-populated or a less dense region, and so the probability of a vacant bond being found is considerably higher. The net effect is to cause a given carrier to diffuse away from the regions of high density. The selection of the algorithm for controlling the carrier movement is consistent with the overall method of using a functional model.

4.5.3 Carrier Drift

This form of movement results from the behaviour of the negatively charged electron or the positively charged hole in an electric field ($E - Field$). The presence of an $E - Field$ causes a small bias in the net motion of the carrier in the direction of the field. This causes the distribution in Figure: 3.5 to be skewed by a small offset, which is proportion to the strength of this field. The problem of representing this field in the lattice is resolved by predefining statistical distributions for certain field levels, and allows the concept of applied voltage to be introduced. An arbitrary limit of 0 to $+/-10$ $E - Field$ units is set in the model, with 10 representing saturation velocity.

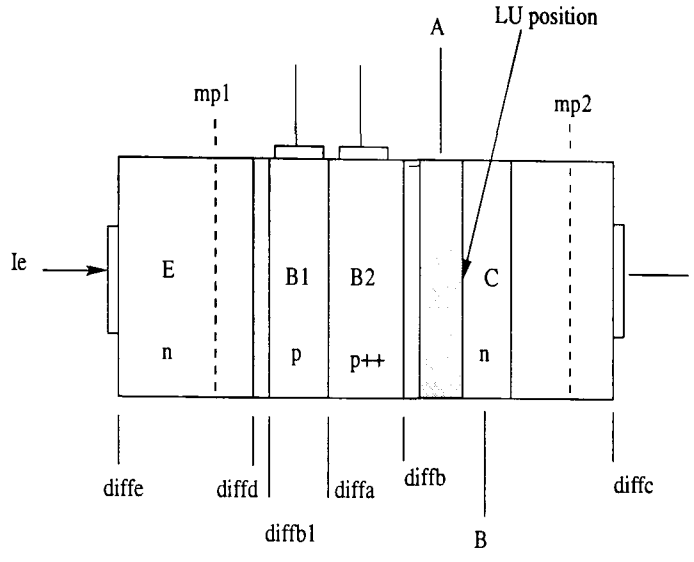

Fig. 4.2. Example of different carrier density regions

The problem of reducing the amount of calculation and speeding execution is resolved by computing preset probabilities , and storing them in a reference integer array or ROM , for the program to use in selecting the direction of movement. The $E - Field$ vector is defined as $\overrightarrow{E_{x,y,z}}$, as values of lateral field are required in some of the doped regions. The normal direction used will be in the direction of the carrier flow i.e. in the z direction or $\overrightarrow{E_{0,0,z}}$ direction. The new base region will require an $E - Field$ component in a direction orthogonal to this direction, and so an $E - Field$ vector $\overrightarrow{E_{0,y,z}}$ will be used. The individual regional $3 - D$ $E - Fields$ can be independently set i.e. for the base regions, collector and emitter.

4.5.4 Recombination

The two matrices, one to represent holes and the other electrons, evolve concurrently from their initial states during the program execution. The problem of representing recombination is where the electron and hole recombine in the lattice. This is given by $e + p \rightarrow p_n$, where p_n is the new hole created by the electron e in its previous location, as it combines. This was solved by using an algorithm which checks the state of each bond location in the E matrix with the same bond location in the P matrix. If they are both occupied after the move is complete , the location

in the P matrix will be set to zero (no hole) and the E matrix unchanged. The effect of a carrier being removed from the P matrix causes an imbalance in the $n.p$ equilibrium and the addition of an additional hole will be injected from one of the regions boundaries. This preserves the space charge neutrality of the crystal. The function of the original BASE1 and the new BASE2 both require recombination to correctly model transistor action in these regions. The recombination of holes and electrons is proportional to the minority-carrier charge in the region.

4.6 Overall carrier flow

4.6.1 Emitter injection

The following description assumes that an NPN device is defined in the crystal array with the appropriate doping profiles. The diagram shown if Figure: 4.1 shows the partitioning required to create an NPN structure.The emitter contact previously described, uses an infinite recombination algorithm to maintain the emitter surface of the crystal with all the atoms and bond states in this surface layer (1 LU deep) without any vacant states. This means that as an electron drifts from this surface layer (emitter) , a vacancy will be left behind. If this vacancy has not been filled by the movement of a random carrier, the algorithm will scan this part of the array, and will replace the electron. This means that the number of vacancies filled will represent the number of electrons flowing into the emitter contact. The current flowing into the emitter can then be determined by either counting the carrier vacancies filled, or by placing a measurement plane at this position.The carriers then move by diffusion or drift away from the emitter, assuming the $E - Field$ is correctly biased, toward the next region defined as P type. The charge equilibrium algorithm ensures that the charge entering the emitter region, does not continue to build up an electron concentration, and that the carriers must exit the region to permit the equilibrium to be maintained.

4.6.2 The base region.

The electrons cross the potential-barrier through the CCA (charge containment algorithm), and into the dopant profile for the base region. The exit of a carrier from the N type (emitter) region permits a new electron to be injected from the emitter recombination contact by means of the CCA. The electron is now a minority carrier in the base region , and alters the charge in this region. This in turn permits any electron, that has satisfied the conditions to leave the base region, to do so. There are two ways for the carriers to exit the base region, via the base contact, or through the collector base junction. The base region of a conventional BJT requires a compromise between a low combination rate of minority carriers in the base, and as low an intrinsic base resistance as possible. These two factors determine the high frequency performance of the device. This mechanism will be now briefly described.

4.6.3 Transistor action

Transistor action is achieved in an NPN structure, when two N type regions are separated by a thin P type base region. The emitter base junction is forward biased as described under emitter injection, however the base collector junction is reverse biased, and only leakage current flows under zero emitter current conditions. The relatively high reverse bias voltage creates a wide carrier depletion region, between the metallurgical junction of the base and collector. When the emitter base junction is forward biased to the point that emitter injection occurs, the electrons, are injected into the P type base, where they are now minority carriers. The design of the base region is such that the majority of the electrons have a *lifetime* τ_b in the base region greater than the average recombination time, and so the electrons cross this thin base region, and are swept into the depletion region of the collect base junction. The percentage of electrons that recombine in the base require an additional supply of holes to retain charge equilibrium, and so this current is supplied from the infinite recombination contact on the base region. This effect is controlled by the charge control algorithm for the base, however on this occasion, it has an input source into the region, and two possible outputs from either the base or the collector. The

charge control algorithm allows an electron to be accepted in balance to the base and recombination current, and the collector carrier flow out of the region.

4.6.4 The collector region

The electrons once they have swept through the reverse biased base-collector junction, are now part of the majority carrier population, and diffuse and drift toward the collector contact. The depletion region extends over only relatively few LU's around the metallurgical junction, and so the $E-Field$ defined as $\frac{V_{cb}}{t_w}$, where V_{cb} is the collector base voltage ,and t_w is the width of the depletion region. The carriers experience a very high $E-Field$ in the depletion region, and are swept through from the base to the collector, with a very small transit time. The problem of modelling this region is resolved in the model by using an approximation to the accelerating effect of this reverse field.When the carrier reaches the boundary of the collector region, the carrier is immediately transferred to the surface 1 LU after the collector boundary, in the N type region. Reverse transport is not permitted by the depletion control algorithm for majority carriers. The carrier will now move towards the collector contact. This assumes the transit time across the base is equal to one 'NDTU' in this model. The infinite recombination surface at the end of the collector region is defined as the reverse of the emitter contact. This means that the end boundary of the collector is maintained by the collector algorithm at an empty state. An electron arriving in this plane of 1 LUs width, is removed and reset to zero, and this is accumulated as part of the collector current.

4.7 The problem of shot noise reduction

Many different scenarios were evaluated through the JAMES model, in an attempt to find a mechanism able to reduce the level of shot noise. Ideally this mechanism should help reduce the other noise forms also, but to a lesser extent. The objective was to propose a structure that did not impact the conventional device performance greatly.

The most appropriate solution to provide these objectives, to some degree, was the introduction of a second base region , close to the collector. This base needed

a different design criteria for the normal base contact. This new base needed to be optimised for maximum noise reduction rather than maximum gain as in the case of BASE1.The design criteria are somewhat of an anti-base region. in that they are opposite design objectives to the signal base.

4.7.1 BASE2 design objectives

The ideal structure for BASE2 would require the following

1. A very low resistance between the centre of the charge flow and the BASE2 external contact.

2. A high recombination rate in the BASE2 region for minority carriers.

3. A straightforward method of implementing it.

4. A minimum effect on the behaviour of BASE1 in terms of recombination rate.

NB. This is somewhat conflicting with the design requirements for a conventional base, and so the addition of another base with different characteristics appeared to be the most appropriate solution. The requirements of 1 and 2 are supportive requirements , and a much higher BASE2 doping level will satisfy both these objectives. A doping density approximately ten times that of the BASE1 would be appropriate. The requirement in 3 would seem to be best implemented as an additional doping implant or diffusion before the BASE1 is formed. The requirement of 4 is very dependent on the physical design of the BASE2, and should ideally have a base contact well separated from the BASE1 contact. This would avoid interaction between the bases and the reduction of the signal base gain β_1. The use of a much higher doping level in BASE2 will cause a small retarding field to be set up between BASE1 and BASE2, due to the initial outward diffusion from BASE2 into BASE1.The voltage is approximately $58mV$ for a doping level density difference of 10. The BASE2 needs to have a low impedance to the external capacitor, so that any fluctuation in the charge of the BASE2 region is integrated by the external capacitor, and so reducing the spectral density of the noise voltage on this base. This provides a constant energy for the minority carriers right

on the edge of the high $E - Field$ collector base depletion region. The carriers that leave this layer towards the collector, are swept into the field with a fixed departure energy. The energy of the carriers arriving in the collector region, now majority carriers, will not be exposed to further shot noise mechanisms en route to the collector. The electrons arriving in the collector region will proceed to the collector primarily through drift, and at or approaching v_{sat} , the saturation velocity. In the presence of a space-charge effect, if the current is dominated by the drift component of the injected carriers, it is called the space-charge-limited current[31] . Since it is a drift current, it is given by, in the case of electron injection,

$$J = qnv.$$

The space charge is determined by the injected carriers, giving rise to the Poisson equation

$$\frac{d^2\Psi}{dx^2} = \frac{qn}{\varepsilon_s}$$

The carrier velocity v is related to the electric field by the equation

$$v = \mu\varepsilon$$

where u is the permeability and ε is the $E - Field$. In the velocity saturation regime v_{sat} is independent of the field, and in the ballistic regime, where there is no scattering

$$v_{sat} = \sqrt{\frac{2q\Psi}{m_e^*}}$$

where m_e^* {B.1} is the effective mass mobility for the electron.

4.7.2 The BASE2 region

The BASE2 region is defined in the main matrix between the BASE1 and collector region. The region also needs a BASE2 infinite recombination contact, and this is defined on the side wall of the BASE2 region, with its axis orthogonal to the axis of the main carrier flow. The addition of this high conductivity region between the signal base BASE1 and the bulk collector acts to reduce the collector-BASE1 capacitance. This Miller capacitance in an ordinary BJT is magnified by the voltage gain A_v of the

transistor, and so reduces the high-frequency gain as the input frequency increases. The reduction of this Miller capacitance by decoupling the BASE2 to signal ground via an external capacitor has significant high-frequency benefits. The increase in gain, and the noise reduction effects, both act to increase the signal to noise ratio (SNR) of the transistor.

4.8 Introduction to the Program

The software structure and algorithms used in the JAMES model to represent the physical mechanisms will now be described, including the representation of the new base region. The intention here is that the additional BASE2 will be justified by the results obtained from its incorporation in the structure, and as demonstrated by the results achieved. The remainder of this section describes how the functional model has been structured, to satisfy the objectives defined in previous sections. The program flow is outlined in Figure:4.3, and a description of each functional block is given.

4.8.1 Program flow

The program flow is shown in Figure: 4.3. The flow is fairly straightforward at the top level, and is described briefly in the following sections. The model has several major sections.

4.8.2 Program modes

There are two modes, a de-bug mode, and a batch mode. The de-bug mode will allow all the interactions with the MP's to be observed during the simulation, and the batch mode which suppresses all the console messages, and stores the results in files, for analysis after the run is finished. This allows many simultaneous runs to be made for comparison after the batch run. The larger crystal structures above $200nm$ representing the state of the art silicon fabrication limits of today, which may take 8 hours or so to complete, can be run overnight on a PC or main-frame system. An additional feature has been added that allows snapshots of the carrier matrix, viewed from different planes to be stored in log files during the program run. This allows

behaviour such as carrier crowding to be viewed after termination of the program run. The program will also accept command line parameters to avoid the necessity of re-compilation after a parameter change.

4.8.3 Program **modules**

The program listing is divided into a number of modules containing the algorithms used to provide the functionality of the JAMES program.

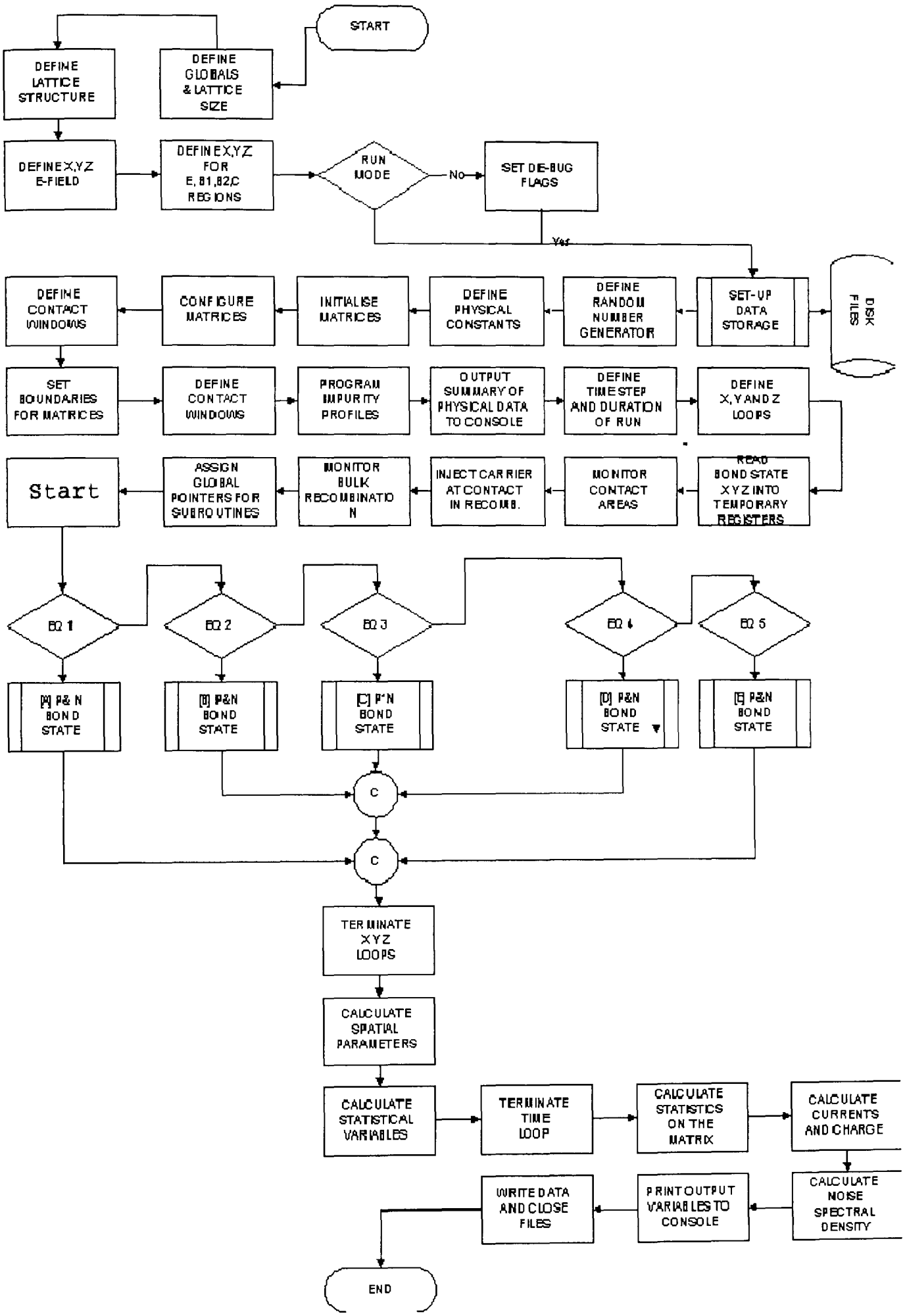

Fig. 4.3. Simplified flow chart

List of Algorithms

4.8.4 Command Line modes

There are two methods of inputting data into the program; by directly entering the parameters in the variables or in the matrices, and/or by entering a few important variables directly on the command line. This is a benefit when simulation times are short and a key variable needs to be varied in order to gather more data.

4.8.5 Global variable definitions

The global variables available to the whole model are initialised here. TIME_LIMIT is the maximum run time in terms of time units, TEMPERATURE the crystal temperature in ^{o}K, and EX_FIELD, EY_FIELD and EZ_FIELD set the x, y and z field components of the $\overrightarrow{E_{x,y,z}}$ vector acting on the lattice. The EX_LFIELD, EY_LFIELD and EZ_LFIELD control the BASE2 E-Field environment.

4.9 Define output files for data collection

This section opens files used to collect intermediate data at each internal program state, such as the matrix state at each time step or atom or bond location.

4.9.1 Main matrix definition

This section defines the main arrays used to represent the crystal lattice of the semiconductor.There are several arrays including the main array, there are ROM tables used to store the probability vectors used to determine the type of move and direction a carrier will make in the evolution of the matrix state. There are also shadow arrays of similar dimensions, used to monitor data, and some experimental arrays for enhancing the accuracy of the model. The two main arrays are $Matrix_i[x][y][z].initial.b1$ and $Matrix_i[x][y][z].initial.b2$. The first being the array representing the electron carrier population and the second the hole population.

Algorithm 1 Global variable initialisation

```
#define TIME_LIMIT 300
#define TEMPERATURE 300 /* Degrees Kelvin */
/* ENTER E-FIELD 0 or +/- (1-10) as fraction of Carrier saturation velocity */
/* Normal field [parallel to each axis] between z=0 and z=MAX_LENGTH */
#define EXFIELD 0
#define EYFIELD 0
#define EZFIELD 0
/* ENTER Lateral E-Field 0 or +/- (1-10) as fraction of Carrier saturation velocity
*/
#define EX_LFIELD -5
#define EY_LFIELD 0
#define EZ_LFIELD 10
/* ENTER LATTICE SIZE BELOW in Lattice units */
#define LATTICE_SIZE 32
#define MAX_ARRAY_ELEMENTS LATTICE_SIZE+1
```

Algorithm 2 Create output files for data collection

```
FILE *outfile,*errfile,*statfile1,*stat2,*stat3,*mapfil,*outfile1;
```

Algorithm 3 Main array definition for representing the crystal lattice

```
/* define two variable types one with 8 bits, one with four bit fields */
/* 5 A per ARRAY_ELEMENT structure; */
typedef struct element{
unsigned char a1 : 3; // 3 bit corner position code
unsigned char b1 : 16; // 16 bit body position code
unsigned char a2 : 3; // 3 bit corner position code
unsigned char b2 : 16; // 16 bit body position code
unsigned char p1 : 8; // 8 bit body pointer
unsigned char p2 : 3; // 3 bit corner pointer
signed char p3 : 2; // signed flag for spatial array
}initial;
typedef struct ARRAY{
struct element initial;
}ARRAY_ELEMENT;
/* define two variable types one with 16 bits, one with four bit fields */
/* 5 A per ARRAY_ELEMENT structure; */
typedef struct element1{
unsigned char a2 : 3; // 3 bit corner position code
unsigned char b2 : 16; // 16 bit body position code
}point;
/* Define bit array for holding E-Field probability vectors */
typedef struct e_field{
signed char e : 2;
double p;
}field;
typedef struct FIELD{
struct e_field field;
}ARRAY_ELEMENT_FLD;
```

4.9.2 Matrix Initialisation

This section configures the composite matrix .

Algorithm 4 Matrix initialisation

```
/* define a global variable for the initial 3-D matrix */
ARRAY_ELEMENT Matrix_i[MAX_ARRAY_ELEMENTS][MAX_ARRAY_ELEMEN
```

4.9.3 Random Pseudo Number Generator

This is a very important algorithm in the program, used to create a pseudo random number, but in a repeatable manner. This allowed the program to be de-bugged by being able to trace the program flow leading up to an error in behaviour. This generator can be replaced by a true random number generator once the program is behaving correctly, and trace-ability is no longer required. A true random number generator will be a close approximation to the real crystal.

Algorithm 5 Pseudo random number generation

```
/* Define variables for RANDOM generator */
static unsigned long mt[N];
/* the array for the state vector */
static int mti=N+1;
/* mti==N+1 means mt[N] is not initialized */
/* initializing the array with a NONZERO seed */
void sgenrand(seed) unsigned long seed;
{
/* setting initial seeds to mt[N] using */
/* the generator Line 25 of Table 1 in */
/* [KNUTH 1981, The Art of Computer Programming */
/* Vol. 2 (2nd Ed.), pp102] */
mt[0]= seed & 0xffffffff;
for (mti=1; mti<N; mti++) mt[mti] = (69069 * mt[mti-1]) & 0xffffffff;
}
```

4.9.4 Declare physical constants

This section declares the value of various physical constants used by the model to translate the functional behaviour into behavioural parameters during the program run.

Algorithm 6 Declare physical constants

```
/* SET TIME ITERATIONS HERE */
time_limit=TIME_LIMIT;
max_length=MAX_LENGTH;
vol_m3=6.35065e27;
pi=3.141592654;
inter_lattice=5.4e-10;
m_electron=8.9e-31;
p_constant=6.625e-34;
ue=100e-6;
un=40e-6;
q_electron=1.6e-19;
e0=8.81e-23;
er=12;
eg=1.12;
ni=1.5e16;
boltzmann_c=1.38e-23;
u0=12.5663706e-7;
me=9.612e-31;
m0=9.11e-31;
mh=7.3791e-31;
sat_vel=1.04e5;
E_sat=60; /* Volts m-1 */
```

4.9.5 Set the E-Field probability vectors

The $E - Field$ probability matrix is a ROM matrix look up table, that will determine the direction and velocity of a carrier. There are only ten discrete field levels in this initial model, and they relate to 1/10 of the carrier saturation velocity in the silicon lattice.

Algorithm 7 Sset the E-Field probability vectors

```
/*Set the x-y-z E-Field probability vectors */
set_field(e_xvariable,e_yvariable,e_zvariable,0,Matrix_e[0][0].field.e);
/* Set the Field Constants */
//Normal Fields e.g 1 = 1/10 =0.10
Fx=1;
Fy=1;
Fz=1;
Px= (float) Fx/MAX_PROB;
Py= (float) Fy/MAX_PROB;
Pz= (float) Fz/MAX_PROB;
printf("Bulk Diffusion Constants Dx Dy Dz %3.3f %3.3f %3.3f\n\n",Px,Py,Pz);
//Diffusion Lateral Field
Fxl=1;
Fyl=1;
Fzl=1;
Pxl= (float) Fxl/MAX_PROB;
Pyl= (float) Fyl/MAX_PROB;
Pzl= (float) Fzl/MAX_PROB;
```

4.9.6 Defining the location of the different regions of the lattice.

The different doping regions are defined in this section of the program. The collector, the emitter, the BASE1 and the BASE2 region. They are defined in x, y, z coordinates. This is the physical location of each region, however the doping concen-

trations are not defined until later.The location of the two viewing planes are also defined here to collect information on the region of interest. e.g spectral density, current flow, charge concentration etc. The boundaries of the different *regions* of the semiconductor structure are defined by six different planes as shown in the algorithm: 8. The boundaries are used to define a region such as the emitter or base region, and the type of region N type or P-type. The doping levels are entered into the N or P matrix depending on their type e.g. The P type BASE1 region would be defined in the $Matrix_i[x][y][z].initial.b2$ array. A typical configuration is shown in Figure: 4.1.

Algorithm 8 Definition of the different physical regions

```
/* Set run variables here */
/* Start of E boundary */
diffe=1;
/* Start of Depletion zone boundary */
diffd=7;
/* Start of Base1 boundary */
diffb1=10;
/* Start of Base2 boundary */
diffa=13;
/* Start of C boundary */
diffb=28;
/* End of C boundary */
diffc=MAX_LENGTH-1;
/* Set planes to observe e traffic */
// e traffic mplane = 11;
mplane1=30;
/* Set planes to observe h traffic */
// h traffic mplaneh= 6;
mplaneh1=26;
```

4.10 Matrix Initialisation

This algorithm resets all the elements of the lattice to zero representing an empty state. The loop formed by the three for loops increments the array to each *element* in turn, and assigns zero to each matrix element.

4.10.1 Printing Summary of structure defined to this point

The various parameters entered in the start of the program are summarised at this point before the main program execution is started.

4.10.2 Definition of Matrix boundaries

The main matrix has now been defined and initialised to zero, and the matrix must now be partitioned in such a way as to create natural boundaries for the carrier flow. The boundaries separate the crystal region of interest from the edges of the lattice. If this were not done, then carriers would not be reflected from the surface states back into the body of the crystal. The input and output planes of the crystal are defined here. This is where carriers will enter and leave the crystal through an external current path. These planes are infinite recombination surfaces where the conduction process in the crystal change from one region to another i.e. from the semiconductor to a metal contact.

4.10.3 Setting the structure limits

The outside edges of the crystal are defined here. Since the matrix is initialised to zero, the outside boundaries are all set to a logic one or filled state. This represents fully occupied bond states at the edge of the lattice.

4.10.4 Definition of the BASE2 region contact window

The BASE2 region is the highly doped region located between the collector and the BASE1 region. This is a window cut in the outer boundary layer of the lattice to allow a recombination surface to be created. This region will allow carriers to migrate through the region and recombine at this mono-layer contact, and so exit into the external conductor.

Algorithm 9 Matrix initialisation

```
printf("Initializing main MATRIX\n\n");
/* initialise matrix */
for(k=0; k <MAX_LENGTH+1; ++k)
{
for(j=0; j <MAX_LENGTH+1; ++j)
{
for(i=0; i <MAX_LENGTH+1; ++i)
{
Matrix_i[i][j][k].initial.a1=0;
Matrix_i[i][j][k].initial.b1=0;
Matrix_i[i][j][k].initial.a2=0;
Matrix_i[i][j][k].initial.b2=0;
Matrix_i[i][j][k].initial.p1=0;
}
}
}
/* New maskb character array */
Matrix_i[0][0][0].initial.p1=1;
Matrix_i[1][0][0].initial.p1=2;
Matrix_i[2][0][0].initial.p1=4;
Matrix_i[3][0][0].initial.p1=8;
Matrix_i[4][0][0].initial.p1=16;
Matrix_i[5][0][0].initial.p1=32;
Matrix_i[6][0][0].initial.p1=64;
Matrix_i[7][0][0].initial.p1=128;
Matrix_i[8][0][0].initial.p1=256;
Matrix_i[9][0][0].initial.p1=512;
Matrix_i[10][0][0].initial.p1=1024;
Matrix_i[11][0][0].initial.p1=2048;
Matrix_i[12][0][0].initial.p1=4096;
Matrix_i[13][0][0].initial.p1=8192;
Matrix_i[14][0][0].initial.p1=16384;
```

Algorithm 10 Print summary of the structure

```
printf("\n\n");
printf("Crystal size = %3f0 Angstroms, Vancant site Population %2d
\n\n",MAX_LENGTH*5.4,MAX_LENGTH*MAX_LENGTH*MAX_LENGTH);
printf("Crystal size = %3f0 nM \n\n",(MAX_LENGTH*5.4/10));
printf("n++ density between limits = %d %d \n\n",diffa,diffb);
printf("n+ Base region between limits = %d %d \n\n",diffd,diffb);
```

4.10.5 Definition of the BASE1 region window

The BASE1 region is the doped region located between the emitter and the BASE2 region.This is similar to the BASE2 contact window, except it forms the BASE1 external contact.

4.10.6 Definition of the EMITTER region

There are two matrices for each region of the doped semiconductor, as there are two carrier types electrons and holes. This is the definition for both the N-type region and the P-type region. The initialised bond sites in the lattice having been initialised can now have precisely defined dopants positioned in the desired profile throughout the region. This will define the dopant concentration of this region.

4.10.7 Definition of the COLLECTOR region

The collector region extents from the end contact or recombination surface to the edge of the BASE2 region.

4.10.8 Definition of the Bulk BASE2 region

This is a high impurity concentration region,and the total carriers defined in this area will be roughly ten times that of the BASE1 region.

4.10.9 Definition of the BASE1 region

This region extends from the emitter infinite recombination surface or contact to the edge of the depletion region set up between the BASE1 region and the emitter.

Algorithm 11 Definition of matrix boundary

```
printf("Defining Matrix boundaries of Lattice\n\n");
for(k=0; k<MAX_LENGTH+1; k++)
{
for(j=0; j<MAX_LENGTH+1; j++)
{
for(i=0; i<MAX_LENGTH+1; i++)
{
/* set Input / Output recombination surfaces for main lattice at 1 for e c */
Matrix_i[i][j][0].initial.a1=7;
/* set Input /Output recombination surfaces for main lattice at 1 for e b */
Matrix_i[i][j][0].initial.b1=0xffff;
/* set output barrier at 0 for e c */
Matrix_i[i][j][MAX_LENGTH].initial.a1=0;
/* set output barrier at 0 for e b */
Matrix_i[i][j][MAX_LENGTH].initial.b1=0;
/* set input barrier at 1 for [h] c */
Matrix_i[i][j][MAX_LENGTH].initial.a2=7;
/* set input barrier at 1 for [h] b */
Matrix_i[i][j][MAX_LENGTH].initial.b2=0xffff;
/* set output Barrier at 0 for [h] c */
Matrix_i[i][j][0].initial.a2=0;
/* set output Barrier at 0 for [h] b */
Matrix_i[i][j][0].initial.b2=0;
}
}
}
```

Algorithm 12 Structure limits

```
/* Set the structure limits */
/* 4 sides (planes) for [e] c */
for(j=0 ; j <MAX_LENGTH+1; j++)
{
for(i=0 ; i <MAX_LENGTH+1; i++)
Matrix_i[0][i][j].initial.a1=7; }
for(j=0 ; j<MAX_LENGTH+1; j++)
{
for(i=0 ; i<MAX_LENGTH+1; i++)
Matrix_i[MAX_LENGTH][i][j].initial.a1=7;
}
for(j=0 ;
j<MAX_LENGTH+1; j++)
{ for(i=0 ; i<MAX_LENGTH+1; i++)
Matrix_i[i][0][j].initial.a1=7;
}
for(j=0 ; j<MAX_LENGTH+1; j++)
{
for(i=0 ; i<MAX_LENGTH+1; i++)
Matrix_i[i][MAX_LENGTH][j].initial.a1=7;
}
/* Set the structure limits */
/* 4 sides (planes) for b */
for(j=0 ; j <MAX_LENGTH+1; j++)
{
for(i=0 ; i <MAX_LENGTH+1; i++)
Matrix_i[0][i][j].initial.b1=oxffff;
}
for(j=0 ; j<MAX_LENGTH+1; j++)
{
for(i=0 ; i<MAX_LENGTH+1; i++)
Matrix_i[MAX_LENGTH][i][j].initial.b1=0xfff;
```

Algorithm 13 Base2 region contact window definition

```
/* Define the Base2 window at x= 0 [e] */
/* x = 0 */
for(j=diffa+1 ; j<diffb; j++)
{
for(i=1 ; i<MAX_LENGTH; i++)
Matrix_i[0][i][j].initial.b1=0;
}
/* Define the Base1 [P] window at x=0 */
for(j=diffb1+1; j<diffa; j++)
{
for(i=1; i<MAX_LENGTH;i++)
{
Matrix_i[0][i][j].initial.b2=0;
}
}
```

Algorithm 14 Definition of BASE1 contact window region

```
/* Define the Base1 [P] window at x=0 */
for(j=diffb1+1; j<diffa; j++)
{
for(i=1; i<MAX_LENGTH;i++)
{
Matrix_i[0][i][j].initial.b2=0;
}
}
/* Define the Base1 [P] window at x=MAX_LENGTH */
for(j=diffb1+1; j<diffa; j++)
{
for(i=1; i<MAX_LENGTH; i++)
Matrix_i[MAX_LENGTH][i][j].initial.b2=0;
}
/* x = MAX_LENGTH-1 for [e] */
for(j=diffa ; j<diffb+1; j++)
{
for(i=1 ; i<MAX_LENGTH; i++)
Matrix_i[MAX_LENGTH][i][j].initial.b2=0;
}
```

Algorithm 15 Definition of emitter N junction

```
/* N - EMITTER */
/* program Nd [e] impurity position in emitter */
for(l=diffe+1; l < diffd; ++l)
{
for(k=2; k < MAX_LENGTH-1; ++k)
{
for(j=2; j < MAX_LENGTH-1; ++j)
{
Matrix_i[j][k][l].initial.a1=0;
Matrix_i[j][k][l].initial.b1=0;
/* NB Stagger the a1 and a2 x impurity co-ordinates or the recombination */
/* centre will gobble all the impurity holes & electrons */
}
}
}
/* P - EMITTER */
/* program Na [h] impurity position in emitter */
for(l=diffe+1; l <diffd; l=l+2)
{
for(k=2; k <MAX_LENGTH-4; k=k+2)
{
for(j=2; j <MAX_LENGTH-4 ;j=j+2)
{
Matrix_i[20][20][20].initial.a2=0;
Matrix_i[j][k][24].initial.b2=0;
}
}
}
```

Algorithm 16 Definition of collector region

```
/* N - COLLECTOR */
/* program Nd [e] impurity position in collector */
for(l=diffb+1; l < diffc; l=l+2)
{
for(k=2; k < MAX_LENGTH-1; k=k+2)
{
for(j=2; j < MAX_LENGTH-1; j=j+2)
{
Matrix_i[j][k][l].initial.a1=0;
Matrix_i[j][k][l].initial.b1=0;
/* NB Stagger the a1 and a2 x impurity co-ordinates or the recombination */
/* centre will gobble all the impurity holes & electrons */
}
}
}
/* N - COLLECTOR */
/* program Na [h] impurity position in collector */
for(l=diffb; l < MAX_LENGTH-1; l=l+2)
{
for(k=2; k < MAX_LENGTH-1;
k=k+2)
{
for(j=2; j < MAX_LENGTH-1; j=j+2)
{
Matrix_i[j][k][l].initial.a2=0;
Matrix_i[j][k][l].initial.b2=0;
/* NB Stagger the a1 and a2 x impurity co-ordinates or the recombination */
/* centre will gobble all the impurity holes & electrons */
}
}
}
```

Algorithm 17 Definition of the bulk BASE2 region

```
/* N++ BASE2 */
/* program Nd [e] high density LATERAL implant region Base2 */
for(l=diffa+1; l< diffb;l=++l)
{
for(k=1; k < MAX_LENGTH-1;k=k+2)
{
for(j=1; j < MAX_LENGTH-1;j=j+2)
{
Matrix_i[j][k][l].initial.a1=0; Matrix_i[j][k][l].initial.b1=0;
}
}
}
/* P++ BASE2 */
/* program Na [h] high density LATERAL implant region Base2 */
for(l=diffa+1; l < diffb;++l)
{
for(k=1; k < MAX_LENGTH;++k)
{
for(j=1; j < MAX_LENGTH;++j)
{
Matrix_i[j][k][l].initial.a2=0;
Matrix_i[j][k][l].initial.b2=0;
}
}
}
```

Algorithm 18 Definition of the bulk BASE1 region

```
/* N TYPE BASE1 MINORITY CARRIER */
/* Define [e] Base1 region between Depletion zone and Base2 region */
/* Leave 1 lu between edge of Depletion and Base2 */
for(l=diffb1+1; l < diffa;l=l+2)
{
for(k=1; k<MAX_LENGTH;k=k+2)
{
for(j=1;j<MAX_LENGTH;j=j+2)
{
Matrix_i[j][k][l].initial.a1=0;
Matrix_i[j][k][l].initial.b1=0;
}
}
}
/* temp b1 carrier */
//Matrix_i[10][10][11].initial.b2=1;
/* P TYPE BASE1 MAJORITY CARRIER */
/* Define [h] Base1 region between Depletion zone and Base2 region */
for(l=diffb1+1; l < diffa;l=l+2)
{
for(k=1; k<MAX_LENGTH;k=k+2)
{
for(j=10;j<MAX_LENGTH;j=j+2)
{
Matrix_i[j][k][l].initial.a2=0;
Matrix_i[j][k][l].initial.b2=0;
}
}
}
```

4.10.10 Definition of the BASE1-EMITTER Depletion region

The contact of two regions of different doping concentration will set up an electric field to counteract further diffusion between the two regions. The model assumes that this depletion region is constant. In a more elaborate model this region width would be calculated and be dependent on the voltage between the two regions.

4.11 Output summary of region sizes to the console

This algorithm provides a summary of the regions created before the program begins. This allows the program to be aborted in the case of very long execution times in a large crystal.

Output number of carriers in the region

This is a similar summary as in the previous case.

Calculate the carrier concentrations

The carrier concentration should be checked here to ensure the correct doping profile has been instantiated.

Calculate the conductivity and resistance of the region

The conductivity is a useful measurement to ensure the correct values of base resistance has been achieved.

Test Random Number generator

The random number generator is important to ensure the correct evolution of the state of the matrix. When different generators are being inserted in the program, the frequency of each number is computed here, and printed on the console to check the correct entropy is achieved. A true random sequence should give an equal average frequency of numbers in the range.

Algorithm 19 Definition of the BASE-EMITTER depletion region

```
/* N - DEPLETION */
/* Define [e] depletion region between emitter region and Base1 */
for(l=diffd; l < diffb1;++l)
{
for(k=1; k<MAX_LENGTH;++k)
{
for(j=1;j<MAX_LENGTH;++j)
{
Matrix_i[j][k][l].initial.a1=0;
Matrix_i[j][k][l].initial.b1=0;
}
}
}
/* N - DEPLETION */
/* Define [h] depletion region between emitter region and Base1 */
for(l=diffd; l < diffb1;++l)
{
for(k=1;k<MAX_LENGTH;++k)
{
for(j=1;j<MAX_LENGTH;++j)
{
Matrix_i[j][k][l].initial.a2=0;
Matrix_i[j][k][l].initial.b2=0;
}
}
}
```

Algorithm 20 Output summary of region sizes to the CONSOLE

```
/* Print Summary of the different regions */
printf("\n\nEmitter region between [%d] and [%d] \n",2,diffd);
printf("Depletion region between [%d] and [%d] \n",diffd,diffb1);
printf("Base1 region between [%d] and [%d] \n",diffb1,diffa);
printf("Base2 region between [%d] and [%d] \n",diffa,diffb);
printf("Collector region between [%d] and [%d] \n\n",diffb,MAX_LENGTH-2);
```

Algorithm 21 Outputthe number of active carriers to the CONSOLE

```
/* Sweep area before run */
for(j=diffa+1;j<diffb;++j)
{
for(k=1;k<MAX_LENGTH;++k)
{
for(l=1;l<MAX_LENGTH;++l)
{
for(m=0;m<8;++m) { if(Matrix_i[j][k][l].initial.b1&maskb[m]>0)
++vals.cntr[71];
}
}
}
}
printf("\n\nCarriers found in Base2 %d\n\n",vals.cntr[71]);
```

Algorithm 22 Output the carrier concentrations to the CONSOLE

```
/* Calculate the concentrations in cm-3 */
Nd=(float)nebe/((inter_lattice*LATTICE_SIZE)*(inter_lattice*LATTICE_SIZE)*(inter_l
*LATTICE_SIZE));
Na=(float)neh/((inter_lattice*LATTICE_SIZE)*(inter_lattice*LATTICE_SIZE)*(inter_la
*LATTICE_SIZE));
printf("Impurity Dopant elements ACTIVE [e] Nd Na %4d %4d \n\n",neb,nebe);
printf("Impurity Dopant elements ACTIVE [h] Nd Na %4d %4d \n\n",neh,nehh);
printf("Nd concentration.m-3 %3e\n\n",Nd);
printf("Na concentration.m-3 %3e\n\n",Na);
printf("Nd lateral count %3d\n\n",ne_lat0);
if(diffb!=diffa)
{
ppm=neh/(diffb-diffa)*MAX_LENGTH*MAX_LENGTH;
printf("n++ density ppm = %4.2f\n\n",((neh*1.0e6)/((diffb-
diffa)*MAX_LENGTH*64*MAX_LENGTH)));
}
ppme = (float) neh/(diffb-diffa)*MAX_LENGTH*MAX_LENGTH;
printf("n++ [e] density ppm = %4.2f\n\n",((nebe*1.0e6)/((diffb-
diffa)*MAX_LENGTH*64*MAX_LENGTH)));
```

Algorithm 23 Calculate the conductivity SNF resistance of region

```
/* Calculate conductivity at 10e-23m-3 */
sige= (float) ue*Nd*q_electron; sigh= (float) un*Na*q_electron;
printf("Conductivity sigma(e) ohm-cm %3.6f\n\n",sige);
printf("Conductivity sigma(h) ohm-cm %3.6f\n\n",sigh);
/* Calculate the Resistance of the lateral region */
r_lateral_e=1/(sige*MAX_LENGTH*inter_lattice*100);
r_lateral_h=1/(sigh*MAX_LENGTH*inter_lattice*100);
printf("Resistance of lateral [e] region [face to face] %3.12f\n\n",r_lateral_e);
printf("Resistance of lateral [h] region [face to face] %3.6f\n\n",r_lateral_h);
```

Algorithm 24 Test random number generator

```
/* test random generator */
for(j=0; j<100000; ++j) { k=newrand(10);
if((k>=0.001)&(k<=1)) ++cnt_r[0];
if((k>=1.001)&(k<=2)) ++cnt_r[1];
if((k>=2.001)&(k<=3)) ++cnt_r[2];
if((k>=3.001)&(k<=4)) ++cnt_r[3];
if((k>=4.001)&(k<=5)) ++cnt_r[4];
if((k>=5.001)&(k<=6)) ++cnt_r[5];
if((k>=6.001)&(k<=7)) ++cnt_r[6];
if((k>=7.001)&(k<=8)) ++cnt_r[7];
if((k>=8.001)&(k<=9)) ++cnt_r[8];
if((k>=9.001)&(k<=10)) ++cnt_r[9];
}
printf("\n\n [0]=%d [1]=%d [2]=%d [3]=%d [4]=%d [5]=%d [6]=%d [7]=%d [8]=%d
[9]=%d \n\n",cnt_r[0],cnt_r[1],cnt_r[2],cnt_r[3],cnt_r[4],cnt_r[5],cnt_r[6],cnt_r[7],cnt_r[8]
```

Algorithm 25 Setting the TIME STEP /END TIME and LU address

```
/* SET NUMBER OF ITERATIONS [TIME] */
for(t=0; t < time_limit; ++t)
{
/* Reset counters */
plus_0=0;
minus_0=0;
plus_1=0;
minus_1=0;
end_val=0;
/* read initial array */
for(z=1; z < MAX_LENGTH; z++)
{
z1[0]=z;
z1[1]=z;
z2[0]=z;
z2[1]=z;
z4[0]=z;
z4[1]=z;
z5[0]=z;
z5[1]=z;
for(y=1; y < MAX_LENGTH; y++)
{
y1[0]=y;
y1[1]=y;
y2[0]=y;
y2[1]=y;
y4[0]=y;
y4[1]=y;
y5[0]=y;
y5[1]=y;
for(x=0; x < MAX_LENGTH+1; x++)
{
```

4.11.1 Setting the time step and LU address

This setting will determine how many times the lattice will be scanned from end to end. This determines the length of the simulation run, and is also proportional to the total current that will flow through the lattice.

4.11.2 Incrementing the covalent bond address

This section provides three loops for each time step to enable the selection of each LU , and allows the corresponding bond states to be addressed. These loops are defined for x, y and z variables.The "posb" variable defines the current bond address in the current LU being addressed. The current LU is $Matrix_i[x][y][z].initial.b1$, for the electron carrier matrix. The array is defined as an unsigned integer with 16 bits, and so each element in this 4-D matrix can be written to or read. The range is $0- > 15$ corresponding to positions arbitrarily defined in the LU shown in Figure: 3.2. The current program has no awareness of the actual geometric position of the bonds, only their logical position.

Algorithm 26 Bond state selection

```
for(pos=0; pos<19; pos++)
{
if(pos<16)
{ posb=pos;
posc=11;
}
if(pos>15)
{ posb=15;
posc=pos-16;
}
```

4.11.3 Scanning the lateral BASE2 contact for carriers

This algorithm is performed every time step. The purpose is to scan for the presence of a carrier having diffused into the lateral BASE2 contact. If a carrier is

detected it is extracted and removed from the carrier population. A new carrier is injected into the emitter region adjacent to the emitter recombination surface. This is the situation in a real device, where the emitter current equals the Base current(s) plus the collector current. This is defined by Kirchoffs laws for high carrier populations.

Algorithm 27 Scanning the lateral BASE2 contact

```
/* Maintain the lateral Base2 diffusion boundary conditions [x=0] and
[x=MAX_LENGTH] */
/* keep the first [e] [0][y][z] x,y,z area for e full */
if((z>=diffa)&(z<diffb))
{
if((Matrix_i[0][y][z].initial.a1)< 7)
{
/* printf(" -0- released \n"); */
Matrix_i[0][y][z].initial.a1=7;
}
/* keep the last [x][y][MAX_LENGTH] x,y,z area for H full */
if((Matrix_i[x][y][MAX_LENGTH].initial.a2)< 7)
{
printf(" -[h]- released \n");
Matrix_i[x][y][MAX_LENGTH].initial.a2=7;
}
if(Matrix_i[MAX_LENGTH][y][z].initial.b1<0xffff)
Matrix_i[MAX_LENGTH][y][z].initial.b1=0xffff;
if(Matrix_i[0][y][z].initial.b2< 255) Matrix_i[0][y][z].initial.b2=0xffff;
}
```

4.11.4 Emitter carrier injection

The emitter as the name suggests emits carriers from the emitter contact into the crystal lattice. This mechanism is provided by this algorithm.

Algorithm 28 Emitter carrier injection

```
// inject an [e] into row 1 c /*
disable when debugging h */ if(flag[0] >10)
{
++ne;
//printf("flag0\n"); flag[0]=0;
n1 = newrand (7);
x1[0]=matx[n1]+x;
y1[0]=maty[n1]+y;
z1[0]=matz[n1]+z;
if(y1[0]<0) y1[0]=0;
if(z1[0]<0) z1[0]=0;
if(y1[0] > MAX_LENGTH)
y1[0]=MAX_LENGTH;
if(z1[0] > MAX_LENGTH)
z1[0]=MAX_LENGTH;
n=newrand (3);
if(n == 0) valh[0]=2;
if(n==1) valh[0]=1;
if(n==2) valh[0]=4;
++cnt[0];
Matrix_i[x][y][1].initial.a1=valh[0];
}
```

4.11.5 BASE2 recombination

This algorithm monitors the BASE2 carrier flow in both the P lattice and in the N lattice. If an electron and a hole carrier are detected at the same physical location i.e. at the same x, y, z co-ordinate and the same bond location in both matrices then the P carrier (or hole) is removed from its current position in the the P matrix. The electron combining with a hole generates another hole at its previous location, and due to the charge imbalance caused by the electron being removed, another electron is injected from the recombination contact for the particular region i.e. the BASE1 region. This represents the recombination of an electron and hole in the crystal. The removal of the hole results in the increase of the negative space charge in this region, and so a hole must be injected or allowed to be accepted from a recombination surface or from an adjacent region. The print statement allows the recombination event to be recorded on the console when in de-bug or analysis mode. This console message will also identify the exact location in the crystal of the recombination event. The recombination current can be measured by the variable $++recome$. This is an example of a variable that can not be physically measured in a laboratory situation.

4.11.6 BASE1 recombination

This is identical to the BASE2 recombination.These algorithms are executed every time unit or time step (NDTU), so they are constantly updated.

4.12 Start of the state modules

This section defines the main algorithms defining the evolution of the carriers in their respective matrices. The state module control the evolution of one type of carrier through each region in the semiconductor, and each one uses a separate matrix. A region is defined as a discrete doping area and type P or N, as defined by the boundaries specified in Alg: 8. There are five main regions numbered one to five, and they represent the emitter, potential-barrier, BASE1, BASE2, and collector regions respectively. There are two state modules one for electrons and one for holes. The module is selected at random by a random number generator. Each module contains

Algorithm 29 BASE2 recombination

```
/* Recombination here */ /* Base 2 region */
if((z>=diffa+1)&(z<diffb)&(x>1)&(x<=MAX_LENGTH-
1)&(y>=1)&(y<=MAX_LENGTH-1))
{
if((Matrix_i[x][y][z].initial.b1&maskb[posb]                    >0)&(Ma-
trix_i[x][y][z].initial.b2&maskb[posb]>0))
{
Matrix_i[x][y][z].initial.b1=0&maskb[posb];
Matrix_i[x][y][z].initial.b2=0&maskb[posb];
printf("b2RRRRRRRRRRRRRRRRRRRRRRRRRRRRRRRRRRRRRxyz    %d
%d %d
Mat[]=%d\n",x,y,z,Matrix_i[x][y][z].initial.b2);
/* Decrement [h] and [e] counters */
--vals.cntr[65];
--vals.cntr[29];
++recome;
}
}
```

Algorithm 30 BASE1 recombination

```
/* Base 1 region */
if((z>=diffb1+1)&(z<diffa)&(x>=1)&(x<=MAX_LENGTH-
1)&(y>=1)&(y<=MAX_LENGTH-1))
{
if((Matrix_i[x][y][z].initial.b1&maskb[posb]                    >0)&(Ma-
trix_i[x][y][z].initial.b2&maskb[posb]>0))
{
Matrix_i[x][y][z].initial.b1=0&maskb[posb];
Matrix_i[x][y][z].initial.b2=0&maskb[posb];
printf("b1RRRRRRRRRRRRRRRRRRRRRRRRRRRRRRRRRRRRRRRxyz%d%d%dMat[]=
/* Decrement [h] and [e] counters */
--vals.cntr[67];
--vals.cntr[36];
++recomh;
}
}
```

the control of each region in the lattice. The carrier state is either occupied or vacant in this model implementation , and it has a restricted number of transitions available to it when it moves from its present location to an adjacent state (another $LU\ x.y.z$ location). In the absence of an $E - Field$, assumed to be the only influence on the carriers, the carriers will randomly move to adjacent bond states. This corresponds to the random movement of carriers observed in practice, and is in fact the cause of the thermal noise generated across the resistive elements of the semiconductor. The presence of an $E - Field$ causes a bias to be created in the probability of this random movement, in the direction of the field, resulting in carrier drift. The modules are identical for both hole and electron matrices, and so they will not all be listed here.The principle is however the same and the collective operation can be seen from the flow diagram at the start of this section. The random number generator selects a module at random and the algorithm processes the state of that module before returning to the next time state, and so the next random number.

The algorithm for the emitter region Alg: 32 is entered when the carrier satisfies the z-axis requirement in that it lies between *diffe* and *diffd.* The control is then passed to the *diffusion_le* , Alg: 37 subroutine where the carrier movement and charge control are located. The algorithm for the potential-barrier Algorithm:33, emitter to base junction is entered when the carrier reaches the z-axis position *diffd.* The depletion subroutine controls the transition from one side of the potential-barrier to the other. The $E - Field$ variables are also passed to the subroutine. The BASE1 region (region 3) is entered when the carrier drifts/diffuses to the edge of the *diffb1* position , and the *diffusion_leb1* subroutine is entered with the $3D\ E - Field$ variables, as well as the lateral $E - Field$ values. The Base1 region Alg: 34 in this particular NPN implementation of the model has an infinite recombination contact cut in the side wall of the lattice, and if carriers recombine in this region they will be replaced by a hole from this surface. BASE1 current is generated externally for each carrier injected into the BASE1 region.

The BASE2 region Alg:35 is similar to BASE1, and the *diffusion_leb2* subroutine

Algorithm 31 Start of the state modules

```
/* [e] B -> B select body to body */
if(d==1)
{
if(((((Matrix_i[x][y][z].initial.b1)&(maskb[posb]))                    >0)&(((Ma-
trix_i[x][y][z].initial.b1))!=0xffff)))
{
if(Matrix_g[70].var.gen==1)
printf("B->B    [e]    Mat[]=%4x    posb=%d    x=%d    y=%d    z=%d
\n",Matrix_i[x][y][z].initial.b1,posb,x,y,z);
/* New test */
/* scan base1 for hole injection */
//this h_inject(MAX_LENGTH,posb,diffa,diffb1,x,y,z,uniform,Matrix_i[0][0][0].initial.b2);
/* scan base2 for hole injection */
//this h_injectb2(MAX_LENGTH,posb,diffa,diffb,x,y,z,uniform,Matrix_i[0][0][0].initial.b2);
/* from d0 */
//Ez=e_sine(quant_size,t,sine_on); cum_z=cum_z+Ez;
if(sine_on<1) m4=m4; else { Ez=e_sine(quant_size,t);
}
k=newrand(12);
/* Check on Pseudo random generator bias */
if((z>=diffa)&(z<=diffb))
x_cum=x_cum+Matrix_e[e_xlvariable][k].field.e;
y_cum=y_cum+Matrix_e[e_yvariable][k].field.e;
z_cum=z_cum+Matrix_e[e_zvariable][k].field.e;
```

Algorithm 32 Emitter region control

```
if((z>=diffe)&(z<diffd))
{
region=1;
diffusion_le(region,t,uniform,diffa,diffb,diffb1,diffd,diffe,diffc,x,y,z,e_xvariable,e_yvariable,e_
//printf(" NEXT z %d [42] %d\n",z,Matrix_g[42].var.gen);
/* Transfer o_plane count to arrays */
vale[t]=Matrix_g[73].var.gen;
vale1[t]=Matrix_g[72].var.gen;
vale2[t]=Matrix_g[74].var.gen;
}
```

Algorithm 33 Potential-barrier control

```
if((z>=diffd)&(z<diffb1))
{
region=2;
depletion(region,eq_flg,uniform,diffa,diffb,diffd,diffb1,x,y,z,e_xvariable,e_yvariable,e_zvariat
/* Transfer o_plane count to arrays */
vale[t]=Matrix_g[73].var.gen;
vale1[t]=Matrix_g[72].var.gen;
vale2[t]=Matrix_g[74].var.gen;
}
```

Algorithm 34 BASE1 region control

```
if((z>=diffb1)&(z<diffa))
{
region=3;
diffusion_leb1(region,t,uniform,diffa,diffb,diffb1,diffd,diffe,diffc,x,y,z,e_xvariable,e_yvariable,
/* Transfer o_plane count to arrays */
vale[t]=Matrix_g[73].var.gen;
vale1[t]=Matrix_g[72].var.gen;
vale2[t]=Matrix_g[74].var.gen;
}
```

is used if the carrier is in the z-axis range between *diffa* and *diffb*. The Collector

Algorithm 35 BASE2 region control

```
if((z>=diffa)&(z<diffb))
{
region=4;
diffusion_leb2(region,t,uniform,diffa,diffb,diffb1,diffd,diffe,diffc,x,y,z,e_xvariable,e_yvariable,
//printf("7-Mat[]=%X posb=%d x=%d y=%d z=%d\n",Matrix_i[x][y][z].initial.b1,posb,x,y,z
/* Transfer o_plane count to arrays */
vale[t]=Matrix_g[73].var.gen;
vale1[t]=Matrix_g[72].var.gen;
vale2[t]=Matrix_g[74].var.gen;
}
```

region, 5, Alg: 36 is shown to pass control to the *diffusion_lec* routine if the carrier lies in the *diffb* to *diffc* location. The function for the emitter only will be shown here as it is representative of the others. The maskb[n]variable is a 16 bit register, with the index 0 to 15 selecting only that bit i.e. maskb[10] selects only the 10th bit. This register when operated on by the logical AND function with another 16-bit register will filter out all the other bits. The vals.cntr[n] counter variables are used to count

Algorithm 36 Collector region control

```
if((z>=diffb)&(z<diffc))
{
region=5;
diffusion_lec(region,t,uniform,diffa,diffb,diffb1,diffd,diffe,diffc,x,y,z,e_xvariable,e_yvariable,e
/* Transfer o_plane count to arrays */
vale[t]=Matrix_g[73].var.gen;
vale1[t]=Matrix_g[72].var.gen;
vale2[t]=Matrix_g[74].var.gen;
}
```

the number of carriers entering a region, and ensure that the same number leave, to preserve space-charge neutrality. The *next_move* function is called at the start of each regions control function, and passes the x, y, z co-ordinates to the $3D\ E-Field$ function, and returns a random relative position for the next proposed move. This can be accepted or rejected depending on the adjacent state of the *LU*. The final function to be called after the charge control function is *move_e* , this function will take the actual carrier position and the next potential x, y, z coordinates, and will move the carrier to the recommended location if the move rules, Alg:41 are obeyed. The FINAL SCANS algorithm Alg: 39, is the algorithm responsible for checking the collector recombination contact to detect a carrier arriving at the collector end of the crystal. The SEM algorithm Alg: 40 is called by the *next_move* function, and since the input data vector it is passed have some values in the range $-1/-0/+1$ this algorithm converts the vectors to positive address vectors only, for the SEM ROM. The SEM ROM Alg: 41 holds the $3D$ paths of each *LU* and the vector returned from the Matrix_s[x][y][z][pos].vecmove.sem=0xnnnn, provides the move algorithm with the valid move locations. This $4D$ array is arranged so that a 4-bit address vector is supplied to it through the 3-bit [x][y][z] integers, and the current bond location is supplied through the final 4th bit. The vector returned is the 16-bit (0xnnnn) mapping for the relative move.

Algorithm 37 Emitter charge control

```
/* Function for [e] protected areas */
diffusion_le(int region,int t,int uniform,int diffa,int diffb,int diffb1,int diffd,int
diffe,int diffc,int x,int y,int z,int e_xvariable,int e_yvariable, int e_zvariable
,int e_xlvariable,int e_ylvariable,int e_zlvariable,int MAX_LENGTH,int posb,int
eq_flg,void use_struct(struct ARRAY))
{
int newz,k1,n,matx[7],matxhl[7],k,j,cext,distl[6],distn[7],p,matz[8],dist[8],flg,distnz[6],matzl[6],
maskb[0]=1;
maskb[1]=2;
maskb[2]=4;
maskb[3]=8;
maskb[4]=16;
maskb[5]=32;
maskb[6]=64;
maskb[7]=128;
maskb[8]=256;
maskb[9]=512;
maskb[10]=1024;
maskb[11]=2048;
maskb[12]=4096;
maskb[13]=8192;
maskb[14]=16384;
maskb[15]=32768;
maskb[16]=0;
/* Start of Emitter flow control */
next_move(region,x,y,z,diffa,diffb,posb,e_xvariable,e_yvariable,e_zvariable,e_xlvariable,e_y
MAX_LENGTH,Matrix_i[0][0][0].initial.p3);
flg=0;
newz=Matrix_g[42].var.gen;
if((z<diffd-1))
{
if(z<diffe+1) { if((z==diffe)&(Matrix_g[42].var.gen==diffe-1))
```

Algorithm 38 Carrier transfer algorithm

```
/* Function to check new adjacent [e] location and move if feasible */
move_e(int region,int t,int x,int y,int z,int posb,int MAX_LENGTH,int eq_flg,int
e_xvariable,int e_yvariable,int e_zvariable,void use_struct(struct ARRAY))
{
int m1,status,lim,x5[4],y5[4],z5[4],l,k,m,maskb[16];
maskb[0]=1;
maskb[1]=2;
maskb[2]=4;
maskb[3]=8;
maskb[4]=16;
maskb[5]=32;
maskb[6]=64;
maskb[7]=128;
maskb[8]=256;
maskb[9]=512;
maskb[10]=1024;
maskb[11]=2048;
maskb[12]=4096;
maskb[13]=8192;
maskb[14]=16384;
maskb[15]=32768;
maskb[16]=0;
/* Check for FF */
if(((Matrix_i[x][y][z].initial.b1&maskb[posb])>0)&(Matrix_i[x][y][z].initial.b1!=0xffff))
{
m1=newrand(15);
/* find an empty slot in new location */
/* position can be x,y,z +/- 1 */
printf("x=%dy=%dz=%dnewx=%dnewy=%dnewz=%dm1=%d\n",x,y,z,Matrix_g[40].var.ge
Matrix_g[42].var.gen,m1);
Matrix_s[1][0][0][0].vecmove.var=maskb[m1];
lim=0; while((((Matrix_i[Matrix_g[40].var.gen][Matrix_g[41].var.gen][Matrix_g[42].var.gen].
```

Algorithm 39 Final scans

```
/* new lateral diffusion x returned in Mat[14] from the diffusion_test function */
//this diffusion_x(e_xvariable,e_xlvariable,uniform,diffa,diffb,x,y,z,Matrix_g[40].var.gen,Ma
/* Transfer o_plane count to arrays */
vale[t]=Matrix_g[73].var.gen; vale1[t]=Matrix_g[72].var.gen;
vale2[t]=Matrix_g[74].var.gen;
if(pop_st<temp)
{
temp=pop_st; fprintf(outfile," pop_down x y z x5 y5 z5 %d %d %d %d %d
%d\n",x,y,z,x5[0],y5[0],z5[0]);
}
/* observation planes */
//o_planes(&vale[0],&vale1[0],&vale2[0],mplane,mplane1,t,x,y,z,pos,MAX_LENGTH,Matrix
//serial=cume(t,time_limit,Matrix_g[0].var.gen);
/* b [e] crossing end */
//if((Matrix_g[42].var.gen==MAX_LENGTH)&(z==MAX_LENGTH-
1)&(Matrix_i[Matrix_g[40].var.gen][Matrix_g[41].var.gen]
[Matrix_g[42].var.gen].initial.b1>0)&(Matrix_i[Matrix_g[40].var.gen][Matrix_g[41].var.gen][
0xffff))
/* scan the z = MAX_LENGTH surface */
scanze(t,x,y,z,&valet[0],Matrix_g[40].var.gen,Matrix_g[41].var.gen,Matrix_g[42].var.gen,MA
Matrix_i[0][0][0].initial.b1);
}
}
```

Algorithm 40 SEM algorithm

```
/* SME function to define the carrier movements in the electron and hole lattice */
/* THE JUNGLE! in a LUT */
/* m1 = the bond number */
sem_lut(int x,int y,int z,int m1, int i_x,int i_y, int i_z,void use_struct(struct AR-
RAY))
{
int s_vect_out;
i_x=i_x-x+1;
i_y=i_y-y+1;
i_z=i_z-z+1;
printf("IN SEM_LUT x_i y_i z_i m1 %d %d %d %d
Mat[%x]\n",i_x,i_y,i_z,m1,Matrix_i[0][m1][0].initial.p1);
/* Start the SEM LUT (Look Up Table) */
/* Corner of LU's */
s_vect_out=Matrix_s[i_x][i_y][i_z][m1].vecmove.sem;
return s_vect_out;
}
```

Algorithm 41 SEM rom

```
sem_prog(void use_struct(struct ARRAY))
{
/* THE JUNGLE! */
/* The range for the first matrix is -1 0 +1 representing the incremental step */
/* Program the SEM ROM */
/* BODY CENTERED Adjacent LU's */
Matrix_s[2][0][1][15].vecmove.sem=0x8000; Matrix_s[1][2][2][15].vecmove.sem=0x0001;
Matrix_s[1][0][0][15].vecmove.sem=0x0200;
Matrix_s[1][2][2][0].vecmove.sem=0x0001;
Matrix_s[2][1][2][0].vecmove.sem=0x8000;
Matrix_s[2][2][1][0].vecmove.sem=0x0200;
Matrix_s[0][0][1][9].vecmove.sem=0x0001;
Matrix_s[1][0][2][9].vecmove.sem=0x8000;
Matrix_s[0][1][2][9].vecmove.sem=0x0020;
Matrix_s[1][2][2][5].vecmove.sem=0x0001;
Matrix_s[2][2][1][5].vecmove.sem=0x0200;
Matrix_s[2][0][1][5].vecmove.sem=0x8000;
Matrix_s[0][1][1][1].vecmove.sem=0x1400;
Matrix_s[1][1][1][1].vecmove.sem=0x000f;
Matrix_s[1][0][1][3].vecmove.sem=0x0140;
Matrix_s[1][1][1][3].vecmove.sem=0x4007;
Matrix_s[0][1][1][4].vecmove.sem=0x1400;
Matrix_s[1][1][1][4].vecmove.sem=0x0072;
Matrix_s[0][1][1][14].vecmove.sem=0x0140;
Matrix_s[1][1][1][14].vecmove.sem=0x0072;
Matrix_s[0][1][1][6].vecmove.sem=0x0140;
Matrix_s[1][1][1][6].vecmove.sem=0x7001;
Matrix_s[0][1][1][8].vecmove.sem=0x4004;
Matrix_s[1][1][1][8].vecmove.sem=0x00f0;
Matrix_s[0][1][1][10].vecmove.sem=0x4004;
Matrix_s[1][1][1][10].vecmove.sem=0x0d40;
Matrix_s[0][1][1][12].vecmove.sem=0x0012;
```

4.12.1 Observation planes

Observation planes are located at the end of each state module to analyse the carrier movements through the selected plane. Collectively they can provide snapshots of the matrix evolution. They can be placed anywhere in the matrix except on the recombination surfaces. They can be placed within 1 LU of these boundary planes, and can even be placed in the depletion regions to study the carrier behaviour here with time. The planes are available for hole and electron carriers.

Algorithm 42 Observation planes

```
//printf("BEFORE\n");
/* e Observation plane */
if(z1[0] == mplane)
{
if( z < mplane)
++plus;
if(z > mplane) ++minus;
}
}
```

4.12.2 Final positional computations

This collection of algorithms use each unique x ,y, z vector to store any intermediate data, and compute any variables required for external storage or for later in the program.

A typical console summary of the program at completion is shown in Figure: 44, and shows the number of carrier entering and leaving the recombination surfaces. The summary includes the summary of some calculations such as the *spectral density* (SD) of the measurement planes.

Algorithm 43 Final positional computations

```
if(Matrix_i[x][y][z].initial.a1 >0)
{
elements=0;
//elements=probee(t,MAX_LENGTH,Matrix_i[z][y][z].initial.a1);
//printf(" active C elements = %2d\n",elements);
}
++q;
if(Matrix_i[x][y][z].initial.b1>0)
{
elements=0;
//elements=probeb(t,MAX_LENGTH,Matrix_i[x][y][z].initial.b1);
//printf(" active B elements = %2d\n",elements);
}
if(prot_flag>0)
{
//pop_st=probeb(t,MAX_LENGTH,Matrix_i[0][0][0].initial.b2);
//
printf(" ACTUAL POPULATION AT START %d\n",pop_st); prot_flag=0;
}
/* close pos */
}
/* close x */
}
/* close y */
}
/* close z */
}
```

Algorithm 44 A typical program summary

HIGHEST X Y Z 0 0 0

LOWEST X Y Z 32 32 32

Net current 26

Total I/P count e = 7

Total O/P count e = 7

Total I/P count h = 59

Total O/P count h = 59

Output count[>max] = 0

Output count[>max] = 0

Output count[>max] = 0

Output count[<min] = 0

Output count[<min] = 0

Output count[<min] = 0

mplane1 + e count = 8

mplane1 - e count = 83

mplane2 + e count = 26

mplane2 - e count = 59

mplane1 + h count = 0

mplane1 - h count = 0

mplane2 + h count = 0

mplane2 - h count = 0

ENPplane + e count = 7

ENPplane + h count = 44

base1 + h count = 0

base2 + h count = 0

mplane2 current = 0

Population crossing = 0

Ave transit time epS = 0.0000000071

Ave transit time hpS = 9999.0000000000

Ave.lateral transit epS = 1.076625e-09

Base2 h Recomb count = 0

Base1 h Recomb count = 0

Algorithm 45 Program summary (continued)

e lateralin count = 0

e lateralout count = 0

e count X diffa [14]= 0

e count X diffb [18]= 0

Act shot[e] rms ENP [32]= 1.056324e-15

Theor SD A^2.rthz-1 ENP [32]= 4.826936e-33

Act SD A^2.rthz-1 ENP [32]= 1.115821e-35

Act shot [e] mp1 [5]= 1.206422e-15

Theor SD A^2.rhz-1 mp1 [5]= 8.274747e-30

Act SD e A^2.rhz-1 mp1 [5]= 1.455454e-35

Act shot [e] mp2 [11]= 0.000000e+00

Theor SD pA.hz-1 mp2 [11]= 8.874667e-40

Act SD A^2.rthz-1 mp2 [11]= 4.360535e-40

Act shot [e] END [32]= 1.056324e-15

Theor SD pA.hz-1 END [32]= 4.826936e-33 <=**T**

Act SD A^2.rthz-1 END [32]= 1.115821e-35 <=**A**

e Current mp1 [5]= 2.585859e-11

e Current mp2 [11]= 2.773333e-21

e Current END [32]= 1.508417e-14 <=**I**

e RMS uA current mp1 [5]= 0.000000e+00

e RMS uA current mp2 [11]= 0.000000e+00

END e current Ie/Ang sq = 5.051660e+01

h Current Base1 = 0.000000e+00

e Current Base2 = 0.000000e+00

h lateralin count = 0

h lateralout count = 0

h count X diffa [14] = 0

h count X diffb [18] = 0

Noise carriers = 0

Base1 Forward Gain = 0.000000e+00

Base2 Forward Gain = 0.000000e+00

Theor shot [h] p (rms) noise= 0.000000e+00

5. RESULTS

5.1 Introduction

The evaluation of the results produced by the model will be divided into three sections. The first will be to evaluate the results of the model and determine if they correspond to a real semiconductor device. This will provide validation of the model accuracy, and also to build its credibility for other predictions to be made. The second part of building further credibility, will be to use parameters measured or derived by other means to equate the crystal to a form that can be validated using well tried and tested simulation methods in use. The third and final validation will be to carry out a simple bench test on a conventional device, and equate the observations to the results obtained from the first two simulation tests. The derived parameters from the semiconductor being modelled will be converted to Spice parameters. This will permit both AC and noise analysis using conventional techniques. The analysis of the results should support the predictions from the model, and support its use in deriving very detailed analysis that is not possible using conventional techniques.

5.2 Results obtained from the JAMES program

The JAMES model is simulating the carrier transport behaviour for an average DC current see the calculated current Algorithm: 45. The model was run with a small carrier population, and the initial results described below in Figure: 5.1. The 3-D array was set for 32 atomic units per side, and the time steps set to 1320 time units (NTDU's). The first correlation aspect of the model to be checked was the current flow across two faces of the lattice in the z direction. The crystal was defined as a single homogeneous structure, i.e. with effectively only the emitter-base junction operating, with an impurity population defined in the region as extending from $z = 5$

to $z = 10$ cell LU's see Figure: 5.4. The behaviour of the carriers in the DIODE-MODE, i.e. a simple P-N junction, at the $z = 32$ surface was then plotted with respect to time. Figure: 5.1 shows the number of carriers crossing the end surface MP[32], for each quanta size on the $y - axis$. Figure: 5.2 shows the same data as a statistical distribution. The total carriers (electrons) crossing the end plane MP[32] used in the simulation for deriving Figure: 5.2 was 280. An electron crossing the end-plane is defined as a unidirectional event, and so only a half of the distribution is observed in Figure:5.2. The behaviour of the model is demonstrated at a simple level, showing that it represents results obtained in actual calculations of the shot noise from the model, at the same current.

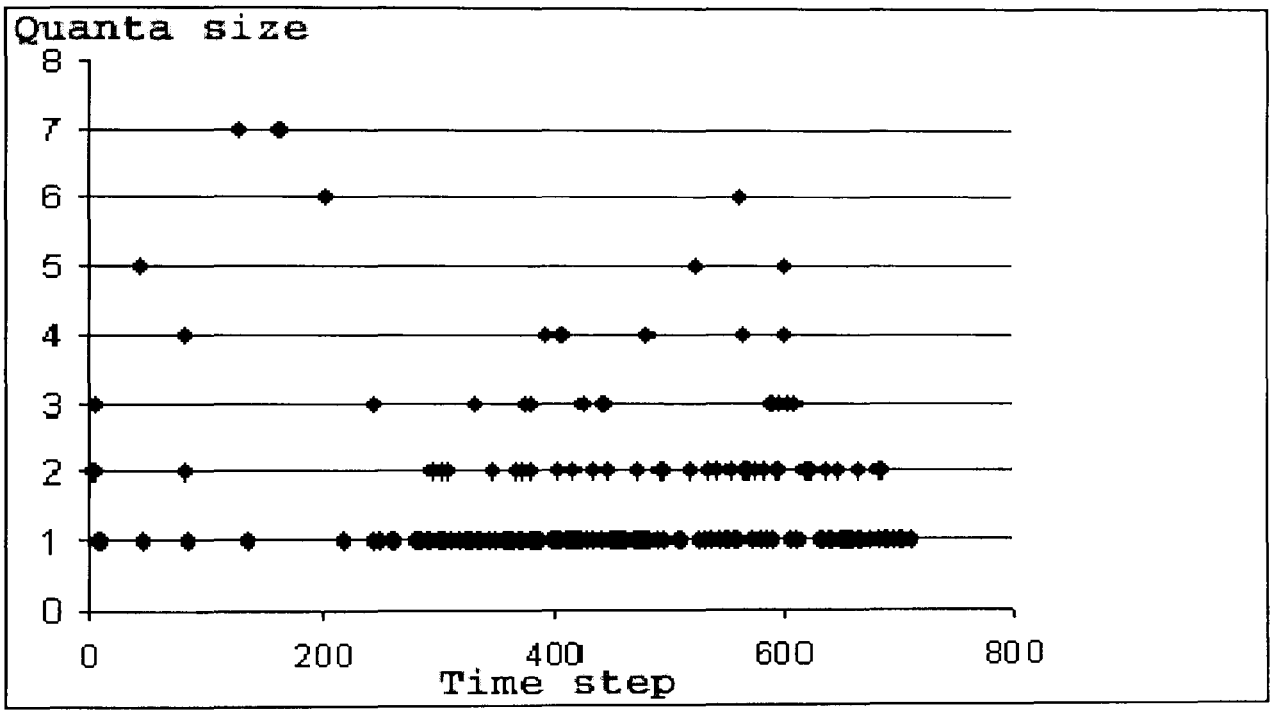

Fig. 5.1. Carrier population crossing end plane z=30, MP[30]

The model allows ten positive and ten negative equal increments of the $E - Field$ vector $\overrightarrow{E_{x,y,z}}$ to be applied across the lattice faces in the z plane. The plot in Figure: 5.3 shows the current that flows as a result of the $E - Field$ vector $\overrightarrow{E_{0,0,z}}$ in the z lattice direction, applied to opposite ends of the lattice, over the range 0 to +9 units ($\overrightarrow{E_{0,0,0}}$ to $\overrightarrow{E_{0,0,9}}$). The current, or the number of carriers flowing out of the end

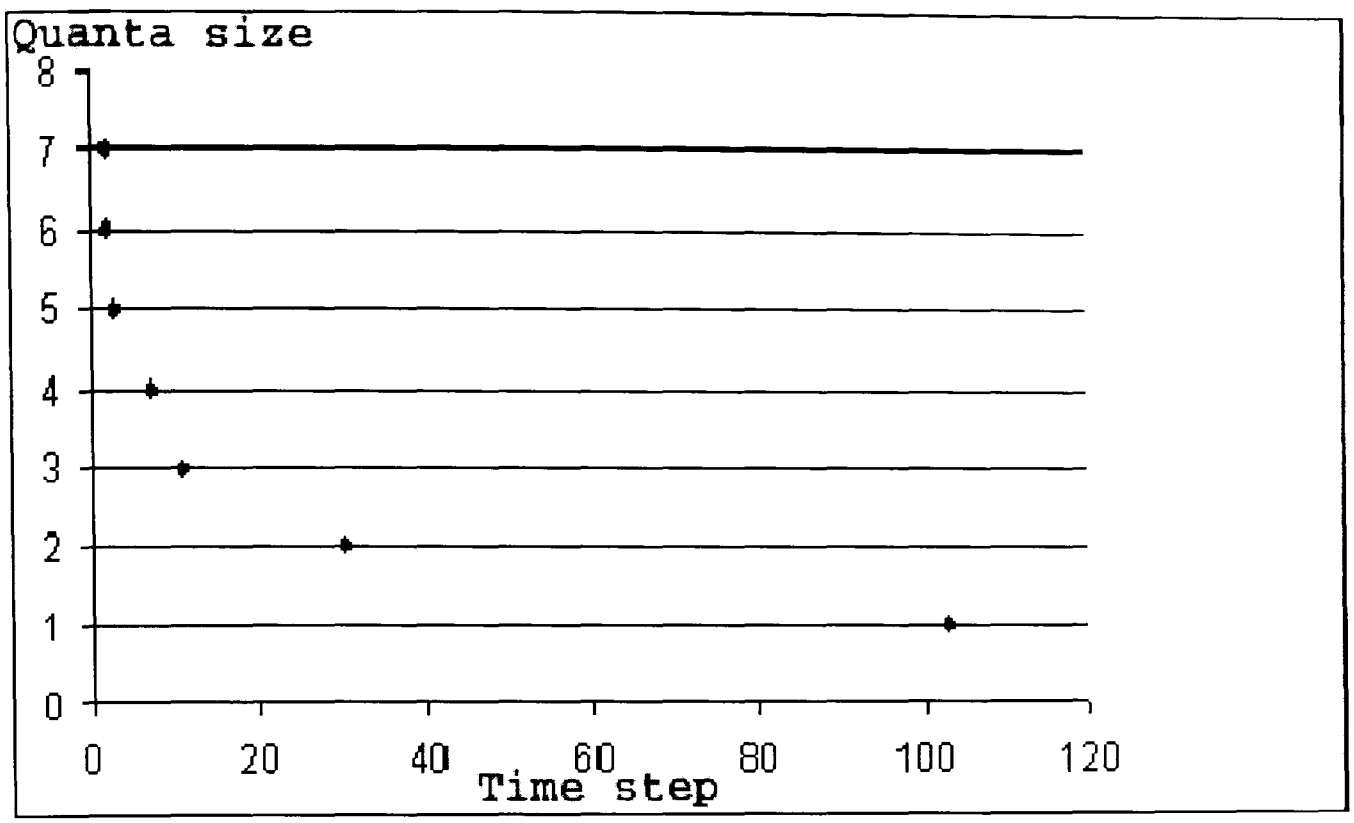

Fig. 5.2. Right half of carrier distribution measured at MP[30]

measurement plane, MP[32], is shown on the vertical y-axis, and the $E-Field$ on the x-axis. The solid line in Figure: 5.3 is the best linear equation fit, to the data points taken from the output of the JAMES model. The slope of this equation indicates a linear dependence of the current on the $E-Field$ as expected. The model in this instance used a carrier population of 16 electrons at $(N_d = 3.87 \times 10^{23}).m^{-3}$, in a lattice of $32,768$ cell $LU's$.

5.2.1 Shot Noise

The shot noise behaviour was chosen to illustrate the ability of the model to represent the carrier transport behaviour in a real semiconductor junction. The base region of width was defined between $12-18$ lattice units as represented by B1 in the idealised simulation structure is shown in Figure: 5.4. The P and N region impurities were defined in the appropriate regions, and the field was set at a fixed value. The carrier population was increased on a number of runs where only the carrier density was increased. The total simulation time was left constant, at a constant field in

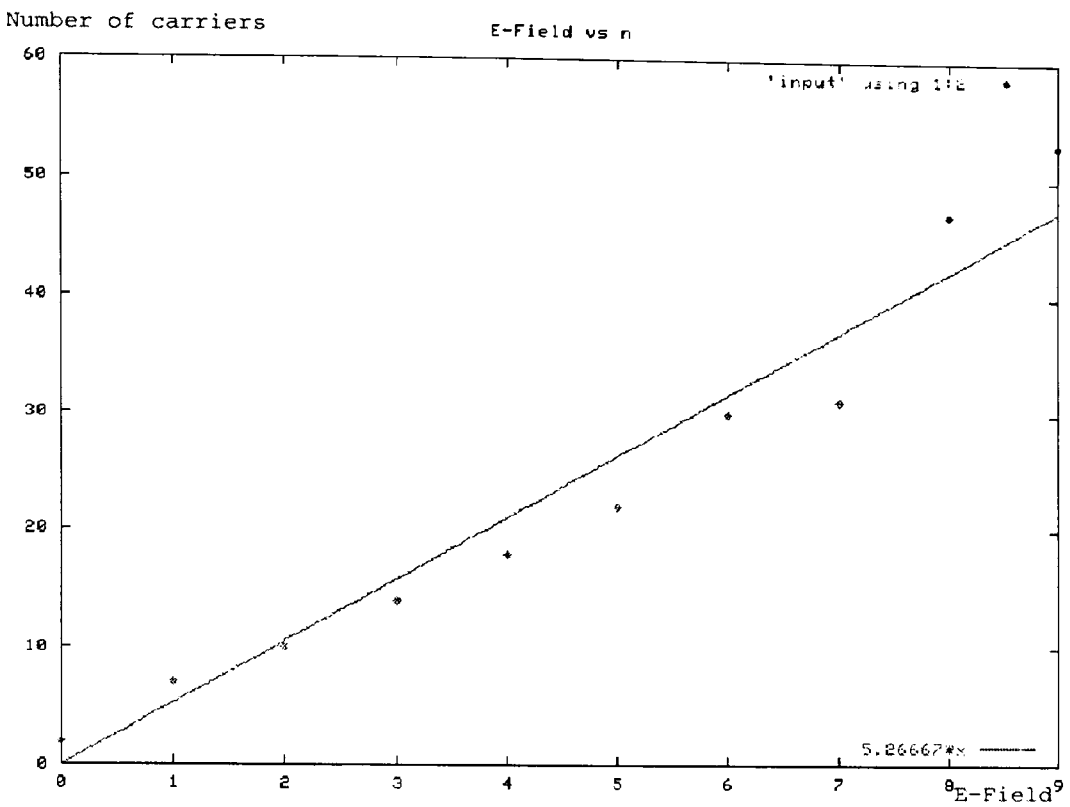

Fig. 5.3. Current vs E-Field

the direction of the current flow. The current flowing was calculated, and also the spectral density of the individual carrier population crossing the measurement plane, see Algorithm: 45. The measurement planes were chosen to coincide with the ends of the crystal in this case as shown on Figure: 5.4. The value obtained from the JAMES simulator, see Algorithm: 45, indicates that $_{K_{SA}}$ can be reduced from 1.0 to 2.31×10^{-3} giving a $-26.4dB$ reduction in spectral density. For a typical BJT device shown in Figure: 7.5, with the following parameters; the transconductance $gm = 0.71$, the DC gain $\beta_F = 100$, and the intrinsic base resistance $r_b = 12\Omega$. Before the application of the noise reduction mechanism, $K_{SA} = 1$, and the total input referred base noise shown in Figure:C.1 is $S_i = 4.8 \times 10^{-20}$. The optimum source resistance R_{Sopt} for lowest total noise in a conventional device, using the Gray model [15] , can be shown to be 60Ω, with the parameters above. This represents a noise factor of 1.41 and a noise temperature of $122^{o}K$. The reduction in total input referred base noise, due to the reduction of the factor K_{SA}, means a total input referred noise of $S_i = 1.67 \times 10^{-22}$. is achieved, as shown in Appendix: {C.1}. This is an improvement of $-24.6dB$ in the

spectral density of the shot noise, and an improvement of $-9.7dB$ in the equivalent total input referred base noise current. With $K_{SA} = 3.47 \times 10^{-3}$, it can be shown that the optimum value of R_{Sopt} at the input of 7.13 increases to 345Ω under the same conditions.

5.2.2 Simulation conditions

The simulator was set for a $3D$ cube of 30 $LU's$ per side, to give a reasonable execution time, i.e. a total of $27,000$ $LU's$, as shown in Figure: 5.4.

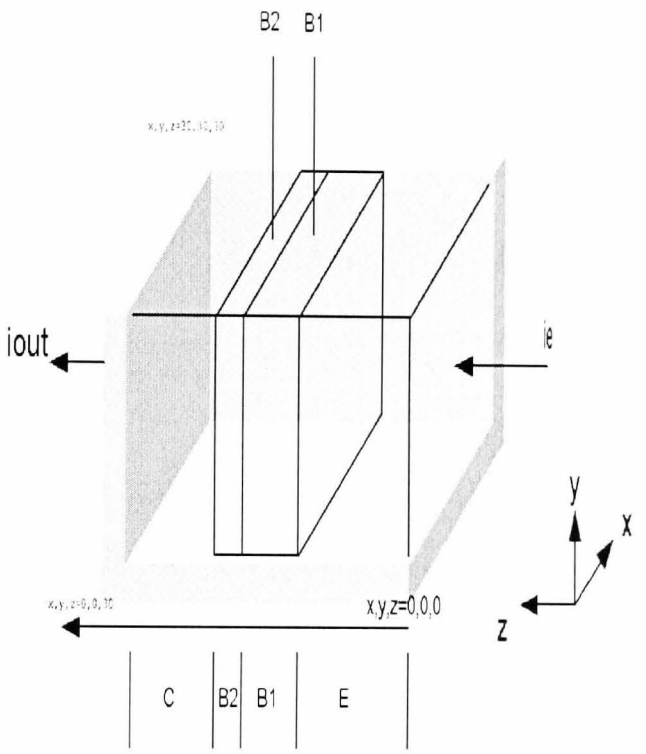

Fig. 5.4. 3-D crystal structure 30x30x30 cell LUs

The size of the lattice chosen is much smaller than an actual device, even by todays small transistor geometry. The state of the art at the time of writing is approximately $0.10um$. The transistor length, defined as the physical distance between the emitter and collector junction, is about the same as an integrated BJT device. The average transit time for a carrier was measured to be around $5.2pS$, after a broad correlation with real-time. A chart showing the correlation between the theoretical Poisson limit for the shot noise spectral density, and the actual measured value from the simulator is shown in Figure: 5.5.

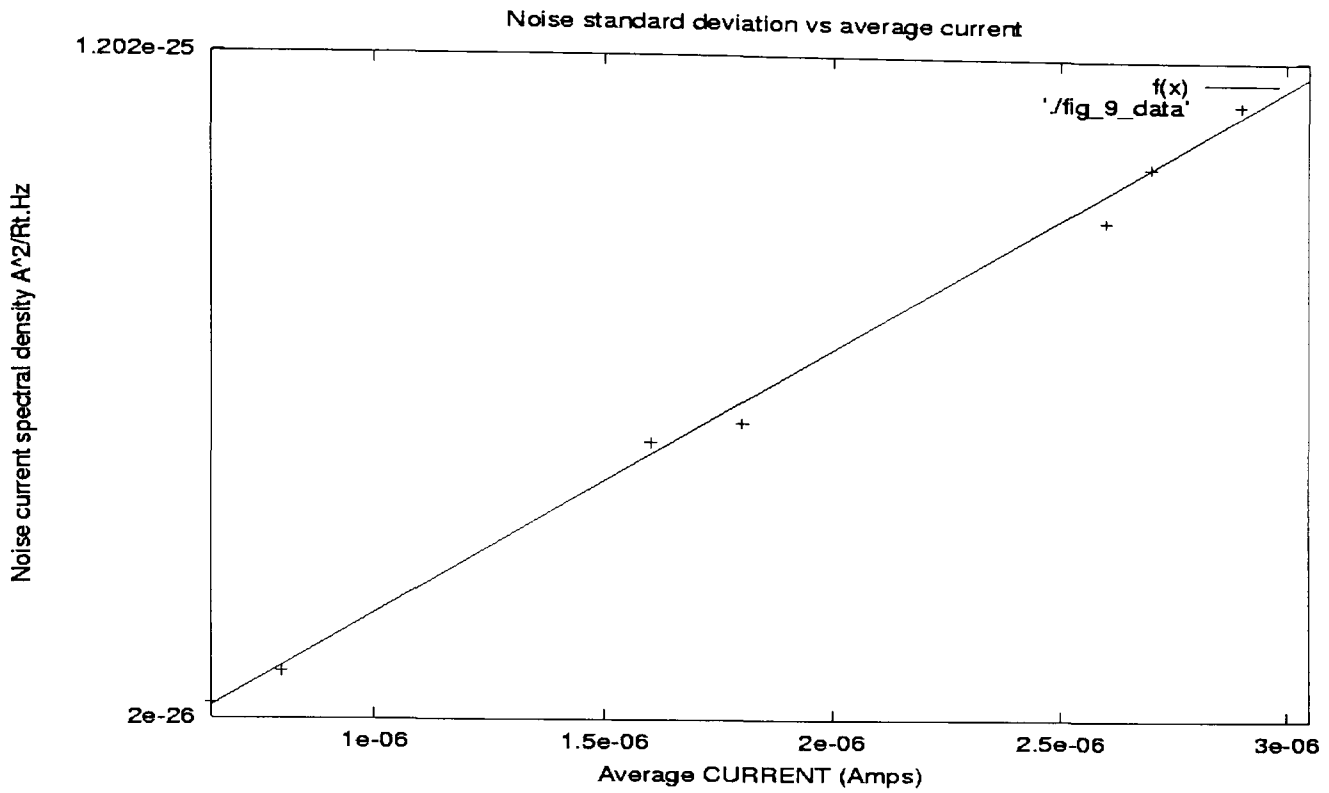

Fig. 5.5. Spectral density vs average current

The plot in Figure: 5.5 shows the theoretical spectral density and the actual modelled (calculated) value of spectral density calculated on the movement of the individual carriers at the end surface $z = 30$ of the crystal. They are both measured against the average current flowing through the lattice. The two plots should be identical if the model is accurately representing the carrier behaviour, and there is a large population of carriers. There is a switch at each of the entry and exit points for each of the device regions to allow charge control. The switch (the uniform variable) allows the charge control of the BASE1, BASE2 and the *collector* regions to be abandoned, and the device behaves as a single P-N junction or *diode*. The output is observed under the following conditions. The P-type dopant concentration was set to $N_a = 10 \times 10^{16}.m^{-3}$, and the N-type region impurity concentration set to $N_d = 3.876 \times 10^{23}.m^{-3}$. This simulation is carried out on a crystal size $30 \times 30 \times 30$ or $27,000$ silicon $LU's$. The first measurement plane MP_1 is placed near the *emitter* recombination surface at $z = 4$, and the second measurement plane MP_2 is placed at $z = 12$, just beyond the *emitter-base* contact region. The MP_2 plane therefore

observes the spectral density of the carrier flow as the carriers emerge from the emitter region. This corresponds to the carriers crossing the potential-barrier in an actual diode. The actual spectral density can be compared to the theoretical value calculated from the Poisson equation Eq. 1.4, and this is shown in Figure: 5.5. The graph in Figure: 5.5 shows a good correlation between the two as expected, considering the very small population of about 36 carriers crossing the measurement plane. The data in Figure: 5.5, represents the computed shot noise spectral density calculated during each NTDU, and the solid line the best fit linear function represents the theoretical spectral density from the Poisson equation Eq. 1.4.

5.2.3 Low noise structures

The objective declared at the start was to model the carrier transport behaviour in relation to noise and the physical structure of the semiconductor device. This gives a specific objective, and provides a vehicle to refine the model. The model has been used to analyse some new physical semiconductor structures, and to study the charge transport and charge density at each stage of the simulation. The structure of a BJT shown in Figure: 5.4 was defined in the model, and used as an initial idealised model for studying the shot noise. The graphs shown in Figures: 5.6, 5.7 and 5.8, show results obtained from the putting the structure of Figure: 5.4 into the model. The graph in Figure: 5.6 shows the probability density of carriers crossing from the emitter E into the base1 B1 region MP[0,0,12] of the crystal in Figure: 5.4 during the simulation without the additional BASE2 in operation. The wide variation in the amplitudes of the quanta shows the normal spectral density from the collector current. The graph in Figure: 5.8 shows the same histogram with the BASE2 algorithm operating without the by-pass and with its external connection. The much smaller amplitude variance and the higher incidence of single carriers show the reduction in the spectral density of the current. The comparison here is a simple visual one. The time duration, and hence the number of carriers recorded on the x-axis was truncated in Figure: 5.8.

The P type base region and the N type emitter and collector doping levels are

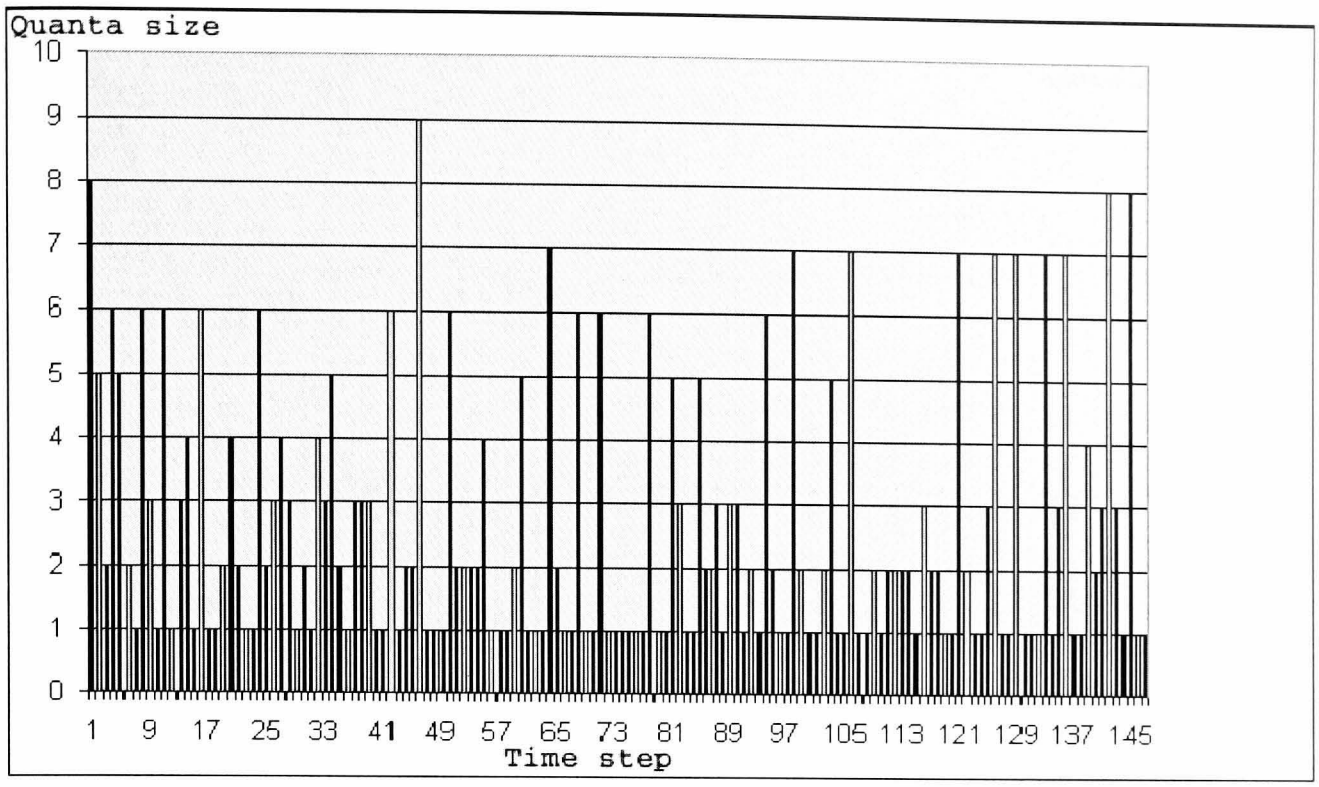

Fig. 5.6. Input spectral density

defined at the initialisation of the model. The three contacts E, B and C represent the emitter, base and collector of the BJT. The Emitter N type region was set to an impurity level of $N_D = 2 \times 10^{23}.m^{-3}$, the base P type region was set to $N_A = 2 \times 10^{24}.m^{-3}$, and the collector N type region to $N_D = 2 \times 10^{22}.m^{-3}$. The graph in Figure: 5.6 shows the collector current flow at the individual carrier level. This represents the normal shot noise and the noise spectral density measured at the collector. The graph in Figure: 5.7 shows the right side of the carrier probability distribution as it emerges from the end plane at MP[30] with the new BASE2 doping conditions included. The spectral density of the individual charge carriers is equal to the variance of the individual charge impulse-function, around the mean value, in this case the y-axis. The variance can be seen to be reduced in Figure: 5.7, between the normal shot-noise variance labelled "input", and the narrower spread or variance labelled "output" after the BASE2-collector junction. The "output" trace also has a higher number of "singulated" carriers i.e. quanta = 1.

Since the variance σ of each of the distributions "input" and "output" in 5.7, gives

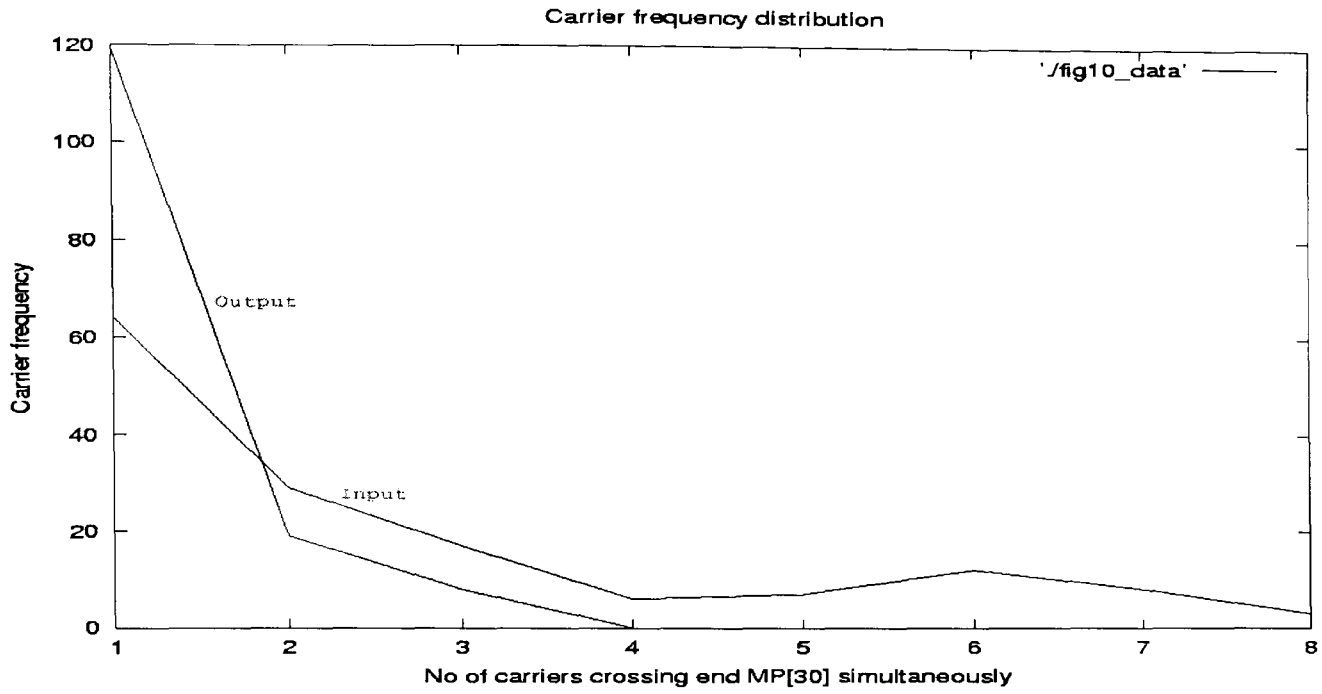

Fig. 5.7. Output spectral density with and without suppression

the spectral density, the ratio of the two gives the new factor K_{SA}, so

$$K_{SA} = \frac{\sigma_{output}}{\sigma_{input}} = \frac{SD_o}{SD_i}$$

By inspection of the two distributions in Figure: 5.7, it is evident there is a reduction in the value of K_{SA}, validating the usefulness of the model, at a broad level.

5.2.4 Summary of simulation results from JAMES

The spectral density of the carriers at the output can be seen to be considerably reduced, because of the small number of impulses varying from the value 1.0 in Figure: 5.8. The perfect current with a $S_i = 0\ A^2/Hz$ would be a histogram where all amplitudes were equal to one, indicating all the carriers were singulated and cross the barrier at a separate time step. The average number of carriers in the noise quanta before shot noise reduction Figure: 5.6 is 3.3 , and this is reduced to 1.2 in Figure: 5.8.

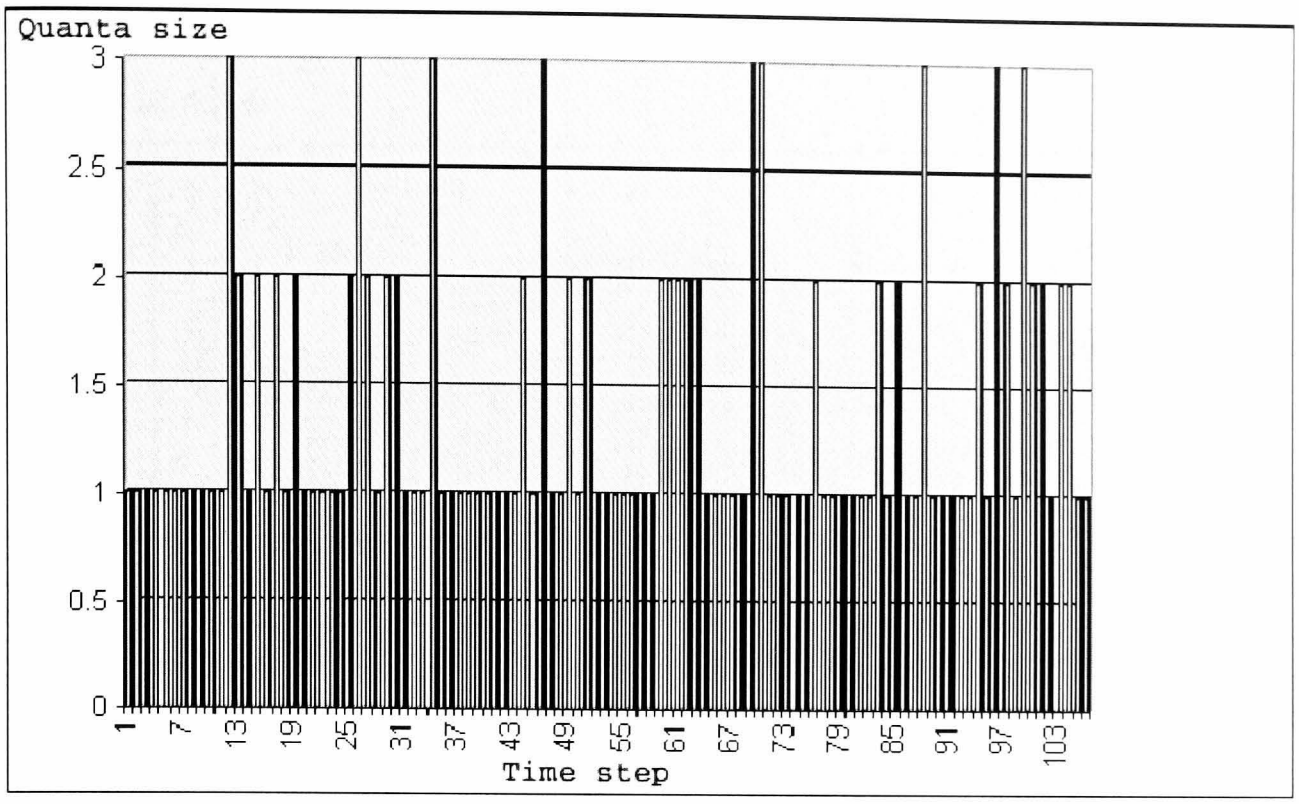

Fig. 5.8. Output spectral density

5.2.5 Post run output analysis

During program execution the spatial and temporal results are stored at each time step in the shadow matrix. The graphical interface for post-processing permits additional observation planes (OP's) to be positioned in any plane to observe matrix carrier activity. Although the charge transport can be monitored and analysed at LU or bond level, the shadow matrix implemented in the present model holds the activity at a maximum of one LU resolution only, and the electron shell level storage would increase the memory requirements to 16 times the present resolution. The model currently implemented allows the charge or current density $J_{i(x,y,z,t)}$ and any LU in the crystal to be monitored. This feature allows the current density in the lattice to be evaluated and displayed to see the behaviour with doping level, physical parameters such as region length, electric field $E_{(x,y,z)}$, applied across the ends of the crystal, or $E_{(x,y,z)}$ within specific regions e.g. in the BASE region. The surface plot of Figure: 5.9 shows a plane taken across the z-axis orthogonal to the $E_{(0,0,z)}$ field.

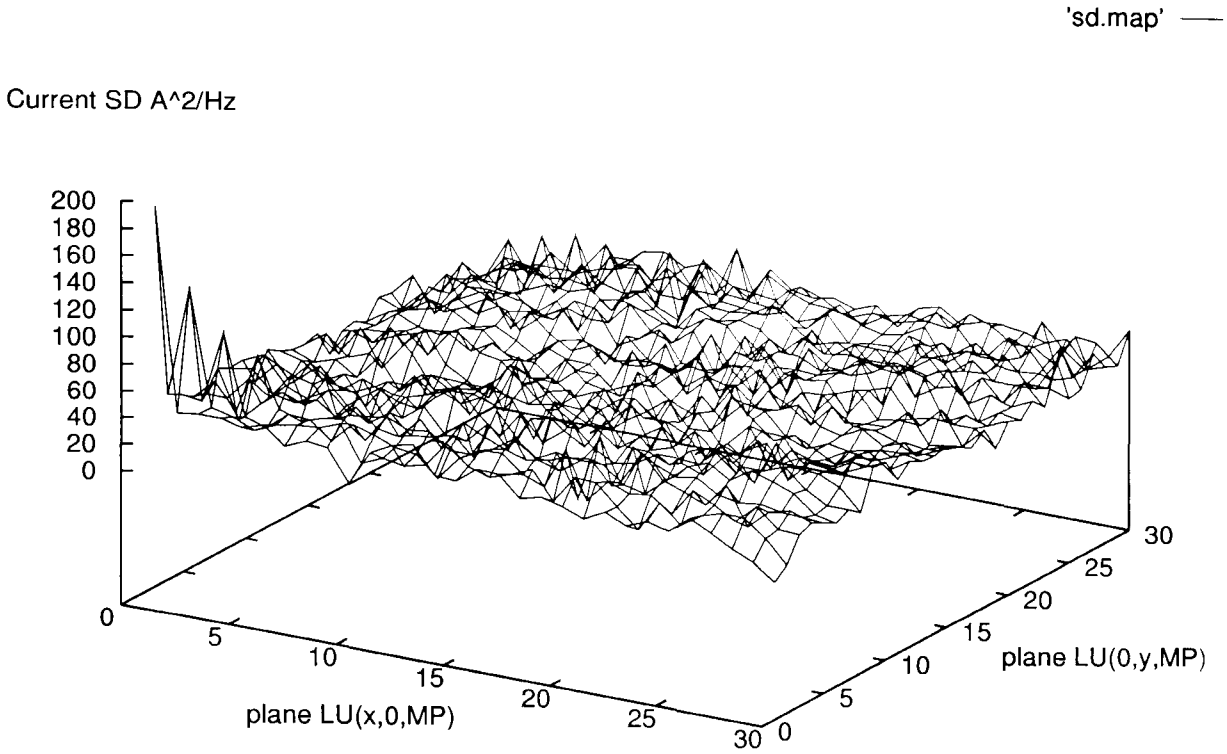

Fig. 5.9. Spatial distribution of charge transport OP[16]

The surface plot was captured on the surface of a OP (observation plane), orthogonal to the $E_{(0,0,0.33)}$ field when the OP was positioned at $z = 16$ in the BASE2 region just above the BASE1 and BASE2 junction. The plot shows a reasonably uniform distribution of carriers in steady state across the OP.

The 2D histogram shown in Figure: 5.10 shows a typical plot of the current density $J_{(x,y,z)}$ with the z-axis showing the axis with an $E_{(0,0,0.33)}$ field units applied in the direction from $z = 0$ to $z = 30$. The idealised physical structure is shown in Figure: 5.4, with the *emitter* region defined from $z = 0$ to $z = 4$ LUs ,the *emitter-base* junction from $z = 4$ to $z = 9$, the BASE1 region from $z = 9$ to $z = 14$, the BASE2 region from $z = 14$ to $z = 20$, and the collector region from $z = 20$ to $z = 32$. The histogram shows the current density $J_{(x,y,z)}$ of the x-axis vs the z-axis with the number of carriers at that location on the z-axis. The vacant region across the x-axis from $z = 4$ to $z = 9$ is the potential barrier region. The histogram in Figure: 5.11 shows the graph in Figure: 5.10 rotated to view the opposite side, where the base1 and BASE2 infinite recombination surfaces are located. The region from $z = 14$ to

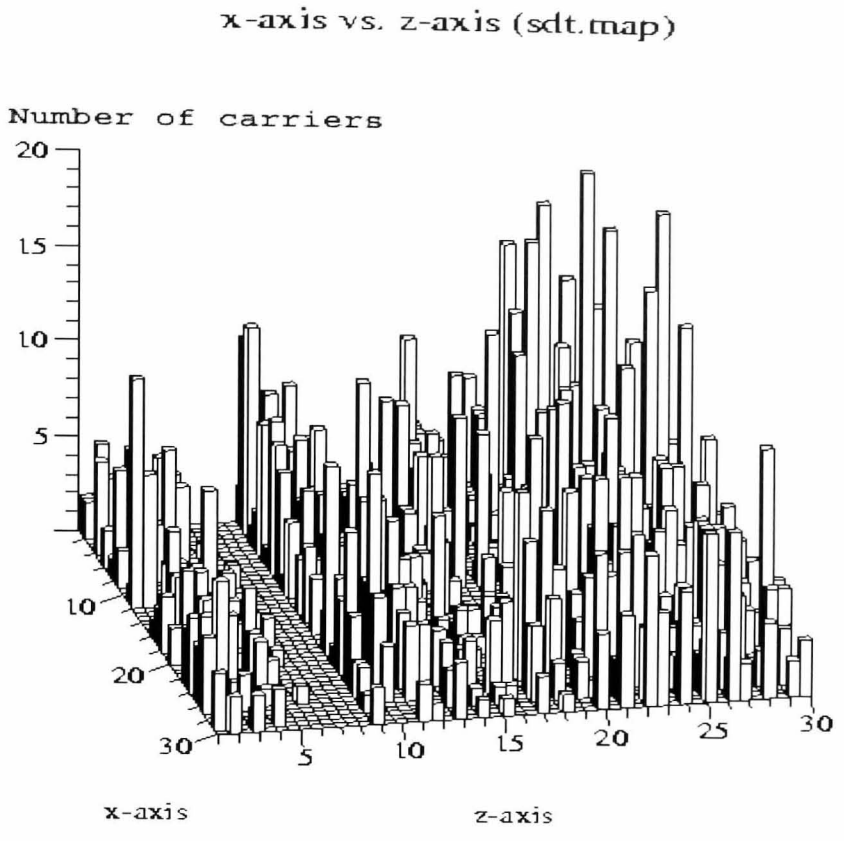

Fig. 5.10. Current density $J_{(x,y,z)}$ vs position (x, z)

$z = 20$ shows much lower current density levels near the contact surface located at $x = 0$. The plots in Figures: 5.9, 5.10 and 5.11 are derived over the full range of time steps, in this case 300.

The plot shown in Figure: 5.12 shows the same physical conditions, however instead of showing the current density $J_{(x,y,z)}$ in the lattice, the histogram shows the current density $J_{(x,12,t)}$ where a horizontal OP is positioned across the lattice parallel to the $< x, y >$ plane and plot the z histogram versus the time step t.

The x-axis (left) is shown against the time axis (right). The evolution of the matrix can be visualised by observing each of the rows parallel to the z-axis evolving one time step away from $t = 0$ towards $t = 300$.

5.2.6 The effect of the new BASE2 structure

The use of the model to study the shot noise in true 3-D at the *emitter-base* junction reveals the following conclusions. The cause of the shot noise is due to multiple

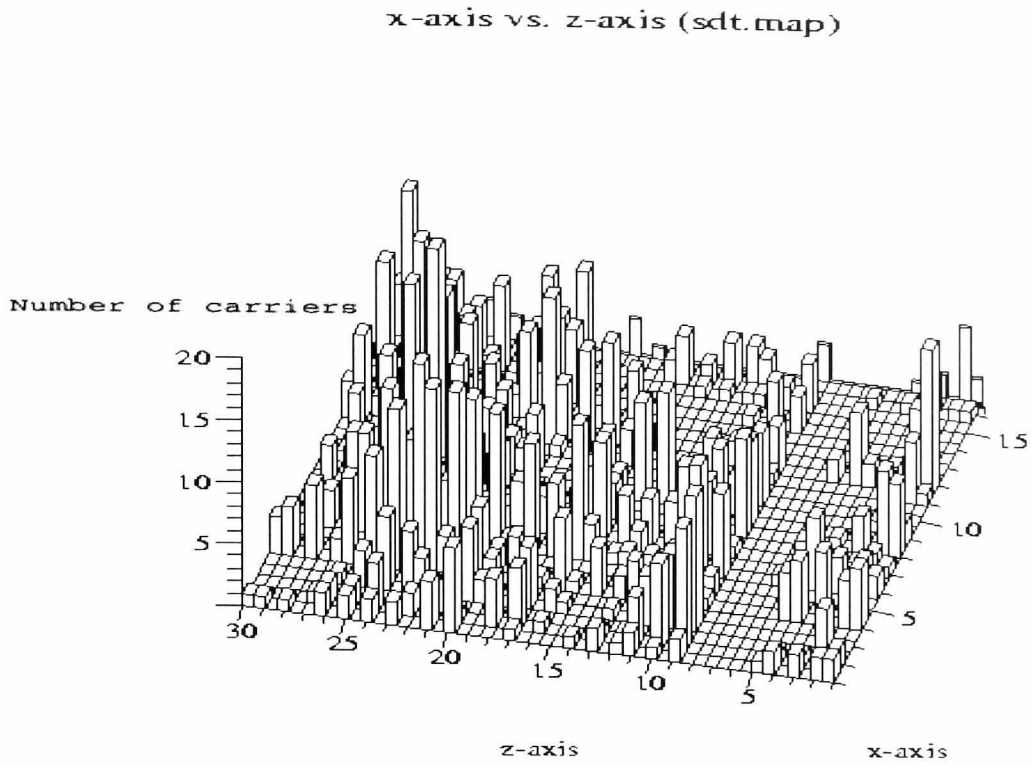

Fig. 5.11. Current density near the BASE2 contact vs position (x, z)

carriers crossing the emitter-base junction simultaneously as mentioned previously. The shot noise can be reduced by re-thermalising the minority carriers in the base. The graded base transistor is a well known technique used in fabricating a BJT to speed up the base transit time and so increase the high frequency cut-off. This is achieved by creating a built-in $E - Field$ to help accelerate the minority carriers. The base conduction is the sum of the drift and diffusion of these carriers. The normal ungraded base BJT has no drift component due to a uniform doping gradient in the base, and so the base transit time is due only to the diffusion length and the base width. The minority carriers are rapidly swept into the collector region, and so the shot noise is un-attenuated. The technique of speeding up the transit time to increase the f_T of the device does nothing to reduce the shot noise,and so they are contradictory requirements in a simple homo-junction device. The proposal outlined here is to create an *inverse graded* base over a part of the combined base region in order to reduce the shot noise. The necessity of reducing the maximum potential f_T in order to reduce the shot noise seems clear, if the BASE2 width can not be

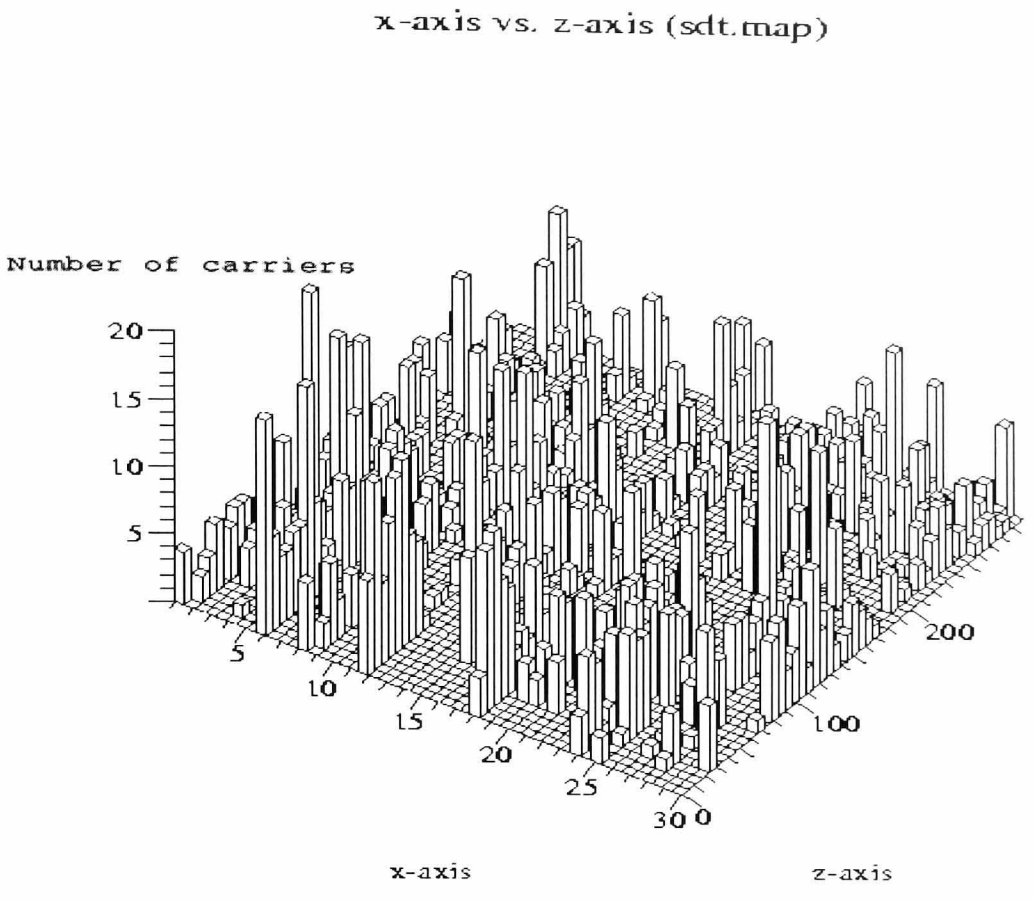

Fig. 5.12. Histogram of current density $J_{(x,12,t)}$ vs position (x, z)

accommodated inside the available BASE1 dimension. This can be done by forcing recombination in the BASE2 region long enough to re-thermalise the carriers. This can have some disadvantages when compared to an optimised high-frequency device. The increased recombination in the new region will also increase the recombination current through the external contact to that region. A number of ways exist to create a high recombination region in between the signal base and the collector region. The intention here is to demonstrate the principle rather than design the BJT device, and so the following section illustrates the principle of using a highly doped region in the base of a homo-junction silicon BJT.

6. CONVENTIONAL ANALYSIS OF THE ADDITIONAL BASE REGION

ANALYSIS OF THE BASE1 AND BASE2 DIFFUSION CHARGE

Assuming a step change in the BASE1 to BASE2 doping profiles for this analysis, the minority carrier recombination rate in the base region of a BJT can be shown to be proportional to the excess minority charge above the equilibrium level. The equilibrium minority carrier level in a P-type region is equal to

$$n_o = \frac{ni^2}{N_A}$$

where n_i is the intrinsic level and N_A is the doping level of the region in the absence of any $E - Fields$. The minority carrier level at the base edge of the emitter-base junction is given by

$$p_{n1} = n_i^2 exp \frac{eV_D}{kT} \tag{6.1}$$

and is shown in Figure: 6.3. The current flowing from the emitter to the collector is assumed to be constant, and for the purposes of this 2-D analysis the recombination is assumed to be negligible in the base regions, relative to the emitter current. Since the current flow is due to diffusion the current flow is given by

$$I_c = A_e D_n \frac{dn}{dx}$$

from Eq. 3.15, the slope of the minority carrier profile is assumed to be linear from the value p_{n0} to zero at the base edge of the base-collector depletion region. The distribution of charges in both bases are shown in Figure: 6.1, where $-Q_{B1}$ is the minority charge.

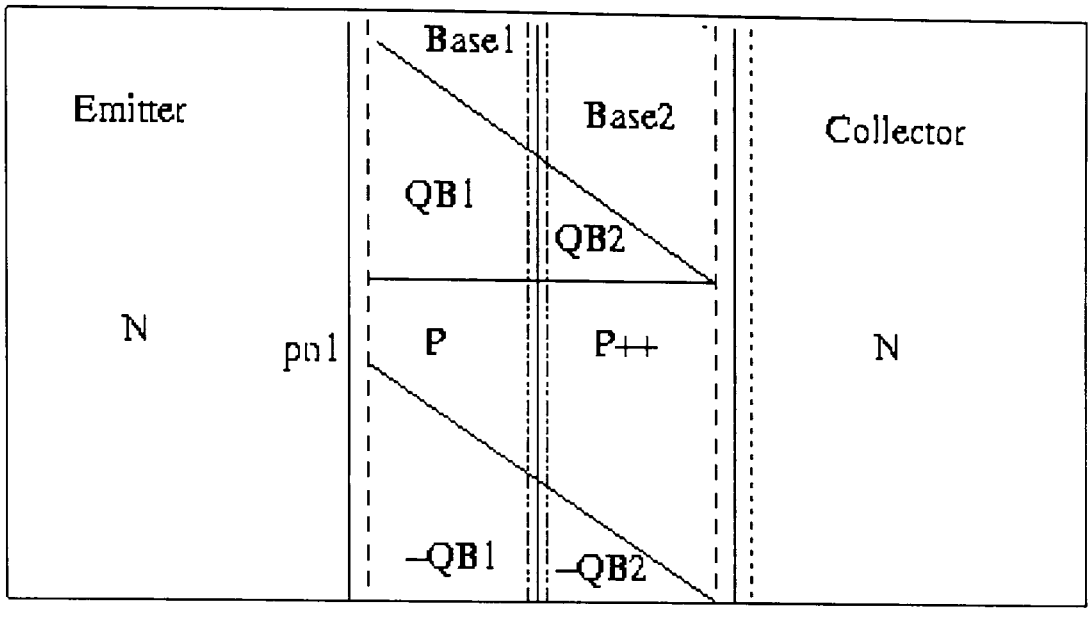

Fig. 6.1. Charge in LNBJT bases

The minority charge $-Q_{EB1}$ is given by

$$-Q_{EB1} = q \cdot A \int_0^{W/2} n_p dx$$

$$= q \cdot A \int_0^{W/2} pn_{(0)} \left[1 - \frac{x}{W}\right] dx$$

$$= q \cdot A \cdot pn_{(0)} \int_0^{W/2} (1 - \frac{x}{W}) dx$$

$$= q \cdot A \cdot pn_{(0)} \left[x - \frac{x^2}{2W}\right]_0^{W/2}$$

giving

$$-Q_{EB1} = \frac{3 \cdot q \cdot W \cdot A \cdot pn_{(0)}}{8} \tag{6.2}$$

repeating for BASE2

$$-Q_{EB2} = q \cdot A \int_{W/2}^{W} pn_{(0)} dx$$

$$= q \cdot A \cdot pn_{(0)} \left[x - \frac{x^2}{2W}\right]_{W/2}^{W}$$

$$-Q_{EB2} = \frac{q \cdot W \cdot A \cdot np_{(0)}}{8} \tag{6.3}$$

now

$$-Q_{EB} = -(Q_{EB1} + Q_{EB2})$$

giving

$$-Q_{EB} = \frac{3 \cdot q \cdot W \cdot A \cdot np_{(0)}}{8} + \frac{q \cdot W \cdot A \cdot np_{(0)}}{8} \tag{6.4}$$

The BASE2 charge is 33% of the BASE1 charge for equal BASE1 and BASE2 lengths. The reduced diffusion capacitance in the BASE2 region means this base is capable of greater high frequency performance, for the same source impedance as compared with the signal base, BASE1.

THE EFFECT OF THE ADDITIONAL BASE2 ON TRANSIT TIME

Again assuming that BASE2 is the same length as BASE1, the simplified expression for minority carrier lifetime is given by

$$\tau_B = \frac{Q_B}{I}$$

this gives

$$\tau_{B1} = \frac{3qWAnp_{(0)}}{8} \cdot \frac{1}{qAD_{eB1}\frac{np_{(0)}}{W}}$$

$$= \frac{3 \cdot W^2}{8.De_{B1}}$$

and

$$\tau_{B2} = \frac{qWAnp_{(0)}}{8} \cdot \frac{1}{qAD_{eB2}\frac{np_{(0)}}{W}}$$

$$= \frac{W^2}{8.D_{eB2}}$$

and assuming the current is the same through both base regions

$$\tau_B = \frac{W^2}{8}\left[\frac{3}{D_{eB1}} + \frac{1}{D_{eB2}}\right]$$

now where u_e is the non graded base mobility

$$D_e = V_t.\mu_e$$

which gives

$$D_e = \frac{kT\mu_e}{q}$$

putting in terms of the base mobility factors

$$\tau_B = \frac{W^2 q}{8kT}\left[\frac{3}{\mu_{eb1}} + \frac{1}{\mu_{eb2}}\right] \tag{6.5}$$

The base transit time for a non-graded base is given by

$$\tau_B = \frac{W^2}{2D_e}$$

or in terms of mobility

$$\tau_B = \frac{W_B^2 q}{2kT \cdot \mu_e}$$

comparing the effect on τ_B of adding the additional base where τ_B is the *total* (BASE1+BASE2) transit time, the degradation factor F is given by

$$F = \frac{W^2.q}{8 \cdot kT}\left[\frac{3}{\mu_{e_{b1}}} + \frac{1}{\mu e_{b2}}\right] \cdot \frac{1}{\frac{W^2 q}{2kT\mu_e}}$$

$$= \frac{\mu_e}{4}\left[\frac{3}{\mu eB_{b1}} + \frac{1}{\mu_{e_{b2}}}\right]$$

the mobility factor for BASE2 is approximately half that of BASE1 for this relative doping level and substituting in Eq. 6.5 gives

$$\tau_B = \frac{\mu_e}{4}\left[\frac{3}{\mu_e} + \frac{2}{\mu_e}\right]$$

If $\mu_{e_{b1}}=\mu_e$, this gives the new value for $\tau_B = 1.25$ times the value of an ungraded base. Considering the effect of the overall BASE1 and BASE2 grading with no current flowing

$$J_h = qp_p\mu_h E(x) - qD_h\frac{dp_p}{dx}$$

Then if $J_h = 0$ then

$$E(x) = \frac{D_h}{\mu_h} \cdot \frac{1}{p_p} \cdot \frac{dp_p}{dx}$$

giving

$$E(x) = \frac{kT}{q} \cdot \frac{1}{p_p} \cdot \frac{dp_p}{dx}$$

This is approximately correct for low levels of injection also. Assuming the case where the overall base region doping varies linearly with distance, as is typical of a standard diffused BJT, and assuming $N_a(0)$ is the doping level at the edge of the base region near the emitter.

$$N_a(x) = N_a(0) + \frac{(N_{a2} - N_{a1})x}{W}$$

where W is the overall base region width , and x is the distance from the start of the base region up to the edge of the base-collector depletion region, and therefore

$$p_p(x) = p_p(0) + \frac{(N_{a2} - N_{a1})x}{W}$$

$$\frac{dp_p}{dx} = \frac{(N_{a2} - N_{a1})}{W}$$

and so

$$\frac{1}{p_p} \cdot \frac{dp_p}{dx} = \frac{(N_{a2} - N_{a1})}{W \cdot p_p}$$

since

$$E(x) = \frac{kT}{q} \cdot \frac{1}{p_p} \cdot \frac{dp_p}{dx}$$

and the base transit time is given by

$$\tau_t \simeq \frac{W_B}{\mu_e \cdot E(x)}$$

and so

$$\tau_t = \frac{qW_B^2 \cdot p_p}{\mu_e kT(N_{a2} - N_{a1})}$$

for $N_{a2} \neq N_{a1}$. Since the non-graded base transit time

$$\tau_{ngt} = \frac{W_B^2 q}{2kT\mu_e}$$

The overall change in the transit time is given by the factor δ

$$\delta = \frac{\tau_t}{\tau_{ngt}}$$

this gives

$$\delta = \frac{2p_p}{(N_{a2} - N_{a1})}$$

where $N_{a2} \neq N_{a1}$. For a p-type inverse graded base with a linearly graded doping density of 1×10^{20} at the emitter end up to 1×10^{21} at the collector end, where BASE2 is equal to the BASE1 width. The increase in the overall τ_b would be

$$\frac{2 \times 0.5 \times 10^{21}}{(1 \times 10^{21} - 1 \times 10^{20})} = 1.11$$

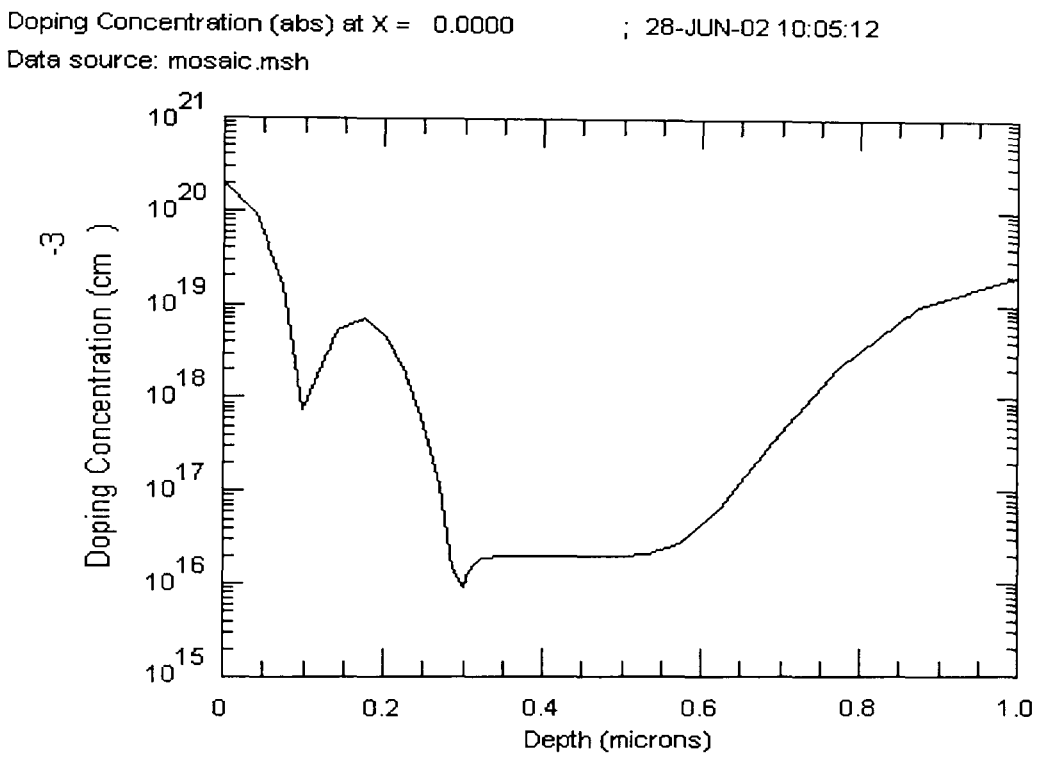

Fig. 6.2. An example of a LNBJT device doping profile

The grading profile of Figure: 6.2 however can be created, and due to the symmetrical nature of the profile , the increase in the delay transit time of the low to high dopant density boundary, can be offset with an identical or greater high to low density step or drop on the collector side. This gives no net increase in the base transit time, and can reduce it with the correct doping profile.

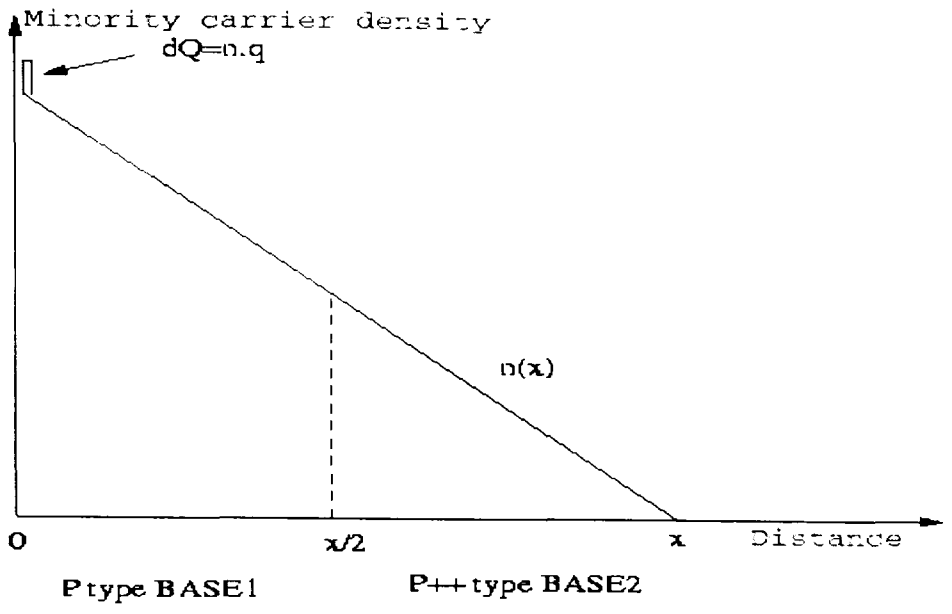

Fig. 6.3. Minority carrier profile in the base regions

RECOMBINATION AND GENERATION

The dynamic behaviour of the minority carrier profile can be calculated as follows. Recombination and generation are always closely related; a high recombination rate is always accompanied by a high generation rate, also different recombination and generation rates lead to different rates of recovery to equilibrium after the carrier densities have been disturbed. The result is that in equilibrium $p_0 \cdot n_0 = ni^2$ whatever the recombination rate. The number of carriers recombining per unit volume per unit time, the recombination rate is proportional to the carrier densities. The recombination rate

$$r = \alpha \cdot n \cdot p \tag{6.6}$$

where α is a constant. In equilibrium $r = g$, whose value depends on the material and on the energy inputs, usually thermal and optical. Consequently, in equilibrium, $r = \alpha \cdot n_0 \cdot p_0 = g$. Given $\frac{g}{\alpha}$ is a constant for a particular semiconductor under given energy inputs, $p_0 \cdot n_0$ =constant. This constant is n_i^2 when the only energy input is thermal, and it is very temperature dependent. The pulse at the top left of Figure: 6.3 disturbs the equilibrium caused by the constant slope of the diffusion profile. The recombination rate for this pulse will be increased until equilibrium is restored i.e.

the constant slope of the profile. The lifetime in the BASE1 region is relatively long , many times the base1 transit time τ_{B1}, and so the pulse will propagate down the slope, with relatively little decay until it reaches the BASE1 to BASE2 junction at $\frac{x}{2}$. The BASE2 region is designed to have a relatively high recombination rate, and the pulse will decay much more rapidly when it enters this region. The minority carrier level with the noise quanta superimposed at the instant of injection is given by $n = n_{e1} + n_0$, where $n_{e1}$where n_0 is the density of the stable profile at that instant. Assuming n_{e1} is not too large , so that the change in electron density is negligible, then the net decrease in electron density (recombination - generation) is proportional to the excess, $n_e = n - n_0$, so that

$$-\frac{dn_e}{dt} = \frac{n_e}{\tau_e}$$

this gives

$$n_e = n_{e1} exp(-t/\tau_e)$$

where τ_e is the electron lifetime in the p-type region of interest. The value of τ_e is the average time taken for the extra electrons to recombine in the region. The profile in Figure: 6.3 assumes the minority carriers are being constantly injected at the left hand side of the figure from a constant emitter current, and the magnitude of the carrier density is given by Eq. 6.1. The relationship between the minority carrier decay after a disturbance and the distance now needs to be determined. The continuity equation for a one dimensional flow is given by

$$| -\frac{1}{e} \cdot \frac{dJ_n}{dx} = \frac{dne}{dx}$$

since the electron current is a diffusion current

$$J_n = -e \cdot D_n \cdot \frac{dn_e}{dx}$$

so

$$\frac{n_e}{\tau_n} = \frac{1}{e} \cdot \frac{d}{dx} \cdot \left[eD_n \frac{dn_e}{dx} \right] = D_e \frac{d^2 n_e}{dx^2}$$

Solving the second order linear differential equation , and for the boundary conditions $n_e = n_{e1}$ when $x = 0$ and $n_e = 0$ when $x = \infty$. This gives

$$n_e = n_{e1} \cdot exp\frac{-x}{\sqrt{(D_e\tau_e)}}$$

This can be written as

$$n_e = n_{e1} \cdot exp\frac{-x}{L_e} \tag{6.7}$$

where

$$L_n = L_e = \sqrt{(D_e\tau_e)} \tag{6.8}$$

L_e being the electron diffusion length. The is the length shown in Figure: 3.7.

CALCULATING THE LENGTH OF THE BASE2 REGION

The minority carrier lifetime for the electrons in the P type region is given by the equation

$$\tau_e \equiv \frac{1}{c_n N_T}$$

where τ_e is a constant for the particular P region at given conditions. The minority carrier profile with a noise pulse is shown in Figure: 6.3, the noise pulse is a noise quanta with a charge of $n.q$, where n represents the number of electrons simultaneously crossing the emitter base potential barrier at the left side of the figure. The profile assumes negligible recombination in the base regions. Figure: 6.3 shows BASE1 and BASE2 of equal length, and so the metallurgical junction between the two occurs at $x/2$. The minimum length required of the BASE2 region to be an effective recombination centre should be sufficient to allow the incident noise quanta to be reduced to say 10% of its incident value i.e. at the left hand side of the BASE2 region shown as $\frac{x}{2}$ in the Figure: 6.3. The lifetime of minority carriers (electrons) in the $P-type$ region is dependent on the doping level of that region. The lifetime decreases with increasing values of N_A , and at very high doping level has a value determined by the Auger lifetime for Silicon. The Auger lifetime is given by the equation

$$\tau_e = \frac{1}{G_p \cdot p^2}$$

where G_p is a constant for Silicon and has a value of 1.5×10^{-31} . and p is the $P - type$ doping level. This gives an electron lifetime of

$$\frac{1}{1.5 \times 10^{-31} \cdot (10 \times 10^{20})^2} = 6.6 \times 10^{-12}$$

This gives $\tau_e = 6.6\, pS$ at a BASE2 doping level $N_A = 10 \times 10^{20}$. Substituting this electron lifetime in the Eq. 6.8 gives

$$L_e = \sqrt{36 * 6.6 \times 10^{-12}}$$

$L_e = 1.54 \times 10^{-5}\ cm$, or $154\, nm$. Substituting the value for L_e back into Eq. 6.7 allows the length of the BASE2 region to be calculated. Since

$$n_e = n_{e1} \cdot exp\frac{-x}{L_e} \tag{6.9}$$

for a decay to 10% of its incident value,

$$\frac{n_e}{n_{e1}} = 0.1$$

giving

$$exp\frac{-x}{L_e}$$

The value of x , to give this decay is then

$$x = -L_e \cdot ln(0.1)$$

or

$$x = 2.3025 \cdot L_e$$

The minimum length of the BASE2 region required to reduce the incident noise quanta to 10% of its initial value is

$$x = 2.3025 \times 1.54 \times 10^{-7} m$$

or 354 nm. The BASE2 region can be inserted into an existing BASE1 length as long as the total base length is greater than this size. The overall length would have to be increased by this amount if the total base length (BASE1 + BASE2) is less than this dimension.

DC GAIN OF BASE1 and BASE2

The base current in a BJT is caused by recombination of minority carriers in the base region. The recombination rate is given by Eq. 6.6, and is proportional to the average minority diffusion current above the equilibrium value in each base. The average minority carrier level in the BASE1 region is three times that of the BASE2 region, and so the recombination rate in BASE1 is three times that of BASE2. The minority carrier lifetime is however much lower in BASE2 due to the high doping level, in this case ten times that of BASE1, and so the BASE2 current is given by

$$I_{B2} = 0.33 \cdot \frac{\tau_{b2}}{\tau_{b1}} \cdot I_{B1} \tag{6.10}$$

where I_{B1} and I_{B2} are the base currents of BASE1 and BASE2 respectively, and τ_{b1} and τ_{b2} are the BASE1 and BASE2 lifetimes respectively. This gives I_{B2} a value of 3.3 times the BASE1 current, for the same BASE1 and BASE2 lengths. This means the DC gain β for BASE2 $\beta_{B2} = 0.33 \cdot \beta_{B1}$. The DC gain will be higher at low levels of emitter current using Eq. 6.2, because the equilibrium value of the BASE2 region is higher than that of BASE1 , given by $pn_{(x)} = \frac{ni^2}{NA_{b2}}$.

6.1 New LNBJT Transistor Small signal AC Transfer Function

The introduction of the new BASE2 region , and the associated external capacitance clearly alters the dynamic characteristics of the LNBJT device. This section shows the changes in the small signal AC model and the transfer function of the device. A small signal AC model commonly used for the BJT, is the Hybrid Pi model. The Hybrid Pi model is used here in order to simplify the calculation of the transfer function. This model is used here, recognising its limitations, in representing the real physical device. The approximation of the base resistance r_π can not model the PN junction very accurately, but is useful for deriving the small signal high frequency transfer function $H(s)$. A model based on the actual physical implementation of the LNBJT has been used to show the additional mechanisms, providing the improvement in performance from an AC small signal perspective, as opposed to the noise performance already reviewed in this work. The small signal model used here accurately

shows the effect of the BASE2 region and the new external capacitance in relation to the AC performance. The new schematic for deriving the transfer function is shown in Figure: 6.4. The model does not show all the parasitic components for brevity in deriving the transfer function.

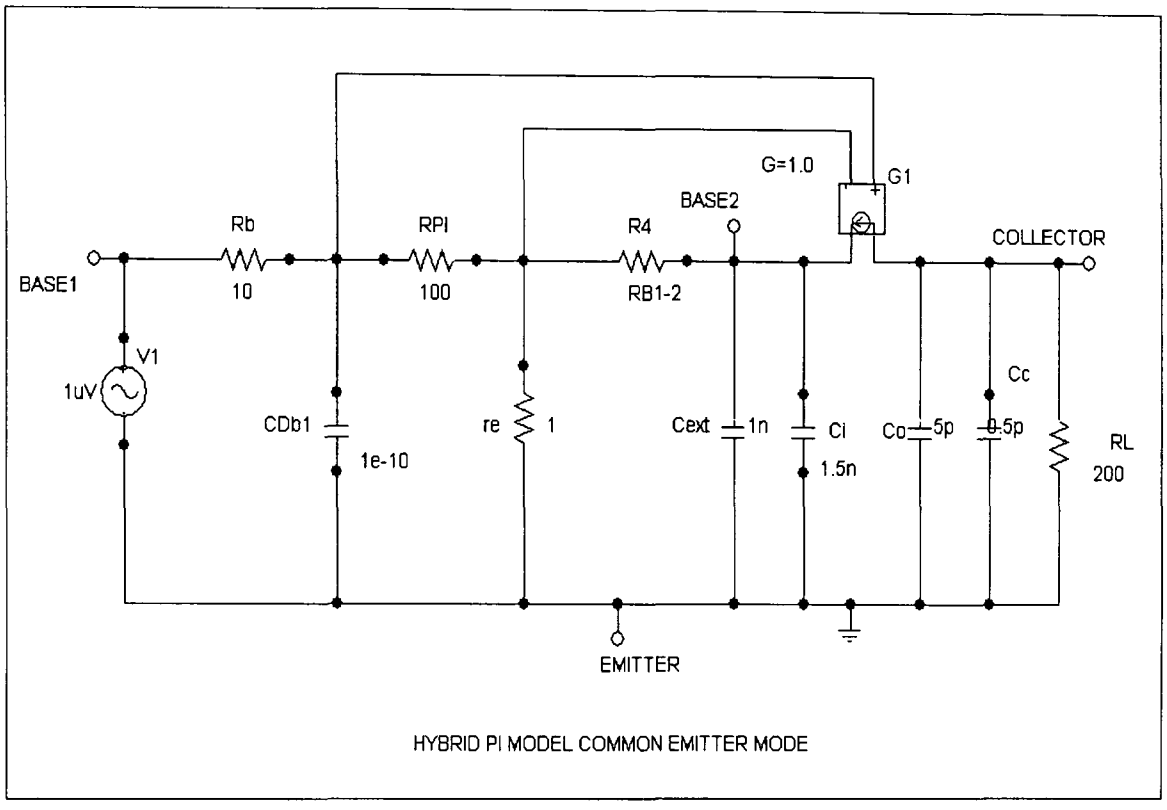

Fig. 6.4. High frequency small signal equivalent circuit of the LNBJT

The schematic shown in Figure: 6.4, is a popular representation used for the high-frequency small signal analysis of the BJT. This particular form is a simplification of the general hybrid-pi in common emitter mode, showing the Miller capacitance as C_i and C_o. The Miller capacitance is reduced to an equivalent input capacitance Ci and an equivalent output capacitance Co. The values for Ci and Co are given as follows

$$Ci = (1 - A_v) \cdot Cbc$$

and

$$Co = (1 - \frac{1}{A_v}) \cdot Cbc$$

where Cbc is the collector to BASE2 capacitance, and A_v is the amplifier voltage gain. In a single base device the Miller capacitance Ci would appear directly across

the base depletion capacitance $CDb1$. The parameters used here are the main parameters of interest, and are as follows. The parameter r_{pi} is the incremental base resistance. The capacitor $CDb1$ is the BASE1 diffusion capacitance and $CDb2$ the diffusion capacitance of the BASE2 region. The capacitor C_{ext} is the external capacitor for reducing the device noise, and RB_{12} is the inter-base resistance. The AC voltage source $V_1 = Vi$ is the input signal voltage, and the transconductance generator $G1$ is the collector current generator with a value equal to $gm \cdot V_\pi$, where V_π is the voltage created across r_{pi} . The output load for the BJT amplifier is shown as RL , and the amplified signal is present across this resistance. The transfer function for the network in Figure: 6.4 is defined as

$$H(s) = Gain = \frac{V_{out}}{V_i}$$

where V_{out} is the voltage across RL. The transfer function can be derived by considering each source generator in turn , and has the form

$$H(s) = \frac{\frac{F+sG}{Rb+F+sG}(1 - \frac{D+sE}{R_\pi+D+sE})}{\frac{1}{gm \cdot Z_0} + \frac{L+sM}{Z_0} \cdot \frac{J+sK}{R_2+J+sK}\left\{1 - \frac{H+sI}{R_\pi+H+sI}\right\}}$$

where $F+sG$ is the complex impedance across the capacitance $CDb1$, and $D+sE$ the complex impedance across re both viewed from the current generator. The value of $L+sM$ is the complex impedance across the capacitance C_{ext} , $J+sK$ the complex impedance across re , and $J+sK$ the complex impedance across re, and $H+sI$ the complex impedance across $DCb1$, all viewed from the source generator side of the network. The term Z_0 is the complex output impedance formed by RL, C_0 and C_5 , and g_m is the transconductance between v_π and the current generator, where v_π is the voltage across r_π .The creation of the BASE2 introduces the inter-base resistance RB_{12} and the associated external capacitor C_{ext} creates a transfer function where the transfer function $H(s)$ has a maximum peak, when the complex term $1 - \frac{H+sI}{R_\pi+H+sI}$ is at a minimum, and the term $1 - \frac{D+sE}{R_\pi+D+sE}$ is also at a relative minimum. This can be viewed as the relationship between the forward and reverse gain of the network. The operation of a BJT in common emitter mode has a small negative feedback term

across the incremental resistance of the base emitter diode re, where re is given by Eq. H.4,and is inversely proportional to the emitter current I_e. This is due to the emitter current having to pass through the emitter diode along with the base current. The incremental base resistance r_{pi} is connected to re at one end, and since the voltage across r_{pi} generates the gain of the device in this model through the dependent current source shown as $G1$ in Figure: 6.4. This negative feedback effectively reduces the gain of the common emitter configuration, particularly at lower frequencies , where the current generator is in anti-phase to the signal V_{pi} . The transfer function $H(s)$ in effect reduces the extent of this negative feedback across re , and so increase the AC gain. This will be approximately 1.7 times the gain of a single base BJT with the parameters shown in Figure: 6.4. The effect of the Miller capacitance reduces the high frequency performance of a BJT where the voltage gain A_v is high. This capacitance in a single base device is effectively transformed across the input capacitance $CDb1$, reducing the high frequency gain , and is the dominant factor in limiting the $-3dB$ frequency in a conventional BJT transistor. Because of the addition of the new BASE2 region , this capacitance is effectively across C_{ext} , so reducing its effect and improving the high frequency gain.

6.1.1 Summary of device behaviour

The previous sections show that the effect of the additional base region reduces the peak to peak noise, and the effect of this additional capacitance on the BASE2 region is effectively removed by including its effect in the transfer function $H(s)$.The addition of the new base may have the adverse effect of increasing the base transit time, due to the extra thickness of the base, if it is not incorporated into the existing base. This would happen with a simple abrupt profile at the BASE1-BASE2 region, and with the other edge of the BASE2 on the collector depletion region. The impact of putting the BASE2 region here would also reduce the collector breakdown voltage, due to the high BASE2 doping. There would be a single adverse $E - Field$ between BASE1 and BASE2 , caused by the inverse step doping profile, which would add a further 11% to the transit time, with a BASE2 width of $1/8^{th}$ that of BASE1. The

higher recombination rate of minority carriers in the BASE2 region, required to reduce the noise, has an adverse effect on the DC gain or β, if the BASE2 is not biassed i.e. has only a connection to the external capacitor C_{ext} . The recombination current in BASE2 is calculated to be 3.3 times, the BASE1 current using Eq. 6.10, if BASE2 is the same width as BASE1. Fortunately the BASE2 can be biassed to supply the BASE2 part of its recombination current, so improving the DC gain of the BASE1 signal input. The magnitude of the BASE1-BASE2 potential Φ_{B1-2} caused by the difference between the BASE1 and BASE2 doping level, shown as the difference in doping level between $0,1\mu$ and $0,2\mu$ in Figure: 6.2, is $-59.5mV$ as calculated by Eq. I.5. By positioning the right hand side of the base doping profile in Figure: 6.2, back from the collector junction, the same or greater potential will exist, of the opposite polarity, due to the other side of the base doping profile, between $0,2\mu$ and $0,3\mu$ creating an accelerating voltage of 178.7 mV, more than compensating for the introduction of BASE2. The net insertion voltage of BASE2, for this example, is $178.7 - 59.5 = 119.2\,mV$. This effectively returns the overall base region "built in" $E - Field$ to assist the minority carrier transit time. Also by keeping the right hand edge of BASE2 back from the collector junction, as in Figure: 6.2, the collector base breakdown voltage can be preserved. The doping levels shown in Figure: 6.2, are shown as an example, and are not the actual doping levels proposed here. There is an AC gain increase due to the presence of the external capacitor C_{ext} . This can be thought of as reducing the effect of the Miller capacitance $C_{in} = (1 - A_v)c_{cb}$, where C_{in} is the input capacitance, and A_v is the AC voltage gain of the amplifier, this being the dominant pole in many high frequency AC amplifiers. The reduction in the AC impedance for the transconductance current source i_2, near its "grounded side" , by the action of C_{ext} also increases the AC gain. The AC gain increase is approximately 1.7 times that of a single base device using the values in Figure: 6.4, at the peak response. The lower the value of emitter current, the larger the value of re from Eq. {H.4}, and the greater the gain improvement provided by C_{ext}. The thinner the BASE2 region relative to the signal base BASE1, the smaller these effects will be. The example

used in this work, for the purpose of validating the JAMES model, is illustrated using a Silicon homogeneous device, with a simple mechanism for increasing the BASE2 recombination rate, by increasing the Na_{b2} doping level. The use of the silicon device in *current source applications* and *lower frequency amplifier applications*, would be a good match for the characteristics of this device. The thickness of this BASE2 region would be calculated to allow the amount of recombination required to reduce the noise level by the desired amount. The component C_{ext} does not increase the component count required for an AC amplifier, because a de-coupling capacitor would normally be used to de-couple the emitter bias resistor of the BJT. The emitter de-coupling capacitor would be replaced by the BASE2 de-coupling capacitor C_{ext}.

NOISE LEVELS IN A BJT TRANSISTOR

The graph in Figure: D.1 shows a graph of the noise levels in a typical BJT over the full spectrum of operating frequency. The mid and top end of the frequency spectrum is the region of interest in terms of AC gain and noise amplitude. A brief calculation of the noise levels in a typical bipolar junction transistor are given in Appendix: {D.1}.

7. MODEL VALIDATION BY CONVENTIONAL SPICE SIMULATION

This is the third method for validating the results obtained from the JAMES ATOMISTIC simulation model. The very elementary nature of the analysis performed by JAMES gives microscopic detail about the carrier transport and behaviour, and the charge movements in the crystal lattice. This is a form of transient analysis but although it gives detailed information on the physical/electronic behaviour over very small time steps, it lacks as yet the speed on a simple PC to model the larger currents over long periods of time i.e. times of several microseconds or greater. The SPICE method of simulating at circuit level however works assuming large carrier populations (currents) and over relatively long time periods when compared with an atomistic simulation, and trades speed against very detailed analysis of the carrier behaviour. The noise simulations in SPICE are carried out by taking each of the noise equations and applying them to all the PASSIVE and ACTIVE devices in the schematic, and then applying a transformation to sum the individual noise components at the output (or input). The H-Spice methodology uses a sine wave signal to represent the particular noise type for the particular circuit element, and transforms it through the transfer function of the device to obtain the noise contribution, and total noise. The use of SPICE provides a well understood and accepted analysis method, and the results of the JAMES model should approximate to the SPICE analysis IN THE LIMIT . This means that the JAMES model should converge with the SPICE results for very large carrier populations. The JAMES model was used to derive the basic mechanisms involved in studying SHOT NOISE in a BJT. The lumped physical parameters for a typical device have been calculated using a 3-D field solver, and this allows SPICE sim-

ulation to be used as a means to validate the overall noise reduction results predicted from JAMES.

7.0.2 Deriving the physical parameters

A 3-D planar construction of a BJT model was used to create a physical model of the BJT in a 3-D field solver, with the approximate doping levels and sizes that could be achieved in a practical implementation. The representation was made in rectangular sections for ease of analysis, as opposed to circular sections that would exist in practice. The cross section of the BJT is shown in Figure: 7.1. A highly doped region is also included under the BASE1 junction directly beneath the emitter diffusion. The contacts are all rectangular in section, and form a near complete loop, contacting the appropriate junction at all its surface points. This reduces the contact resistance of the device parasitics.

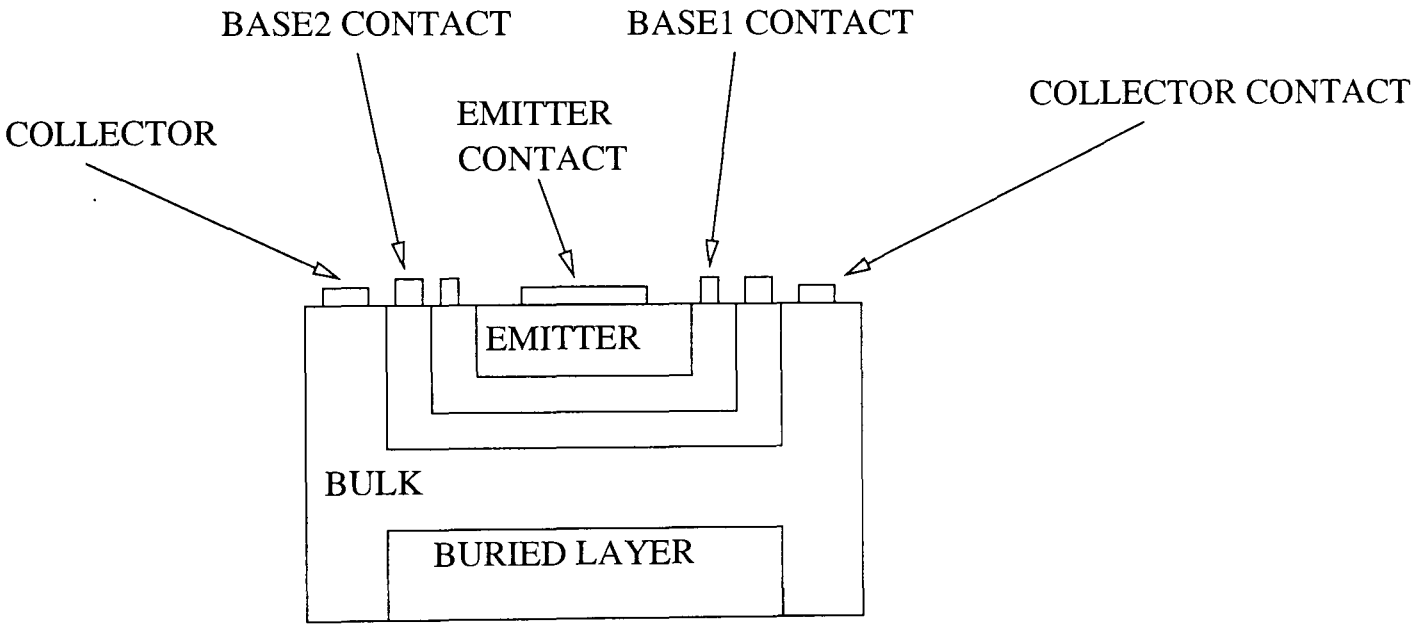

Fig. 7.1. Physical model of a planar BJT

This is treated as a four port network as shown in Figure: 7.2

The resistance and inductance values are extracted and used to provide the lumped values used in the SPICE simulation model of Figure:7.4. The diodes are typical and of an appropriate area, complete with diffusion capacitance. The physical dimensions were entered into the FASTHENRY software, and used to calculate the 3-D resistance

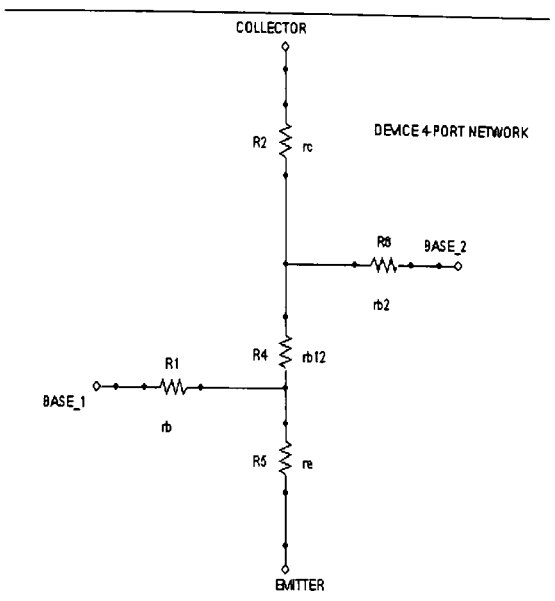

Fig. 7.2. 4-port BJT lumped model

values for the "lumped" model. The input file listing for the FASTHENRY program is shown in Appendix: K.1 along with the resistance values calculated by the program.

7.0.3 Conventional Lumped BJT Noise models

The conventional SPICE models that may be used to model noise in a BJT semiconductor devices are shown in Figure: 7.3. The Gray and Meyer model [15] can be used to derive the equations for parameters such as R_{Sopt}, while the Van der Ziel model [32] can be used for the Spice simulation models, as it is more accurate for representing the true physical approximations.

The use of the SPICE simulation program should therefore show broadly similar results to that obtained in the JAMES simulator. There will be one major difference however, the study of relatively small numbers of carriers will not give identical results to a SPICE simulation, as the paradigm is different between the two approaches.

7.0.4 Representing the new BASE2 region in SPICE

The higher doping density in the BASE2 region reduces the resistance between the BASE2 contact and the region of the main current density, i.e. between the emitter and collector. The high recombination region in this base has no exact parallel, in terms of the SPICE elements of resistors, capacitors, or current sources, as they are

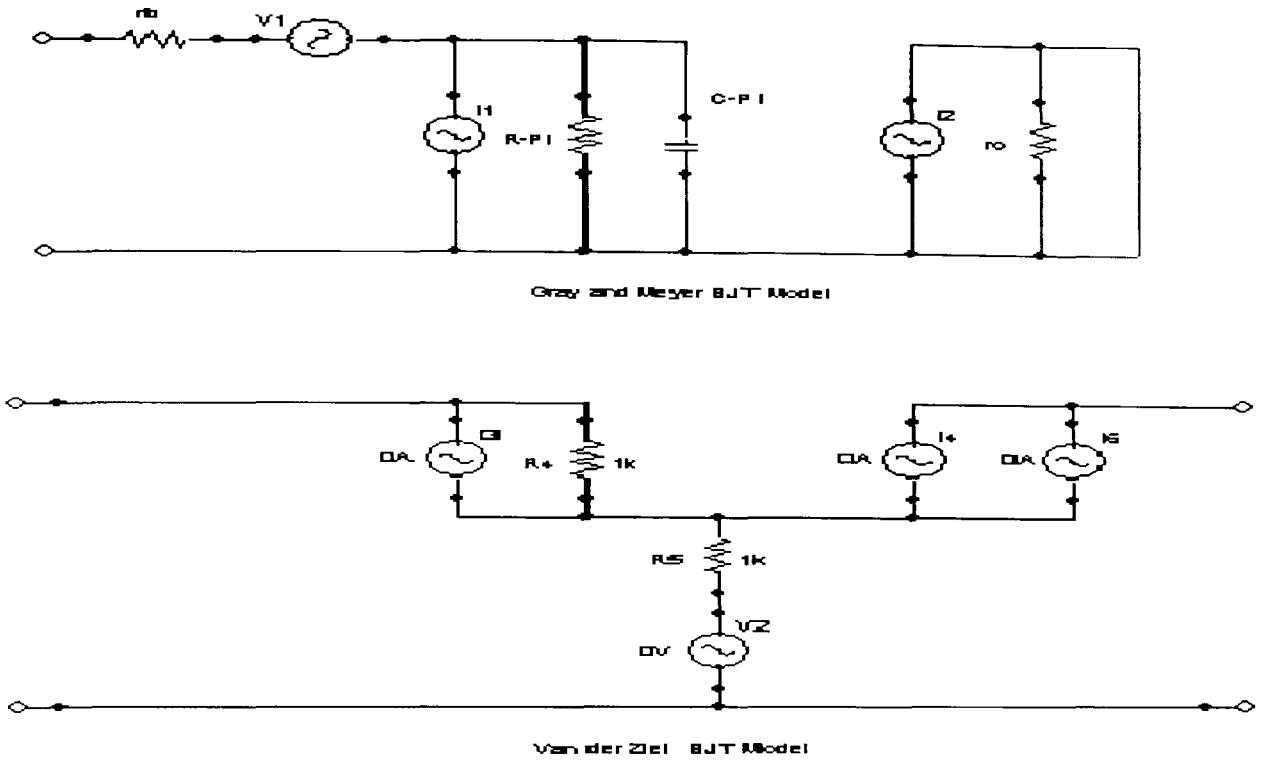

Fig. 7.3. Noise models for BJTs

designed for "macro" parameters.The resistance parameter for example, is suitable for high population carrier levels , and the resistance R is defined as $R = V/I$, where V is the applied voltage and I the average current nq/t resulting from the voltage difference. However with this approximation in mind, an equivalent circuit of the new device is shown in Figure: 7.4.

7.0.5 The SPICE model parameters

The resistance R39 in Figure: 7.4 represents the resistance of the bulk, highly doped BASE2 region, to the external BASE 2 contact, and R33 represents the discrete part of the base resistance rb. The current generator F3 represents the current gain β_F. and $R49$ of Figure: 7.4 the BASE1-BASE2 resistance.

A test environment must be defined to analyse the electrical behaviour of the Spice model, and to allow measurements of various behavioural aspects such as AC gain, and signal to noise ratio (S/N). The design of an RF amplifier has been chosen and is shown in the Figure: 7.5. This is a simple capacitively coupled arrangement.

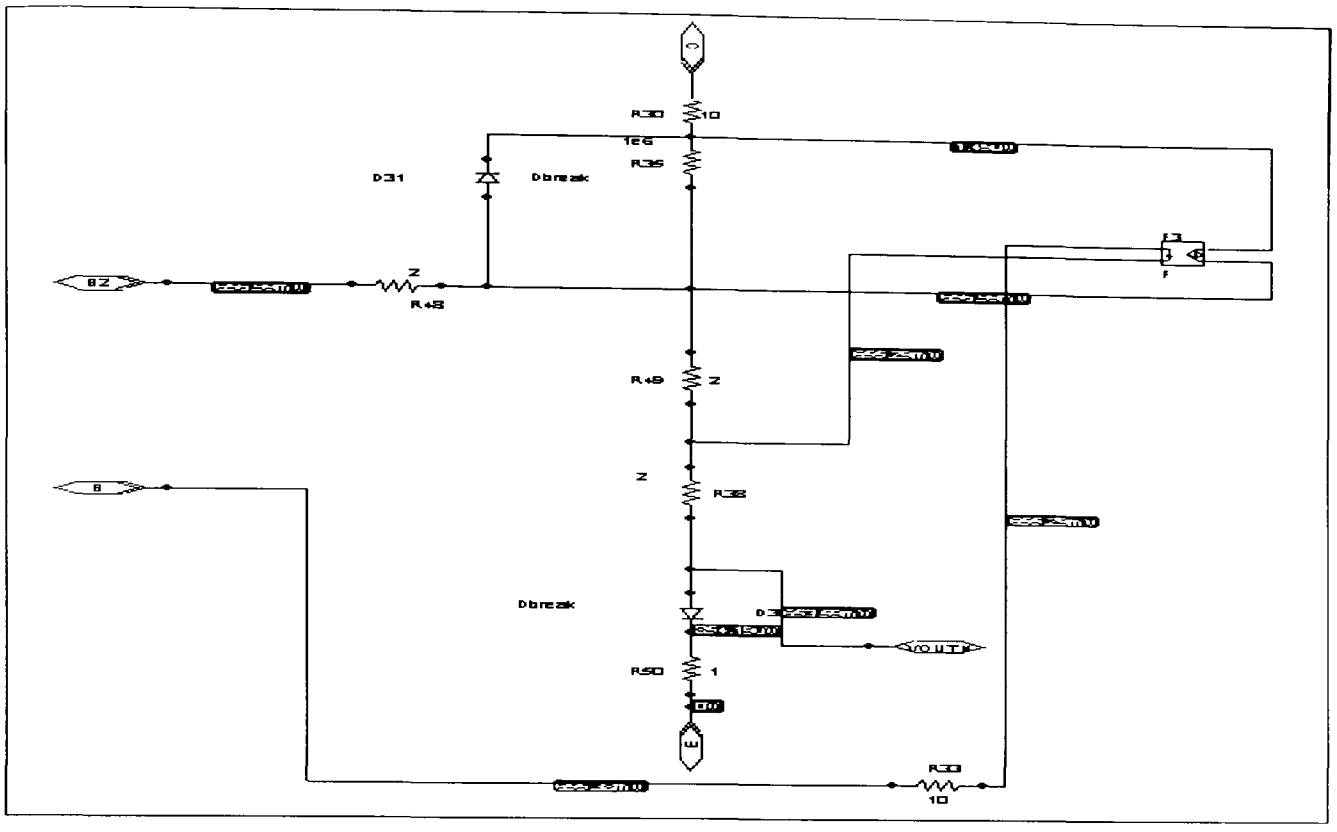

Fig. 7.4. Lumped electrical approximation to the new structure

with no attempt to optimise the noise performance. This will be done later. Various noise parameters will also be measured. The input signal source is shown as V_{10} with the source resistance given by R_3. The noise factor F can then be measured at the port marked OUT. In order to show the comparison between a conventional device and the new structure, the capacitor C_{ext} (C_4 schematic reference), is swept across 6 values pre defined in the SPICE simulator. The 1st value is effectively zero, and this represents an approximation to a conventional device i.e. without any external capacitor or BASE2 connection. Under the conditions where there is zero external capacitance the BASE2 region is not in use, and the device will behave in a similar way to a conventional BJT. The response of the new device can now be evaluated with different degrees of decoupling, in relation to a conventional BJT device.

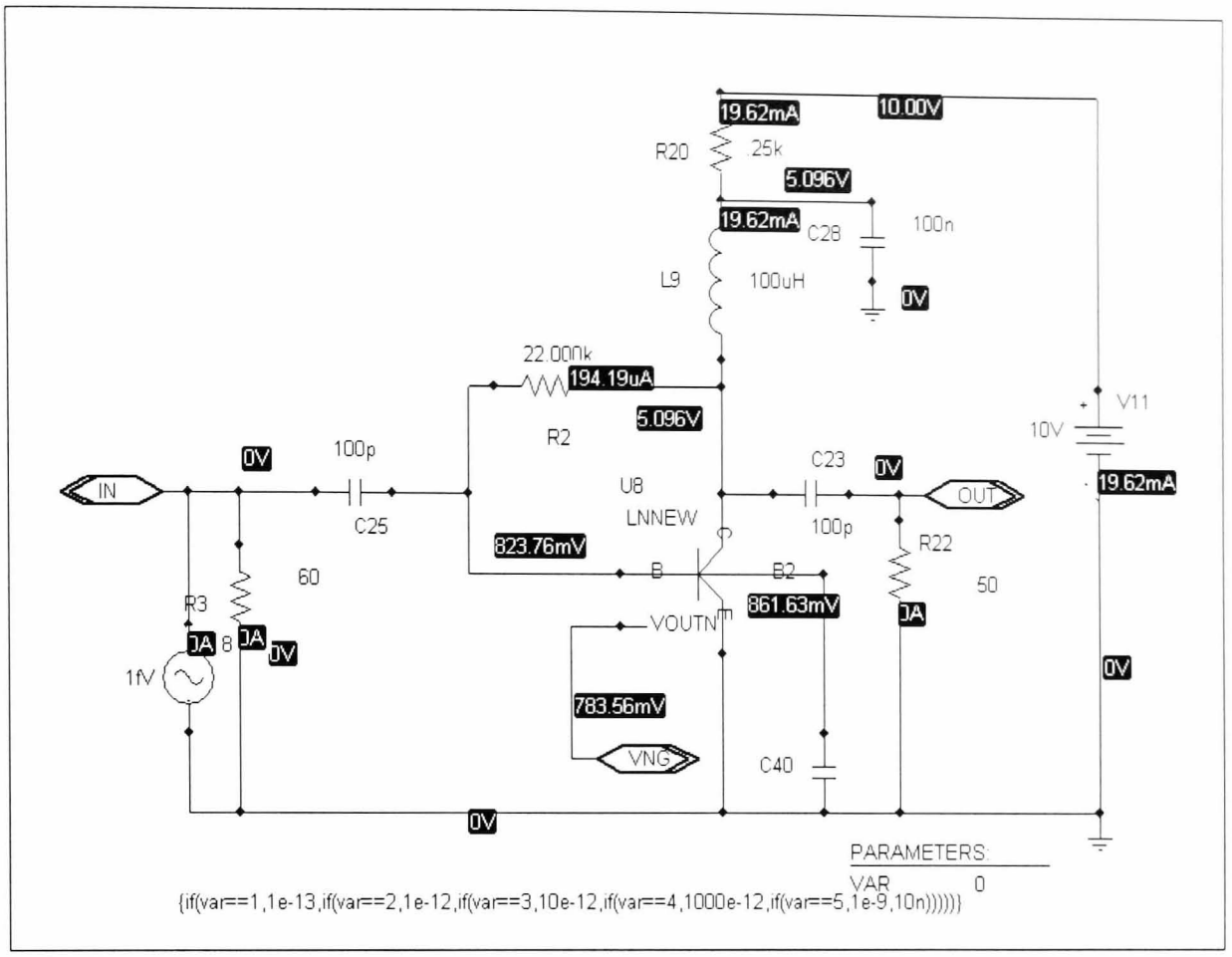

Fig. 7.5. Test schematic for the proposed device ,Vcc=10v, .

7.1 Spice Results

The Spice simulator was run for several important parameters of the new low-noise BJT design. This section examines the various parameters commonly regarded as the metrics of high frequency low-noise amplifiers.

7.1.1 Interpretation of graphs

In this chapter extensive use will be made of graphical information. The following Icons are key to understanding the results shown on the graphs. The external capacitor used to reduce noise C_{ext} is incremented over the range from 0 to 1000×10^{-12} $(1000pF$) in pre-selected steps. The key to the graphs, is displayed in the lower left corner as a row of icons, and looks like this □ ◇ ▽ △ □ IP_SD . The zero value of C_{ext} is the left-most icon, and the highest value is right icon, just before the trace label , in this case IP_SD. The actual values used can be identified

from the parameter statement listed on the schematic in use. The parameter list {if(var==1,1e-13,if(var==2,1e-12,if(var==3,10e-12,if(var==4,100e-12,if(var==5,1000e-12,100p))))))} , can be found on the schematic in use at the mid bottom position, and shows the actual capacitance value corresponding to the icon on each trace. The intention is to show the LNBJT approximating to a conventional device with $C_{ext} = 0pF$, as the BASE2 region becomes a small local ,highly doped floating region in the device structure without any effective electrical connection.

7.1.2 The Amplifier Gain

The noise characteristics examined include the device AC-GAIN in the test schematic Figure: 7.5, the noise of the amplifier, the SIGNAL to NOISE RATIO $[SNR]$, the NOISE FACTOR F, the NOISE FACTOR in dB , and the Noise Temperature T. The graph of stage GAIN is shown in Figure: 7.6. The 6 traces shown increase the C_{ext} capacitance value from 0 through to $1000pF$ in five steps.

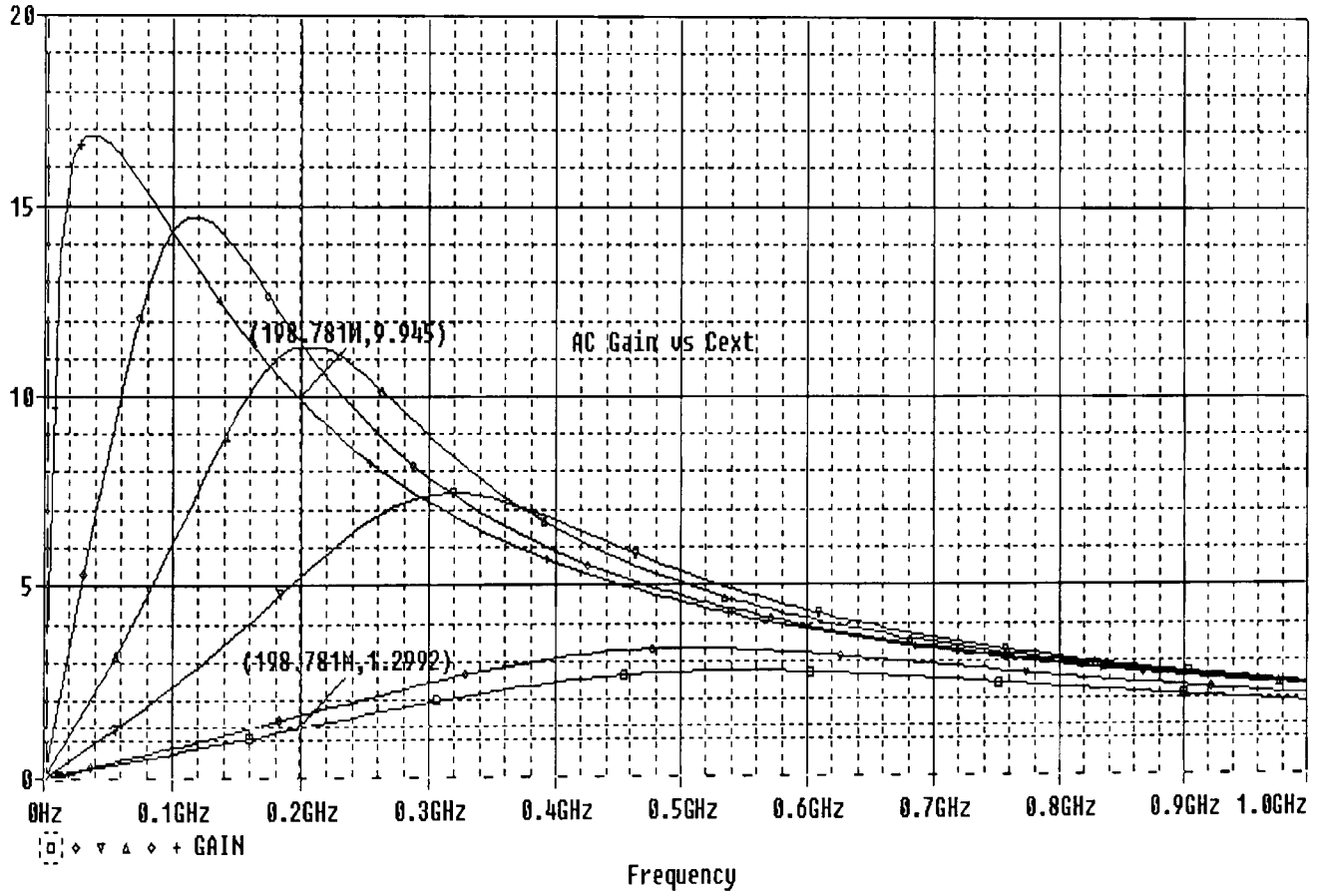

Fig. 7.6. Gain vs frequency

7.1.3 The Amplifier noise

This parameter can be measured at the input or output. The normal method is to measure the INPUT REFERRED noise, which normalises the noise taking the stage gain into account. The noise levels are TOTAL noise levels including thermal noise. shot noise and flicker noise. The graph in Figure: 7.7 shows the *rms* value of the noise v_{rms}. The input referred noise in Figure: 7.7 shows that with the second base

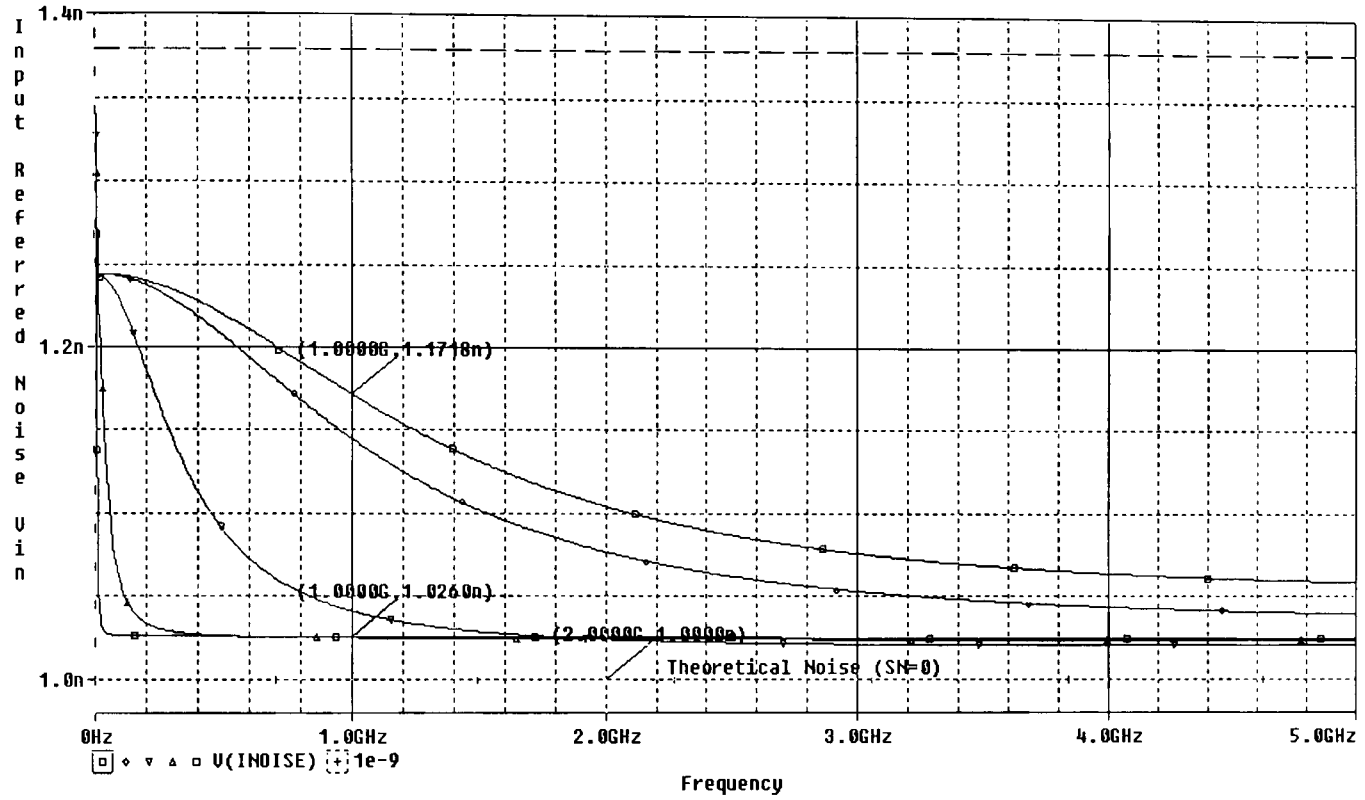

Fig. 7.7. Total (input referred) noise

in operation, the noise is very close to the theoretical minimum. This does not apply to frequencies in the range where BASEBAND or $1/f$ noise is present. This component of noise would be present in the approximate frequency range $DC - 100kHz$. There will be some reduction in the baseband noise, however the attenuation will not be as great as that of the shot noise. This is believed to be due to larger charge variations in the $1/f$ noise quanta , as opposed to the small quanta $n \cdot q$, see Figure: 6.3. charge variation of the shot noise. The reduction in the input referred noise can be seen from an inspection of Figure: 7.7. The Unity Gain measurement gives a indication of the

upper usable gain of a particular device where the gain drops to unity. A graph of the Unity Gain point for this particular BJT is shown in Figure: 7.8, and shows the usable frequency being increased from $37Ghz$ to $51Ghz$.

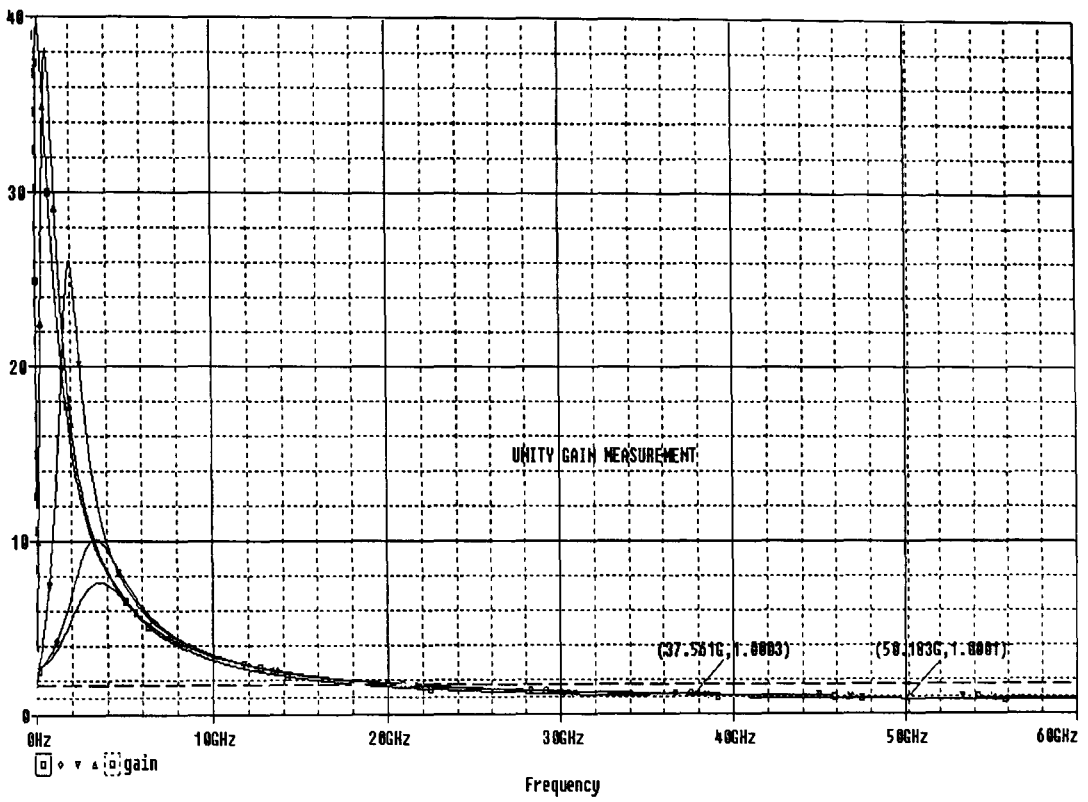

Fig. 7.8. Unity gain graph

7.1.4 Signal to Noise Ratio

The signal to noise ratio is given by the equation

$$SNR = \frac{v_{in}}{v_{irn}}$$

where v_{in} is the input signal voltage, and v_{irn} is the input referred noise voltage. The graph in Figure: 7.9 shows the value of the SNR for all five values of C_{ext}

The SNR shows the higher level of SNR achieved by using a large external value of C_{ext} The SNR falls off most rapidly on the lower trace (with $0pF$) . This is equivalent to the behaviour of the conventional BJT with only one base i.e. no second "AC base". The noise levels drop off due to the reduction in the gain of the conventional BJT with higher frequencies.

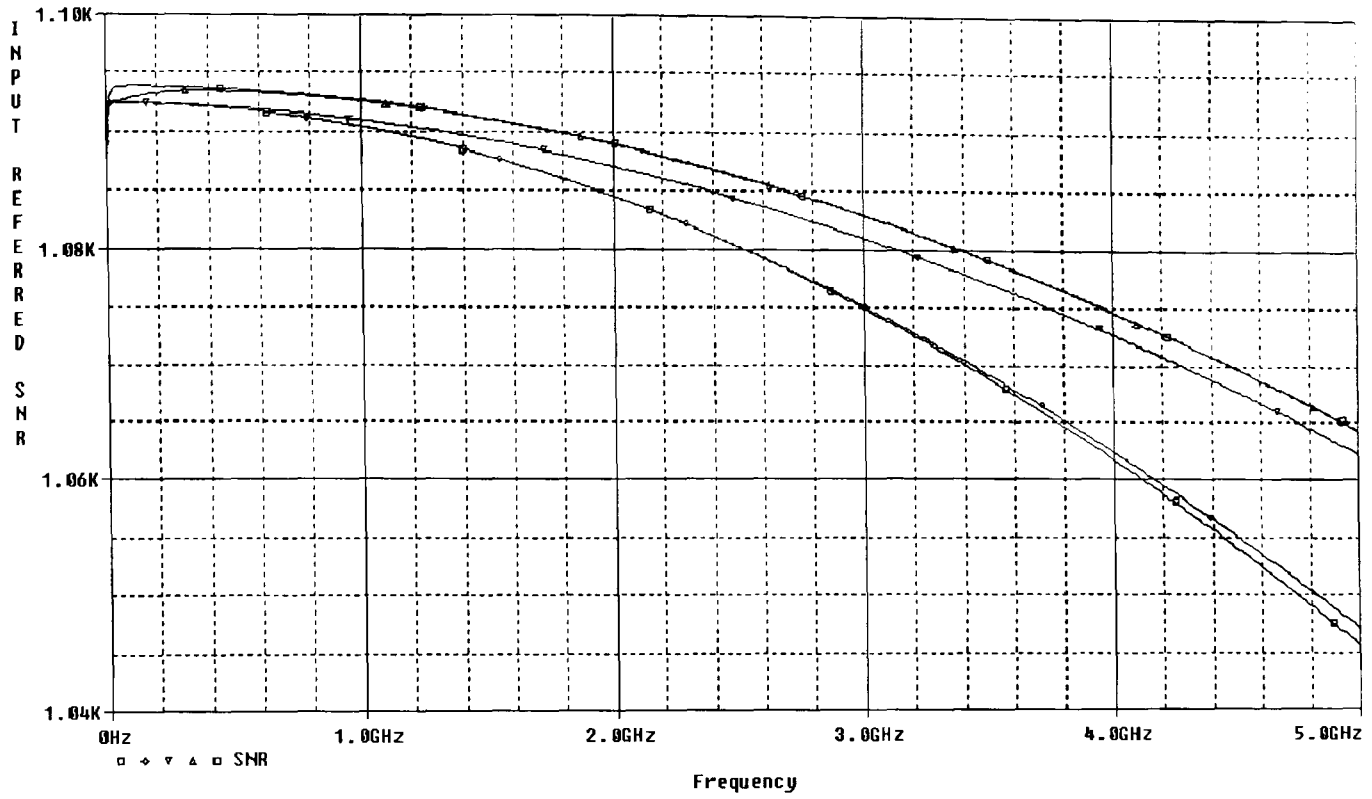

Fig. 7.9. Signal to Noise Ratio (SNR)

7.1.5 Noise Factor

The noise factor F is defined as

$$F = \frac{Total - Noise - Power[From(all - sources)]}{Total - Noise - Power[From(input - resistance)]}$$

The noise factor F shown on the upper trace of Figure: 7.10 shows the conventional BJT performance, and the lower traces show an improvement in F with the external capacitance.

7.1.6 Noise Factor in dB

This metric is commonly used in defining the noise performance of the BJT, and is defined as

$$F_{db} = 10.log(F)$$

The lower trace in Figure: 7.15, is the noise with a large $(1000pF)$ capacitance connected as C_{ext} , and this curve can be observed to provide the lowest value of F. The minimum theoretical NOISE FIGURE F_{min} is shown in Figure:7.15. The upper trace shows the conventional BJT is well above the calculated value of F_{min} .

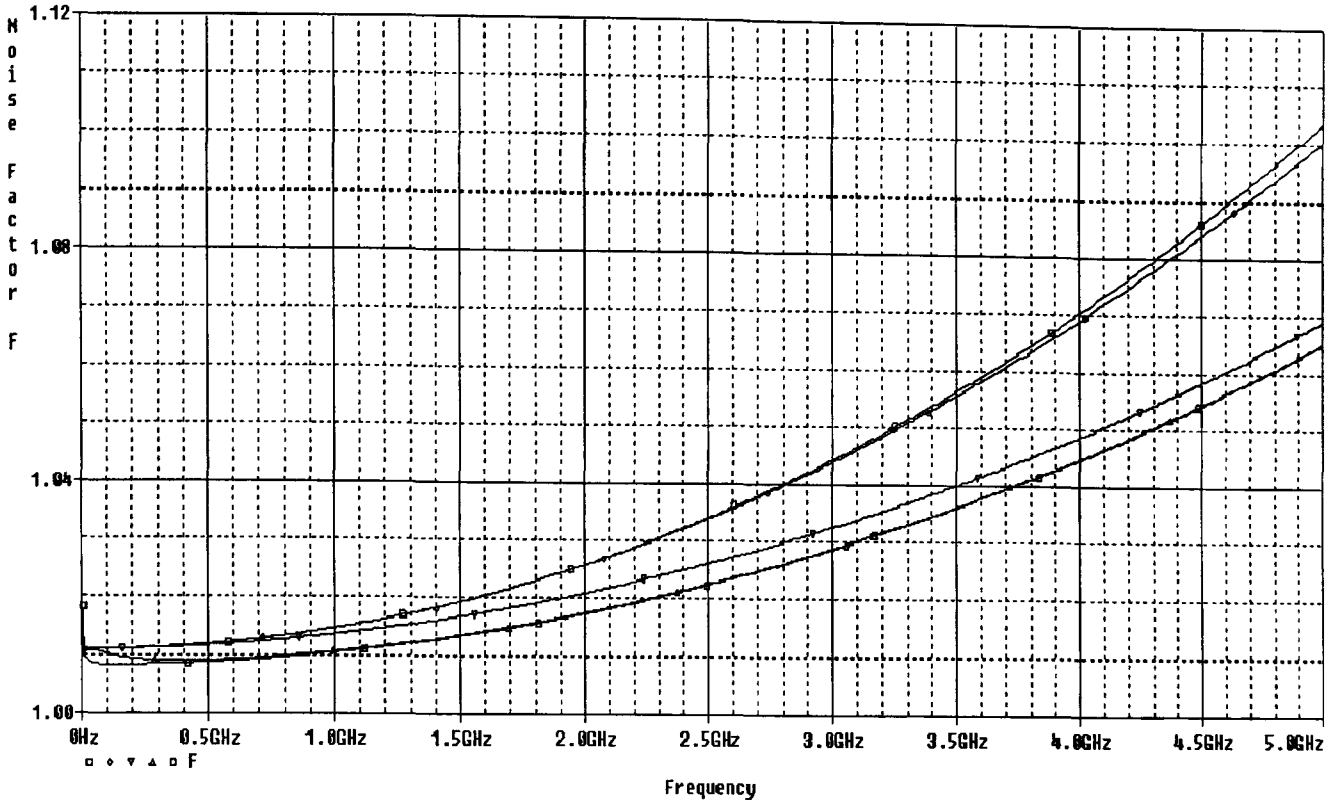

Fig. 7.10. Noise factor F vs frequency

The improvement in the Noise Figure [dB] can be seen from in Figure: 7.11. The Noise Factor for the conventional BJT with this physical design given here is $5.0dB$ @ $1Ghz$. The Noise Factor improves to $2.4dB$ @ $1Ghz$. By using modern fabrication techniques such as planar epitaxial, or Hetero-junction BJT (HBJT) the frequency and noise figures can be considerably improved beyond those shown in the example given here.

7.1.7 Noise Temperature

The metric of Noise Figure is commonly used in radio communications for quantifying noise. The metric of noise temperature is also used in satellite communications systems, and is given in terms of the Noise Figure F by

$$T_n = T(F - 1)$$

where T is the temperature at which the measurement is taken, normally $300^\circ K$. The noise temperature shows a consistent improvement with an increasing value of C_{ext} .

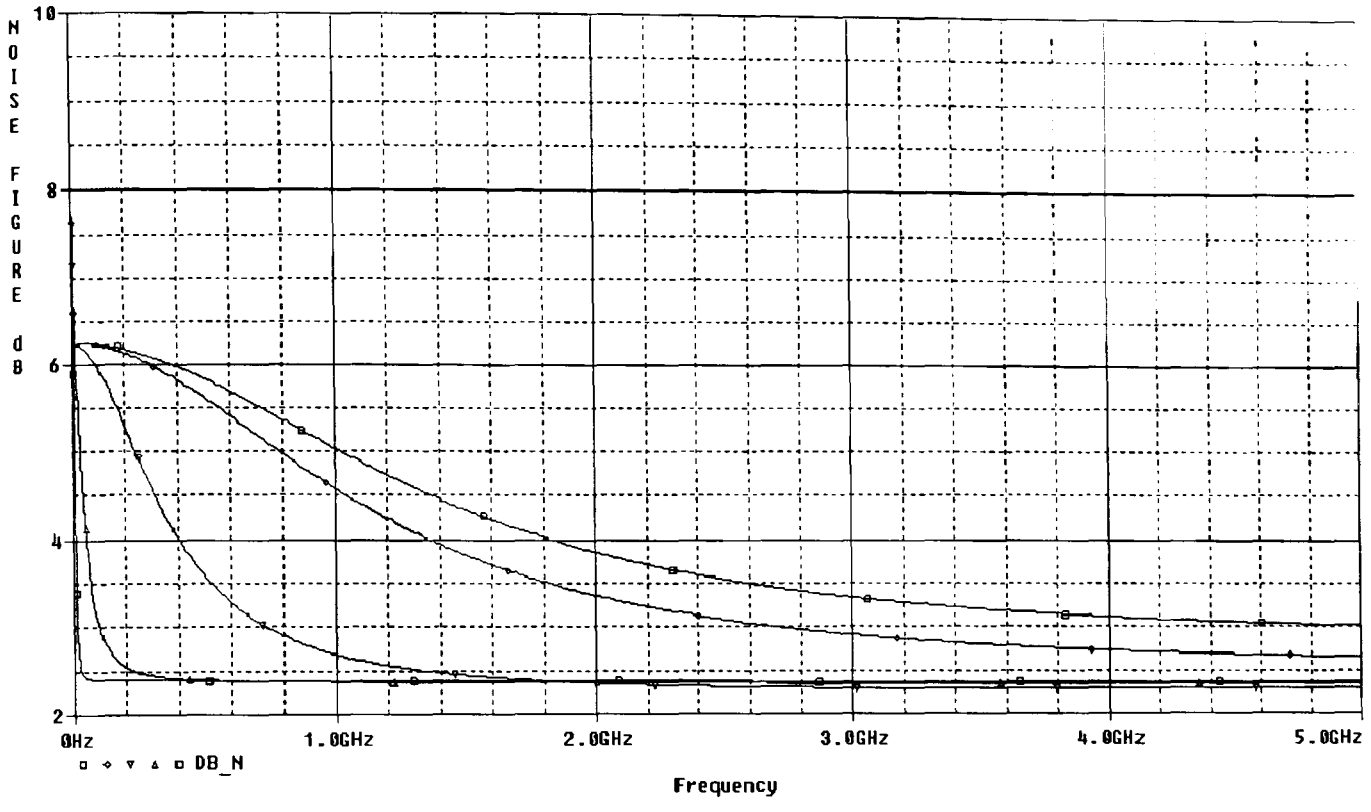

Fig. 7.11. Noise figure dB

7.1.8 Achieving the optimum source resistance

The lowest noise occurs at the optimum value of source resistance for a BJT. The TEST SCHEMATIC providing the optimum matching transformer is shown in Figure: 7.13. The transformer $TX4$ is used to match the source resistance of the signal to the optimum source resistance required to give the optimum resistance R_{Sopt} defined in the Eq. C.5.

Some of the simulations are repeated for this new matching arrangement, and are shown in Figure: 7.15. The graphs of theoretical noise give a comparison of the improvement in gain achieved, also in relation to the theoretical noise for the BJT. The use of this optimum matching shows that F improves from 1.6567 to 1.270 @ $1Ghz$, where the theoretical limit is 1.1200 defined at $R_s = 100\Omega$. The presence of an extra base considered in this new BJT, if successful should ideally suppress shot noise in the base-emitter junction, from reaching the collector. This would mean that ideally the shot noise component would be removed as a contributor to the the

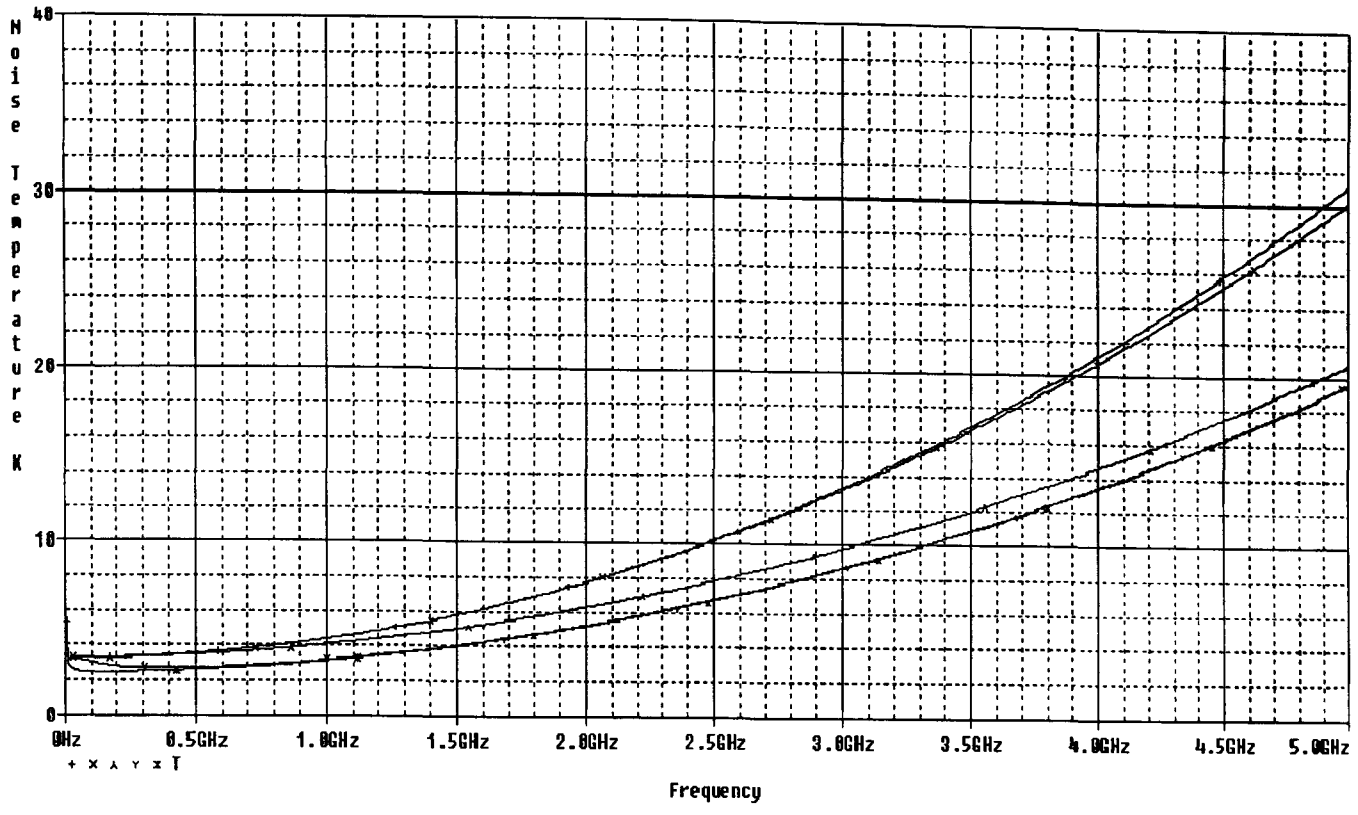

Fig. 7.12. Noise temperature

total device noise. The input referred noise level $v_{in}(rms)$ is shown below in Figure: 7.14 , with the *theoretical minimum noise level* added to the graph. This noise level *assumes* that the shot noise *is reduced to zero amplitude*, and only the Thermal noise component remains. This is something that is *not attainable* with a conventional BJT structure.

The graph in Figure: 7.14 shows that the noise level of the BJT *does indeed converge* at *lower frequencies* on the theoretical minimum input referred noise level.

The lower trace is the Noise Figure at a $C_{ext} = 1000\ pF$, and can be seen *to approach* the *minimum theoretical* value of F_{min}. The graph of Noise temperature is shown in Figure: 7.16.

The noise temperature is a similar result of course, showing the Noise temperature for the conventional device to be $197.013^{o}K$ *at* $1GHz$, and this drops to $81.009^{o}K$ at $1Ghz$, with the LNBJT. The *theoretical minimum* noise temperature for this BJT with its *physical design constraints,* in the absence of shot noise is $36.29\ ^{o}K$.

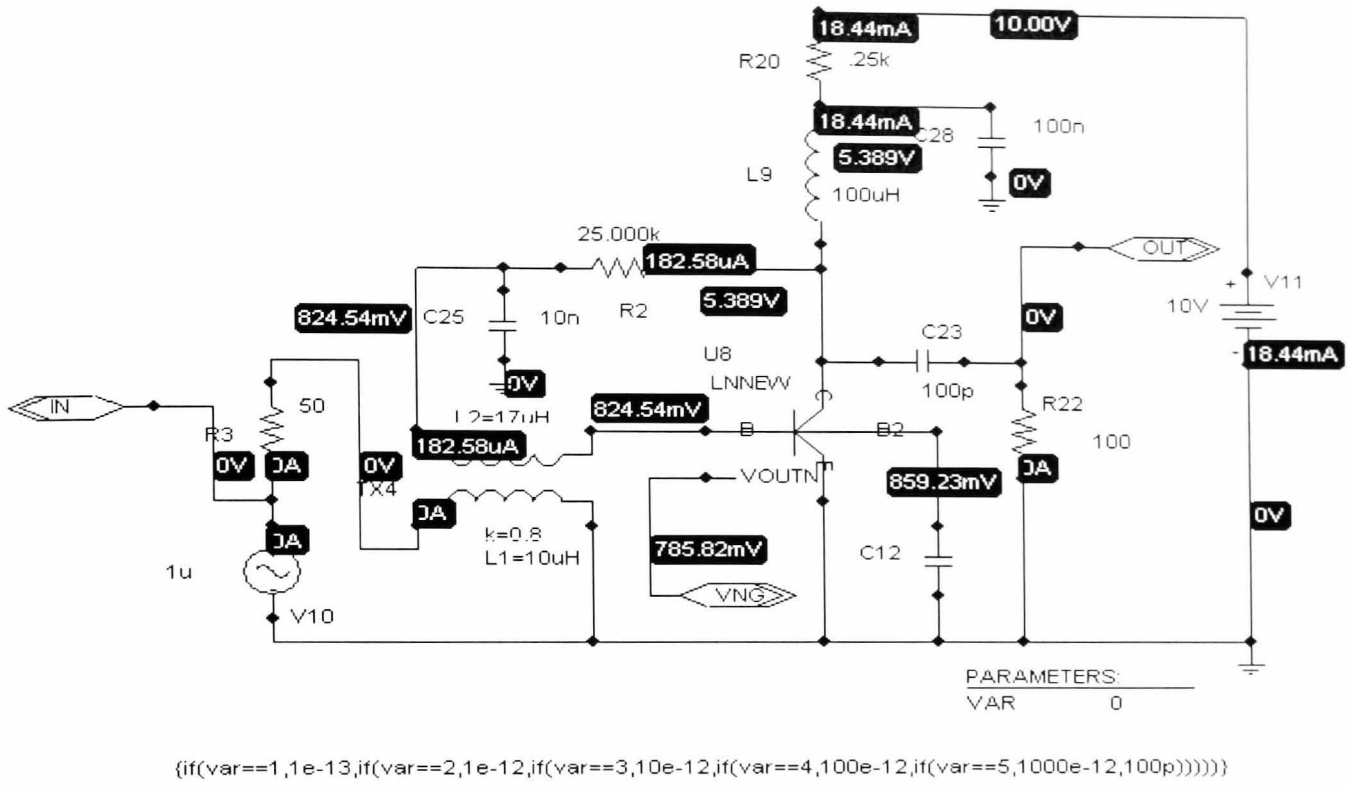

Fig. 7.13. Test schematic for optimum performance

7.1.9 Validation of shot noise attenuation factor

The value of K_{SA} will differ to some degree between the JAMES model and the spice simulation, due to the small carrier populations and short time periods represented. The value of the theoretical spectral density from the output of the JAMES model is 4.83×10^{-33} see Algorithm:45 with label "<=**T**", and the actual spectral density from the simulator measured at MP[32] is 1.116×10^{-35} see Algorithm: 45 with label "<=**A**" , giving K_{SA} a value of $-26.4dB$. The value of K_{SA} was also measured using the SPICE simulator. This is shown in Figure: C.1, and has a maximum attenuation of $-24.6dB$ at frequencies near DC.

7.2 Practical laboratory measurements.

Without the fabrication of an actual device, and subsequent testing, the only test possible in the laboratory was to take a conventional BJT, bias it, and to observe the noise spectra, with and without an external capacitance. The conventional device has only one base of course, and so the only test that could be made, was to add

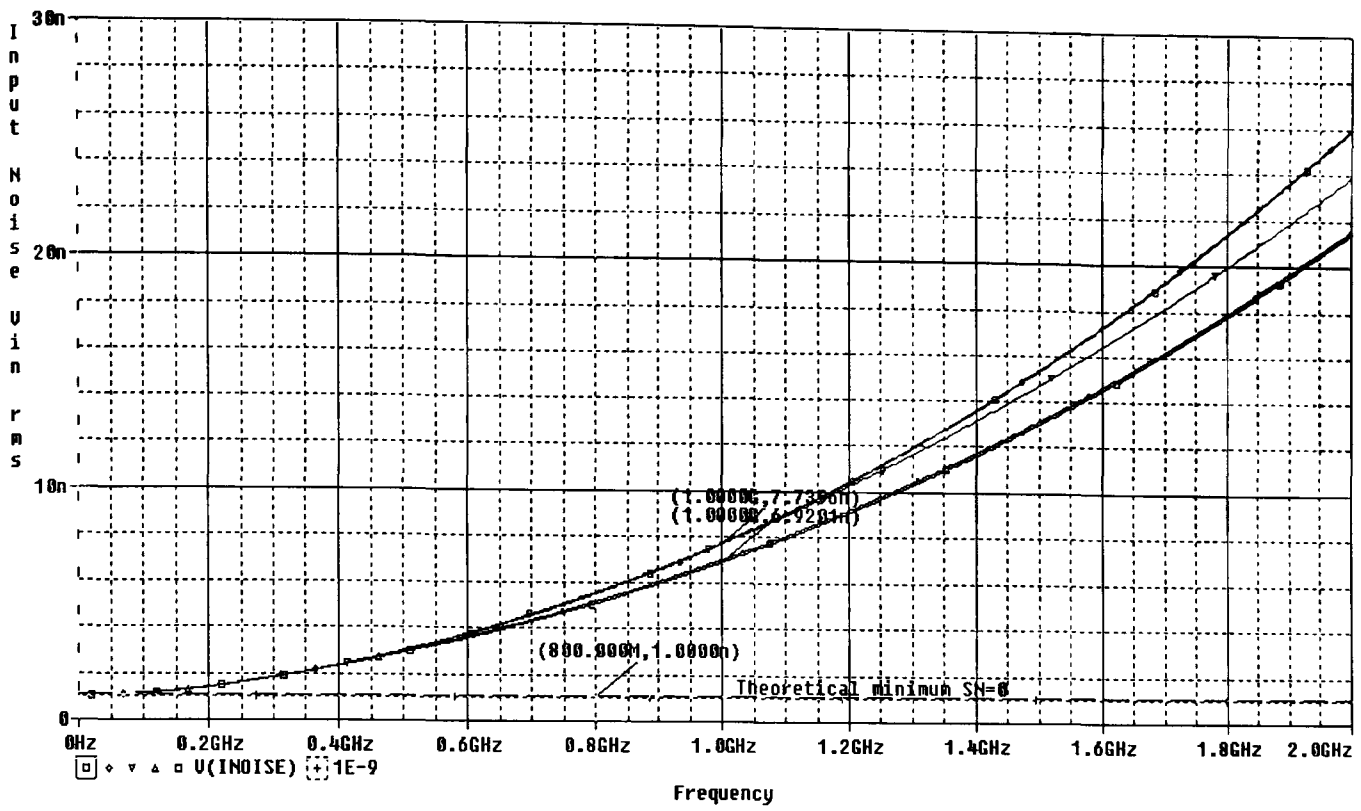

Fig. 7.14. Input referred noise vs theoretical (Shot Noise=0)

an external capacitance on to the base connection. This is a poor approximation at best to the new structure, but the principle is broadly similar, in that providing an external low impedance path to the shot noise variations, reduces the noise. This method would severely limit the frequency of operation of the conventional BJT device, and would not provide the gain advantages of the second base, as shown in Figure: 7.6, and of course the improved SNR in Figure: 7.9. The experiment does show that if the complete BASE1 region is decoupled to signal ground , the bulk effect in the base is to reduce the shot-noise contribution. This is not the same effect as decoupling the new BASE2 region at or near the BASE2-COLLECTOR depletion region, to achieve the shot-noise reduction, and also increasing the high-frequency gain. The measurements were made with a $BC547A$ BJT using the TEST SCHEMATIC shown in Figure: 7.17. The results were measured on a Tektronix spectrum analyser, and are shown Figures: 7.18, and 7.19, using the schematic of Figure: 7.17.

The output noise was measured with and without the base capacitance C1. and the results are shown in Figure: 7.18.

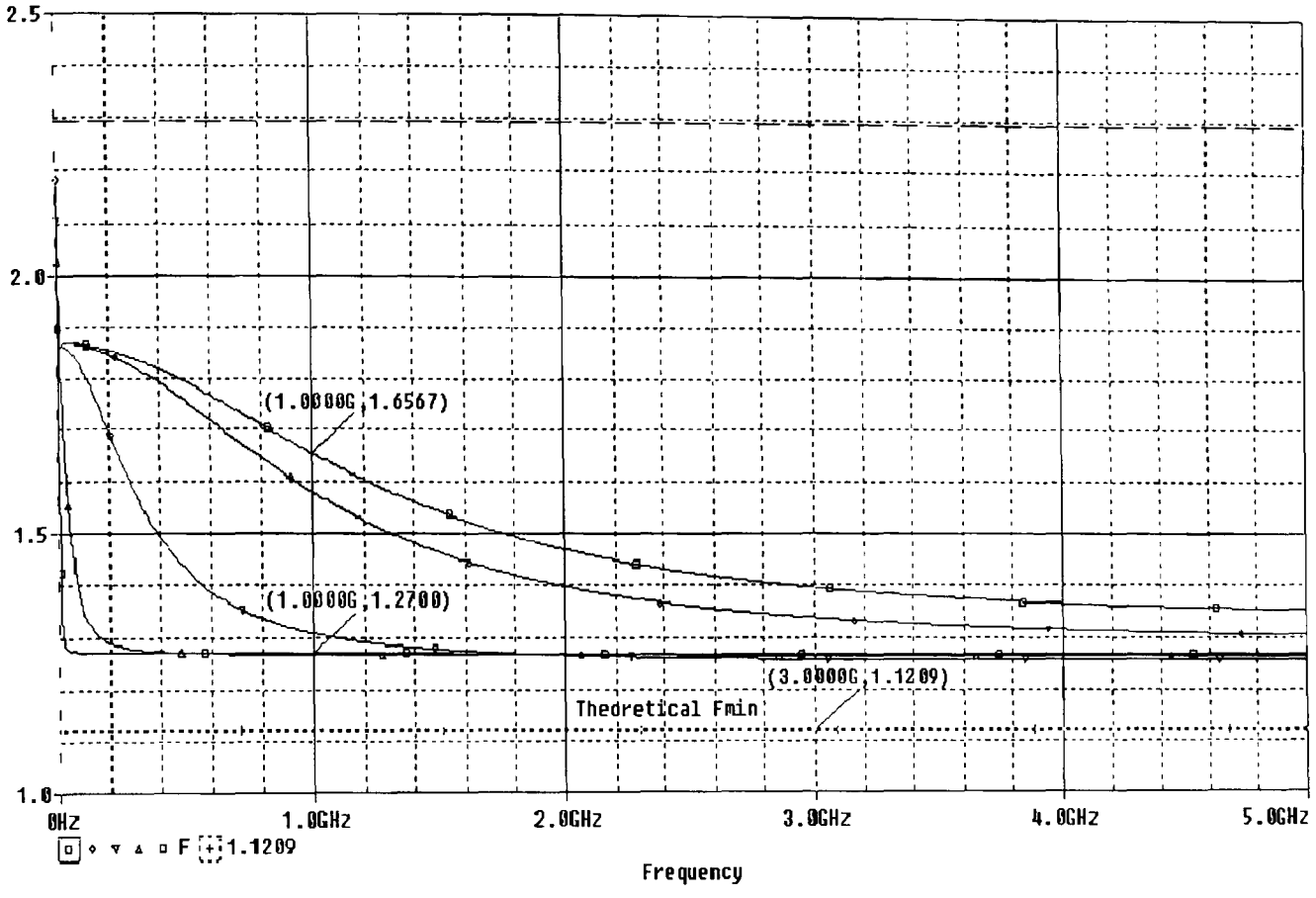

Fig. 7.15. Noise figure F vs frequency

The upper trace in Figure: 7.18 shows the peak-peak noise voltage as $1200mV$ peak-peak, without the base capacitor.

The trace shows the comparison with the base capacitance C1 connected. The peak-peak voltage is reduced to $420mV$. This is a reduction of $680mV$ peak-peak noise voltage. The results show the presence of the base capacitor reduce the peak-peak noise voltage by $-4.9dB$. The capacitor acts to smooth the shot noise in the base-emitter junction, and this in turn reduces the shot noise measured in the collector, and at the output.

7.2.1 Summary of Spice simulation results

The above simulations have shown the considerable improvement to the noise and the gain for the new BJT. The signal to noise (SNR) improves significantly. The comparisons were carried out on the most basic BJT structure, and this shows considerable improvements. A typical value of F for a good low noise BJT is between

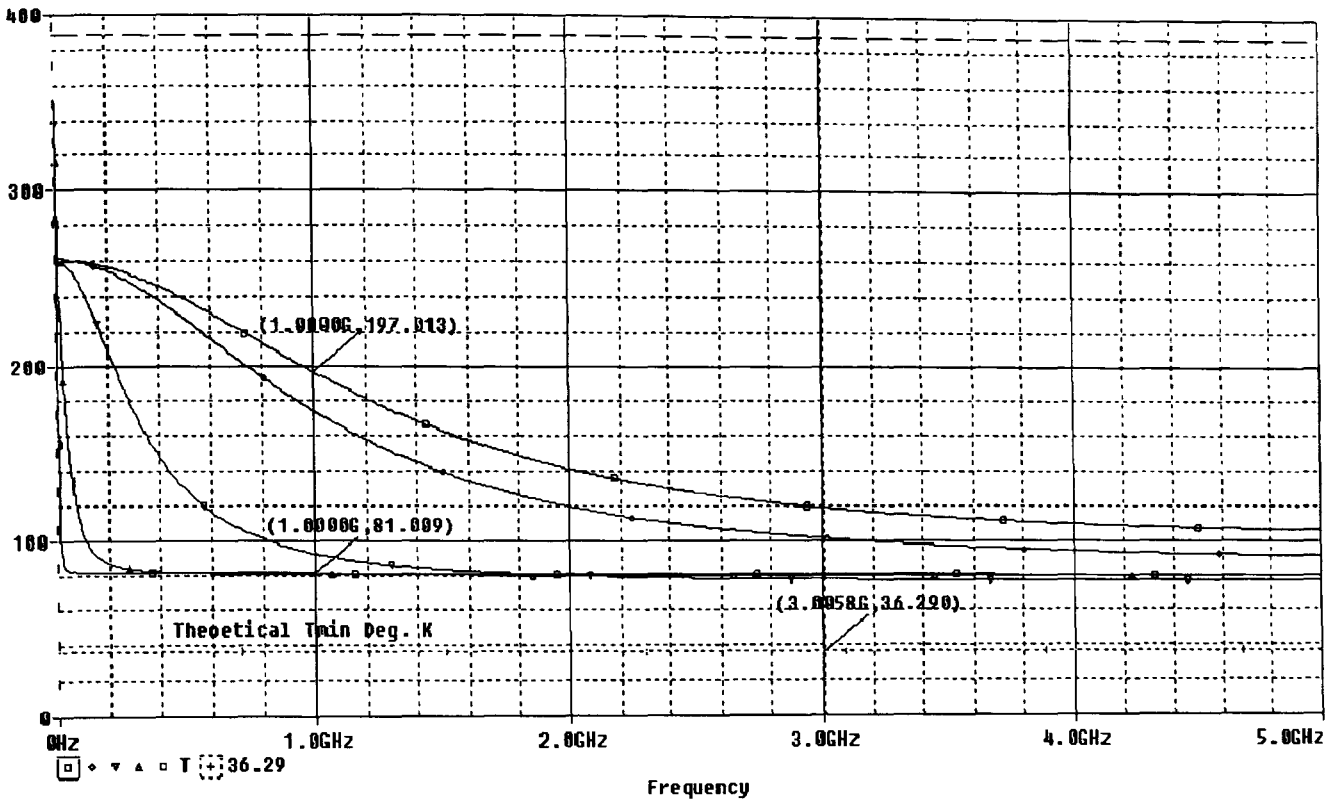

Fig. 7.16. Noise temperature vs frequency

$2.0dB$ and $5dB$ e.g. the BC547A has a noise figure $F = 2.5dB$ to $10dB$ @ $I_c = 200uA$. The minimum theoretical noise figure attainable by a conventional BJT can be calculated, and this is given by the equation in Appendix: {G.3}. The value of F_{min} for the LNBJT can be calculated from the values in the test schematic shown on Figure: 7.4. The theoretical value of F_{min} will be calculated assuming $K_{SA} = 0$ i.e. the shot noise equal to zero. The value of r_e is small and will be ignored for this calculation. Substituting the values for R_s and r_b in the equation for F_{min} {C.8} gives $F_{min} = R_s + r_b/R_s$. This gives F_{min} a value of 1.1200. The noise factor F can be a little misleading as it does not take account of the voltage gain A_v . A different metric called the *noise measure, M* Eq. G.7, takes gain into account. The smaller the value of M results in better noise/gain performance of a device in an amplifier application. Using this metric the *noise measure* for the BC547A has a value between 2.0 and 12.0. and the LNBJT described here has a value of 0.127 . The spice simulation show a reasonably good correlation with the JAMES model predictions and the theoretically derived values.

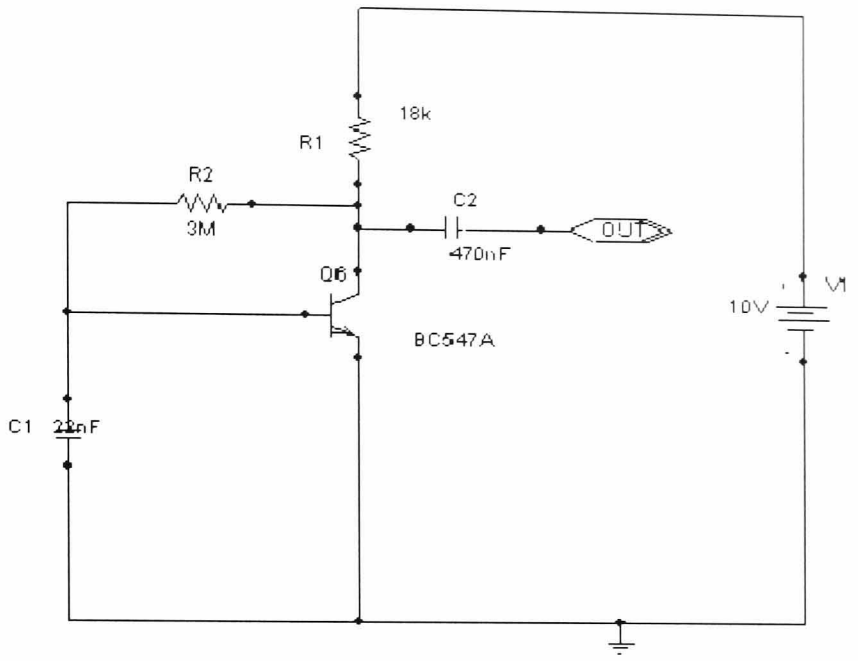

Fig. 7.17. Bench test schematic

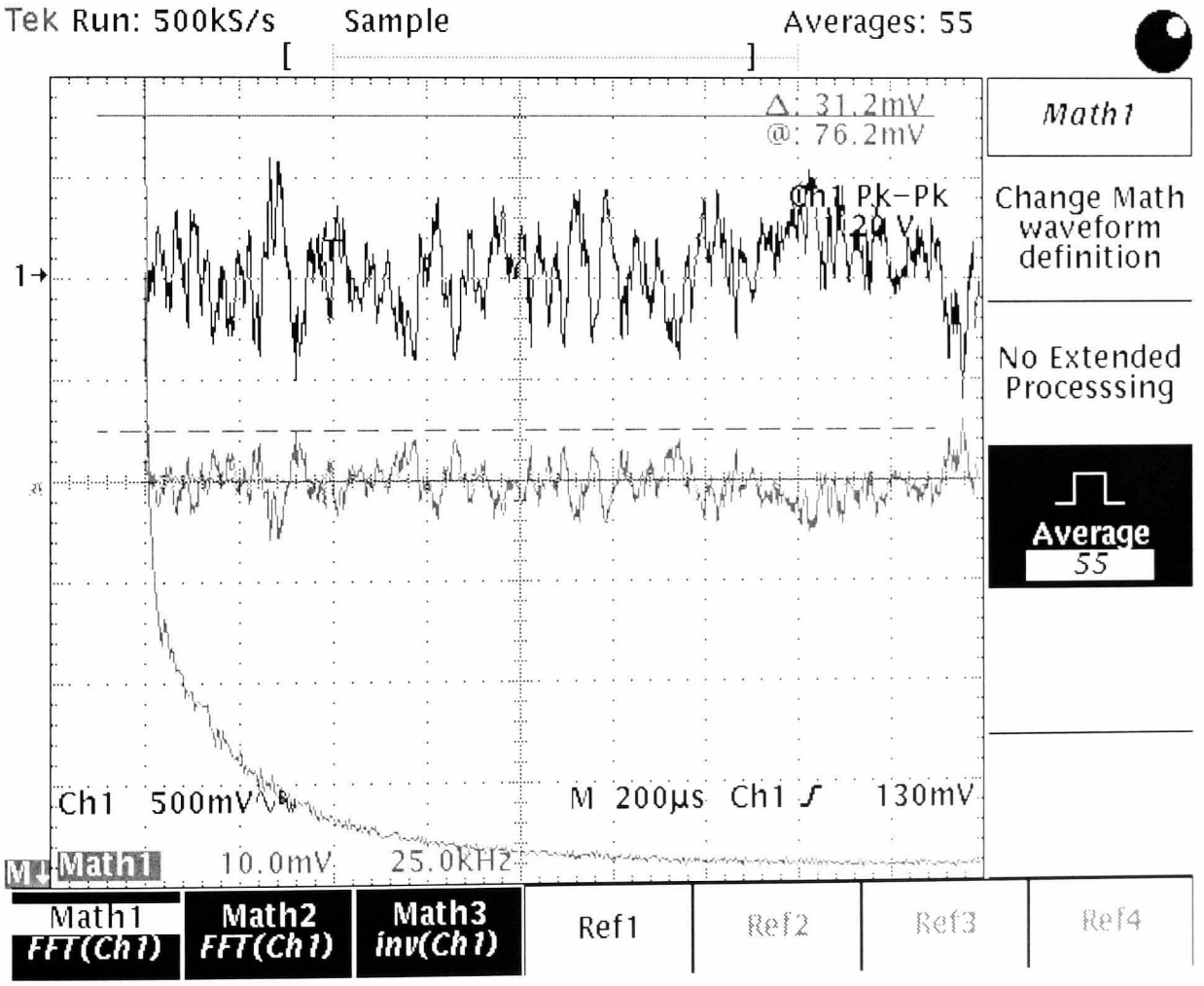

Fig. 7.18. Noise without capacitor

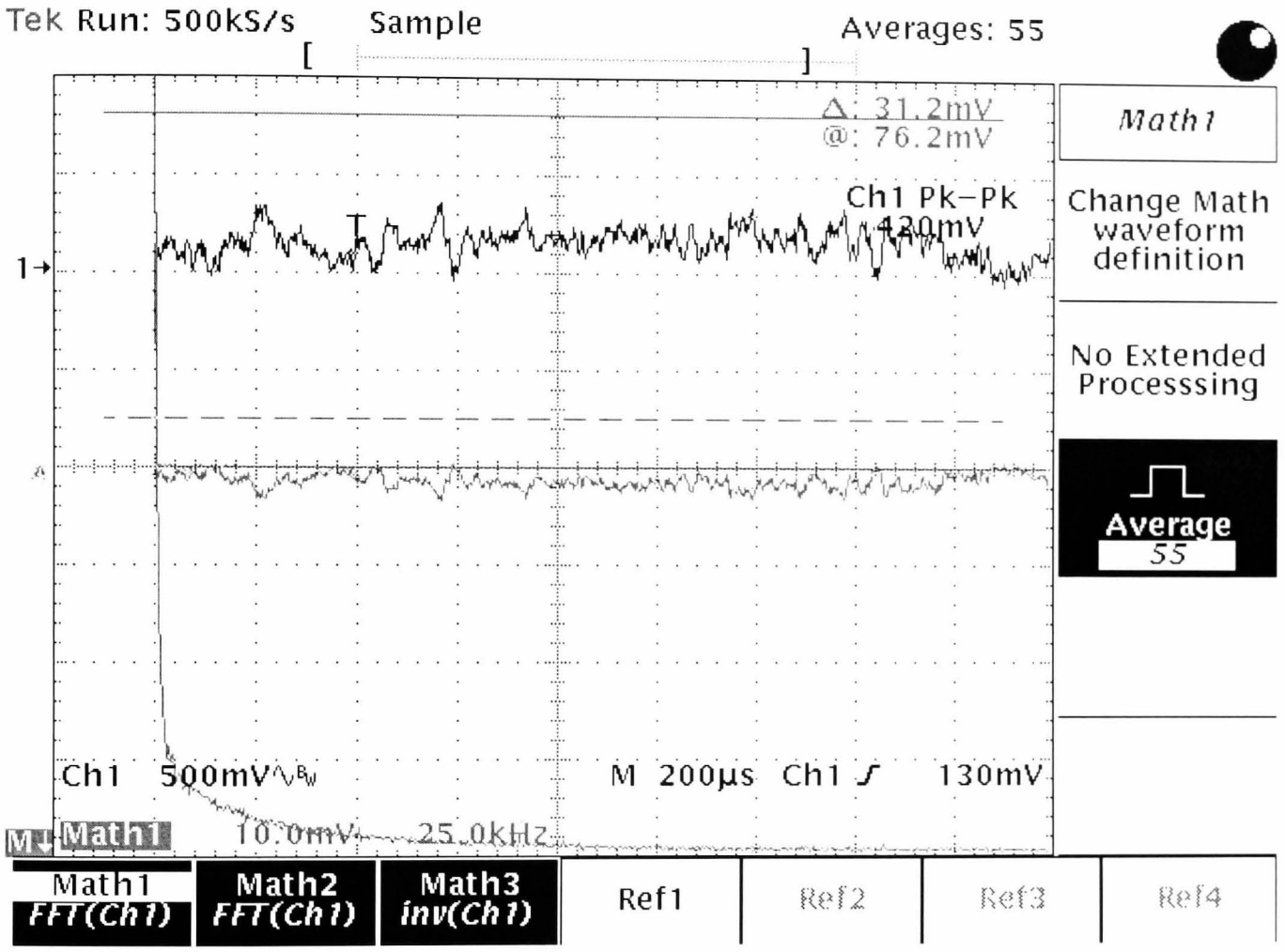

Fig. 7.19. Noise with capacitor connected

8. CONCLUSIONS

1. The use of a true 3-D diffusion based model of individual charge carrier flow through the lattice has been demonstrated as a means of analysing noise in the semiconductor structure.

2. The model provided detailed spatial and temporal analysis of the charge transport with short execution times.

3. The model showed the expected behaviour of current flow as a result of applied electric field (Ohms law).

4. The model showed the expected linear shot noise relationship with average current flow through the lattice.

5. Shot noise is proposed here as being due to an integer *n charge carriers simultaneously crossing a potential barrier.*

6. The new base region is used to re-thermalise the shot noise carriers and reduce the spectral density of the noise current.

7. The new BASE2 structure *reduces the Miller capacitance* from the collector bulk to the signal base.

8. The high frequency *AC voltage gain* of the device has been *increased* by using the model, and shows a marked improvement over the single base device.

9. Shot noise is generated *primarily by emitter injection into the base* of a BJT and transferred to the collector.

10. The significant reduction of the *shot noise* mechanism allows the total noise to approximate to the thermal noise of the device over a limited range of frequencies.

11. Ignoring $1/f$ noise, Burst and G-R noise, after shot noise reduction, the only other major improvement in noise for the BJT structure is gained by lowering the absolute temperature of the junction.

12. The shot noise in a BJT can be substantially reduced near DC using a source follower or current mirror mode.

8.1 Summary of Contributions

The contributions provided by this work include the following:

GENERAL

1. The development of a relationship between the THERMAL noise in the bulk silicon in relation to the SHOT NOISE in a P-N junction.

2. The proposition from the results of the JAMES model that the shot noise is only generated in the emitter base junction and not in the base or collector junction.

3. The proposition that shot noise is due to multiple carriers crossing a P-N junction potential barrier concurrently, and in the case of a simple BJT , propagating down the base region minority carrier density profile to the collector, where the charge quanta appears as shot noise.

4. A proposed method of propagation of shot noise quanta in a BJT device that is consistent with physical explanations.

5. A way of reducing the amplitude of the physical mechanism of shot noise formerly thought to be a fundamental mechanism.

6. A rapid method of simulating a large number of carriers in the semiconductor lattice.

7. A method of representing noise in the semiconductor lattice at the atomistic level.

SIMULATION MODEL

1. The use of a novel full 3-D simulation model called JAMES providing a rapid simulation of individual hole and electron carrier behaviour in the semiconductor lattice.

2. The use of a software model to provide evaluation of semiconductor structures and current flow behaviour more detailed than is currently available.

3. The use of the JAMES software kernel to model noise behaviour in a semiconductor structure.

4. The use of a PSEUDO-RANDOM noise generator to develop and de-bug a program with a random execution sequence in the simulator.

5. A method of representing a functional model of the semiconductor lattice and the carriers by using a binary field.

6. A basis for analysing the spectral density at a lattice unit (LU) level or by atomic bond in the LU cell.

7. A model which allows the creation of point defects in the lattice to allow study of the effects on the carrier flow and spectral density at a specific point in 3 dimensions.

8. A model to allow specific point doping profiles to be entered in the lattice.

9. A basis to allow current density analysis at the LU level at any point within the structure.

10. A simulation environment to permit the effect of lattice point-defects on the carrier transport to be evaluated.

11. The results have satisfied the objective of providing a tool for studying mechanisms that are not physically able to be measured.

LOW-NOISE BJT STRUCTURE

1. A new design of BJT incorporating a second base able to reduce the spectral density of the shot noise by $-26.4dB$ at DC.

2. A new BASE2 region reducing the Miller capacitance between the signal base and the bulk collector.

3. A new BASE2 region increasing the AC gain of the device over a broad range of input frequencies.

4. A new BASE2 region increasing the Signal to Noise Ratio of the device when used as a high frequency amplifier.

5. The transition time of the device is improved when used in switch mode, due to the BASE2 region removing diffusion charge.

6. A new BASE2 region suitable for incorporation into VLSI fabrication technologies.

EDA SOFTWARE TOOLS

1. A new approach and basis for providing a design tool suitable for modelling idealised semiconductor devices in the range $15nm - 150nm$.

PUBLICATIONS

1. A paper has been prepared for submission to the AIP Appl. Phys. Letters publication titled "A Novel approach to modelling charge transport in the semiconductor lattice".

2. A paper for the LOW NOISE DUAL BASE BJT device has been prepared for electronic letters , this submission is pending the UK patent finalisation.

3. A potential publication on the relationship between THERMAL and SHOT NOISE as introduced in Appendix: {E.1}.

4. A paper titled "A low current noise source" is being prepared.

5. A future paper for the AIP proposing the mechanism of generation and propagation of shot noise in the BJT structure.

PATENTS

1. A patent application has been filed in the UK for the design of the DUAL-BASE LNBJT device.

2. A patent application has been filed in the USA for the same device.

3. A potential patent application for the low noise current source, Appendix:{L.1 }.

8.1.1 Atomistic modelling

The use of this approach allows future fabrication technologies to be evaluated, and for models to be generated, well before the physical realisation is possible. This permits the evaluation of new semiconductor technologies, particularly the noise implications, in enough time to decide on their suitability. No EDA tool is known to exist at this time, able to achieve this. The use of the JAMES simulator to potentially reduce shot noise has been demonstrated by incorporating different diffused regions in the BJT, in addition to those required in the basic device. This approach is highly suited to BJTs used in current source circuits, which commonly use high source resistance, medium levels of collector current, and high frequency collector signals. The presence of high levels of shot noise in this application would benefit considerably from the use of this new structure. The application of those devices would permit much smaller signals to be processed in electronic systems, and permit more precise measurements and control of time critical functions due to reduced phase noise error or jitter.

8.1.2 Structure for reducing shot noise

The use of an additional highly doped base has been demonstrated, by the use of a simulation model, to reduce the shot noise of the minority carriers in a BJT device, by introducing a mechanism for reducing the spectral density of the collector current.

8.2 What have been the aims of the project

The objective was to understand the charge carrier transport within the semiconductor, the temporal and spatial behaviour, and how this relates to electrical noise observed in a BJTs operation, and use this to validate the JAMES model by proposing a new LNBJT device. The highest ranking factors affecting the noise were taken as the object for improvement, and used to propose a solution for reducing the overall noise in a BJT. The creation of a new model was required to represent this behaviour, and for accuracy, needed to be based on the physical processes in the semiconductor. Testing of the model was required to ensure it behaved in an appropriate way for other mechanisms apart from noise. This would give the model credibility , and then would be applied to studying noise mechanisms. The model was then used to test various physical additions to the transistor structure, and determine if they had a beneficial or detrimental effect on the noise. The final aim was to measure the degree of noise attenuation achievable in a minority carrier BJT transistor.

8.3 What work has been involved, and what has been achieved

The initial work involved the definition of a model which would allow the different physical phenomena to be implemented in a simple way. The next stage identified the important mechanisms relative to the device being studied, and ensure they were implemented in such a way as to correspond to the actual physics of the lattice. This definition was used to write the JAMES model and implement the various mechanisms for de-bug and subsequent validation. The overall simulation was then compared against observed noise phenomena and the correlation of behaviour was used to validate the functional performance of the simulation software. The selection of the programming language and operating system was made with a view to achieving a

program execution time consistent with carrying out many different physical scenarios, on a simple PC . A new model for noise has been developed, and a new BJT proposed with increased AC gain and lower noise. A better understanding of the shot noise mechanism, and a technique for reducing shot noise in minority carrier devices is the result.

8.4 How was it achieved

The main concept which allowed the study of the carrier transport and the shot noise mechanism was the functional noise simulator JAMES. The development and use of this model allowed various possible solutions to be evaluated, and one selected to create a new form of BJT, the LNBJT which is able to reduce shot noise and improve the AC gain of the bipolar structure.

8.5 Novel aspects of work done

The novel aspects of this work have been:

1. The method or representing the carriers as a binary field in a multi-dimensional matrix array.
2. The method of representing the problem in a methodology suitable for rapid analysis.
3. The method for reducing the memory requirements of the simulation kernel.
4. The method for representing the carrier transport mechanisms in a simple, but physically consistent manner.
5. The use of a computer model to study noise mechanisms in a realistic 3-D model up to physically realisable sizes
6. The use of the JAMES model to propose a mechanism for shot noise generation and propagation in the base region of a BJT.
7. The use of this new understanding to propose a solution for reducing the shot noise.

8. The use of a second base in a BJT to reduce the shot noise amplitude by re-thermalising the minority carriers.

9. The use of a second base to screen the signal base and reduce the capacitance from the collector to this base.

10. The use of a second base to increase the transition time of the LNBJT by rapidly removing base diffusion charge through the external BASE2 capacitance

11. The improvement in AC gain over a conventional single base BJT.

12. The combination of noise reduction and gain improvement leading to an improved Signal to Noise ratio.

8.6 Successes

The use of the JAMES kernel has demonstrated a reasonable correlation with several aspects of real devices, namely the spectral density correlation with the current, and the current versus applied voltage. The model was then applied to design a new semiconductor structure, and demonstrate by existing well proven methods, that the structure significantly reduced inherent shot noise in the device, and to some extent the low frequency noise. The AC gain of the new structure was increased by 1.7 times that of a single base BJT for the example given. The signal to noise ratio of the device was substantially improved allowing the application of this concept to many areas of modern micro-electronics. The minimum detectable signal was improved for the new structure when used in amplifier applications. The unity gain bandwidth of the new structure was markedly improved. The work has provided a true 3-D model with significant advantages in simulating noise mechanisms, for the further study of carrier transport in heterogeneous silicon structures, using an intuitive approach. The introduction of an additional doped region into a conventional BJT device, is demonstrated via the model to reduce the shot noise level. The results show that for a given BJT design , the addition of the extra base can reduce the Noise Factor significantly. This example showed the Noise Factor reduced from $5.0dB$ to

$2.4dB$ in a standard amplifier, and in the case of the optimum matching configuration from $1.6567dB$ to $1.27dB$. This approach can be applied to any BJT using other semiconductor materials other than Silicon, e.g. Silicon-Germanium ($SiG\epsilon$). The resolution of some problems using atomistic simulation to model sub-micron semiconductor structures, in a much shorter time than previously attainable, and so making the practical application more feasible. A method for improving the high frequency performance of BJTs, and increasing the signal to noise ratio (SNR) of such devices, to that approaching the levels attainable with MOS FET amplifiers under certain bias conditions. The validation of the shot noise attenuation factor K_{SA} was made by **SPICE** showing a maximum attenuation of $-24.6dB$ at DC. The design of a low current source was given with the noise level reduced from $S_v = 429pV/\sqrt{Hz}$ to $267pV/\sqrt{Hz}$. The demonstration of a new simulation paradigm for application to high performance communications systems in silicon was also made.

8.7 Directions for future research

The previous sections showed an EDA software simulation at the atomic level can be used to represent carrier flow in a semiconductor structure. The nature of shot and thermal noise in relation to the carrier transport processes was also demonstrated. The JAMES simulator kernel was then used to analyse the contributors to noise and to design a new structure specifically for low noise operation. The design of a BJT device to reduce shot noise has been discussed. The plan is to complete the design of such a device and compare it against the predictions from the model, and so to permit further enhancements. The possibility of fabricating such a device would require a slightly modified bipolar fabrication flow. This would allow the creation of a BJT, which would reduce the overall noise figure, and a higher upper usable frequency limit. The contingency in being able to achieve this during the final stage of the research would be to produce an equivalent spice or BSIM model that could represent the new enhanced noise features. This would be an approximation to the equivalent lumped values required to provide equivalent electrical behaviour. This model could be demonstrated in a conventional Spice simulator and its effect, in any

given circuit, analysed. The model developed in its basic form would need further work to develop its full potential. However the possibility of being able to use such a detailed device model in critical areas of a large design, would present a practical and useful alternative. This would enable the computing resource to be used selectively in a large simulation, to achieve the accuracy required. The possibility exists, to use the model available at the end of this research, in an existing simulator, to simulate the front end input stages of an amplifier very accurately. The use of an atomistic model providing a vehicle for noise analysis has been initially demonstrated.

8.7.1 Temperature

The model could be enhanced by representing each bond energy with a greater number of unique electron states. This would allow a more accurate representation of the temperature effects in the model. By using, say 11 internal band energy states out of 14 given by Hund's filling order, the energy levels would be represented by $(E - E_F) \pm 5kT$, where E_F is the Fermi level see Appendices: {I.1, B.1}, could be included. This would allow the model to represent a significant part of the energy probability for the electrons, from 6.693×10^{-3} to 0.993. The total energy-state, of the matrix, would be more accurately represented by having discrete energy levels instead of a single level, so enhancing the model. This could ultimately be expanded to include electron spin. The need for such a detailed representation is not clear at this stage, especially as the conduction process can be represented more accurately with perhaps another 4 states. The complete representation of the energy states would require 64 electron states per bond state, where the more accurate conduction model would require only 4 extra states per bond, a significant saving in memory requirements and program execution time. This additional information would require an extra, four bits per bond-state in the matrix. This is a trade-off between the size of the program matrix and the run-time of the program. In a lattice, the matrix currently needs $704k$ bits of storage. Adding the extra 4 bits would require $906k$ bits, an increase of 36% in each of the two matrices. The bits were not added in the interests of storage and execution time.

8.7.2 Carrier Drift mechanism

The mechanisms of drift are not fully included in the model at this stage. The assignment of charge to each carrier is included, but the electrostatic field and the force on the carriers due to this charge is not. The field influences the width of depletion zones, and the result of this change, would improve the spatial accuracy of the carrier transport modelling. The field set up between the different populations of charge carriers would affect the speed of the carrier movement in high field regions such as a reverse biased junction.

8.7.3 Hardware emulation

The objective was to take the final software model and instantiate the software in hardware to reduce the execution time. The software could then be instantiated in hardware using current EDA tools. This would add a hardware accelerator for the model, if required. The plan was to use behavioural simulation on the JAMES model written in the C programming language, and then synthesise a gate level net-list. This net-list could then be converted to a bit image file, and then loaded into a large Composite Programmable Logic Device (CPLD). This could substantially reduce the model run time, if the hardware could be run at 100 Megahertz.

8.7.4 Transistor modelling to create H-Spice BSIM models

The additional base region of the proposed transistor has been included in an extended lumped H-Spice model, which allows the device to be simulated in a standard AC simulation. This approach would allow a BSIM macro model of the specific semiconductor structure to be derived, for simulations requiring fast execution time such as with the Spice simulators.

8.7.5 Photonics / hole-photon interaction

The JAMES model described in this work may have a useful basis in modelling the behaviour of Photonic crystals. The analogy between hole-electron interaction in the lattice has a parallel with the photon-hole interaction in this technology. The model would require further enhancements e.g. the addition of magnetic field vectors

and enhanced representation of the spatial position of the bonds in the lattice. The model would require an additional $H_{(x,y,z)}$ matrix to be superimposed on the lattice to be addressed by an additional process during program execution.

8.8 Implications for the study

8.8.1 Design of a low noise bipolar transistor

The MOSFET amplifier has been used for many LNA applications due to the lower overall noise when the source resistance is of the order of several hundred ohms. This is due to the MOSFET having an active channel working on the basis of majority carrier operation, as opposed to the BJT which uses minority carrier conduction in the base region. The use of this new LNBJT can improve the Noise Factor in LNA applications with lower source resistance, over MOSFET's. This is due to the MOSFET having some noise contributions greater than the BJT, e.g. reverse channel induced gate noise.

8.8.2 Reduction of Phase noise or "jitter" in PLL systems

The use of the LNBJT in the design of an oscillator or current source reduces the spectral noise density of the active circuit. The use of a constant current source, or current mirror, is a common in discrete and integrated system design to form oscillators and sub-system bias elements for operational amplifiers. The noise on the bias generators can affect the switching point in oscillator designs, and as a result the frequency of the oscillator, has a *phase noise* which reduces its spectral purity. The *Phase Locked Loop* or PLL, is based on a variable frequency oscillator, and so the performance is determined by its phase noise. By reducing the spectral density of the current sources , the oscillator performance and the phase noise or *"jitter"* of the PLL is improved. This can have a *significant* improvement in attaining a higher specification on the performance of timing based electronic systems, such as telecommunications systems operating at high baud rates. The limiting constraint on improvement will be the random thermal jitter once the lower frequency shot noise component is effectively removed.

8.9 Post Script

Enhancements to the simple NPN structure have made during the writing of this thesis, and the model now represents a $3D$ atomistic model of an NPN bipolar structure exhibiting gain characteristics in a limited way via the signal base, and also demonstrating noise attenuation with the additional region superimposed between the signal base and the collector. This mode would require additional work to be regarded as reliable. This creates the possibility of applying signals to the signal base region, and observing carrier operation in full BJT mode, and fast switch mode. This is probably not desirable due to the simulation time required, but does form a basis for studying fast transient analysis, on the BJT structure.

8.10 Endnotes

This approach has provided a natural end-point to this first part of the research, and would result in the design of a Low Noise BJT device. The JAMES model could be used to enhance and analyse other types of semiconductor and certainly other substrate materials apart from silicon.

8.11 VITA

This marks the end of my research that started five years ago at the University of Surrey Research campus in Guilford, Surrey. The intention was to take some time out from a career spend in the semiconductor industry for sabbatical leave, and spend some time in academia pursuing a fundamental area which was inter-disciplinary, in between condensed-matter physics, mathematics and software. My career started with my interests in modelling physical systems, and led to semiconductor physics. The path became a little twisted as time went by and took on more turns than I had anticipated. My ideal challenge is the combination of academia and high technology and I will try to find a balance between the two that allows me to continue my research interests in the physics of semiconductors and exploring the physical limits of this remarkable branch of physics that has become such an important technology.

APPENDICES

Appendix A:

Physical origins of shot noise

Poisson limit (A.1)

To explain the origin of shot noise consider a ficticious experiment, with only one charge carrier. The carrier is incident on a barrier, where the particle is transmitted with probability T or reflected with probability $R = 1 - T$. The incident state is characterised by an occupation number n_{in}, the transmitted state by n_T and the reflected state by n_R . In this experiment $\langle n_{in} \rangle = 1$, $\langle n_T \rangle = T$, and $\langle n_R \rangle = R$. The mean fluctuations in the incident beam vanish $(n_{in} - \langle n_{in} \rangle)^2 = 0$. Finding the mean squared fluctuations of the transmitted and reflected state, we take the average of the product of the occupation numbers of the transmitted and reflected beams $\langle n_T \cdot n_R \rangle$. In each event the particle is transmitted or reflected, the product $n_T.n_R$ vanishes for each experiment, and so the average also vanishes, $\langle n_T n_R \rangle = 0$. This gives a mean square of the transmitted and reflected beam and their correlation is given by

$$\left\langle (\Delta n_T)^2 \right\rangle = \left\langle (\Delta n_R)^2 \right\rangle = - \langle \Delta n_T \Delta N_R \rangle = TR \tag{A.2}$$

where $\Delta n_T = n_T - \langle n_R \rangle$. These fluctuations are called *partition* noise since the scattering divides the incident carrier beam into two streams. The partition noise vanishes both in the limit when the transmission probability $T = 1$, and in the limit when the transmission probability $T = 0$. The partition noise is at a maximum when the transmission probability $T = 1/2$. Enhancing the experiment a little more, and assuming the incident beam is occupied with a probability f. The initial state is empty with probability $1 - f$, and since the average incident occupation number is $\langle n_{in} \rangle = f$, and the particle is transmitted only with probability fT and reflected with probability

fR, we have $\langle n_T \rangle = fT$ and $\langle n_R \rangle = fR$. Repeating the above calculation $\langle (\Delta n_T)^2 \rangle = Tf(1-Tf)$, $\langle (\Delta n_R)^2 \rangle = Rf(1-Rf)$, $\langle \Delta n_T \Delta n_R \rangle = -TRf^2$. At zero temperature $f = 1$, and the previous results are obtained. At $T = 1$ the fluctuations do not vanish, but fluctuate in a similar manner to the incident state. For the transmitted beam the factor $(1-Tf)$ can be replaced with 1 , if either the transmission probability is small, low transparency, or the incident carrier beam is small. Assuming the carriers are moving in one direction only with a velocity $v(E)$ determined by the carrier energy E . In a narrow energy interval dE, the incident current $dI_{in}(E) = e\nu(E)d\rho(E)$, where $d\rho(E)$ is the density of carriers per unit length, $\nu(E) = d\rho/dE$ times the occupation factor $n_{in}(E)$ of the state at energy E. This gives $d\rho(E) = n_{in}(E)\nu(E)dE$. The density of states in this perfect conductor is $v(E) = 1/(2\pi\hbar\nu(E)$. The incident current in a narrow energy interval is then $dI_{in}(E) = \frac{e}{2\pi\hbar} n_{in}(E)dE$. This shows there is a direct link between the current and the occupation number. The total incident current is $I_{in} = (e/2\pi\hbar)\int n_{in}(E)dE$ and the average current is $\langle I_{in} \rangle = (e/2\pi\hbar)\int f(E)dE$. The average transmitted current is $\langle I_T \rangle = (e/2\pi\hbar)\int f(E)TdE$, and the average reflected current $\langle I_R \rangle = (e/2\pi\hbar)\int f(E)RdE$. The current fluctuations in this narrow energy interval are at long times determined by $dI_{in}(E,t) = (e/2\pi\hbar)n_{in}(E,t)dE$ where $n_{in}(E,t)$ is the time dependent occupation number of states with energy E . Since we are interested in the low frequency current noise, we can use a Fourier transform on this equation. In the low frequency limit $I(\omega) = (e/2\pi\hbar)\int dEn(E, E+\hbar\omega)$. This shows the fluctuations in the current and the occupation number are directly related. In the zero frequency limit the current noise power is $S_{II}(E) = e^2 \int dE S_{nn}(E)$, with a mean square value given by $S_{nn}(E) = (1/\pi\hbar)\langle \Delta n \Delta n \rangle$. The transmitted fluctuation spectra is thus

$$S_{I_{in}I_{in}} = 2\frac{e^2}{2\pi\hbar}\int dE\, f(1-f)$$

$$S_{I_T I_T} = 2\frac{e^2}{2\pi\hbar}\int dE\, Tf(1-Tf)$$

$$S_{I_R I_R} = 2\frac{e^2}{2\pi\hbar}\int dE\, Rf(1-Rf)$$

The transmitted and reflected currents are correlated

$$S_{I_T I_R} = -2\frac{e^2}{2\pi\hbar}\int dE\, T f\, R f$$

In the limit that T is small or f is small, the factor $(1 - Tf)$ approximates to 1. In this limit the average current through the barrier is $\langle I\rangle = e/2\pi\hbar \int dE\, T\, f$ and the Schottky's result [, Shottky] is $S_{I_T I_T = 2e\langle I\rangle}$ corresponds to the uncorrelated arrival of carriers (time between carriers) with a Poisson distribution $P(\Delta) = \tau^{-1} exp(-\Delta t/\tau)$, where τ is the mean interval between carriers. The extra factor $(1 - Tf)$ means the Shot noise is always less than the Poisson value. For ballistic systems $T = 1$ the shot noise vanishes even in the zero temperature limit. At high temperatures the factor $(1 - f)$ can be replaced with one. The full Poisson noise given by Schottky's formula is also reached in the case of a barrier with very low transparency, $T \ll 1$.

QUANTUM EQUIVALENCE

The conductance of the system can be expressed in quantum mechanical terms by regarding the system in thermal equilibrium. The quantum statistical average of the product of an electron creation operator and annihilation operator of a Fermi gas is $G = \frac{e^2}{2\pi\hbar} T_r \left[t^\dagger(E_F) t(E_F)\right]$ This equation establishes a relation between the scattering matrix and evaluated at the Fermi energy and the conductance. The matrix $t^{\dagger t}$ has a set of real eigenvalues (transmission probabilities) , each of then having a value between zero and one. This gives $G = \frac{e^2}{2\pi\hbar}{}_{mn}\sum T_{mn}$ where $G_0 = \frac{2e^2}{\hbar}$ is the quantum conductance, and $T_{RL,mn} = |s_{RL,mn}|^2$ are the transmission probabilities.

FANO FACTOR

A measure of the *sub-Poisson* shot noise is the *Fano factor* F which is the ratio of the actual shot noise and the Poisson noise that would be measured if the system produced noise due to single independent carriers, where $F = \frac{S_{LL}}{S_P}$. For energy independent transmission and/or in the linear regime the Fano factor is

$$F = \frac{{}_n\sum T_n(1 - T_n)}{{}_n\sum T_n} \tag{A.3}$$

The Fano factor assumes values between zero (all channels are transparent) and one (Poisson noise). For one channel it becomes $(1 - T)$.

Appendix B:

Physical Constants

$$Physical - constants \tag{B.1}$$

ε_o= 8.854 $\times 10^{-12}$ Farads/m. Absolute permittivity of free space

$\varepsilon_r = 11.9$ Relative permittivity of Silicon (Si)

$q = 1.6 \times 10^{-19}$ coulomb

$k = 8.62 \times 10^{-5} eV/K$

$\hbar = 6.57946 \times 10^{-16} eVs$

$T = -273.16^o K$

$E_F = 1.12eV$ Fermi level at $300^o K$

$n_i[cm^{-3}] = 1.0 \times 10^{10}$ at $300^o K$

$\mu_n[cm^2/V - s] = 1400$ at $300^o K$

$\mu_p[cm^2/V - s] = 450$ at $300^o K$

$\mu_0 = 4\pi \times 10^{-7}$ Henry/meter

$h = 4.134 \times 10^{-15} eV$

$c = 2.998 \times 10^8 m/s$

The Thermal voltage = $V_T = \frac{kT}{q} = 25.875 \times 10^{-3} V$ at $300^o K$

$LU = 5.43095 A^o$

$\frac{a}{4}(\overleftarrow{x} + \overleftarrow{y} + \overleftarrow{z}) = r = 2.3 A^o$

$m_e^* = 0.98$

$m_0 = 5.69 \times 10^{-12} eVs^2 cm^{-2}$

$v_d = 5 \times 10^3\ ms^{-1}$ at 300^o (max)

v_d saturation velocity =$1.05 \times 10^7 cm.s^{-1}$ at 300^o

CONSTANTS

PHYSICAL PARAMETERS USED IN THE LNBJT DESIGN

Boltzmann's k = 8.61700e-05

charge = 1.60200e-19

permittivity = 8.85400e-14

Temperature = 300.

Thermal voltage =0.025851

rel permit = 11.800

log10(ni) = 10.160

n-mobility = 1000.0

p-mobility = 500.00

vsat = 1.03494e+07

taup0 = 1.00000e-07

taun0 = 1.00000e-07

egap(300) = 1.0800

egalpha = 4.73000e-04

egbeta = 636.00

affinity = 4.1700

egap = 1.0800

cnau = 2.80000e-31

cpau = 9.90000e-32

An** = 110.00

Ap** = 30.000

Nc = 2.80000e+19

Nv = 1.04000e+19

gcb = 2.0000

gvb = 4.0000

edb = 4.40000e-02;

eab = 4.50000e-02

Appendix C:

Proof of optimum source resistance

$$K_{SA}factor \tag{C.1}$$

Development of the optimum source resistance R_{Sopt} using the K_{SA} factor, where K_{SA} is real, and defined to be the Shot-noise attenuation factor for electrons, and has a value between 0 and 1.

$$R^2_{Sopt} = \frac{\overline{v_i^2}}{\overline{i_i^2}} \tag{C.2}$$

where v_i is the input equivalent noise voltage, and i_i is the equivalent input noise current, and for $K_{SA} \neq 0$.

$$\overline{v_i^2} = 4kT(r_b + \frac{1}{2gm})\Delta f$$

$$\overline{i_i^2} = 2K_{SA}qI_B\Delta f = 2K_{SA}q\frac{I_C}{\beta_F}\Delta f$$

$$R^2_{Sopt} = 2\beta_F(r_b + \frac{1}{2gm})/K_{SA}gm$$

$$F = \frac{Total - Noise - Power[From(all - sources)]}{Total - Noise - Power[From(input - resistance)]} \tag{C.3}$$

$$R^2_{Sopt} = \beta_F(1 + 2gmr_b)/K_{SA}gm^2$$

$$R_{Sopt} = \frac{\sqrt{\beta_F}}{gm\sqrt{K_{SA}}}\sqrt{1 + 2gmr_b}$$

This shows R_{Sopt} varies as the square root of K_{SA}. when $K_{SA} = 1$, in a conventional BJT, by definition , then

$$R_{Sopt} = \frac{\sqrt{\beta_F}}{gm}\sqrt{1 + 2gmr_b} \tag{C.4}$$

when $\sqrt{K_{SA}} = 0.06$

$$R_{Sopt} = \frac{1}{.06}\frac{\sqrt{\beta_F}}{gm}\sqrt{1+2gmr_b} \tag{C.5}$$

R_{Sopt} increases by a factor of 4.08. By substituting the expression for R_{Sopt} in the equation for the noise factor F, the optimal value of the noise factor can be calculated.

$$F_{opt} = 1 + \frac{\sqrt{1+2gmr_b}}{\sqrt{\beta_F}}\sqrt{K_{SA}} \tag{C.6}$$

The optimum value of the noise factor achievable for a given BJT transistor is reduced as K_{SA} is reduced. It can also be shown that the THEORETICAL minimum noise figure without shot attenuation is given by

$$F_{min} \simeq 1 + \frac{1}{\sqrt{\beta_F}}\sqrt{1+2gmr_b} \tag{C.7}$$

This shows the base spreading resistance is a key parameter in determining the minimum noise figure for a BJT. When $K_{SA} = 0$, (no shot noise from Eq. C.2 $i_i = 0$), there is no optimum value for R_S and hence no value for R_{Sopt} and F_{opt} . The minimum value of F_{min} is given by C.8 in the limit $K_{SA} \to 0$.

$$F_{min} = (R_s + r_b)/R_s \tag{C.8}$$

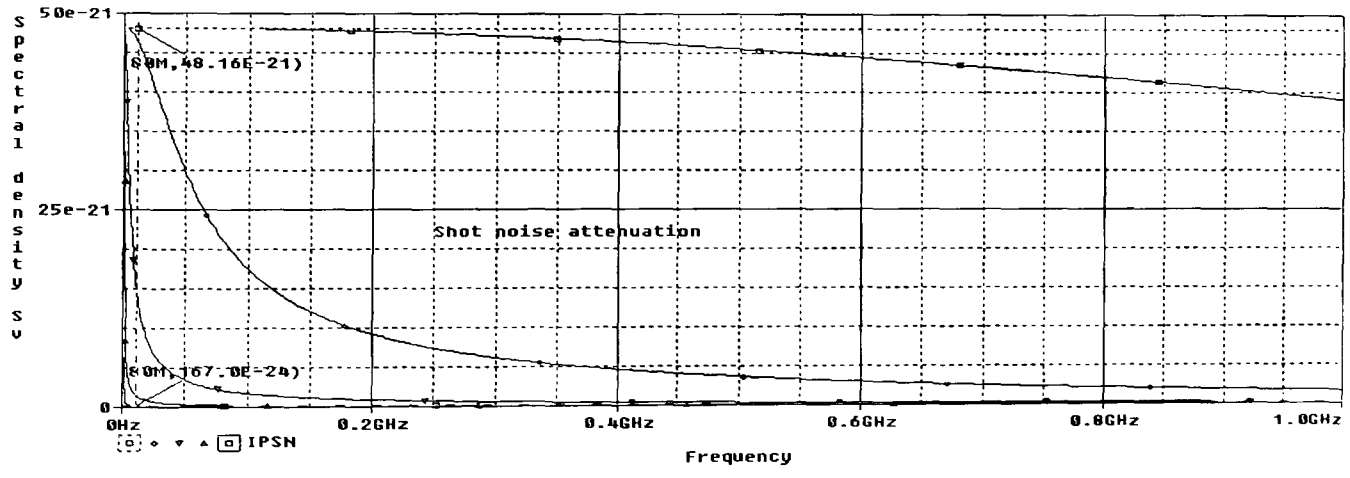

Fig. C.1. SPICE simulation of the shot noise attenuation factor K_{SA}

Appendix D:

Noise levels in the BJT device

The resistance dominating the thermal noise model of a bipolar device is the base resistance. The typical value for a high-frequency BJT is about $5 - 20\Omega$ in practice . Taking 20Ω for this example; the thermal noise due to r_b is therefore

$$S_i = 4kT.\frac{1}{20}.\Delta f \tag{D.1}$$

$$S_i = 8.28 \times 10^{-22}\ A^2/Hz.$$

The graph in Figure: D.1 below shows the approximate magnitudes of each of the noise types described above. The graph shows the noise spectral density measured against the log frequency on the horizontal axis.

Frequency f_1 represents the onset of Flicker noise at low frequencies, and f_2 the onset of shot noise effects. The mid band region between $f_1$and f_2 is dominated primarily by Thermal noise effects. The noise below f_1 increases at an approximate rate of $1/f$, and the frequency above $f_2$increases at approximately f^2[15].

The Flicker and Burst noise are taken from measurements of typical BJT devices. and the shot and thermal noise levels are superimposed. The input referred voltage noise spectral density S_v above , can be written in another form. The *transconductance* parameter gm is defined as the forward current ratio, or the ratio of the collector to base current. Given the transconductance gm is given by

$$gm = \frac{qI_c}{kT} \tag{D.2}$$

where $q = 1.6 \times 10^{-19}$, k = Boltzmann's constant , $T = 300^o K$ {B.1} , and I_c is the

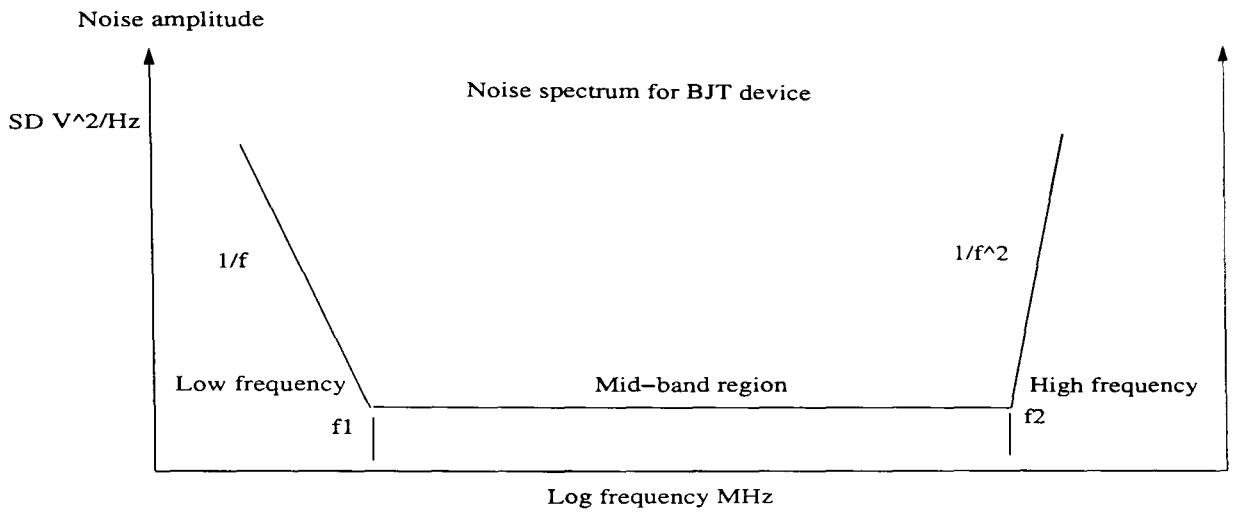

Fig. D.1. BJT noise spectrum vs Frequency

collector current giving

$$S_v = 4kT(r_b + (\frac{kT}{2qI_c}))\ V^2/Hz$$

This is the input referred equivalent noise resistance. Substituting with $I_c = 100 \times 10^{-6}$, and $r_b = 20\Omega$.

$$S_v = 4 \times 1.38 \times 10^{-23} \times 300 \times (20 + 129)$$

and so

$$S_v = 3.3 \times 10^{-19} + 2.14 \times 10^{-18} = 2.47 \times 10^{-18}\ V^2/Hz$$

The thermal noise spectral density of the base resistance for $r_b = 20\Omega$ would be

$$S_v = 4kTr_b = 4 \times 1.38 \times 10^{-23} \times 300 \times 20 = 3.3 \times 10^{-19}\ V^2/Hz$$

The approximate mid-band shot-noise [15] is given by

$$S_i = 2q[I_B + (\frac{I_C}{\beta_0^2})]$$

For $\beta_F = 100$, and $f_T = 500MHz$, then $f_b = 50MHz$. This gives a mid-band equivalent input shot-noise current spectral density of

$$S_i = 2 \times 1.6 \times 10^{-19}[\frac{1 \times 10^{-3}}{100} + \frac{1 \times 10^{-3}}{100^2}]$$

$$S_i \cong 2qI_B = 3.2e^{-24}\ A^2/Hz$$

at a collector current I_c of $100uA$. From the equation for the total input referred noise of the device given in Eq. D.3.

$$\frac{\overline{v_{in}^2}}{\Delta f} = 2kT(R_s + r_b + \frac{1}{2gm}) + K_{SA}R_S^2\, 2q\left[I_b + \frac{I_c}{|\beta(jf)|^2}\right] \tag{D.3}$$

The above Eq. [15] shows total noise omitting Flicker noise.

$$Test - conditions \tag{D.4}$$

The standard test conditions for reference throughout this work is given as:
$T = 300^o K$ and $I = 10^{-3}A$;

$$S_i = 2 \cdot I_D \cdot q$$

$$S_i = 2 \cdot 1.6 \times 10^{-19} \cdot 1 \times 10^{-3} = 3.2 \times 10^{-22}$$

The shot noise of a junction device sets a fundamental lower limit to the attainable noise figure in a simple P-N junction; for example such a junction at $300^o K$ and with a forward current of $1mA$ flowing, generates a spectral density $S_v = 2.14 \times 10^{-19} V^2/Hz$ or by using Eq. H.6 a voltage of

$$S_v = \frac{2k^2T^2}{qI_d} = 463pV\ rms \tag{D.5}$$

of noise voltage across the base emitter junction of a typical BJT. The value of S_v therefore increases with the magnitude of the current.

Appendix E:

The relationship between Thermal noise and Shot noise

There is a direct relationship between Thermal noise and Shot noise as demonstrated below. The shot noise is derived in relation to a simple P-N junction, in this case the *base-emitter* junction of the BJT. Thermal noise is given by

$$\overline{v_T}^2 = 4kT \tag{E.1}$$

Shot noise is given by

$$\overline{v_S}^2 = 2Iqr_D^2 \tag{E.2}$$

where $r_D = \frac{dV_{be}}{dI}$, the dynamic resistance or slope of the I/V characteristic.

$$\overline{v_T}^2 = \overline{v_S}^2.F \tag{E.3}$$

where

$$F = \frac{2kT}{qI_D r_D} \tag{E.4}$$

where I_D is the current through the junction and r_D is the dynamic resistance of the junction. The diode equation is given by

$$I_D = I_S(exp^{\frac{qV_D}{kT}} - 1) \tag{E.5}$$

where I_S is the junction saturation current and is given by

$$I_S = \frac{qAD_n}{W_B N_A} \tag{E.6}$$

where D_n is the hole diffusion constant, and W_B is the length of the Base region from the edge of the base-emitter depletion layer to the edge of the collector Base depletion region in a conventional single base BJT. Substituting in the equation above

$$\overline{v_T}^2 = \overline{v_S}^2.2\frac{(I_D + I_S)}{I_D} \tag{E.7}$$

substituting for I_S

$$\overline{v_T}^2 = \overline{v_S}^2.2(1 + \frac{aAD_n}{W_B N_A I_D}) \tag{E.8}$$

where $I_D >> I_S$

$$\overline{v_T}^2 \simeq 2.\overline{v_S}^2 \tag{E.9}$$

or

$$\overline{v_S}^2 \simeq \frac{1}{2}\overline{v_T}^2 \tag{E.10}$$

This is true for all I_D unless I_D approaches I_S.

N.B. In practice $I_D = 10^{-10}$ and I_D is in the range 10^{-6} to 10^{-1}. This means that the Spectral density of the Thermal noise is double the Spectral density of the Shot noise in a $P - N$ junction under normal operating conditions.

Appendix F:

Carrier mobility vs Doping

$$u_n \; and \; u_p \tag{F.1}$$

The electron and hole mobilities have similar doping dependence. For low doping concentrations the mobility is almost constant, and is primarily limited by phonon scattering. At higher doping concentrations the mobility decreases due to ionised impurity scattering with the ionised doping atoms. The actual mobility also depends on the type of dopant. The empirical calculation for the mobility for electrons and holes are shown below.

$$\mu_n = 68.5 + \frac{(1414 - 68.5)}{1 + (\frac{N}{9.2 \times 10^{16}})^{0.711}} cm^2/V - s \tag{F.2}$$

and

$$\mu_p = 44.9 + \frac{(470.5 - 44.9)}{1 + (\frac{N}{2.23 \times 10^{17}})^{0.719}} cm^2/V - s$$

These are obtained by curve fitting experimental values and not theoretically derived. The temperature dependence for mobilities are also shown below for electrons:

$$\mu_n(N,T) = 88(\frac{T}{300})^{0.57} + \frac{7.4e^8 T^{-2.33}}{1 + (\frac{N}{1.26 \times 10^{17}(\frac{T}{300})^{2.4}} 0.88(\frac{T}{300})^{0.146}} cm^2/V - s \tag{F.3}$$

and for holes

$$\mu_p(N,T) = 54.3(\frac{T}{300})^{0.57} + \frac{1.35e^8 T^{2.33}}{1 + (\frac{N}{2.35 \times 10^{17}(\frac{T}{300})^{2.4}} 0.88(\frac{T}{300})^{0.146}} cm^2/V - s \tag{F.4}$$

Appendix G:

Noise Parameters of BJTs

This section provides some noise parameters for BJTs derived from small signal AC analysis techniques [43]. The Equivalent resistance is given by:

$$R_{eq} = R_b + \frac{(1/2)}{g_m} \tag{G.1}$$

Equivalent capacitance:

$$C_{eq} = C_{be} + C_{bc} + C_p \tag{G.2}$$

Minimum noise figure:

$$F_{min} = 1 + \sqrt{\frac{2q}{kT}(R_{eq} I_B) + \frac{2R_{eq}}{gm}(\omega C_{eq})^2} \tag{G.3}$$

Noise figure:

$$F = \frac{v_n^2 + R_S^2 . i_n^2 + 4kTBR_S}{4kTBR_s} \tag{G.4}$$

Optimum source resistance:

$$R_{opt} = \sqrt{R_b^2 + \frac{2gmR_{eq}}{(\omega C_{eq})^2}} \tag{G.5}$$

Noise conductance:

$$g_n = \frac{(\omega C_{eq})^2}{2gm} \tag{G.6}$$

Noise measure

$$M = \frac{F-1}{1-(1/G)} \tag{G.7}$$

where G is the associated gain of the device. The Minimum Detectable Signal is given by:

$$MDS = \overline{v_{iNT}^2} \tag{G.8}$$

where $\overline{v_{iNT}^2}$ is the equivalent input noise generator that would produce the output noise for a noiseless BJT.

Appendix H:

P-N Junction characteristics

$$Diode - eqn \tag{H.1}$$

The relationship between current and voltage for an abrupt P-N junction is given below

$$I_D = I_S(\frac{qV_{BE}}{kT} - 1) \tag{H.2}$$

where I_S is the P-N junction saturation current see E.6, and $V_{BE}$is the forward voltage across the $P - N$ junction. The slope resistance of the diode at the operating point set by I_D is given be

$$r_d = \frac{v_{be}}{I_D} \tag{H.3}$$

This can be written as

$$r_d = \frac{kT}{qI_D} \tag{H.4}$$

The spectral current density is given by

$$S_i = 2qI_d A^2/Hz$$

and the spectral voltage density across the diode can be found by

$$S_v = S_i r_d^2 \tag{H.5}$$

giving the spectral voltage density as

$$S_v = \frac{2k^2T^2}{qI_D} \tag{H.6}$$

Appendix I:

FERMI Energy Level

Fermi level (I.1)

The relationship between the Fermi energy level E_F and the Intrinsic energy level E_i is given by

$$\Phi_B = \frac{kT}{q}\left[ln(\frac{N_D}{n_i})\right] \tag{I.2}$$

if $N_D = 10^{24}$

$$\Phi_B = \frac{1.38 \times 10^{-23} \times 300}{1.6 \times 10^{-19}}\left[ln(\frac{10 \times 10^{24}}{1 \times 10^{10}})\right] \tag{I.3}$$

giving $\Phi_B = 0.8937V$ difference in energy between E_F and E_i. where N_D is the doping level (n-type), and n_i is the intrinsic equilibrium level of carriers.

Junction potential (I.4)

The BASE1-BASE2 potential between $0,1\mu$ and $0,2\mu$ in Figure: 6.2, and is given by the equation

$$\Phi_{B1-2} = \frac{kT}{q} \cdot ln\left(\frac{N_{aB2}}{N_{aB1}}\right) \tag{I.5}$$

This voltage is equal to $59.5mV$ at a temperature of $300^{o}K$, and $N_{aB2} = 10N_{aB1}$. The BASE2-BASE1 potential between $0,2\mu$ and $0,3\mu$ in Figure: 6.2 using Eq. I.5 is $178mV$ at the same temperature, where $N_{aB2} = 10^3 N_{aB1}$.

Appendix J:

Electronic Design Auomation

$$EDA - brief - synopsis \tag{J.1}$$

The development of Electric Design Automation has been concurrent to some extent with the development of the large scale integration of systems on silicon. The usual process that has evolved is that the lead design engineers create the cutting edge of the performance , and so develop the initial processes. These processes are taken by the EDA corporations and built in to software tools to allow the processes themselves to be more systematic, much faster to use, and so enhanced. This drives the reduction of time to market, and makes a solid commercial base for the high-technology products.The need to provide new EDA tools that speeds up VLSI development time and reduces the large financial risk will drive the direction of this technology in the future.

Appendix K:

BJT 3-D PARAMETERS

FastHenry (K.1)

The FASTHENRY 3-D solver program was used to extract the lumped parameters of the BJT illustrated in Figure: 7.1. The model assumes there are no P-N junctions and that the contact resistance between the different regions will be the same as the small signal resistance in the limit. The device selected would be one implementation, and could be made using a quadruple diffusion planar structure. This assumes the diode slope resistance is zero. The resistance values of the structure are all that are required in the SPICE simulation , as the diode functions will be inserted also, so this is a reasonable approach. The data input file for FASTHENRY is shown below: The Planar BJT device is divided into a number of sections representing the different doped regions of the BJT. The ".units" statement sets the actual dimensions to be used, in this case micro-meters. There a four sections for the emitter, collector etc.

The nodes described as Nxxx have a description of the x,y, and z coordinates of each 3-D region. The terms shown as Exxx describe filaments that connect the nodes to one another called branches, and build up to represent the 3-D regions. The next part of the statement defines the resistivity σ of the branch in mhos. The section of the E statement after the connectivity e.g "nhinc=8 nwinc=8" defines the number of filaments in the branch. The greater the number of filaments the higher the accuracy of the resistive and inductive values calculated. The device has a buried collector region defined under the collector base. This is used to reduce the collector resistance of the device. The statement ".equiv N3 N1 N16 N20 N30 N37 " defines the nodes as having the same potential at each node. This is used in this as an example to

circumnavigate some of the difficulties in using this software to model a single crystal with different doped regions. Finally the statement ".external N4 N6 .freq fmin=1e4 fmax=1e8 ndec=1" defines the two nodes of interest in the calculation. This example shows that the parameters between nodes 4 and 6, this is the resistance measurement between the collector and BASE2 contact. The final part of this statement defines the minimum and maximum frequency of interest, and the incremental frequency step to be used. FASTHENRY creates an output file called *Zc.mat* , and an example of this file is shown below Algorithm: 60. The inductance values are ignored as the example here is being analysed at a relatively low frequency.

The output file shows the Impedance between the Base and emitter contacts (node4 to node 11). The real component (or resistive part is 7.07Ω) and the imaginary component is $9.35 \times 10^{-9}\Omega$ inductive at a frequency of $100Mhz$.

Algorithm 46 Fasthenry input file

```
.default z=0

.units um

N1 x=.25 z=1.0 y=0.25

N1A x=.250 z=1.010 y=0.25

N1B x=.250 z=1.020 y=0.25

N1C x=.250 z=1.030 y=0.25

N1D x=.250 z=1.040 y=0.25

N2 x=.25 z=1.050 y=0.25

N2A x=.250 z=1.060 y=0.25

N2B x=.250 z=1.070 y=0.25

N2C x=.250 z=1.080 y=0.25

N2D x=.250 z=1.090 y=0.25

N3 x=.025 z=1.0 y=0.25

N3A1 x=.025 z=1.010 y=0.25

N3A2 x=.025 z=1.020 y=0.25

N3A3 x=.025 z=1.030 y=0.25

N3A4 x=.025 z=1.040 y=0.25

N3A5 x=.025 z=1.050 y=0.25

N3A x=.025 z=1.060 y=0.25

N3B x=.025 z=1.070 y=0.25

N3C x=.025 z=1.080 y=0.25

N3D x=.025 z=1.090 y=0.25

N3E x=.025 z=1.100 y=0.25

N3F x=.025 z=1.11 y=0.25

N3G x=.025 z=1.12 y=0.25

N3H x=.025 z=1.13 y=0.25

N3I x=.025 z=1.14 y=0.25

N3J x=.025 z=0.15 y=0.25

N3K1 x=.025 z=1.16 y=0.25

N3L1 x=.025 z=1.17 y=0.25

N3M1 x=.025 z=1.18 y=0.25

N3N1 x=.025 z=1.19 y=0.25
```

Algorithm 47 Part 2

N5B x=.075 z=1.070 y=0.25

N5C x=.075 z=1.080 y=0.25

N5D x=.075 z=1.090 y=0.25

N5E x=.075 z=1.100 y=0.25

N5F x=.075 z=1.11 y=0.25

N5G x=.075 z=1.12 y=0.25

N5H x=.075 z=1.13 y=0.25

N5I x=.075 z=1.14 y=0.25

N5J x=.075 z=1.15 y=0.25

N5K1 x=.075 z=1.16 y=0.25

N5L1 x=.075 z=1.17 y=0.25

N5M1 x=.075 z=1.18 y=0.25

N5N1 x=.075 z=1.19 y=0.25

N6 x=.075 z=1.200 y=0.25

N7 x=0.125 z=1.050 y=0.25

N7A x=0.125 z=1.060 y=0.25

N7B x=0.125 z=1.070 y=0.25

N7C x=0.125 z=1.080 y=0.25

N7D x=0.125 z=1.090 y=0.25

N7E x=0.125 z=1.100 y=0.25

N7F x=0.125 z=1.11 y=0.25

N7G x=0.125 z=1.12 y=0.25

N7H x=0.125 z=1.13 y=0.25

N7I x=0.125 z=1.14 y=0.25

N7J x=0.125 z=1.15 y=0.25

N7K1 x=0.125 z=1.16 y=0.25

N7L1 x=0.125 z=1.17 y=0.25

N7M1 x=0.125 z=1.18 y=0.25

N7N1 x=0.125 z=1.19 y=0.25

N8 x=0.125 z=1.200 y=0.25

N9 x=.250 z=1.100 y=0.25

N9A x=.250 z=1.11 y=0.25

Algorithm 48 Part 3

N10 x=.250 z=1.15 y=0.25

N10A x=.250 z=1.16 y=0.25

N10B x=.250 z=1.17 y=0.25

N10C x=0.25 z=1.18 y=0.25

N10D x=0.25 z=1.19 y=0.25

N11 x=0.25 z=1.20 y=0.25

N12 x=.375 z=1.050 y=0.25

N12A x=.375 z=1.060 y=0.25

N12B x=.375 z=1.070 y=0.25

N12C x=.375 z=1.080 y=0.25

N12D x=.375 z=1.090 y=0.25

N12E x=.375 z=1.100 y=0.25

N12F x=.375 z=1.11 y=0.25

N12G x=.375 z=1.12 y=0.25

N12H x=.375 z=1.13 y=0.25

N12I x=.375 z=1.14 y=0.25

N12J x=.375 z=1.15 y=0.25

N12K1 x=.375 z=1.16 y=0.25

N12L1 x=.375 z=1.17 y=0.25

N12M1 x=.375 z=1.18 y=0.25

N12N1 x=.375 z=1.19 y=0.25

N13 x=.375 z=1.200 y=0.25

N14 x=.425 z=1.050 y=0.25

N14A x=.425 z=1.060 y=0.25

N14B x=.425 z=1.070 y=0.25

N14C x=.425 z=1.080 y=0.25

N14D x=.425 z=1.090 y=0.25

N14E x=.425 z=1.100 y=0.25

N14F x=.425 z=1.11 y=0.25

N14G x=.425 z=1.12 y=0.25

N14H x=.425 z=1.13 y=0.25

N14I x=.425 z=1.14 y=0.25

Algorithm 49 Part 4

N14M1 x=.425 z=1.18 y=0.25

N14N1 x=.425 z=1.19 y=0.25

N15 x=.425 z=1.20 y=0.25

N16 x=.475 z=1.00 y=0.25

N16A1 x=.475 z=1.010 y=0.25

N16A2 x=.475 z=1.020 y=0.25

N16A3 x=.475 z=1.030 y=0.25

N16A4 x=.475 z=1.040 y=0.25

N16A x=.475 z=1.050 y=0.25

N16B x=.475 z=1.060 y=0.25

N16C x=.475 z=1.070 y=0.25

N16D x=.475 z=1.080 y=0.25

N16E x=.475 z=1.090 y=0.25

N16F x=.475 z=1.100 y=0.25

N16G x=.475 z=1.11 y=0.25

N16H x=.475 z=1.12 y=0.25

N16I x=.475 z=1.13 y=0.25

N16J x=.475 z=1.14 y=0.25

N16K x=.475 z=1.15 y=0.25

N16L x=.475 z=1.16 y=0.25

N16M x=.475 z=1.17 y=0.25

N16N x=.475 z=1.18 y=0.25

N16O x=.475 z=1.19 y=0.25

N17 x=.475 z=1.200 y=0.25

N20 x=.250 z=1.0 y=0.025

N20A x=.250 z=1.01 y=0.025

N20B x=.250 z=1.02 y=0.025

N20C x=.250 z=1.03 y=0.025

N20D x=.250 z=1.04 y=0.025

N20E x=.250 z=1.05 y=0.025

N20F x=.250 z=1.06 y=0.025

N20G x=.250 z=1.07 y=0.025

Algorithm 50 Part 5

N20K x=.250 z=1.11 y=0.025

N20L x=.250 z=1.12 y=0.025

N20M x=.250 z=1.13 y=0.025

N20N x=.250 z=1.14 y=0.025

N20O x=.250 z=1.15 y=0.025

N20P x=.250 z=1.16 y=0.025

N20Q x=.250 z=1.17 y=0.025

N20R x=.250 z=1.18 y=0.025

N20S x=.250 z=1.19 y=0.025

N21 x=.250 z=1.20 y=0.075

N22 x=.250 z=1.05 y=0.075

N22B x=.250 z=1.06 y=0.075

N22C x=.250 z=1.07 y=0.075

N22D x=.250 z=1.08 y=0.075

N22E x=.250 z=1.09 y=0.075

N22F x=.250 z=1.10 y=0.075

N22G x=.250 z=1.11 y=0.075

N22H x=.250 z=1.12 y=0.075

N22I x=.250 z=1.13 y=0.075

N22J x=.250 z=1.14 y=0.075

N22K x=.250 z=1.15 y=0.075

N22L x=.250 z=1.16 y=0.075

N22M x=.250 z=1.17 y=0.075

N22N x=.250 z=1.18 y=0.075

N22O x=.250 z=1.19 y=0.075

N23 x=.250 z=1.20 y=.075

N24 x=.250 z=1.100 y=.125

N24A x=.250 z=1.11 y=.125

N24B x=.250 z=1.12 y=.125

N24C x=.250 z=1.13 y=.125

N24D x=.250 z=1.14 y=.125

N24E x=.250 z=1.15 y=.125

Algorithm 51 Part 6

N24I x=.250 z=1.19 y=.125

N25 x=.250 z=1.20 y=.125

N26 x=.250 z=1.100 y=.375

N26A x=.250 z=1.11 y=.375

N26B x=.250 z=1.12 y=.375

N26C x=.250 z=1.13 y=.375

N26D x=.250 z=1.14 y=.375

N26E x=.250 z=1.15 y=.375

N26F x=.250 z=1.16 y=.375

N26G x=.250 z=1.17 y=.375

N26H x=.250 z=1.18 y=.375

N26I x=.250 z=1.19 y=.375

N27 x=.250 z=1.20 y=.375

N28 x=.250 z=1.05 y=0.425

N28B x=.250 z=1.06 y=0.425

N28C x=.250 z=1.07 y=0.425

N28D x=.250 z=1.08 y=0.425

N28E x=.250 z=1.09 y=0.425

N28F x=.250 z=1.10 y=0.425

N28G x=.250 z=1.11 y=0.425

N28H x=.250 z=1.12 y=0.425

N28I x=.250 z=1.13 y=0.425

N28J x=.250 z=1.14 y=0.425

N28K x=.250 z=1.15 y=0.425

N28L x=.250 z=1.16 y=0.425

N28M x=.250 z=1.17 y=0.425

N28N x=.250 z=1.18 y=0.425

N28O x=.250 z=1.19 y=0.425

N29 x=.250 z=1.20 y=0.425

N30 x=.250 z=1.0 y=0.475

N30A x=.250 z=1.01 y=0.475

N30B x=.250 z=1.02 y=0.475

Algorithm 52 Part 7

N30F x=.250 z=1.06 y=0.475

N30G x=.250 z=1.07 y=0.475

N30H x=.250 z=1.08 y=0.475

N30I x=.250 z=1.09 y=0.475

N30J x=.250 z=1.1 y=0.475

N30K x=.250 z=1.11 y=0.475

N30L x=.250 z=1.12 y=0.475

N30M x=.250 z=1.13 y=0.475

N30N x=.250 z=1.14 y=0.475

N30O x=.250 z=1.15 y=0.475

N30P x=.250 z=1.16 y=0.475

N30Q x=.250 z=1.17 y=0.475

N30R x=.250 z=1.18 y=0.475

N30S x=.250 z=1.19 y=0.475

N31 x=.250 z=1.20 y=0.475

* AXIS N32 x=0 y=0 z=0

N33 x=0 y=0.6 z=0

N34 x=0.6 y=0 z=0

N35 x=0 y=0 z=0.6

* ADD BURIED COLLECTOR LAYER

N36 x=0.25 y=0.25 z=0

N37 x=0.25 y=0.25 z=1.0

E1 N1 N1A w=0.4 h=0.4 rho=4.34 nhinc=8 nwinc=8

E2 N1A N1B w=0.4 h=0.4 rho=4.34 nhinc=8 nwinc=8

E3 N1B N1C w=0.4 h=0.4 rho=4.34 nhinc=8 nwinc=8

E4 N1C N1D w=0.4 h=0.4 rho=4.34 nhinc=8 nwinc=8

E5 N1D N2 w=0.4 h=0.4 rho=4.34 nhinc=8 nwinc=8

E6 N2 N2A w=0.3 h=0.3 rho=6.5 nhinc=8 nwinc=8

E7 N2A N2B w=0.3 h=0.3 rho=6.5 nhinc=8 nwinc=8

E8 N2B N2C w=0.3 h=0.3 rho=6.5 nhinc=8 nwinc=8

E9 N2C N2D w=0.3 h=0.3 rho=6.5 nhinc=8 nwinc=8

E10 N2D N9 w=0.3 h=0.3 rho=6.5 nhinc=8 nwinc=8

Algorithm 53 Part 8

E25 N3A3 N3A4 w=0.05 h=0.5 rho=4.34e3 nhinc=8 nwinc=8

E25A N3A4 N3A5 w=0.05 h=0.5 rho=4.34e3 nhinc=8 nwinc=8

E26 N3A5 N3A w=0.05 h=0.5 rho=4.34e3 nhinc=8 nwinc=8

E27 N3A N3B w=0.05 h=0.5 rho=4.34e3 nhinc=8 nwinc=8

E28 N3B N3C w=0.05 h=0.5 rho=4.34e3 nhinc=8 nwinc=8

E29 N3C N3D w=0.05 h=0.5 rho=4.34e3 nhinc=8 nwinc=8

E30 N3D N3E w=0.05 h=0.5 rho=4.34e3 nhinc=8 nwinc=8

E31 N3E N3F w=0.05 h=0.5 rho=4.34e3 nhinc=8 nwinc=8

E32 N3F N3G w=0.05 h=0.5 rho=4.34e3 nhinc=8 nwinc=8

E33 N3G N3H w=0.05 h=0.5 rho=4.34e3 nhinc=8 nwinc=8

E34 N3H N3I w=0.05 h=0.5 rho=4.34e3 nhinc=8 nwinc=8

E35 N3I N3J w=0.05 h=0.5 rho=4.34e3 nhinc=8 nwinc=8

E36 N3J N3K1 w=0.05 h=0.5 rho=4.34e3 nhinc=8 nwinc=8

E37 N3K1 N3L1 w=0.05 h=0.5 rho=4.34e3 nhinc=8 nwinc=8

E38 N3L1 N3M1 w=0.05 h=0.5 rho=4.34e3 nhinc=8 nwinc=8

E39 N3M1 N3N1 w=0.05 h=0.5 rho=4.34e3 nhinc=8 nwinc=8

E40 N3N1 N4 w=0.05 h=0.5 rho=4.34e3 nhinc=8 nwinc=8

E46 N5 N5A w=0.05 h=0.4 rho=6.5 nhinc=8 nwinc=8

E51 N5A N5B w=0.05 h=0.4 rho=6.5 nhinc=8 nwinc=8

E52 N5B N5C w=0.05 h=0.4 rho=6.5 nhinc=8 nwinc=8

E53 N5C N5D w=0.05 h=0.4 rho=6.5 nhinc=8 nwinc=8

E54 N5D N5E w=0.05 h=0.4 rho=6.5 nhinc=8 nwinc=8

E55 N5E N5F w=0.05 h=0.4 rho=6.5 nhinc=8 nwinc=8

E56 N5F N5G w=0.05 h=0.4 rho=6.5 nhinc=8 nwinc=8

E57 N5G N5H w=0.05 h=0.4 rho=6.5 nhinc=8 nwinc=8

E58 N5H N5I w=0.05 h=0.4 rho=6.5 nhinc=8 nwinc=8

E59 N5I N5J w=0.05 h=0.4 rho=6.5 nhinc=8 nwinc=8

E60 N5J N5K1 w=0.05 h=0.4 rho=6.5 nhinc=8 nwinc=8

E61 N5K1 N5L1 w=0.05 h=0.4 rho=6.5 nhinc=8 nwinc=8

E62 N5L1 N5M1 w=0.05 h=0.4 rho=6.5 nhinc=8 nwinc=8

E63 N5M1 N5N1 w=0.05 h=0.4 rho=6.5 nhinc=8 nwinc=8

E64 N5N1 N6 w=0.05 h=0.4 rho=6.5 nhinc=8 nwinc=8

Algorithm 54 Part 9

E173 N7C N7D w=0.05 h=0.30 rho=5.7e1 nhinc=8 nwinc=8

E174 N7D N7E w=0.05 h=0.30 rho=5.7e1 nhinc=8 nwinc=8

E175 N7E N7F w=0.05 h=0.30 rho=5.7e1 nhinc=8 nwinc=8

E176 N7F N7G w=0.05 h=0.30 rho=5.7e1 nhinc=8 nwinc=8

E177 N7G N7H w=0.05 h=0.30 rho=5.7e1 nhinc=8 nwinc=8

E178 N7H N7I w=0.05 h=0.30 rho=5.7e1 nhinc=8 nwinc=8

E179 N7I N7J w=0.05 h=0.30 rho=5.7e1 nhinc=8 nwinc=8

E180 N7J N7K1 w=0.05 h=0.30 rho=5.7e1 nhinc=8 nwinc=8

E181 N7K1 N7L1 w=0.05 h=0.30 rho=5.7e1 nhinc=8 nwinc=8

E182 N7L1 N7M1 w=0.05 h=0.30 rho=5.7e1 nhinc=8 nwinc=8

E183 N7M1 N7N1 w=0.05 h=0.30 rho=5.7e1 nhinc=8 nwinc=8

E184 N7N1 N8 w=0.05 h=0.30 rho=5.7e1 nhinc=8 nwinc=8

E10A N9 N9A w=0.2 h=0.2 rho=5.7e1 nhinc=8 nwinc=8

E10B N9A N9B w=0.2 h=0.2 rho=5.7e1 nhinc=8 nwinc=8

E10C N9B N9C w=0.2 h=0.2 rho=5.7e1 nhinc=8 nwinc=8

E10D N9C N9D w=0.2 h=0.2 rho=5.7e1 nhinc=8 nwinc=8

E10E N9D N10 w=0.2 h=0.2 rho=5.7e1 nhinc=8 nwinc=8

E10F N10 N10A w=0.2 h=0.2 rho=1.3 nhinc=8 nwinc=8

E10G N10A N10B w=0.2 h=0.2 rho=1.3 nhinc=8 nwinc=8

E10H N10B N10C w=0.2 h=0.2 rho=1.3 nhinc=8 nwinc=8

E10I N10C N10D w=0.2 h=0.2 rho=1.3 nhinc=8 nwinc=8

E10J N10D N11 w=0.2 h=0.2 rho=1.3 nhinc=8 nwinc=8

E70 N12 N12A w=0.05 h=0.30 rho=5.7e1 nhinc=8 nwinc=8

E72 N12A N12B w=0.05 h=0.30 rho=5.7e1 nhinc=8 nwinc=8

E73 N12B N12C w=0.05 h=0.30 rho=5.7e1 nhinc=8 nwinc=8

E74 N12C N12D w=0.05 h=0.30 rho=5.7e1 nhinc=8 nwinc=8

E75 N12D N12E w=0.05 h=0.30 rho=5.7e1 nhinc=8 nwinc=8

E76 N12E N12F w=0.05 h=0.30 rho=5.7e1 nhinc=8 nwinc=8

E87 N12F N12G w=0.05 h=0.30 rho=5.7e1 nhinc=8 nwinc=8

E88 N12G N12H w=0.05 h=0.30 rho=5.7e1 nhinc=8 nwinc=8

E89 N12H N12I w=0.05 h=0.30 rho=5.7e1 nhinc=8 nwinc=8

E90 N12I N12J w=0.05 h=0.30 rho=5.7e1 nhinc=8 nwinc=8

Algorithm 55 Part 10

E94 N12M1 N12N1 w=0.05 h=0.30 rho=5.7e1 nhinc=8 nwinc=8

E95 N12N1 N13 w=0.05 h=0.30 rho=5.7e1 nhinc=8 nwinc=8

E100Z N14 N14A w=0.05 h=0.4 rho=6.5 nhinc=8 nwinc=8

E101 N14A N14B w=0.05 h=0.4 rho=6.5 nhinc=8 nwinc=8

E102 N14B N14C w=0.05 h=0.4 rho=6.5 nhinc=8 nwinc=8

E103 N14C N14D w=0.05 h=0.4 rho=6.5 nhinc=8 nwinc=8

E104 N14D N14E w=0.05 h=0.4 rho=6.5 nhinc=8 nwinc=8

E105 N14E N14F w=0.05 h=0.4 rho=6.5 nhinc=8 nwinc=8

E106 N14F N14G w=0.05 h=0.4 rho=6.5 nhinc=8 nwinc=8

E107 N14G N14H w=0.05 h=0.4 rho=6.5 nhinc=8 nwinc=8

E108 N14H N14I w=0.05 h=0.4 rho=6.5 nhinc=8 nwinc=8

E109 N14I N14J w=0.05 h=0.4 rho=6.5 nhinc=8 nwinc=8

E110 N14J N14K1 w=0.05 h=0.4 rho=6.5 nhinc=8 nwinc=8

E111 N14K1 N14L1 w=0.05 h=0.4 rho=6.5 nhinc=8 nwinc=8

E112 N14L1 N14M1 w=0.05 h=0.4 rho=6.5 nhinc=8 nwinc=8

E113 N14M1 N14N1 w=0.05 h=0.4 rho=6.5 nhinc=8 nwinc=8

E114 N14N1 N15 w=0.05 h=0.4 rho=6.5 nhinc=8 nwinc=8

E120 N16 N16A1 w=0.05 h=0.5 rho=4.34e3 nhinc=8 nwinc=8

E121 N16A1 N16A2 w=0.05 h=0.5 rho=4.34e3 nhinc=8 nwinc=8

E122 N16A2 N16A3 w=0.05 h=0.5 rho=4.34e3 nhinc=8 nwinc=8

E123 N16A3 N16A4 w=0.05 h=0.5 rho=4.34e3 nhinc=8 nwinc=8

E124 N16A4 N16A w=0.05 h=0.5 rho=4.34e3 nhinc=8 nwinc=8

E125 N16A N16B w=0.05 h=0.5 rho=4.34e3 nhinc=8 nwinc=8

E126 N16B N16C w=0.05 h=0.5 rho=4.34e3 nhinc=8 nwinc=8

E127 N16C N16D w=0.05 h=0.5 rho=4.34e3 nhinc=8 nwinc=8

E128 N16D N16E w=0.05 h=0.5 rho=4.34e3 nhinc=8 nwinc=8

E129 N16E N16F w=0.05 h=0.5 rho=4.34e3 nhinc=8 nwinc=8

E130 N16F N16G w=0.05 h=0.5 rho=4.34e3 nhinc=8 nwinc=8

E131 N16G N16H w=0.05 h=0.5 rho=4.34e3 nhinc=8 nwinc=8

E132 N16H N16I w=0.05 h=0.5 rho=4.34e3 nhinc=8 nwinc=8

E133 N16I N16J w=0.05 h=0.5 rho=4.34e3 nhinc=8 nwinc=8

E134 N16J N16K w=0.05 h=0.5 rho=4.34e3 nhinc=8 nwinc=8

Algorithm 56 Part 11

E138 N16N N17 w=0.05 h=0.5 rho=4.34e3 nhinc=8 nwinc=8

E170 N20 N20A w=0.4 h=0.05 rho=4.34e3 nhinc=8 nwinc=8

E170A N20A N20B w=0.4 h=0.05 rho=4.34e3 nhinc=8 nwinc=8

E170B N20B N20C w=0.4 h=0.05 rho=4.34e3 nhinc=8 nwinc=8

E170C N20C N20D w=0.4 h=0.05 rho=4.34e3 nhinc=8 nwinc=8

E170D N20D N20E w=0.4 h=0.05 rho=4.34e3 nhinc=8 nwinc=8

E170E N20E N20F w=0.4 h=0.05 rho=4.34e3 nhinc=8 nwinc=8

E170F N20F N20G w=0.4 h=0.05 rho=4.34e3 nhinc=8 nwinc=8

E170G N20G N20H w=0.4 h=0.05 rho=4.34e3 nhinc=8 nwinc=8

E170H N20H N20I w=0.4 h=0.05 rho=4.34e3 nhinc=8 nwinc=8

E170I N20I N20J w=0.4 h=0.05 rho=4.34e3 nhinc=8 nwinc=8

E170J N20J N20K w=0.4 h=0.05 rho=4.34e3 nhinc=8 nwinc=8

E170K N20K N20L w=0.4 h=0.05 rho=4.34e3 nhinc=8 nwinc=8

E170L N20L N20M w=0.4 h=0.05 rho=4.34e3 nhinc=8 nwinc=8

E170M N20M N20N w=0.4 h=0.05 rho=4.34e3 nhinc=8 nwinc=8

E170N N20N N20O w=0.4 h=0.05 rho=4.34e3 nhinc=8 nwinc=8

E170O N20O N20P w=0.4 h=0.05 rho=4.34e3 nhinc=8 nwinc=8

E170P N20P N20Q w=0.4 h=0.05 rho=4.34e3 nhinc=8 nwinc=8

E170Q N20Q N20R w=0.4 h=0.05 rho=4.34e3 nhinc=8 nwinc=8

E170R N20R N20S w=0.4 h=0.05 rho=4.34e3 nhinc=8 nwinc=8

E170S N20S N21 w=0.4 h=0.05 rho=4.34e3 nhinc=8 nwinc=8

E171A N22 N22B w=0.3 h=0.05 rho=5.21e1 nhinc=8 nwinc=8

E171B N22B N22C w=0.3 h=0.05 rho=5.21e1 nhinc=8 nwinc=8

E171C N22C N22D w=0.3 h=0.05 rho=5.21e1 nhinc=8 nwinc=8

E171D N22D N22E w=0.3 h=0.05 rho=5.21e1 nhinc=8 nwinc=8

E171E N22E N22F w=0.3 h=0.05 rho=5.21e1 nhinc=8 nwinc=8

E171F N22F N22G w=0.3 h=0.05 rho=5.21e1 nhinc=8 nwinc=8

E171G N22G N22H w=0.3 h=0.05 rho=5.21e1 nhinc=8 nwinc=8

E171H N22H N22I w=0.3 h=0.05 rho=5.21e1 nhinc=8 nwinc=8

E171I N22I N22J w=0.3 h=0.05 rho=5.21e1 nhinc=8 nwinc=8

E171J N22J N22K w=0.3 h=0.05 rho=5.21e1 nhinc=8 nwinc=8

E171K N22K N22L w=0.3 h=0.05 rho=5.21e1 nhinc=8 nwinc=8

Algorithm 57 Part 12

E171O N22O N23 w=0.3 h=0.05 rho=5.21e1 nhinc=8 nwinc=8

E172A N24 N24A w=0.2 h=0.05 rho=5.7e1 nhinc=8 nwinc=8

E172B N24A N24B w=0.2 h=0.05 rho=5.7e1 nhinc=8 nwinc=8

E172C N24B N24C w=0.2 h=0.05 rho=5.7e1 nhinc=8 nwinc=8

E172D N24C N24D w=0.2 h=0.05 rho=5.7e1 nhinc=8 nwinc=8

E172E N24D N24E w=0.2 h=0.05 rho=5.7e1 nhinc=8 nwinc=8

E172F N24E N24F w=0.2 h=0.05 rho=5.7e1 nhinc=8 nwinc=8

E172G N24F N24G w=0.2 h=0.05 rho=5.7e1 nhinc=8 nwinc=8

E172H N24G N24H w=0.2 h=0.05 rho=5.7e1 nhinc=8 nwinc=8

E172I N24H N24I w=0.2 h=0.05 rho=5.7e1 nhinc=8 nwinc=8

E172J N24I N25 w=0.2 h=0.05 rho=5.7e1 nhinc=8 nwinc=8

* AXIS

E175 N32 N33 w=0.01 h=0.01

E176 N32 N34 w=0.01 h=0.01

E177 N32 N35 w=0.01 h=0.01

E178A N26 N26A w=0.2 h=0.05 rho=5.7e1 nhinc=8 nwinc=8

E178B N26A N26B w=0.2 h=0.05 rho=5.7e1 nhinc=8 nwinc=8

E178C N26B N26C w=0.2 h=0.05 rho=5.7e1 nhinc=8 nwinc=8

E178D N26C N26D w=0.2 h=0.05 rho=5.7e1 nhinc=8 nwinc=8

E178E N26D N26E w=0.2 h=0.05 rho=5.7e1 nhinc=8 nwinc=8

E178F N26E N26F w=0.2 h=0.05 rho=5.7e1 nhinc=8 nwinc=8

E178G N26F N26G w=0.2 h=0.05 rho=5.7e1 nhinc=8 nwinc=8

E178H N26G N26H w=0.2 h=0.05 rho=5.7e1 nhinc=8 nwinc=8

E178I N26H N26I w=0.2 h=0.05 rho=5.7e1 nhinc=8 nwinc=8

E178J N26I N27 w=0.2 h=0.05 rho=5.7e1 nhinc=8 nwinc=8

E179A N28 N28B w=0.3 h=0.05 rho=5.21e1 nhinc=8 nwinc=8

E179B N28B N28C w=0.3 h=0.05 rho=5.21e1 nhinc=8 nwinc=8

E179C N28C N28D w=0.3 h=0.05 rho=5.21e1 nhinc=8 nwinc=8

E179D N28D N28E w=0.3 h=0.05 rho=5.21e1 nhinc=8 nwinc=8

E179E N28E N28F w=0.3 h=0.05 rho=5.21e1 nhinc=8 nwinc=8

E179F N28F N28G w=0.3 h=0.05 rho=5.21e1 nhinc=8 nwinc=8

E179G N28G N28H w=0.3 h=0.05 rho=5.21e1 nhinc=8 nwinc=8

Algorithm 58 Part 13

E179K N28K N28L w=0.3 h=0.05 rho=5.21e1 nhinc=8 nwinc=8

E179L N28L N28M w=0.3 h=0.05 rho=5.21e1 nhinc=8 nwinc=8

E179M N28M N28N w=0.3 h=0.05 rho=5.21e1 nhinc=8 nwinc=8

E179N N28N N28O w=0.3 h=0.05 rho=5.21e1 nhinc=8 nwinc=8

E179O N28O N29 w=0.3 h=0.05 rho=5.21e1 nhinc=8 nwinc=8

E180 N30 N30A w=0.4 h=0.05 rho=4.34e3 nhinc=8 nwinc=8

E180A N30A N30B w=0.4 h=0.05 rho=4.34e3 nhinc=8 nwinc=8

E180B N30B N30C w=0.4 h=0.05 rho=4.34e3 nhinc=8 nwinc=8

E180C N30C N30D w=0.4 h=0.05 rho=4.34e3 nhinc=8 nwinc=8

E180D N30D N30E w=0.4 h=0.05 rho=4.34e3 nhinc=8 nwinc=8

E180E N30E N30F w=0.4 h=0.05 rho=4.34e3 nhinc=8 nwinc=8

E180F N30F N30G w=0.4 h=0.05 rho=4.34e3 nhinc=8 nwinc=8

E180G N30G N30H w=0.4 h=0.05 rho=4.34e3 nhinc=8 nwinc=8

E180H N30H N30I w=0.4 h=0.05 rho=4.34e3 nhinc=8 nwinc=8

E180I N30I N30J w=0.4 h=0.05 rho=4.34e3 nhinc=8 nwinc=8

E180J N30J N30K w=0.4 h=0.05 rho=4.34e3 nhinc=8 nwinc=8

E180K N30K N30L w=0.4 h=0.05 rho=4.34e3 nhinc=8 nwinc=8

E180L N30L N30M w=0.4 h=0.05 rho=4.34e3 nhinc=8 nwinc=8

E180M N30M N30N w=0.4 h=0.05 rho=4.34e3 nhinc=8 nwinc=8

E180N N30N N30O w=0.4 h=0.05 rho=4.34e3 nhinc=8 nwinc=8

E180O N30O N30P w=0.4 h=0.05 rho=4.34e3 nhinc=8 nwinc=8

E180P N30P N30Q w=0.4 h=0.05 rho=4.34e3 nhinc=8 nwinc=8

E180Q N30Q N30R w=0.4 h=0.05 rho=4.34e3 nhinc=8 nwinc=8

E180R N30R N30S w=0.4 h=0.05 rho=4.34e3 nhinc=8 nwinc=8

E180S N30S N31 w=0.4 h=0.05 rho=4.34e3 nhinc=8 nwinc=8

* Base of structure

E185 N36 N37 w=0.5 h=1.0 rho= 4.34 nhinc=8 nwinc=8

*.equiv N37 N16

.equiv N3 N1 N16 N20 N30 N37

.equiv N3A1 N1A N16A1

.equiv N3A2 N5A2 N1B N16A2

.equiv N3A3 N5A3 N1C N16A3

Algorithm 59 Part 14

```
.equiv N3B N5B N7B N2B N12B N14B N16B
.equiv N3C N5C N7C N2C N12C N14C N16C
.equiv N3D N5D N7D N2D N12D N14D N16D
.equiv N3E N5E N7E N9 N12E N14E N16E N20J N22F N24 N26 N28F N30J
.equiv N3F N5F N7F N9A N12F N14F N16F N20K N22G N24A N26A N28G N30K
.equiv N3G N5G N7G N9B N12G N14G N16G N20L N22H N24B N26B N28H N30L
.equiv N3H N5H N7H N9C N12H N14H N16H N20M N22J N24C N26C N28I N30M
.equiv N3I N5I N7I N9D N12I N14I N16I N20N N22K N24D N26D N28J N30N
.equiv N3J N5J N7J N10 N12J N14J N16J N20O N22L N24E N26E N28K N30O
.equiv N3K1 N5K1 N7K1 N10K1 N12K1 N14K N16K N20P N22L N24F N26F N28L
N30P
.equiv N3L1 N5L1 N7L1 N10L1 N12L1 N14L N16L N20Q N22M N24G N26G N28M
N30Q
.equiv N3M1 N5M1 N7M1 N10C N12M1 N14M N16M N20R N22N N24H N26H N28N
N30R
.equiv N3N1 N5N1 N7M1 N10D N12N1 N14N N16N N20S N22O N24I N26I N28O
N30S
.equiv N5 N2 N14
* Equiv to ring base and collector contacts at z=0.5
.equiv N6 N15 N23 N29
.equiv N4 N17 N21 N31 N36
.equiv N8 N13 N25 N27
* Equiv ring bases and collector contacts at z=0.2
.external N4 N6 .freq fmin=1e4 fmax=1e8 ndec=1
.end
```

Algorithm 60 Output of fasthenry

Row 1: n11 to n4

Impedance matrix for frequency = 10000 1 x 1

7.06909 +9.35085e-12j

Impedance matrix for frequency = 100000 1 x 1

7.06909 +9.35085e-11j

Impedance matrix for frequency = 1e+06 1 x 1

7.06909 +9.35085e-10j

Impedance matrix for frequency = 1e+07 1 x 1

7.06909 +9.35085e-09j

Impedance matrix for frequency = 1e+08 1 x 1

7.06909 +9.35085e-08j

Appendix L:

LOW-NOISE CURRENT SOURCE/(SINK)

The use of the Low-noise BJT as a very low constant current source is shown below in Figure:L.1. This configuration is different from the normal approach of creating the constant current in the collector circuit. The approach provides a current sink in this instance with a very low output impedance.

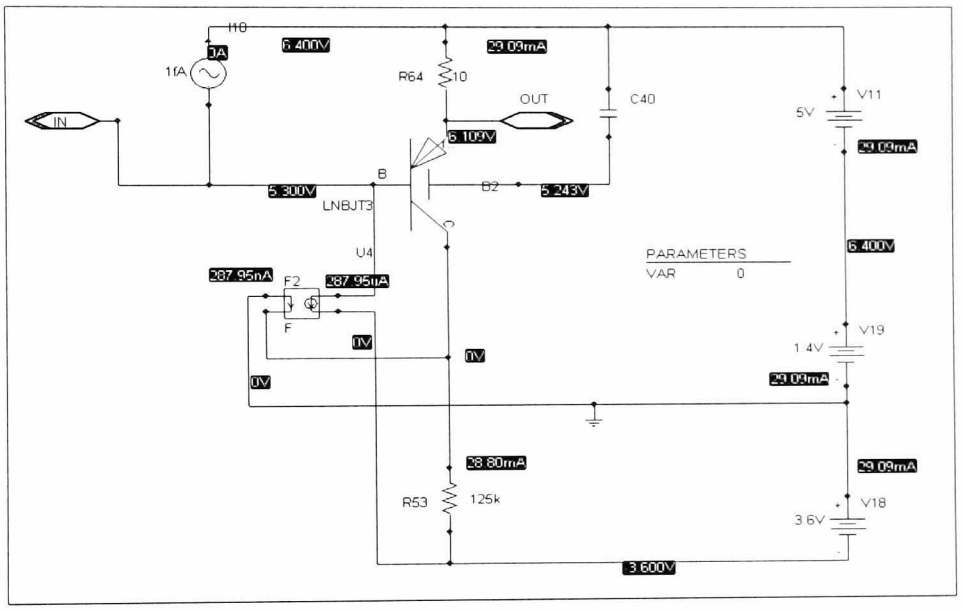

Fig. L.1. Graph of current noise vs frequency

Normally the shot-noise current generator would appear unattenuated as the input referred noise, making the conventional approach quite noisy. By reducing the output impedance to the load, the output noise of the schematic shown in Figure: L.1 decreases, and this can be further reduced by using the LOW NOISE BJT. This current source as shown with the BJT parameters defined, will provide a reduction in spectral density from $S_v = 1.8 \times 10^{-21} V^2/Hz$ to $S_v = 0.73 \times 10^{-21} V^2/Hz$, or from a noise voltage of $v_n = 429.8pV/\sqrt{Hz}$ to a noise voltage of $v_n = 267.4pV/\sqrt{Hz}$, or

$-4.1dB$, against a similar conventional current source approach.

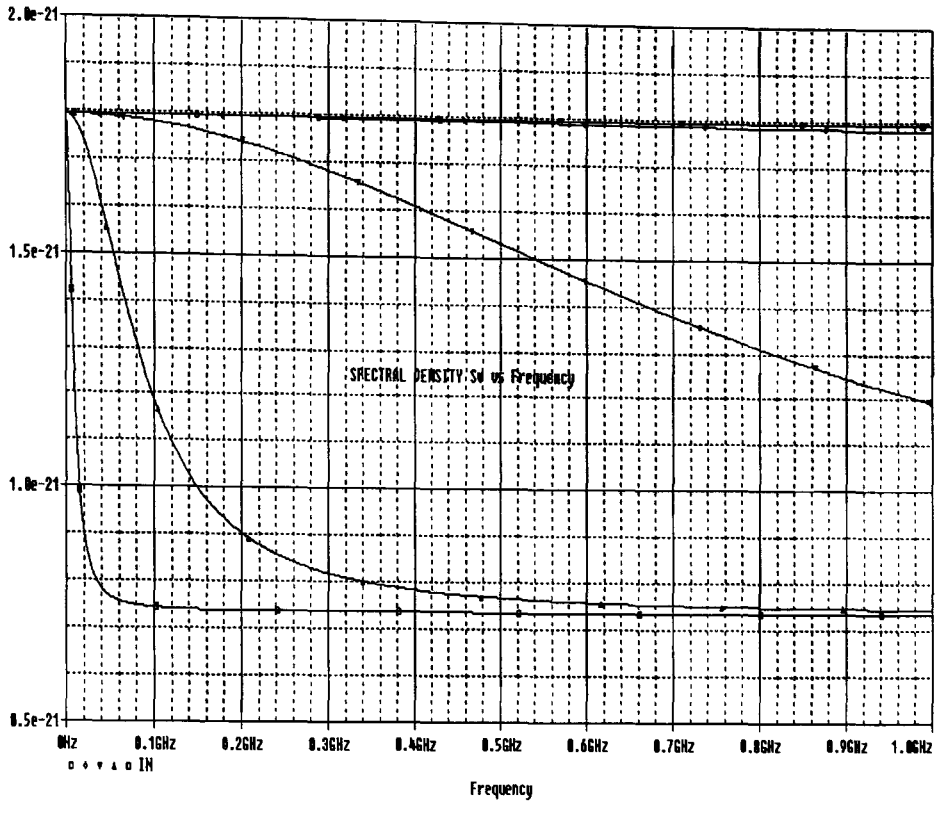

Fig. L.2. Spectral density plot of the current source

The current source is formed by creating a high gain amplifier to maintain the collector voltage, and hence collector current through $R53$ at the same voltage as $V18$. This means the emitter current is the collector current plus the base current. If the gain of the BJT is high, then the emitter current will be very close to the collector current. Changes in the value of $R64$ will not change the current from the emitter to any great extent, and the effective output resistance of the emitter (or current-source) will be high. The output impedance of the BJT will however be low and this will in effect appear in parallel with the noise current generator, so reducing the spectral density of the output noise.

Appendix M:

BJT DERIVED PARAMETERS FROM FASTHENRY

This table shows the parameters obtained from running FASTHENRY for each of the different ports.

Parameter	Symbol	Value	Units
Current Gain	hFe	100	-
Collector-Emitter resistance	rs	100K	Ohms
Collector-BASE2 capacitance	ccb2	2.5p	Farads
Base spreading resistance	rb	7.07	Ohms
Collector -Base2 resistance	rbb2	2	Ohms
Collector Bulk resistance	rcb	10	Ohms
Base2-Base1 capacitance	cb12	8p	Farads
Base2 thickness	w_{b2}	0.15	um
Base2 Minority carrier lifetime	τ_{b2}	6.6×10^{-12}	seconds

BJT parameters for the device shown in Figure:7.1

The value of ccb1 the Collector to Base1 capacitance was unable to be measured directly by this method.

Minority carrier lifetime in BASE2 τ_{b2}= 0.1 of BASE1 or typically $6.6 \times 10^{-12} s$.

Appendix N:

Summary of the amplitudes of the different noise types in a BJT device

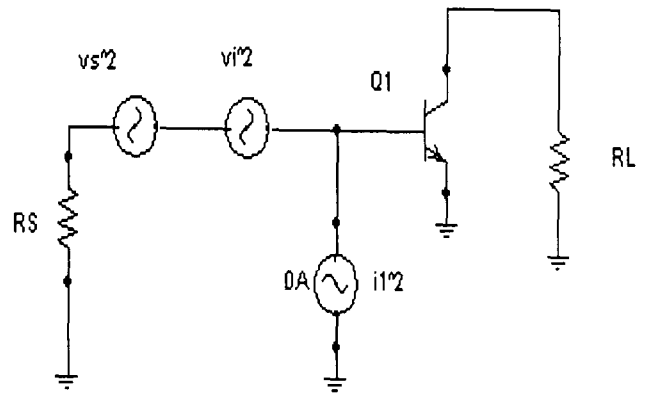

Fig. N.1. BJT diagram

The known noise types have been defined previously. In order to determine the most effective way of reducing the noise levels in a BJT device, and it is now necessary to calculate the amplitudes of the different types. This will allow an analysis of different options to be made, and aid in the design of a mechanism to reduce the noise process of the BJT device. The equivalent-input-noise generators, for a bipolar transistor, can be calculated from the common-emitter equivalent circuit of N.1. An approximation [15] can be used to show the value of this equivalent noise $\overline{v_i^2}$ .to be given by

$$\overline{v_i^2} = 4kTr_b\Delta f + \frac{2qI_c\Delta f}{gm^2} \qquad \text{(N.1)}$$

where k =Boltzmann constant, r_b is the transistor base resistance, I_c is the collector current, and gm the forward current gain of the device. This is the sum of the thermal noise, due to r_b, and the shot noise of the collector current referred back to the input

by using g_m in the second term. This gives the spectral density [15]

$$S_v = \frac{\overline{v_i^2}}{\Delta f} = 4kT(r_b + \frac{1}{2gm}) \tag{N.2}$$

with reference to N.1 The equivalent voltage noise spectral density is therefore composed of two parts. The thermal noise due to the base resistance r_b , and the component due to shot noise of the collector current I_c referred back to the input by gm, so $I_c = gm.I_b$. The AC current gain gm tends to reduce at high frequencies, and at high collector currents. To calculate the equivalent input noise current generator $\overline{i^2}$, the shot noise of the base and collector are combined. Using rms noise

$$\beta(j\omega)i_i = i_c + \beta(j\omega)i_b$$

solving for i_i this gives

$$i_i = i_b + \frac{i_c}{\beta(j\omega)} \tag{N.3}$$

and because i_a and i_b are both independent generators

$$\overline{i_i^2} = \overline{i_b^2} + \frac{i_c^2}{\mid \beta(j\omega) \mid^2} \tag{N.4}$$

where

$$\beta(j\omega) = \frac{\beta_0}{1 + j\frac{\omega}{\omega_b}} \tag{N.5}$$

where β_0 is the low frequency, small signal gain, and so

$$\frac{\overline{i_i^2}}{\Delta f} = 2q[I_b + \frac{I_c}{\mid \beta(j\omega) \mid^2}] \tag{N.6}$$

This is the spectral density of the equivalent input noise generator. Referring to Figure: D.1, frequency f_2 is the point where the high frequency noise asymptote intersects the mid-band asymptote. The value f_2 can then be calculated from

$$\beta(jf) = \frac{\beta_0}{1 + j\frac{f}{f_r}\beta_0} \tag{N.7}$$

where β_0 is the low frequency, small-signal current gain. The collector current noise term [15] is

$$2q\frac{I_c}{\mid \beta(jf) \mid^2} = 2q\frac{I_c}{\beta_0^2}(1 + \frac{f^2}{f_T^2}\beta_0^2) \cong 2qI_c\frac{f^2}{f_T^2} \tag{N.8}$$

and so

$$f_b = f_T\sqrt{\frac{I_B}{I_C}} \tag{N.9}$$

The large-signal (or DC) current gain is defined as

$$\beta_F = \frac{I_C}{I_B} \tag{N.10}$$

and so

$$f_b = \frac{f_T}{\sqrt{\beta_F}} \tag{N.11}$$

The approximate mid-band shot-noise [15] is given by

$$S_i = 2q[I_B + (\frac{I_C}{\beta_0^2})] \tag{N.12}$$

The gm of the device falls at high frequencies, and so this percentage increases with the frequency of operation. This means shot-noise becomes more dominant above f_2. Larger value of I_c reduce the input referred noise at low frequencies, but in situations where high-frequency low collector current amplifiers are required, or in low noise high-frequency current sources, then it is vital these noise figures are minimised. The greatest opportunity to reduce the noise levels, in these regions of operation, in a bipolar device, would be by improving the high frequency usable boundary. This would be achieved by reducing the shot noise. The total input referred noise for both thermal and shot noise, ignoring modulation noise for the moment is

$$\overline{v_{in}^2} = \overline{v_S^2} + \overline{v_i^2} + \overline{i_i^2.R_S^2} \tag{N.13}$$

Where v_i is the referred input noise source for the BJT transistor, i_i is the input referred shot noise current, and R_S the input source resistance, v_{in} is a single voltage source representing the total noise, and v_s is the noise in the source resistance . The expression for the total noise voltage spectral density [15] is now

$$\frac{\overline{v_{in}^2}}{\Delta f} = 4kT(R_S + r_b + \frac{1}{2gm}) + 2K_{SA}R_S^2q[I_B + \frac{I_C}{\mid \beta(jf) \mid^2}] \tag{N.14}$$

where gm is the transconductance term, I_B the base current, I_C the collector current, and β the small signal gain, and K_{SA} is a constant. This is a proposed new constant first introduced here, to represent the reduction factor of shot noise in the new BJT profile developed here. The shot noise attenuation factor K_{SA}, is defined as

$$K_{SA} = \frac{S_{i4}}{S_{i3}} \tag{N.15}$$

where S_{i3} is the spectral density with the three region (normal) BJT, and S_{i4} the spectral density with the new noise attenuation mechanisms proposed. This factor is therefore defined as unity in a conventional BJT. The need for the K_{SA} factor will become clear as the analysis continues. The contribution of each type of noise depends on the operating conditions of the BJT, and can be determined from the equation above. To minimise noise, v_{in} should be kept as low as possible, which means the thermal noise v_i should be small, and the shot-noise component on the left i_i , should be as small as possible. For conventional BJTs this means that r_b the intrinsic base spreading resistance, and the collector current I_c , should be as low a value as possible, and β as high as possible. The source resistance R_S should be selected for the optimum value. For a given amplifier, as the frequency increases β drops, and the shot-noise component begins to rise, making the shot-noise the more dominant. This is the situation at higher end of lower source resistance values, and higher collector currents. The situation changes when the BJT is used in common-emitter configurations with high source resistance, and higher collector currents. This is the situation with current source configurations. For applications at the mid to high frequency range,the shot-noise component then dominates the total noise value. The design of a BJT where the SNA factor K_{SA} , could be reduced, would allow an entirely new range of applications to be found. Using the BJT noise model proposed by Gray and Meyer [15], the total input referred noise is given by Eq. N.13, the best achievable noise figure ignoring modulation noise N.2. The noise figure is defined as

$$F(dB) = \frac{input(S/N)ratio}{output(S/N)ratio} \tag{N.16}$$

or

$$F = 1 + \frac{\overline{v_i^2}}{4kTR_S\Delta f} + \frac{\overline{i_i^2}}{4kT\frac{1}{R_S}\Delta f} \tag{N.17}$$

at R_{sopt} where

$$R_{sopt} = \frac{\sqrt{\beta_f}}{gm}\sqrt{1 + 2gmr_b} \tag{N.18}$$

This gives

$$F_{opt} \equiv 1 + \frac{1}{\beta_F}\sqrt{1 + 2gmr_b} \tag{N.19}$$

The Noise temperature is given by

$$\frac{T_n}{T} = (F - 1) \tag{N.20}$$

where T is the absolute temperature .

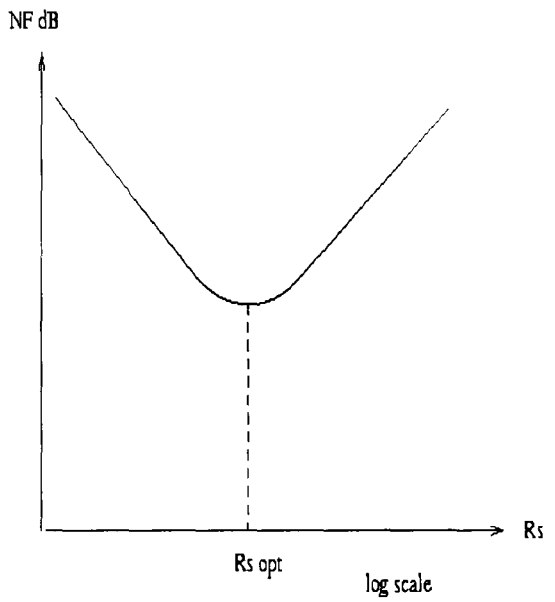

Fig. N.2. Noise figure NF vs source resistance

Appendix O:

BAND STRUCTURE OF SILICON

$$BAND - STRUCTURE - S_i \tag{O.1}$$

The energy gap in semiconductors tends to increase as the temperature is increased. This effect is quantified by the linear expansion coefficient of the material. The temperature dependence is given by

$$E_g = E_{g(0)} - \frac{\alpha T^2}{T + \beta} \tag{O.2}$$

Where T is the absolute temperature, and α and β are fitting parameters. The table shown in Table: O.1 lists the parameters for Silicon.

	Silicon
$E_g(0)(eV)$	1.166
$\alpha(meV/K)$	0.473
$\beta(K)$	636

Table O.1
Parameters as a function of temperature

The bandgap of Silicon at $300^o K$ equals

$$E_g(300K) = E_g(0K) - \frac{\alpha T^2}{T + \beta} = 1.166 - \frac{0.473 \times (300^{2)}}{300 + 636} = 1.12eV \tag{O.3}$$

Appendix P:

EQUIPMENT TYPE

The details of the equipment used to make the measurements on the TEST schematic 7.17 are shown below.

TEKTRONIX LOGIC ANALYSER WITH SPECTRUM ANALYSER MODULE type TEK 4182

SPECIFICATION:

EG&G ULTRA LOW NOISE PRE-AMPLIFIER

PRINCETON APPLIED RESEARCH

SPECIFICATION:

Gain $60\,dB$

FET input circuit

Noise input $v_n = 0.5\,nV/\sqrt{Hz}\ rms.$

ACCURACY $\pm 1\%$

STABILITY $\pm 800\,ppm\ /Deg.C.$

INPUT IMPEDANCE $5M\Omega/\ 35pF$

LIST OF REFERENCES

[1] Dermir,"*Analysis and Simulation of noise in nonlinear circuits and systems*",Kluwer International series in Engineering and computer science, p425, 1997

[2] Van der Ziel,"*Fluctuation phenomena in semiconductors*", Butterworths Scientific Pub., London, (1959).

[3] Jaeger and Brodersen,"*Low frequency noise sources in bipolar junction transistors*", IEEE Tran. Electronic Devices, vol17, No. 2, pp. 128-136, 1979

[4] "*A physical model for random telegraph signal currents in semiconductor devices*", Applied Physics, Journal of , vol. 66, no 2, pp. 937-948, 1989

[5] L.J.K. Vandamme ",*Noise in Physical Systems and 1/f Noise*", edited by M. Savelli,, G. Lecoy, and J.P Nougier (Elsevier, Amsterdam) p.183, (1983).

[6] Handel and Chung (Eds.),"*Noise in Physical systems and 1/f fluctuations* ", New York: AIP Press, pp. 200-205, 1993.

[7] K.W.Boer,"*Survey of Semiconductor Physics*", Van Nostrand, New York, (1990).

[8] T.S Sherif and P.H Handel,"*Unified Treatment of Diffraction and 1/f Noise*",Phys. Rev. A26, p.596-602, (1982).

[9] "*1/f noise in b+ p-n microwave transistors*", Solid State Electronics, vol.28, no 5, pp.473-477,1985

[10] Buckingham M.J.,"*Noise in Electronic devices and systems*", John Wiley and Sons, London, (1983).

[11] Ninth International Conference on Noise,in "*Physical systems/Including 1/f noise and noise in Biological systems Membranes Including L/F noise and n*", International conference on noise in physical systems, Montreal, 1987

[12] Ghione and Filicori , "*A computationally efficient unified approach to the numerical analysis of the sensitivity and noise of semiconductor devices*",1993.

[13] Ya. M. Blanter and M. Buttiker,"*Shot noise in Mesocopic Conductors*", Phys. Rep. **336**, 1 , 2000

[14] Asenov,"*Efficient 3D 'Atomistic' simulation technique for studying of random dopant induced threshold voltage lowering and fluctuations in decanano MOSFETs*": University of Glasgow. `http://www.elec.gla.ac.uk`

[15] Gray and Meyer ,"*Analysis and design of Analog Integrated circuits*", Wiley press,1993

[16] Vempati , "*Low-frequency noise in UHV/CVD Epitaxial Si and SiGe bipolar transistors*", IEEE Journal of Solid state circuits, p1458-1465, Oct 1996.

[17] D. M. Cughey and R. E. Thomas, "*Carrier Mobilities in Silicon Empirically Related to Doping and Field*", Proceedings of IEEE, vol. 55, pp. 2192-2193, (1967).

[18] Roderick,"*Metal-semiconductor contacts*",IEE Proc., 129, 1, 1982.

[19] *Solid State Electronics* 9,1035, Diodes, Sci. Technology, Vol. A3, pp. 176-182, 1996

[20] Grubin,"*The Physics of sub-micron structures*" edited by (Plenum, New York), p.211,1984

[21] Savelli,"*Noise in Physical Systems and 1/f Noise*" (Elsevier, Amsterdam), p15,1983

[22] Ferry,"*Physics of Submicron Devices*" (Plenum press, New York, p380, 1991).

[23] Sarantini,"*An efficient Multigrid Poisson Solver for Device Simulations,Physik Department ans Walter Schottky Institut, Technische Universitat Muenchen:IEEE Transaction on Computer Aided Design of Integrated Circuits and Systems*", NR.2,VOL.15,141-150, (1996).

[24] Wein, "*The Monte Carlo Method for Semiconductor Device Equations*", Springer Verlag, New York,1989

[25] "*Lattice-gas cellular-automation method for semi-classical transport in semiconductors*" , Physical Review B, vol. 46, pp. 1382-1394, July 1971.

[26] Selberherr,Springer-Verlag, "*Analysis and Simulation of Semiconductor Devices*" Vienna, New York,1984

[27] Hilger, "*Computer Simulation using particles*" Bristol, 1998

[28] Sze, "*Physics of Semiconductor Devices*", 2nd Edition, Wiley Inter science publication, 1981

[29] A. Asenov, A.R.Brown, S. Roy, J.R Barker,"*Topologically Rectangular Finite Element Grids in the Parallel Simulation of Semiconductor Devices*", Department of Electronics, University of Glasgow.

[30] Pana,"*Finite Element Simulation of Semiconductor Devices on Multiprocessor Computers*", vol. 20, pp. 1130-1159,1993

[31] Kwok, 1995,"*Complete Guide to Semiconductor devices*", pp. 564-565.

[32] *Aldert* van der Ziel, "*Noise Sources, Characterization, Measurement*", New Jersey, Prentice Hall,1970.

[33] Johnson J.B,"*Thermal agitation of Electricity in Conductors*", Nature, vol 119, pp.50-51,1927

[34] Johnson J.B,"*Thermal Agitation of Electricity in Conductors*", Physical Review. vol.32, no 7, pp. 97-109, July 1928

[35] Nyquist H,"*Thermal Agitation of Electric Charge in Conductors*",Physical Review, vol.32,no 7, pp. 110-113, July 1928

[36] Nougier J.P,"*Fluctuations and Noise of Hot Carriers in Semiconductor Materials and Devices*", IEEE Transactions in Electron Devices. vol. 41. no. 11. pp. 2034-2049, Nov. 1994.

[37] Johnson J.B,"*The Schottky effects in Low Frequency Circuits*". Physical Review. vol.26, pp. 71-85,1925.

[38] Motchenbacher and F.C. Fitchen,"*Low-Noise Electronic Design* ", John Wiley & Sons, Inc., New York, NY,1973.

[39] Friis H.T.,"*Noise Figures of Radio Receivers*". Proceeding of the Institute of Radio Engineers, vol. 32,no 7,pp.419-422, July 1956.

[40] Shockley W. J A Copeland, and R. P. Thames, "*The impedance Field Method of Noise Calculation in Active Semiconconductor Devices*", in Quantum Theory of Atoms, Molecules and the Solid-State, Academic, New York,N.Y, pp.537-563, 1996.

[41] Vliet van K.M."*General Transport Theory of Noise in PN Junction-Like Devices-I. Three-Dimensional Green's Function Formulation*", Solid State Electronics, vol.15, pp.1033-1053, 1972.

[42] F.Bonani, G. Ghione, M.R. Pinto, R.K. Smith, "*An efficient Approach to Noise Analysis Through Multidimensional Physics-based Models*", IEEE Trans. Electron Devices, 45, 261 (1998).

[43] Martin, Archer,Boulin,"*Device Noise in Silicon RF Technologies*", Bell Labs Technical Journal, July 1997.

[44] G.B. Levovik, JETP Lett. **49**, 683 , 1989

[45] M. Buttiker, Phys. Rev. Lett. **65**, 2901, 1990

[46] Th. Martin and R. Landauer, Phys. Rev. B **45**, 1742 , 1992

[47] Gruzinskis, Starikov and Shiktorov, "*Hydrodynamic approach to noise spectra in unipolar semi-conductor structures*" , Semi-conductor Physics Institute, Lithuania, (1994).

[48] Ya. M. Blanter and M. Buttiker,"*Shot Noise in Mesoscopic Conductors*", Phys. Rep. 336,1, 2000

[49] W. Schottky, Ann. Phys. (Leipzig) **57** (1918)

[50] M.J.M. de Jong and C. W. J. Beenakker, Physica A **230** (1996) 219

[51] D.G. Peterson. "*Noise Performance of Transistors*",IRE Transactions on Electron Devices, Vol. **ED-9**, pp. 296-303, May 1962.

[52] J.L. Plumb and E.R. Chenette,"*Flicker Noise in Transistors*". IEEE Transactions on Electron Devices, Vol. **ED-10**, pp. 304-308, September 1963.

[53] M. Schwartz."*Information Transmission, Modulation, and Noise*" MGraw-Hill, New York, 1959, Chapter 5.

[54] J. L. Lawson and G.E. Uhlenbeck, "*Threshold Signals*", McGraw-Hill. New York. 1950, Chapter 4.

[55] W.B. Davenport, Jr., and W.L. Root, "*An introduction to the Theory of Random Signals and Noise*", McGraw-Hill, New York, 1958, Chapter 7.

[56] Chih-Tang Sah, R.N. Noyce and W. Shockley, Proc. IRE, **45** (1957), 1228.

[57] B. Wang and M. Curov, "*Numerical large-signal simulation of diffusion noise in GaAs Gunn devices*", IEEE Trans. Electr. Dev. **ED-39** (1992) 2176-2178.

[58] J.B. Johnson, "*Thermal agitation of electricity in conductors*", Phys. Rev. (1998), July, 110-113

[59] Paul J. van Wijnen, "*On the Characterisation and Optimisation of High-Speed Bipolar Transistors*", Cascade Microtech, Inc., June 1995.

[60] O.M. Bulashenko, G. Gomila, J.M. Rubi and V.A. Kochelap, "*Extension of the impedance field method to the noise analysis of a semiconductor junction*", Analytical Approach, J. Appl. Phys. **83** (1998) 2610-2618.

[61] S.R. Lederhandler, L.J.Giacoletto, "*Measurement of Minority Carrier Lifetime and Surface Effects in Junction Devices*", Proc. IRE, pp. 477-483, April 1955.

[62] Guillermo Gonzalez," *Microwave Transistor Amplifiers–Analysis and Design*",Prentice-Hall, Inc., Englewood Cliffs, NJ, 1984.

[63] E. Strikov, P. Shiktorov, V. Gruzinskis, L. Varani, J.C. Vaiserre, J.P. Nougier, T. Gonzalez, "*Transfer impedance calculations of electronic noise in two-terminal semiconductor structures*", J. Appl. Phys. 83 (1998) 2052-2066.

[64] M.Pinto C.S.Rafferty and R.W. Dutton, "*PISCES-II: Poisson and continuity equation solver*", Stanford, CA, Stanford Electron Lab. Tech. Rep., Sept 1984.

[65] K.M. Van Vliet, A. Friedman, R.J.J. Zijlstra, A. Gisolf and A. Van der Ziel, "*Noise in single injection diodes*", I. A survey of methods, J. Appl. Phys. **46** (1975) 1804-1813.

[66] A. van der Ziel,"*Noise in Solid State Devices and Circuits*",Chapter 5, John Wiley & Sons, N ew York, NY, (1986).

[67] A van der Ziel," *Solid State Physical Electronics*", Chapter 18, Prentice-Hall, Englewood Cliffs,NJ, 3rd Edition, (1976).

[68] F. Brezzi, L.D. Marini and P.Pietra, "*Numerical simulation of semiconductor devices*", Comp. Meths. Appl. Mech. Engr., vol 75, 1989, pp. 493-515.

[69] Kazutaka Tomizawa, "*Numerical simulation of Submicron Semiconductor Devices*", Artech House Publishers, 1993

[70] A. Reklaitis and L. Reggiani, " *Monte Carlo study of shot-noise supression*", J. Appl. Phys. 82, 3161-3163 (1997), 33-83.

[71] Steven E. Koonin and Dawn C. Meridith, " *Computational Physics*", Addison-Wesley (1990).

[72] Foulkes, W.M.C. Mitas, L., Meeds, R.J., and Rajagopal, G., "*Quantum Monte Carlo Simulations of Solids*", Reviews of Modern Physics, Vol. 73, No. 1, (JAN 2001), 33-83

[73] Thijssen, J.M., "*Computational Physics* ", Cambridge: The Cambridge Press, 1999.

[74] Malivin H. Kalos and Paula A. Whitelock," *Monte Carlo Methods*", Vol 1, Basics, John Wiley & Sons, (1986).

[75] Reuven Y. Rubenstein, " *Simulation and the Monte Carlo Method*", John Wiley & Sons, (1981).

[76] Ronald Rohrer, Laurence Nagel, Robert Meyer and Lynn Weber,"*Computationally Efficient Electronic Circuit Noise Calculation*", IEEE J Solid State Circuits, vol. SSC-6, pp. 204-213, Aug 1971.

[77] H.-M Rein and M. Schroter,"*Base spreading resistance of square emitter transistors and its dependence on current crowding*", IEEE Trans. Electron Dev., vol. 36, pp. 730-733, 1989.

[78] W. Shockley,"*Problems related to p-n junctions in silicon*", Solid State Electron., vol. 2, p 35, (1961).

[79] A. van der Ziel, "*Unified presentation of 1/f noise in electronic devices Fundamental 1/f noise sources*", Proc. IEEE, vol. 76, pp 233-258, Mar. (1988).

[80] N.D. Nelson and T.A. Manteuffel and S.F. McCormick,"*A multigrid solver for the semiconductor equations*",pp. 1-15, (1993).

[81] R.K. Coomer and I.G. Graham,"*Massively Parallel Methods for Semiconductor Device Modelling*", Computing v.56, pp 1-27, (1996).

[82] Y.J Park, "*On the Monte Carlo Simulation of Bipolar Devices*",IEDM Tech. Digest,pp 688-691, December (1982).

[83] C.M VAN Vliet. "*Macroscopic and Microscopic Methods for Noise in Devices*", IEEE Trans. Electron Devices 41, 1902 (1994).

[85] Bonani, G. Ghione, "*Generation-Recombination Noise Modelling in Semiconductor Devices Through Population or Approximate Equivalent Current Density Fluctuations*", Solid State Electronics 43, 285 (1998).

[86] Bonani F. Pinto M.R.,"*An Efficient Approach to Multi-Dimensional Impedance Field Noise in Physical Systems and 1/f Noise*", in Proceedings of 13th International Conference on Noise in Physical Systems and 1/f Noise,pp. 379-382, (1995).